THERMODYNAMIC ANALYSIS TECHNIQUES FOR THE STUDY OF COMBUSTION IN COMPRESSION IGNITION ENGINES WITH APPLICATION TO METHANOL/DIMETHYL ETHER FUELLING

DANIELE CIPOLAT

A Thesis submitted to the Faculty of Engineering, University of the Witwatersrand, Johannesburg, in fulfilment of the requirements for the degree of Doctor of Philosophy

Johannesburg 1991

Declaration by Candidate

I, Daniele Cipolat, hereby declare that this thesis is my own work, and the material contained herein has not been submitted by me for the degree of Doctor of Philosophy at any other university.

15 MARCH 1991

ABSTRACT

Thermodynamic analysis techniques for the study of combustion in compression ignition engines were developed and refined. The techniques were validated against test runs of diesel fuelling, and were then applied to the almost unexplored case of combustion of aspirated dimethyl ether (DME), acting as ignition promotor and supplementary fuel, and injected methanol as main fuel.

Combustion chamber pressure versus crank angle data were captured for single engine cycles on normal fuelling (methanol and DME), fuelling with DME alone and pure motoring (no fuel) all at essentially identical engine conditions. These data were analysed by a number of mutually complementary techniques, the most important of which were the superposition of single and dual fuel cycles and the application of a comprehensive energy release model. The model is a refinement of that of Krieger and Borman (1966), capable of accounting for the presence of both fuels (where applicable) and featuring a heat transfer analysis specifically developed for the engine used in this study.

Tests at constant speed and power, and with varying proportions of DME to methanol were conducted. Injection timing was unaltered from that previously optimised for diesel fuelling. The DME contribution to the total combustibles varied from some 25 to 50% by mass, the lower limit corresponding to the onset of misfire and the upper to that of knock. Indicated thermal efficiency fell with increasing DME fuel contribution.

The DME was found to combust during compression in an unusual manner involving three distinct, previously incompletely recognized, stages of reaction. The release of energy and of products of combustion of these DME reactions, furthermore, strongly affected the subsequent burning of injected methanol. The variations in macroscopic engine performance as a function of DME fuel contribution could be adequately explained in terms of the interaction of the individual combustion phenomena. The analysis techniques developed in this thesis are thus seen to have been helpful in the study of a complex case of combustion in a compression ignition engine.

ACKNOWLEDGEMENTS

I wish to express my most sincere appreciation to Professor C J Ballis for suggesting a most challenging and interesting topic for research. His supervision, guidance, advice and the sharing of his experiences and knowledge, made it possible for this research to become a reality.

I also wish to thank Dr H H Jawurek, my colleague and co-supervisor for his advice, assistance and many fruitful discussions. His encouragement, particularly during the analysis, is gratefully acknowledged.

A word of gratitude to those members of the staff of the School of Mechanical Engineering who shared their expertise, offered suggestions and showed interest, particularly Professor A Nurick.

My sincere thanks are also extended to Mrs Hilary Jacobson for her patience and for dedicating many hours to the typing of this manuscript.

My thanks and appreciation go also to the staff of the Mechanical Engineering Laboratory for their technical assistance and encouragement.

The financial assistance of the University of the Witwatersrand, the Foundation for Research and Development and AECI Ltd, is gratefully acknowledged.

I am also grateful to my wife Francesca and my sons Riccardo and Alberto for their patience and encouragement, throughout those years of research. Their concern and constant interest particularly during the most difficult stages of this work is much appreciated.

Last but not least to my father, Angelo and my mother Dirce, a particular word of gratitude for their kindness and encouragement. The dedication they have shown their children is an example I shall always follow.

DEDICATION

To my father Angelo, and my mother Dirce

NOTATION

c_p	specific thermal capacity at constant pressure (J/kgK)
c_v	specific thermal capacity at constant volume (J/kgK)
$\bar{M}$	mean molecular mass (kg)
n	polytropic index
n_c	carbon mole ratio
$\dot{n}_{DME}$	mole flow rate of DME (mol/s)
$\dot{n}_{METHANOL}$	mole flow rate of methanol (mol/s)
$\dot{n}_{TOTAL}$	mole flow rate of methanol and DME (mol/s)
p	combustion chamber pressure (N/m^2)
p_1	combustion chamber pressure at IVC (N/m^2)
Q_a	magnitude of pre-reaction energy absorption of DME (J)
Q_1	magnitude of first energy release of DME (J)
Q_2	magnitude of second energy release of DME (J)
Q_{EVO}	magnitude of modelled energy released at EVO (J)
Q_{FUEL}	magnitude of energy supplied by fuel (J)
R	specific gas constant $(J/molK)$
R^u	universal gas constant $(J/molK)$
s	specific entropy of combustion chamber gases (J/kgK)
T	mean combustion chamber gas temperature (K)
V	combustion chamber volume (m^3)
V_1	combustion chamber volume at IVC (m^3)

The following nomenclature is used in the derivation of the heat transfer equations in Appendix A:

a_1, a_2, a_3	constants
A	combustion chamber exposed area (m^2)
A_c	cross sectional area of cylinder (m^2)
$A_{crown+head}$	area of piston crown and cylinder head (m^2)
A_l	cylinder wall area (m^2)
A_r	piston crown and cylinder head area (m^2)
A_{wall}	exposed area of combustion chamber walls (m^2)
c	crank to connecting rod ratio
c_p	specific thermal capacity at constant pressure (J/kgK)
C_1	constant
d	diameter of bowl in piston crown (m)
$dS(I)$	derivative of distance of piston crown from cylinder head at any crank angle position with respect to time (m/s)
D	cylinder bore (m)
h	convective heat transfer coefficient (W/m^2K)
h_l	longitudinal convective heat transfer coefficient (W/m^2K)
h_r	radial convective heat transfer coefficient (W/m^2K)
$h_{resultant}$	resultant convective heat transfer coefficient (W/m^2K)
I	crank angle position ($^\circ$)
k	conductivity of combustion chamber gases (W/mK)
m	constant
n	constant
N_u	Nusselt number
P_r	Prandtl number
Q	heat transfer (W)
Q_{CONV}	total convective heat transfer (W)
Q_l	longitudinal convective heat transfer (W)
Q_r	radial convective heat transfer (W)
Q_{RAD}	radiation heat transfer (W)
Q_{TOTAL}	total heat transfer (W)
r	connecting rod length (m)
Re	Reynolds number

$S(l)$	distance of piston crown from cylinder head at any crank angle position (m)
T_g	mean cylinder gas temperature (K)
$T_w(l)$	cylinder wall temperature at any crank angle position (K)
v	combustion chamber volume (m^3)
V	piston velocity (m/s)
V_t	longitudinal air flow velocity (m/s)
V_r	radial air flow velocity (m/s)
W_c	air swirl velocity in cylinder during compression (rad/s)
W_o	air swirl velocity in cylinder at beginning of compression (rad/s)

GREEK SYMBOLS

γ	ratio of principal specific thermal capacities
ε	emissivity of combustion chamber gases
θ	crank angle increment (°)
θ_1	crank angle corresponding to the onset of Q_1 (°)
θ_2	crank angle corresponding to the onset of Q_2 (°)
μ	dynamic viscosity of combustion chamber gases (Ns/m^2)
ρ	density of combustion chamber gases (kg/m^3)
σ	Stefan-Boltzmann constant (W/m^2K^4)
ϕ	equivalence ratio
ϕ_{DME}	ratio of stoichiometric to actual air DME ratio
ϕ_{TOTAL}	ratio of stoichiometric to actual air methanol/DME ratio

ABBREVIATIONS

ABDC	after bottom dead centre
ATDC	after top dead centre
BBDC	before bottom dead centre
BDC	bottom dead centre
BMEP	brake mean effective pressure (Pa)
BSEC	brake specific energy consumption (kg/kWh)
BSFC	brake specific fuel consumption (kg/kWh)
BTDC	before top dead centre
BTE	brake thermal efficiency
°CA	degree crank
CI	compression ignition
DME	dimethyl ether
EVO	Exhaust valve open
IMEP	Indicated mean effective pressure (Pa)
ITE	Indicated thermal efficiency
IVC	Inlet valve close
SI	Spark ignition

Contents

1 BACKGROUND, AIMS AND OUTLINE OF STUDY 1

1.1 Background 1

1.2 Overall Aims of Study 2

1.3 Outline of Thesis 2

2 LITERATURE SURVEY: METHANOL AS A FUEL 4

2.1 Historical Background 5

2.1.1 Historical Development of Methanol as a Fuel 6

2.1.2 Alcohol as a Fuel 9

2.1.3 Methanol as a replacement 11

2.1.4 Methanol as an Extender 17

2.1.5 Methanol as an Emulsion or Solution 19

2.1.6 Methanol in a Dual-fuelling System 23

2.1.7 Summary of Fuelling Techniques 26

2.1.8 Dimethyl Ether as an Ignition Promoter 28

2.1.9 Conclusions 30

3 LITERATURE SURVEY: ANALYTICAL METHODS 31
3.1 Energy Release 31
3.1.1 Energy Release Models 32
3.1.2 Heat Transfer 64
3.1.3 Heat Transfer Models 66
3.2 Conclusions 81
4 THERMODYNAMIC ANALYSIS TECHNIQUES 83
4.1 General Analysis Techniques 83
4.1.1 Combustion Chamber Pressure 84
4.1.2 Derivative of Combustion Chamber Pressure 84
4.1.3 Combustion Chamber Pressure versus Volume . . . 84
4.1.4 $ln\,(p/p_1)$ versus $ln(V/V_1)$ 85
4.1.5 Polytropic Index 85
4.1.6 Injector Line Pressure 85
4.2 Energy Release Modelling and Related Techniques 86
4.2.1 The Energy Release Model 86
4.2.2 The Determination of c_p and R 88
4.2.3 Gas Temperature 99
4.2.4 Compression of DME and Air 100
4.2.5 Calculation of Apparent Mass Burnt 100
4.2.6 Entropy 101

4.2.7 Heat Transfer in the Engine 101
4.2.8 Basis of the Heat Transfer Equation 102
4.2.9 Conclusions 103

5 EXPERIMENTAL EQUIPMENT AND PROCEDURE 106

5.1 Experimental Equipment 107
5.1.1 The Engine and Fuel System 107
5.1.2 The Dynamometer 107
5.2 Instrumentation 107
5.2.1 Steady State Parameters 109
5.2.2 Transient Parameters 109
5.2.3 Manual Inputs 110
5.3 Preliminary Tests 111
5.3.1 Location of Top Dead Centre 111
5.3.2 Optimization of Injection Timing 112
5.3.3 Supplying DME to the Engine 118
5.3.4 Heating and Cooling the Inlet Air 119
5.3.5 Data Acquisition Triggering System 120
5.3.6 Computer Programs 122
5.4 Experimental Procedure 122
5.4.1 Testing Procedure 122

6 RESULTS AND DISCUSSION 124

6.1 Diesel Fuelling 125
6.1.1 Test Conditions 125
6.1.2 Analysis and Discussion 126
6.1.3 Interim Conclusions 140
6.2 Methanol/DME Fuelling 140
6.2.1 Engine Performance Characteristics 142
6.2.2 Combustion Characteristics 146
7 CLOSURE 183
7.1 Summary, Conclusion and Comments 183
7.1.1 Suggestions for Further Work 189
APPENDICES 190
A DERIVATION OF THE HEAT TRANSFER EQUATION 190
A.1 Convective Heat Transfer 191
A.1.1 Convective Heat Transfer Coefficient 191
A.1.2 Exposed Combustion Chamber Area 194
A.1.3 Mean Combustion Chamber Wall Surface Temperature 195
A.1.4 Mean Gas Temperature 195
A.1.5 Total Convective Heat Transfer 195
A.1.6 Radiation Heat Transfer 196
A.2 Total Heat Transfer 197

B SPECIFICATIONS 198
B.1 Petter Compression Ignition Engine 198
B.1.1 Instrumentation 199
C CALIBRATION OF INSTRUMENTATION 201
C.1 Load Cell 201
C.2 Tachometer 203
C.3 Fuel Flowmeter 205
C.4 Airflow 207
C.5 Combustion Chamber Pressure 209
C.6 Injector Needle Lift 210
C.7 Fuel Line Pressure 213
C.8 Rotameter 214
D EFFECT OF RESIDUALS ON INITIAL MIXTURE TEMPERATURE 219
E PHYSICAL PROPERTIES OF DME 221

List of Figures

2.1 Techniques for fuelling compression ignition engines with alcohol fuels (Cipolat *et al*, 1986) 26

3.1 Energy release diagrams (Lyn, 1960) 33

3.2 Rate of heat release (Whitehouse *et al*, 1962) 35

3.3 Measured and predicted heat release diagrams (Bowden *et al*, 1969) 38

3.4 Comparison between experiment and both air entrainment models for rate of heat release (Grigg and Syed, 1969) . . . 41

3.5 Comparison between experiment and conical plume model for rate of heat release (Grigg and Syed, 1969) 41

3.6 Actual and substitute rate of heat release dependent upon air-fuel equivalence ratio (Woschni and Anisits, 1974) 43

3.7 6-Hole nozzle, low load, pressure and heat release diagrams (Whitehouse and Abughres, 1975) 44

3.8 Change of $\frac{dQ}{d\theta}$ pattern with the change of swirl (Shimotsu and Erdo, 1982) 46

3.9 Change of $\frac{dQ}{d\theta}$ pattern with the change of fuel injection period (Shimotsu and Erdo, 1982) 47

3.10 Heat release and cylinder pressure of two-fuel system (Hsu, 1984) 47

3.11 Heat release and cylinder pressure of two-fuel system at different injection timing (Hsu, 1984) 48

3.12 Comparison of burning rates at full load (Faletti *et al*, 1982) 49

3.13 Comparison of cumulative energy release (Faletti *et al*, 1982) 49

3.14 Ignition delay, brake thermal efficiency, peak cylinder pressure and maximum rate of pressure rise : comparison at 2000 *rev/min* (Faletti *et al*, 1982) 51

3.15 Comparison of heat release analysis achieved by : Perfect Gas Theory, (—) : Model (···) (Picken *et al*, 1979) 52

3.16 Comparison of normalized mass burning rates at a BMEP of 600*kPa*. The simple heat release model using an assumed initial mass (Hayes *et al*, 1986) 52

3.17 Comparison of normalized mass burning rates at a BMEP of 300 *kPa*. The simple heat release model using an assumed initial mass (Hayes *et al*, 1986) 54

3.18 Rate of heat release for different SDC timings at 1500 *rev/min* and 45 :1 air-fuel ratio (Martin and Ahmad, 1986) 55

3.19 Cumulative heat release for different SDC timings at 1500 *rev/min* and 45 :1 air-fuel ratio (Martin and Ahmad, 1986) 56

3.20 Rate of heat release for different speeds at 45 :1 air-fuel ratio and SDC timing at TDC (Martin and Ahmad, 1986) 56

3.21 Rate of heat release for different air-fuel ratios at 1500 *rev/min* and SDC timing at TDC (Martin and Ahmad, 1986) 57

3.22 Heat release histories for various loads (1200 *rev/min*) (Alkidas, 1987b) 60

3.23 Heat release histories for various loads (1800 rev/min) (Alkidas, 1987b) 60

3.24 Heat release curves for arrangement D-2 at $n = 2200\ rev/min$ $\theta_{inj} = 24°$ CA BTDC (Ghojel, 1982) 61

3.25 Effect of combustion arrangement and engine speed on rate of heat release at IMEP = 0.9 MPa (Ghojel, 1982) 62

3.26 Effect of IMEP and injection timing on rate of heat release for arrangement D-2 at $n = 2000\ rev/min$. (Ghojel, 1982) . 63

3.27 Comparison of experimental simulated results for the effect of fuel-air ratio on power, fuel consumption, and exhaust temperature in a diesel engine. (Sorenson, 1981) 65

3.28 Simulated pressure-time diagrams showing the effect of fuel-air ratio in a diesel engine (Sorenson, 1981) 66

3.29 Heat flux calculated from data of figure 3.31 (Le Feuvre *et al*, 1969) 67

3.30 Thermocouple locations in the open-chamber diesel (Le Feuvre *et al*, 1969) 68

3.31 Surface temperature at five locations shown in figure 3.30. Supercharged at 2000 rev/min and 0.45 equivalence ratio (Le Feuvre *et al*, 1969) 68

3.32 Comparison between measured area averaged heat flux and predictions (Annand and Ma, 1970) 74

3.33 Comparison of heat-transfer coefficients calculated using different formulae for the same engine conditions (Woschni, 1967) 76

3.34 Heat flux data obtained using a CFR engine and calculated heat-transfer coefficients obtained by using measured wall and mass-averaged temperature differences (Overbye, 1961) 77

3.35 Dimensionless heat flux versus dimensionless cylinder pressure for a motored engine (Overbye, 1961) 78

3.36 Measured surface heat flux in piston bowl and predicted flux using bulk mean and hot-zone model with swirl effect (Dent and Suliaman, 1977) 80

4.1 Cumulative energy released versus crank angle for a motoring cycle 104

5.1 Injector pressure versus crank angle 115

5.2 Derivative of cylinder pressure versus crank angle 116

5.3 Ignition delay versus speed 117

Cylinder pressure versus crank angle 118

6.1 Combustion chamber pressure versus crank angle for minimum diesel fuelling 127

6.2 Combustion chamber pressure versus crank angle for maximum diesel fuelling 127

6.3 Injector line pressure versus crank angle for maximum diesel fuelling 129

6.4 Combustion chamber pressure versus volume for minimum diesel fuelling 131

6.5 Combustion chamber pressure versus volume for maximum diesel fuelling 131

6.6 $\ell n(p/p_1)$ versus $\ell n(V/V_1)$ for minimum diesel fuelling . . . 132

6.7 $\ell n(p/p_1)$ versus $\ell n(V/V_1)$ for maximum diesel fuelling . . . 132

6.8 Polytropic index and gamma versus crank angle for minimum diesel fuelling 134

6.9 Polytropic index and gamma versus crank angle for maximum diesel fuelling 134

6.10 Gas temperature versus crank angle for minimum diesel fuelling 135

6.11 Gas temperature versus crank angle for maximum diesel fuelling 135

6.12 Cumulative energy release versus crank angle for minimum diesel fuelling 136

6.13 Cumulative energy release versus crank angle for maximum diesel fuelling 137

6.14 Gas temperature versus entropy for minimum diesel fuelling 138

6.15 Gas temperature versus entropy for maximum diesel fuelling 138

6.16 Brake thermal efficiency versus ϕ_{DME} for low and high loads, methanol / DME fuelling 143

6.17 Indicated power versus ϕ_{DME} for low and high loads, methanol/DME fuelling 144

6.18 Indicated thermal efficiency, versus ϕ_{DME} for low and high loads, methanol/DME fuelling 145

6.19 Mechanical efficiency versus ϕ_{DME} for low and high loads, methanol/DME fuelling 145

6.20 Combustion chamber pressure versus crank angle for low load, low DME fuel contribution 147

6.21 Combustion chamber pressure versus crank angle for low load, high DME fuel contribution 147

6.22 Combustion chamber pressure versus crank angle for high load, low DME fuel contribution 149

6.23 Combustion chamber pressure versus crank angle for high load, high DME fuel contribution 150

6.24 Combustion chamber pressure versus volume for low load, low DME fuel contribution 151

6.25 Combustion chamber pressure versus volume for low load, high DME fuel contribution 151

6.26 Combustion chamber pressure versus volume for high load, low DME fuel contribution 152

6.27 Combustion chamber pressure versus volume for high load, high DME fuel contribution 152

6.28 $ln(P/P_1)$ versus $ln(V/V_1)$ for low load, low DME fuel contribution 154

6.29 $ln(P/P_1)$ versus $ln(V/V_1)$ for low load, high DME fuel contribution 154

6.30 $ln(P/P_1)$ versus $ln(V/V_1)$ for high load, low DME fuel contribution 155

6.31 $ln(P/P_1)$ versus $ln(V/V_1)$ for high load, high DME fuel contribution 155

6.32 Polytropic index versus crank angle for low load, low DME fuel contribution 157

6.33 Polytropic index versus crank angle for low load, high DME fuel contribution 157

6.34 Polytropic index versus crank angle for high load, low DME fuel contribution 159

6.35 Polytsopic index versus crank angle for high load, high DME fuel contribution 159

6.36 Combustion chamber gas temperature versus crank angle for low load, low DME fuel contribution 160

6.37 Combustion chamber gas temperature versus crank angle for low load, high DME fuel contribution 160

6.38 Combustion chamber gas temperature versus crank angle for high load, low DME fuel contribution 161

6.39 Combustion chamber gas temperature versus crank angle for high load, high DME fuel contribution 161

6.40 Cumulative energy release versus crank angle for low load, low DME fuel contribution 162

6.41 Cumulative energy release versus crank angle for low load, high DME fuel contribution 163

6.42 Cumulative energy release versus crank angle for high load, low DME fuel contribution 164

6.43 Cumulative energy release versus crank angle for high load, high DME fuel contribution 164

6.44 Cumulative energy release versus crank angle showing where Q_1 and Q_2 are measured 165

6.45 Combustion chamber pressure versus crank angle for low load at three different DME fuel contributions 166

6.46 Energy release Q_a versus ϕ_{DME} for low and high loads . . . 168

6.47 Exhaust gas manifold temperatures versus ϕ_{DME} for low and high loads 168

6.48 Degree crank angle at Q_1 versus ϕ_{DME} for low and high loads 170

6.49 Energy release Q_1 versus ϕ_{DME} for low and high loads . . . 170

6.50 Calculated gas temperature at the start of Q_1 versus ϕ_{DME} for low and high loads 172

6.51 Energy release Q_2 versus ϕ_{DME} for low and high loads . . . 172

6.52 Degree crank angle at Q_2 versus ϕ_{DME} for low and high loads 174

6.53 Calculated gas temperature at the start of Q_2 versus ϕ_{DME} for low and high loads 174

6.54 Indicated thermal efficiency for cycle 2 (DME only) versus ϕ_{DME} for low and high loads 176

6.55 Initial rate of energy release of methanol versus ϕ_{DME} for low and high loads 176

6.56 Concentrations of CO_2 and O_2 resulting from the complete combustion of DME versus ϕ_{DME} for all tests 178

6.57 Temperature versus entropy for low load, low DME fuel contribution 181

6.58 Temperature versus entropy for low load, high DME fuel contribution 181

6.59 Temperature versus entropy for high load, low DME fuel contribution 182

6.60 Temperature versus entropy for high load, high DME fuel contribution 182

C.1 Torque versus load cell output 203

C.2 Engine speed versus tachogenerator output 205

C.3 Fuel flowrate versus flowmeter output 207

C.4 Pressure drop across orifice versus micromanometer output 208

C.5 Transducer pressure versus output voltage 210

C.6 Injector lift versus LVDT output 213

C.7 Transducer pressure versus output voltage 214

C.8 Calculated and experimental mass flowrate versus rotameter reading using water 217

List of Tables

2.1 Fuel properties of diesel 1 and diesel 2 (Alternative Fuels Committee of the Engine Manufacturers Association, 1982) 12

2.2 Fuel properties of ethanol and methanol (Alternative Fuels Committee of the Engine Manufacturers Association, 1982) 13

2.3 Gaseous emissions at full load (Lawson and Last, 1979) . . 21

3.1 Results of analysis (Bowden *et al*, 1969) 37

4.1 Constants for c_p and M equations (Gulder, 1988) 94

6.1 Test conditions, diesel fuelling 125

6.2 Summary from pressure crank angle diagram 126

6.3 Test conditions, methanol/DME fuelling 141

6.4 Fuelling conditions 141

6.5 Stages of energy release of DME 167

6.6 Modelled energy release and supplied fuel energy 179

C.1 Calibration of load cell 202

C.2 Calibration of tachogenerator 204

C.3 Calibration of fuel flowmeter 208
C.4 Calibration of micromanometer 208
C.5 Calibration of cylinder pressure transducer 211
C.6 Calibration of injector needle lift 212
C.7 Calibration of fuel line pressure transducer 215
C.8 Calibration of rotameter using water 216

Chapter 1

BACKGROUND, AIMS AND OUTLINE OF STUDY

1.1 Background

The study here presented arose from preliminary work carried out by Brook *et al* (1984) in the School of Mechanical Engineering, University of the Witwatersrand, Johannesburg. Brook investigated the fuelling of a compression ignition engine on methanol with aspirated dimethyl ether (DME) as ignition promotor. In practical applications, the DME would be generated by catalytic conversion of methanol, the converter being heated by exhaust gases.

The work of Brook indicated some unusual features in the combustion of this fuel system, but left many questions unanswered. It was thus decided to study methanol/DME combustion in much greater depth. Reference tests were conducted on diesel oil fuelling to provide baseline information that would allow unusual features of the combustion of methanol/DME to be recognized. As the study progressed, it became evident that some thermodynamic techniques, both experimental and analytical, required to be developed, for purposes of advancing the understanding of the combustion of this fuel system.

The thrust of this research is thus twofold: to develop thermodynamic

techniques for the analysis of unusual features of combustion and to apply these methods to the methanol/DME fuel system.

As a first step it was considered appropriate to assess the viability of methanol as a fuel. Thus one chapter of the literature survey is dedicated entirely to considerations of how an engine can be fuelled on methanol. From this investigation, two philosophies emerged. These are, adapting the engine to the fuel, and adapting the fuel to the engine. The present study falls into the latter category.

Having selected this route, a commercially available compression ignition engine was employed. The number of modifications carried out to permit methanol/DME fuelling, were kept to the minimum possible.

1.2 Overall Aims of Study

The overall aims of this study were thus defined as follows:

1. to develop and consolidate thermodynamics techniques, both experimental and analytical, for the study of combustion phenomena in compression ignition (CI) engines,
2. to demonstrate the powers and limitations of these techniques by their applications to the relatively well-known situation of diesel fuelling, and
3. to contribute to the understanding of combustion of methanol/DME in CI engines by application of the above techniques to this fuel system.

1.3 Outline of Thesis

The structure and outline of the thesis are as follows:

- Chapter 2 provides a brief historical background of methanol as a fuel and an overview of the methods of fuelling compression ignition engines with methanol.
- Chapter 3 reviews techniques available for the analysis of combustion with particular reference to compression ignition engines. The emphasis is on energy release and heat transfer models.
- Chapter 4 discusses the development of the thermodynamic analysis techniques used for this research.
- In Chapter 5 a description of the equipment and instrumentation used for the research is given.
- The results are presented and analysed in Chapter 6. The discussion relates to both diesel and methanol/DME fuelling.
- Conclusions and recommendations for further work are given in Chapter 7.
- The Appendices include the derivation of the heat transfer equation used in the energy release model, equipment specifications and calibration of the instrumentation.

Chapter 2

LITERATURE SURVEY: METHANOL AS A FUEL

The literature survey has been divided into two main chapters.

This chapter provides a brief historical background of the development of methanol as a fuel. It is then followed by a description of the different methods of fuelling compression ignition engines using methanol. Generally speaking four categories of fuelling systems are at present in use. These are discussed from the aspects of practicality, performance and emissions. The emissions are restricted to nitrous oxides, carbon dioxide and carbon monoxide.

At the end of this part of the literature survey, a decision regarding the fuel combination to be investigated as alternative to diesel fuel is made. The method of fuelling the engine is also chosen.

The justifications for the selection of both the fuel and the fuelling method are also given.

The next chapter considers various methods for the analysis of the mechanism of combustion with particular reference to compression ignition engines.

A very powerful method of evaluating alternative fuels, is to calculate the

rate at which energy is being released. Therefore, a detailed survey of energy release models has been conducted. There are various levels of sophistication in energy release modelling. In this research only single-zone models are considered, and consequently reported in the survey.

An important aspect very closely related to the rate of energy release, is the heat transfer to and from the combustion chamber surfaces and the working fluid. As for the case of energy release, a survey of the existing heat transfer models has been conducted. Heat transfer in internal combustion engines is a very complex subject. Virtually every researcher in this field has a view of his own as to the most probable mode of heat transfer. This is clearly illustrated in the survey.

Additional analytical methods that could [illegible] assistance in understanding the mechanism of combustion, are also d[illegible]ed.

At the end of this survey the specific methods of evaluating:

a) the rate at which energy is being released, and,

b) the heat transfer taking place in the combustion chamber,

are formulated. As in the previous chapter, the justifications for the selection of the above methods are given.

2.1 Historical Background

This brief historical background has been based on a paper by Hagen (1977). The references are those as cited by Hagen and are quoted to outline the development of the use of methanol as a fuel over the years. These references have been listed separately, as the relevant papers and reports have not been read.

2.1.1 Historical Development of Methanol as a Fuel

Methanol has been used as a fuel for many years. It was used extensively in France from the middle of the nineteenth century as a clean fuel for heating and cooking purposes. Reed and Lerner (1973) report that methanol was replaced by kerosene as a lighting fuel around 1830, for better luminosity. Alcohols were also used as automobile engine fuels at the beginning of the 20th century. However, they were superseded by low cost petrol.

The alcohols have frequently attracted attention as alternative fuels when there was a fear of a shortage of petroleum fuels. For example in the early 1920's considerable research was done on alcohols, until the discovery of large petroleum deposits (Gonnerman *et al* 1975). Alcohols have been used as single fuels or in fuel blends on several occasions as a result of petroleum shortages arising from political, economic or geographic reasons. Typical cases are South Africa and Brazil.

During World War II, many cars and trucks were run on methanol as well as producer gas (carbon monoxide and hydrogen resulting from the burning of wood). Methanol was synthetically prepared in Germany in 1937 at a rate of about 70 000 tons per annum (Reed 1975, Nash and Howes 1938).

In the last twenty years or so there has been increasing concern for and awareness of the rapid depletion of petroleum deposits worldwide (during the present generation). The result of this has been a concerted effort in the search for alternative fuels. Methanol appears to be the most promising solution.

In 1964 a survey was published by the Society of Automotive Engineers, investigating the use of alcohol as a fuel for vehicles. A few years later, in 1971, the American Petroleum Institute published a review on the use of alcohols, primarily ethanol, in petrol as a blend. This was followed by studies of alternative fuels by the Exxon Corp (Kant *et al* 1974), the Institute of Gas Technology (Pangorn and Gillis 1974), and the Aerospace Corp (Lapedes *et al* 1974). These studies were all sponsored by the Environmental Protection Agency, in an effort to reduce pollution. However, the 1973 OPEC oil embargo, followed by an article by Reed and Lerner (1973) indicating that methanol was a versatile fuel for immediate use, sparked off great interest in this fuel. A year later in 1974, the Engineering

Foundation held a conference exclusively on methanol as an alternate fuel. Another study on the practicalities and possibilities of the use of methanol as a fuel was undertaken by the Lawrence Livermore Laboratories, also in 1974 (Anderson *et al* 1974). They proposed various strategies and testing programs.

A study of a different nature was carried out by the City of Seattle (Mathematical Sciences Northwest Inc. 1974). This concerned the conversion of urban refuse into fuel, as methanol, or fertilizer in the form of ammonia, the underlying motive being environmental, energy and economic incentives. As part of this study Cassady (1974 and 1975) undertook a detailed survey of the use of methanol as a fuel for vehicles and of the current methanol literature up to that time.

In Europe the situation has always been different from that in North America, in that Europe is much more dependent on imported crude oil. As a result of the 1973 embargo, the German Federal Ministry for Research and Technology in 1974 sponsored a detailed study of the production, distribution, economics, uses and dangers of hydrogen and methanol as fuels (Fed Ministry for R & T, Bonn 1974). The Research and Development division of Volkswagen has continued on from this, by testing methanol and methanol blends in both conventional and advanced engines. The methanol and blends have also been tested in fleet vehicles.

The number of studies on methanol and its possible use in blends increased during 1975. There was obviously a greater awareness of the difficulties and problems as well as the increasing advantages. At meetings held by the SAE as well as the American Chemical Society, much emphasis was placed on alternative fuels and in particular methanol (Most and Longwell 1975). The Lawrence Livermore Laboratories also continued their studies on the use of methanol in engines (Crothers and Anderson 1975, Crothers 1975). Based upon the feasibility studies sponsored by the Environmental Protection Agency mentioned above, the US Energy Research and Development Administration in turn sponsored efforts at the Universities of Santa Clara and Miami and the ERDA Bartlesville Energy Research Centre. These efforts were directed at investigating in detail the performance of methanol as well as blends in internal combustion engines (Johnson 1975). A comprehensive survey of alcohol fuel technology was also undertaken by the Mitre Corporation (Baratz *et al* 1975, Stokes and Park 1975).

From 1977 the ERDA has sponsored additional projects on methanol and methanol blends, such as : the investigation of the effects of methanol on lubricants by the US Army Fuels and Lubricants Research Laboratory; in depth research into the known problems of methanol as well as the effects of varying fuel formulations (carried out by the Union Oil Company of California); the University of Michigan investigation of engine and fuel problems and possible modifications; and the study by the Stanford Research Institute of the economics and viability of trade-offs in production, fuel composition and engine performance. Furthermore, a quarterly publication entitled 'Alternative Fuels Utilization Report' was started by the ERDA (1977) so as to inform and update researchers and the public on developments in this particular field.

An international symposium on alcohol fuels relating to transportation was held in Germany in November 1977. The papers presented at this conference were primarily involved in blending up to 15% methanol in petrol and problems of phase separation were discussed. A further conference on 'The Future of Methanol as a Motor Fuel' was held in the winter of 1977 in the US. The interest shown by researchers in the field of methanol as a fuel has been growing steadily as seen by the number of papers presented at automotive and fuel related conferences. The development of synthetic fuels has been spurred on by the continuing depletion of petroleum deposits, price hikes, international political uncertainty as well as the potential of renewable fuel supplies. Because of distribution problems, alcohol based fuels have been used mainly in fleets (Jackson *et al* 1984), or in blends with petrol as in South Africa. From 1987 Brazil planned to use ethanol as fuel in vehicles and equipment used in the sugar and alcohol related industries. A special allowance was made for reduced quantities of diesel oil, with a maximum 20% in dual-fuel engines for agricultural tractors (Bindel 1984).

Heywood (1981) reviewed the expected changes in transportation fuels from natural petroleum. He estimated the following time scales :

1980–1990	alternative fuels available in token quantities
1990–2010	alternative fuels contribution modest but increasing
2010–2030	amount of alternative fuels comparable to natural petroleum
–2030	onwards, alternative fuels will dominate.

Heywood predicted a deterioration of fuel quality, increases in price and

availability problems from 1990.

Furthermore, engines would have to be developed for alternative fuels.

The recurrent interest in alcohol fuels, in spite of generally unfavourable economics, relative to petroleum products, can be attributed to at least several different objectives :

a) obtain fuel from secure domestic sources in countries with current or anticipated oil shortages

b) create or stabilize a market for surplus farming products

c) improve antiknock quality without the use of lead compounds

d) increase power output from engines in certain situations, as for racing cars or aircraft at take-off, where extra power is more important than increased fuel consumption

e) reduce exhaust emissions of air pollutants .

f) satisfy ecological and environmental preferences for fuel obtained from renewable rather than fossil sources.

2.1.2 Alcohol as a Fuel

When Rudolph Diesel patented the 'diesel cycle' in 1892, he presumed that any fuel would be suitable for an engine operating in the manner he desired. Although he intended building an engine with pulverized coal as the fuel, the idea was abandoned and the first oil burning engine ran in 1897. Diesel's idea was that his engine could adapt to a wide variety of fuels.

However, the development of the 'diesel cycle' over many years has established that it is best fuelled with liquid petroleum referred to as distillate or gas oil.

Requirements to be satisfied by the fuel used to power high speed CI engines are few but important:

1. The fuel must be able to ignite at temperatures reached when air is compressed at different loads, speeds, as well as during starting.

2. The fuel must lubricate the moving parts in the high pressure pump and injectors.

3. The fuel must not freeze at low temperatures, and must not corrode any parts or accessories of the engine.

Diesel fuel is a mixture of many different hydrocarbon compounds, each with its own boiling point. Alcohol fuels, on the other hand, are essentially pure compounds - having a single boiling point. Thus diesel fuel will have a range of properties, as opposed to alcohol fuels which has specific properties. These two types of fuel also differ considerably in their chemical composition. Therefore if alcohol is to be considered for engine applications, certain important characteristics must be borne in mind. These have been listed by the Alternative Fuels Committee of the Engine Manufacturers Association (1982) as follows :

Cetane rating : Alcohol's high octane rating is best suited for SI engines, and their low cetane number presents difficulty when using them in CI engines.

Energy : alcohols produce less energy per unit mass than diesel fuel when burnt and require less air for complete combustion.

Energy of vaporization : the higher energy of vaporization of alcohol increases the evaporative quenching effect considerably.

Vapour pressure : the low vapour pressure of alcohols at low temperatures presents problems in starting.

Corrosion : alcohols may attack some materials used in diesel fuel systems.

Flammability : the flammability limits of alcohols are wider than diesel fuel. The saturated vapour in the fuel tank of a vehicle could be within the explosive range at ambient conditions. Appropriate precautions must be taken to avert accidents.

Fires : since pure alcohols burn with a clear flame, the correct fire fighting equipment must be used.

Flash point : the flash point of diesel is about $70°C$, while that of alcohols, specifically methanol and ethanol, are $14°C$ and $13°C$ respectively.

Solubility : Alcohols are completely soluble in water, whereas diesel fuel is essentially insoluble in water.

Handling : methanol in particular is toxic. It affects the nervous system, causing blindness. Liquid methanol can penetrate the skin, while vapours enter the body through the lungs. Therefore, particular attention must be paid when handling methanol.

Fuel properties with specific reference to diesel fuel, methanol and ethanol are given in tables 2.1 and 2.2.

Alcohols have been used as CI engine fuels to replace petroleum products in different ways: as a total replacement, an extender, an emulsion and dual-fuelling. These methods will be reviewed with particular reference to methanol. Each section will be discussed under its own heading with attention being focused on performance and emissions.

2.1.3 Methanol as a replacement

From the above indications, it appears that pure methanol cannot be utilized as a CI engine fuel, without some form of modification. Considerable research has been directed towards improving the ability of methanol to ignite on compression. A method of using neat methanol in CI engines is to increase the cetane number sufficiently with ignition improving additives to ensure that compression ignition will occur. However, a drawback is the quantity and the cost of the ignition improver. Most of the effective ignition improvers are nitrogen based compounds, which could aggravate NO_x emissions.

Spark ignition of neat methanol in CI engines provides a method of replacing diesel fuel entirely. A spark plug is introduced into the combustion

Characteristic	No 1 Diesel Fuel	No 2 Diesel Fuel
Chemistry	Mixture of Hydrocarbons	Mixture of Hydrocarbons
Approx Specific Gravity @ 16°C	82	85
Boiling Point °C	190-280	210-325
Net Heating Value (Mass) MJ/kg	43	27
Net Heating Value (Volume) MJ/l	36.6	21.3
Heat of Vaporization kJ/kg	600	600
Vapor Pressure @ 38°C kPa	0.34	0.27
Octane Number - Research - Motor	N/A	N/A
Cetane Number	40-60	40-60
Stoichiometric Air/Fuel Ratio	14,6	14,6
Vapor Flammability Limits % by Volume	0,6–6,5	0,6–6,5
Viscosity @ 40°C Centipoise Centistokes	1,45 1,75	2,41 2,79
Appearance	Colourless to light amber colour	Light amber colour
Vapour Toxicity	Extr[illegible]entration caus[illegible]osis	

Table 2.1: Fuel properties of diesel 1 and diesel 2 (Alternative Fuels Committee of the Engine Manufacturers Association, 1982)

Characteristic	Ethanol	Methanol
Chemistry	C_2H_5OH	CH_3OH
Approx Specific Gravity @ 16°C	0,79	0,79
Boiling Point °C	78,3	65
Net Heating Value (Mass) MJ/kg	27	20,1
Net Heating Value (Volume) MJ/l	21,3	15,9
Heat of Vaporization kJ/kg	900	1110
Vapor Pressure @ 38°C kPa	17	32
Octane Number - Research - Motor	111 92	112 91
Cetane Number	Below 15	Below 15
Stoichiometric Air/Fuel Ratio	9	6,4
Vapor Flammability Limits % by Volume	3,5–15	5,5–26
Viscosity @ 40°C Centipoise Centistokes	0,83 1,1	0,46 0,58
Appearance	Colourless	Colourless
Vapour Toxicity	Irritant toxic only in large doses	Irritant cumulative toxicant. Causes narcosis

Table 2.2: Fuel properties of ethanol and methanol (Alternative Fuels Committee of the Engine Manufacturers Association, 1982)

chamber, and the associated ignition system components must be added to the engine. The approach is advantageous as it uses the high latent energy of vaporization and octane rating of the methanol. The high compression ratio of the CI engine and positive ignition with resulting smooth combustion lead to a better thermal efficiency. However, engine modifications are required. Space must be available for fitting a spark plug, and attention must be given to ensuring that it is adequately cooled.

In both the spark ignition and ignition improver methods, a small percentage of lubricant, such as 1% by volume of castor oil, may have to be added to the alcohol to increase lubricity and to prevent wear (Ecklund *et al* 1984). Anti-corrosion additives may also be added, as well as small amounts of cetane improvers.

Toepel *et al* (1983) investigated the possibility of using neat methanol as a fuel for a two-stroke CI engine. Preliminary tests and studies were carried out on a single cylinder engine, derived from a production type diesel fuelled engine. An important modification was the inclusion of a glow plug to assist in cold starting conditions.

Having completed the preliminary tests, a full scale six cylinder engine was modified as per the test engine to run on methanol. The engine's injection timing was optimized for thermal efficiency at each load and speed. The trends indicated a reduction in NO_x, but no measurement of CO was taken. Smoke readings taken on a Bosch meter were all less than 0,1. For a given power output, the brake specific fuel consumption (BSFC) for the methanol engine was almost double that of the standard diesel engine. This was due to the fact that methanol's energy content per unit mass is about half that of diesel fuel.

Endurance tests of a CI engine running on ignition improved methanol were carried out to establish the viability of a substitute for diesel fuel (Myburgh and Weiss, 1986). The suitability of this fuel for standard production heavy-duty CI engines incorporating minor modifications was also considered. The fuel was 'DIESANOL', (registered trade mark of AECI Ltd) which consists of methanol blended with low percentages of ignition improver, a corrosion inhibitor and a lubricant.

On the performance side, the power output with methanol was found to be higher at low speed and lower at high speeds. This was the result of the

fuel delivery characteristics of the fuel pump. However, for the same fuel energy input, the power output with both fuels was roughly the same. The thermal efficiency was found to be comparable at high engine speeds.

A significant advantage of methanol was the almost smoke-free combustion. This indicated that methanol has the potential for operating with less excess air and developing higher power. Methanol was also found to produce 15 to 50% less NO_x, while unburned HC and CO emissions were found to be similar to those of diesel fuel.

The authors also reported certain difficulties. These related to cold starting, cylinder liner wear, cracks on piston crown and hard ceramic like deposits on the piston.

Yoshida *et al* (1986) developed a particular version of a spark assisted CI engine supplied by two methanol-fuel supplying systems. One of the fuel supplying systems was the direct injection of methanol into the cylinders, while the second system was dissociated methanol fed through the intake manifold. Methanol was dissociated into CO and H_2 by passing it through a catalytic dissociator heated by the exhaust gas of the engine. The dissociated methanol with higher heat of combustion was then fed through the intake manifold. These fuels were switched from one to the other by an electronic controller according to the operating conditions of the engine.

At low loads the intake air was throttled to provide a rich mixture and the exhaust temperature rose. The temperature of the catalytic dissociator also rose, and the conversion rate of dissociated methanol improved. This resulted in a greater advantage of dissociated methanol at low load. High exhaust gas temperature at high load, would raise the temperature of the catalytic dissociator thus degrading the catalyst. The exhaust was therefore bypassed from the superheater when the exhaust temperature was in excess of 650°C so that the temperature of the catalytic dissociator would not become too high.

In addition, it may not have been possible to generate dissociated methanol when the temperature of the cooling water was too low. This was so at cold starting, idling or warm-up because methanol would not be gassified at such conditions. In such cases methanol was directly injected into the cylinders.

The effects of intake air throttling on both thermal and combustion efficiency were reported by the authors. As the intake air was reduced, the pumping losses increased and the combustion efficiency improved. This was found to be so because the ignition stability increased and combustion improved as the mixture changed gradually from lean to rich. The combustion efficiency of dissociated methanol was higher than that of direct injection at all excess air ratios, the reason being that dissociated methanol formed a highly combustible pre-mixed mixture while the combustibility was not as good for direct injection. The authors believed that in the latter case the air and the spray did not mix well due to the weak swirl at low intake air flow.

The brake thermal efficiency of the dissociated methanol was about 3% higher than that of direct injection for all excess air ratios. The maximum efficiency occurred at an excess air ratio of about 1.8. The improved thermal efficiency arose mainly from the higher energy efficiency of about 110% under the conditions of the experiment.

Concentrations of *CO* and unburned methanol emissions of the developed engine were a little higher than those of the diesel engine at low load. However, the intake air flow was throttled at low load. Therefore, exhaust emissions were not more than those of the conventional engine in terms of mass emissions. As for the NO_x emissions, these were less for the developed engines, again in terms of mass emissions.

Field and dynamometer tests on neat methanol with 1% water were carried out by Garcia (1986). The engine used was a CI engine converted to be spark assisted. Although no specific figures were given, the author reported that the required power output was achieved. Observation of cylinder pressure diagrams showed that at lean mixture strengths cycle variability was very low. Emission results were not reported for any of the tests.

Jackson *et al* (1984) carried out extensive tests on two transit coaches using neat methanol. These coaches were used in revenue service for a year. Fuel economy comparisons showed methanol to be 14% less efficient than the diesel baseline for the combined Urban Mass Transportation Administration driving cycle. At steady speeds, however, fuel economy is nearly equivalent. This indicated that methanol was not as efficient during acceleration. No exhaust emission tests were reported by the authors.

Pischinger and Burghardt (1984) investigated the effects of using methanol as a fuel in passenger car engines. They found that a minimum amount of ignition improver of about 12% by volume, as well as a modification of the injection system was required. Test results with a swirl-chamber engine showed marked advantages with regard to efficiency and full load performance compared with diesel fuel operation. With a direct injection engine, however, no marked advantages were obtained using methanol. The authors believed that an improvement would result with a methanol fuelled direct injection engine, if the injection system was optimized. No smoke was produced at part load or at full load with either type of engine when run on methanol. NO_x emissions were on the same level and rose from 500 to 1100 ppm with increasing load. CO emissions at low load showed the same low level with both engines on methanol and on diesel fuel. With increasing load the direct injection methanol operation showed an earlier rise of CO emission compared with diesel fuel operation.

Edo and Foster (1984) developed a model using dissociated methanol as a fuel in compression ignition engines. The model utilizes the energy present in the exhaust gases to dissociate the methanol. The authors predicted a maximum gain of 11% for the dissociated methanol over liquid methanol. The model was, however, not validated by means of real data.

Another model to compare different methods of utilising methanol as a fuel for internal combustion engines was put forward by Swain and Swain (1984). The methods studied were dissociation and vaporization of methanol with waste heat. Theoretical data was generated and used for the model. The authors concluded that a better BSFC would be obtained with dissociated methanol.

2.1.4 Methanol as an Extender

The process whereby an alternative fuel is used as an extender of the main fuel, is generally called fumigation. Part of the fuel, for example methanol, is supplied through the engine air intake. The remaining diesel fuel is supplied normally by the injection system into the cylinder. This is therefore a relatively simple method of extending the fuel supply to the engine without major modifications.

The methanol injected in the air intake vapourizes and forms a combustible mixture. This is then compressed and is ignited by combustion of the main fuel. This represents a combination of premixed methanol charge burning and diesel diffusive combustion. Fumigation permits the use of methanol at various methanol/diesel fuel ratios.

An alcohol fuel system, requiring a tank and delivery components, is needed. The performance of the alcohol system depends upon such parameters as atomization, vapourization, temperature drop and uniformity of the mixture. These will have an effect in the optimization of this dual-fuel system.

A number of fumigation systems have been investigated prior to recent interest in alcohol fuels (Alternate Fuels Committee of the Engine Manufacturers Association, 1982). These are briefly described below :

In-line heated vaporizer : this consists of a heated metal container in the intake air supply line. Liquid alcohol evaporates when dropped on the container bottom and mixes with the intake air stream, and some droplets can be carried by the air stream. However, the heating of the intake air results in a reduced volumetric efficiency.

Mist generator : this produces an alcohol mist which is then conveyed to the air intake manifold. This system has the advantage of not creating a restriction in the manifold as would the venturi of a carburettor.

Carburettor : use is made of a conventional carburettor to supply the alcohol/air mixture to the engine. The carburettor can also be preceded by a heat exchanger to transfer heat from the exhaust gas to the intake air.

Direct manifold injection : this is a more recent development and has been proposed as a method for an engine retrofit kit. Alcohol can be injected directly into the intake manifold. Engine performance is influenced by the location and arrangement of spray nozzles.

Cruz *et al* (1979) investigated the possibility of adding a carburettor to the combustion air intake system of a CI engine, to accomplish at least partial substitution of alcohol for diesel fuel. The alcohols concerned were ethanol and methanol, but particular attention is given to the methanol

results. These authors found that approximately 50% of the fuel energy for a CI engine could be met by carburetted methanol. Higher levels of alcohol substitution caused objectionable knocking in the engine. The investigation revealed that the maximum torque with methanol was 105 per cent of that with diesel fuel alone. This occurred at an air/methanol ratio of 39,2, above which knock would be too severe. If the air intake was preheated the maximum torque was reduced to 90 per cent, but the air/methanol ratio was increased to 63,9.

The proportion of *CO* present in the exhaust was found to be generally greater when methanol was used than when diesel fuel only was used. This difference was minimum at high torque levels, but increased noticeably as torque decreased. Reduction in the richness of the air/methanol ratio reduced the concentration of *CO*. The use of the air preheater was responsible for the noticeable reduction in pollutant concentrations. The concentrations of NO_x were not recorded by the researchers.

2.1.5 Methanol as an Emulsion or Solution

An easy method by which alcohols can be used as a CI engine fuel, is in the form of solutions. Methanol, however, has a limited solubility in diesel fuel. Ecklund *et al* (1984) indicated that methanol's solubility increases as the aromatic content of the diesel fuel increases.

Although solutions present a direct method by which alcohols can be used in CI engines, only small alcohol percentages are practical.

Emulsions of alcohol and diesel fuel, however, solve some of the problems encountered with solutions, and are capable of accommodating higher percentages of alcohol.

Alcohol and diesel fuel emulsions share many of the advantages and characteristics of a solution. Emulsions must contain an emulsifier and generally methanol or ethanol is used as the alcohol. A higher percentage of water is acceptable in an emulsion, relative to a solution. A disadvantage of this approach is the cost of emulsifiers and their poor low temperature physical properties. The quantity of emulsifier is dependent upon the particular alcohol used as well as the characteristics of the diesel used. Researchers have

found that in general equal amounts of alcohol and emulsifier are needed. The cost of the fuel thus becomes an important factor.

Two types of emulsions are evident—stable and unstable. Stable emulsions are in general microemulsions requiring a surfactant so that no separation occurs under normal ambient conditions. These can be easily used in typical diesel injection systems. Unstable emulsions, however, tend to separate when left unused for a period of time as no surfactant is added. This type of emulsion presents an operational problem when left standing in fuel lines and systems. Separated emulsion can cause misfire and severe knock on starting up.

The advantage with both types of emulsions is that no modifications need be done on the engine or fuel injection system. Changes are, however, required in the fuel supply system depending upon the emulsion used.

Lawson and Last (1979) investigated the use of an emulsification device to overcome the problem of phase separation. The device was developed by the Ontario Research Foundation and was known as the Hydroshear. Engine performance data was obtained with a six-cylinder Deutz engine operated at full load and two speeds of 2200 and 1600 rev/min with diesel only and about 20% methanol/diesel fuel emulsion. The emulsion also contained 0,8% water to improve stability.

The authors pointed out that when the engine was set on full load, the governor would compensate for the reduced calorific value of the emulsion fuel. There was thus little change in speed or load due to increase in fuel rate caused by governor compensation. However at full load a reduction of about 5–10% in load would occur when the engine ran on the emulsion.

The results of the fuel consumption rate of the diesel component of the emulsion measured in *lb/hr* was reduced from 11 to 18% for the 18% emulsion and the brake specific diesel fuel consumption was reduced by up to 13%. At the rated speed of 2200 *rev/min* the total fuel consumption was reduced by about 5% for a 6% decrease in power, and an increase in engine efficiency. However, at 1600 *rev/min*, the reverse situation was found.

Exhaust emissions of CO_2, CO and SO_2 were found to decrease, whereas the NO_x's were found to increase, when the emulsion was used as the fuel. These are shown in table 2.3.

Speed *rev/min*	Load *bhp*	Fuel	CO_2 %	*CO* *ppm*	SO_2 *ppm*	NO_x *ppm*
2200	130	Diesel	9,9	300	52	480
2200	122	Emulsion	8,1	230	45	560
1600	105	Diesel	9,4	260	48	435
1600	93	Emulsion	8,0	160	41	510

Table 2.3: Gaseous emissions at full load (Lawson and Last, 1979)

This Hydroshear emulsifier was further developed and tested by Lawson *et al* (1981) when it was fitted on a Detroit Diesel engine mounted in a truck, so as to undergo road and dynamometer tests. The results previously obtained were confirmed, namely, with a 20% methanol emulsion, maximum power decreased by about 9%. Exhaust emissions also showed a similar trend, with NO_x increasing and *CO* decreasing with increasing methanol content.

The possibility of fuelling a CI engine with emulsions and solutions of methanol and diesel was also investigated by Baker (1981). An onboard emulsifier was utilized to ensure good mixing of the two fuels up to the point of injection. Blends of 15, 32 and 39% methanol with an almost equal amount of stabilizer by volume were tested. This author's results confirmed the trends obtained by Lawson and Last (1979) with regard to thermal efficiency and exhaust emissions. Engine smoke levels were very low throughout the test range, usually below 1,0 Bosch unit.

The cyclic combustion variation of alcohol blends was investigated by Chiu *et al* (1984). The blends consisted of methanol with different amounts of diesel, namely 10, 15 and 20% by volume. The parameters considered were maximum cylinder pressure, maximum rate of pressure rise, maximum rate of energy release and the crank angle position where these occurred. The tests were carried out at different speeds and loading conditions.

The investigation revealed that the averaged maximum gas pressure and averaged rate of pressure rise decreased as the methanol content increased. This was particularly so at high engine speed and high load. The cyclic

variation of maximum pressure increased with increased alcohol content, particularly at high alcohol levels. Furthermore the ignition delay increased, whereas the maximum rate of energy release was delayed and decreased sharply with increasing methanol content.

Performance and emissions tests of a fleet of standard Volkswagen 4-cylinder swirl-chamber CI engines run on a methanol-diesel blend were carried out by Weidmann and Menrad (1984). The blend consisted of 15% methanol, 15% solubilizer, 1% ignition improver and 69% diesel by volume. On the performance side, the researchers found that both the mean effective pressures and the specific energy consumptions were similar in the case of diesel fuel and the blend. However, contrary to others, the alcohol blend CO emission was higher than with diesel, and NO_x was found to decrease by 10% by changing from diesel to the blend.

Methanol substitution in an unmodified Deutz FSL-4132 F/W compression ignition engine, used in underground mines, was investigated by Burnett *et al* (1984). It was reported that the combustion of an emulsion containing 12% methanol on an energy basis, increased the peak cylinder pressures and rate of pressure rise. However, these did not exceed the manufacturer's recommended limits. A 15% methanol substitution on an energy basis could be achieved with the addition of 1,5% octyl nitrate cetane enhancer, on a volume basis. In the former case the brake specific energy consumption (BSEC) was found to increase up to nearly 20% depending upon load, speed and timing. In the latter case the BSEC was found to be comparable to straight diesel tests. Emission tests were carried out for the 15% emulsion. Emission of nitrogen oxides and insoluble particulates were reduced at all loads and speeds, at the expense of increased soluble particulates, total hydrocarbons and aldehydes at some engine load/speed conditions. Emission of sulphur oxides was reduced in proportion to the amount of displaced diesel fuel. Furthermore, CO decreased to less than corresponding diesel tests at lower speeds and higher loads.

The operation of a production car CI engine on a methanol-diesel oil blend without any modification to the engine was investigated by Pischinger and Burghardt (1984). Comparing the results of a blend (65% diesel, 20% methanol and 15% solubiliser by volume) with diesel fuel operation, the following was found:

- an increase of up to 1,5% in indicated thermal efficiency in mid and upper load ranges
- mechanical load remained almost constant
- in the lower load range the *HC* and *CO* emissions were higher while in the upper load range gaseous pollutants were about the same as for diesel oil
- near full load NO_x emissions were slightly higher than with diesel oil
- up to 50% decrease in smoke
- combustion duration remained almost constant in the whole load range.

2.1.6 Methanol in a Dual-fuelling System

The methods discussed thus far allow for a maximum substitution of about 20% of the diesel fuel by alcohol. This limitation is the result of mixing and ignition delay problems associated with alcohol. These problems can be partly overcome by directly injecting alcohol into the cylinder. This method allows for the direct injection of both diesel and alcohol into the cylinder, by means of separate fuel injection systems. Diesel fuel is injected first, and is ignited by compression. A very much greater quantity of alcohol is then injected into the burning mixture.

The dual injection system must be optimized for injection timing, number of injector holes and injection rate, so as to cope with various power requirements. At low speeds and loads the amount of alcohol must be adjusted accordingly so as to avoid overfuelling.

The dual injection system is specific to an engine and can not be easily adapted to other engine designs.

Disadvantages of dual injection include the complexity and cost of a second injection system and related fuel supply system. The utilization of different fuels in a CI engine with two separate injection systems has been investigated by Berg *et al* (1979). The fuels tested were methanol, ethanol and crude gasoline.

The quantity of main fuel, diesel in this case, was used for idling and at low loads. No quantity for the diesel used was mentioned. Results with methanol indicated that less smoke and lower exhaust temperatures were observed. The peak pressure and thermal efficiency were found to be higher. The only emission recorded was hydrocarbon, which was found to be consistently lower than with diesel fuel only. Performance was not found to be affected by the addition of 15% by volume of water. Emissions remained virtually the same as without water.

A dual injection system for methanol and diesel was also investigated by Pischinger and Havenith (1979). A single cylinder air cooled CI engine was modified to a two injection system. The pilot fuel was diesel while the main fuel was methanol.

These authors concluded that methanol could largely replace diesel fuel while maintaining reliable ignition and knock-free combustion. Efficiency with dual-fuelling was equal to or better than that of diesel only, while lower peak pressures and maximum rates of pressure rise were achieved.

Very low smoke values were attained, and thus an increase in performance was possible due to the absence of a soot-limit.

NO_x emissions were reduced by more than half in comparison to standard diesel operation, whereas the *HC* and *CO* emissions were equal to or lower than those of the standard diesel operation. Finally the compression ratio could be varied from 14,5 :1 to 19,3 :1 without negatively affecting the normal operating behaviour.

Seko *et al* (1984) modified a standard CI engine to a dual-fuel type with an injector for diesel and one for methanol. The percentage of diesel substituted was 86% by volume in transient mode and 94% by volume in steady state operation.

The injection timing was set at 8° and 7° BTDC at 2800 *rev/min* for diesel and methanol respectively, as this was found to give optimum fuel consumption and *CO* emissions. As the brake mean effective pressure (BMEP) increased the methanol replacement rate was increased, to a maximum of 94% by volume at maximum power output. The brake thermal efficiency was 32% at maximum power, and was 2 to 3% lower than that of the original engine over the whole operating range. The power output of the dual-fuel

engine was 57 *kW* at 3150 *rev/min* which was lower than that of the original version. However, at lower speeds, from about 2100 *rev/min*, the dual-fuel engine developed marginally more power than the diesel version.

The NO_x emission levels were found to be about 50% lower in the case of the dual-fuel engine, varying from about 200 to 400 *ppm*. The *CO* emissions resulted in an opposite trend. At low speeds the *CO* content was 2 to 5 times greater with the methanol and about equivalent at maximum speed. Smoke emissions measured in Bosch units, were minimal at all speeds.

The same type engine used by Baker (1981) to test emulsions, was modified to a dual-fuel by Storment and Baker (1981). Installation of a small pencil type injector for pilot diesel fuel was accomplished by drilling out the normal cylinder pressure relief port, in each cylinder head. The small injector was then inserted in the modified port.

Best engine performance was achieved with pilot fuel inputs of 18% and 22% on an equivalent heat input basis. The thermal efficiency increased about 3% over baseline diesel. This occurred at a pilot injection timing of 23° BTDC, approximately 10° advanced from the start of methanol injection. Both the rate of pressure rise and the peak pressure increased. Exhaust smoke was low, typically less than 0,5 Bosch units, but no NO_x or *CO* emissions were reported.

A modified version of an air-cooled Deutz F8L 413 F production engine was used by Cipolat *et al* (1986) to compare the performance of alcohol-based fuel systems.

The main fuels tested were methanol and ethanol each in combination with diesel oil, sunflower oil ethyl ester and 'DIESANOL' fuel (registered trade mark of AECI Ltd, it consists of methanol with minor additions of ignition promoter, lubricity enhancer and corrosion inhibitor). Injection timing and duration were held unaltered for all fuel combination. With each pilot fuel and over the entire range of operation, ethanol yielded torque and power 10 to 15% higher than those for methanol. Thermal efficiencies were correspondingly lower on ethanol fuelling, and exhaust temperatures some 100°*C* higher. With both methanol and ethanol as main fuels, the performance of diesel oil and sunflower oil ethyl ester as pilot fuel were essentially identical and some 4% higher than with 'DIESANOL' fuel. The contribution to the total fuel of each pilot fuel was approximately 5% by

volume.

2.1.7 Summary of Fuelling Techniques

The fuelling of compression ignition engines with alcohol fuels can be classified under three main headings. These are :

- Single injection
- Single injection with aspiration
- Dual injection

The implementation of each of these is shown diagramatically in figure 2.1 (Cipolat *et al*, 1986)

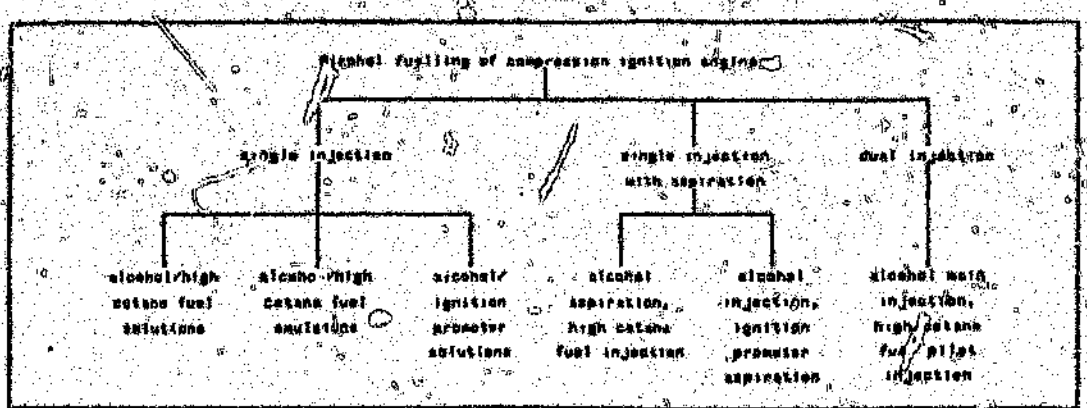

Figure 2.1: Techniques for fuelling compression ignition engines with alcohol fuels (Cipolat *et al*, 1986)

Each of the three fuelling methods will now be discussed.

As is evident from the literature, the fuelling with single injection of an alcohol solution or emulsion, has been well researched. This method is not without it's difficulties, but it appears to be the easiest and most practical from the user's point of view, the main advantage being that it is a single fuel. Once mixed in the correct proportions it is fed to the engine by means of the existing injection system. In some cases, some modifications may be required. It was therefore decided not to research this avenue.

Consider now the third method, namely dual injection. This is probably the neatest method, but it involves costly modifications. Briefly, these are an additional and completely separate injection system with all auxiliary equipment, and a modified cylinder head. Depending upon the engine, this modification may not always be possible without a major re-design of the cylinder head. Very few manufacturers have produced such engines, the leading one being KHD.

The School of Mech[illegible]ng is fortunate in being in possession of such an engine. It [illegible] Deutz F8L 413F production engine. Tests were [illegible] engine as reported previously (Cipolat *et al*, 1986). Ho[illegible]vide is in a way unique and not commonly known nor easily [illegible]ailable, it was decided not to research further into this metho[illegible]

The second technique of fuelling, that of single injection with aspiration was ultimately chosen. A brief background explains the reasons for the choice.

In their early search for alternatives to diesel fuel, AECI Ltd considered the partial dissociation of methanol. A device was built so that a fraction of the methanol supplied was dissociated into dimethyl ether and water. Methanol was injected into the cylinder while the dimethyl ether was aspirated into the manifold.

Preliminary tests carried out by AECI Ltd indicated the occurrence of some unusual phenomenon during the combustion process. A number of discussions took place between the thermodynamics division of the School of Mechanical Engineering and AECI Ltd, relating to these findings.

Although AECI Ltd proceeded to develop other fuels, the idea of methanol injection with dimethyl ether was taken up within the School as an area

very slow, the period extending throughout the complete expansion stroke. Burning by a diffusion flame process takes place in the second and third stage.

The total burning time was found to increase only very slightly with load, and to decrease considerably with increase in engine speed. Thus the burning time in terms of crank angle increased slightly when the speed was doubled. This increase was accounted for by the increase in injection timing at the higher speed. The burning time was reduced by advancing the injection by an amount approximately equal to the increase in delay period. In this way the time from the start of injection to the end of burning remained essentially constant.

From the above findings, Austen and Lyn developed their mathematical relationship between the injection and the heat release behaviour. The rate of burning was defined as :

$$R = R_0(1 - (t/t_b))$$

where
R is the rate of heat release
R_0 is the initial rate
t_b is the total burning time of a droplet of fuel
t is the time after injection.

From tests carried out, the authors found the model to be sufficiently accurate to be of practical value.

The above findings were confirmed in another paper by one of the authors (Lyn, 1962). In addition, the investigation examined the burning rate and its rate-controlling mechanisms. The major factors affecting the burning rate were found to be injection rate, engine speed and combustion chamber design. These in turn all affect the mixing patterns directly.

Depending on the interaction between the fuel spray and air stream, three basic mixing and burning patterns were postulated. These are :

1. Fuel injection across the chamber with considerable momentum : mixing proceeds immediately as it enters the chamber and is little affected

The influence of blower pressure, compression ratio and valve timing were considered in both the calculated and the measured conditions. Close agreement was reached in all cases.

These authors concluded that their methods of calculation provided a valuable insight into how and why a compression ignition engine gives the results it does.

Apparent energy release from internal combustion engines has been computed from pressure-time diagrams (Krieger and Borman, 1966). This computation was based on the assumption that thermodynamic equilibrium exists at each instant. The energy release curve was related to the fuel injection diagram, and to experimentally obtained pressure crank angle diagrams, as was the case with Lyn (1960) and Austin and Lyn (1960).

Krieger and Borman (1966) proposed a model in which the effects of both heat transfer and the dissociation of the products of combustion were considered. The model did not however shed light on the details of the combustion phenomena. Negative burning (negative heat release) was obtained if the calculations were started during the portion of the cycle where significant fuel vaporization but no combustion was occurring.

The authors concluded that about 50% of the fuel was burned during the first third of the heat release period. The effects of dissociation of the products were found to be negligible.

Whitehouse and Way (1969) also obtained basic energy release data by analysing cylinder pressure diagrams from a variety of engines. However their emphasis was to investigate the effect of air supply on combustion. The energy release patterns were then correlated to the fuel injection characteristics.

The authors based the calculations of energy release rates on the single zone model. Although reasonable results were obtained, the model was found to have serious limitations. This was due to the fact that in the cylinder there are considerable differences in the values of temperature and oxygen concentration between the burning zone and the unused air. The use of cylinder average values for both temperature and oxygen concentration was thus unrealistic.

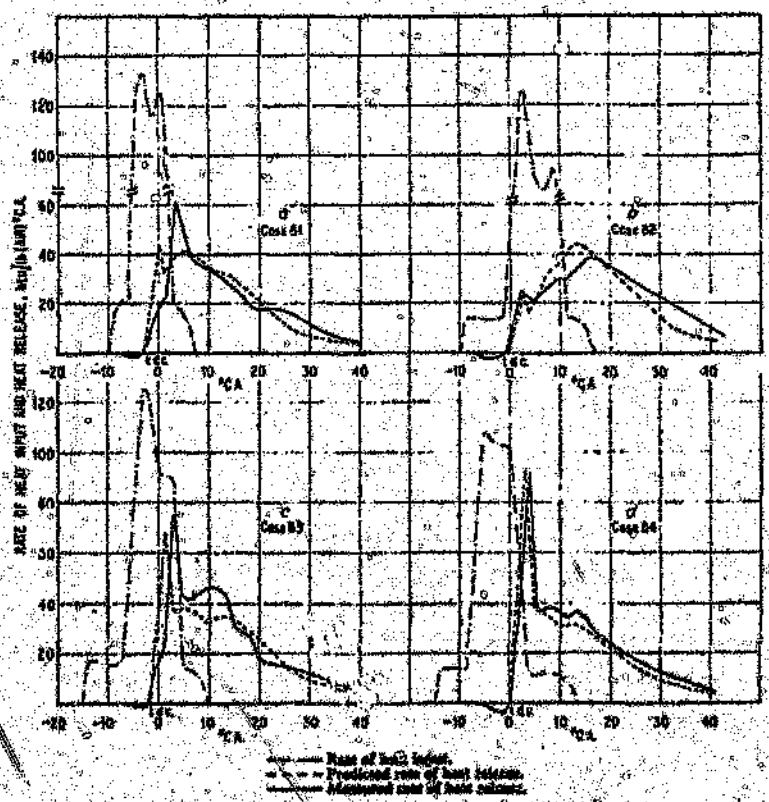

Figure 3.3: Measured and predicted heat release diagrams (Bowden *et al*, 1969)

load was small enough. With retarded timing, combustion would simply be transferred from the pre-chamber to the main chamber, thus merging the two portions of the energy release diagram. With advanced timing, the pre-chamber part of the combustion would be over earlier and the second peak would be more distinct. (See table 3.1).

Boyce *et al* (1969) studied the effects on the combustion process, by introducing directly into the engine air various concentrations of pure fuel fractions, as well as light distillate diesel fuel vapour. The fuels considered were n-heptane, iso-octane, cyclohexane, benzine generated in a reactor and light fraction diesel. The quantities involved were varied from very small quantities, similar to those used in pilot injection, up to 50% of the total

for further research. A need to understand the mechanism of combustion of this fuel combination was identified.

With this knowledge as background, tests with methanol as a fuel and dimethyl ether as an ignition promoter were carried out by Brook *et al* (1984). The findings of these tests are discussed in the next section. Although these were mainly performance tests, some unusual characteristics were evident.

A survey of the literature appeared to reveal that dimethyl ether has been used as an ignition promoter in spark ignition engines. However, very few publications were available for work done on compression ignition engines.

It was then decided to acquire more sophisticated data capturing equipment than that used by Brook *et al* and carry out exploratory tests. Some unusual features were immediately evident in the pressure and the energy release diagrams.

The use of methanol as a main fuel and dimethyl ether as an ignition promoter was thus decided upon as the alternative to diesel fuel.

The literature with dimethyl ether as an ignition promoter is now reviewed.

2.1.8 Dimethyl Ether as an Ignition Promoter

Special reference will now be made to research carried out by Brook *et al* (1984). The aim of this research was to replace diesel with methanol with an ignition promoter, to obtain the characteristics of this combination and to evaluate its feasibility as an alternative to diesel. The ignition promoter was dimethyl ether (DME). The physical properties of DME are given in Appendix E.

The engine used in this work was an unmodified Petter compression ignition engine. The methanol was supplied using the existing injection system, while the DME was aspirated into the inlet manifold through a suitable distributor.

The engine was found to run smoothly on methanol/DME provided that the concentration of DME in the inlet air was maintained within certain

limits. This concentration depended upon engine speed. While the engine power versus speed curve was essentially unchanged, the torque-speed characteristic for methanol/DME was flatter. A six per cent improvement in low-end torque was achieved, whilst a four per cent reduction in peak torque occurred. Peak power output was essentially unchanged.

Estimates of thermal efficiency were presented, which indicate that the methanol/DME fuel combination compares favourably with diesel fuel. In defining thermal efficiency, however, definitional problems regarding regeneration arise which were not entirely resolved by Brook *et al.* This point will be taken up in section 6.2.1 of this thesis.

Heating of the inlet air had two effects :

- the power and brake thermal efficiency were reduced
- the engine showed a greater tolerance to the enrichment quantity of DME without knock.

An interesting feature of this fuel combination was shown up in its pressure crank angle traces. Whereas the diesel oil trace exhibits the generally accepted four stages of combustion, methanol/DME produced a trace similar to that of a normal SI engine. It is believed that the reaction which the DME underwent involved the formation of a number of active radicals which acted as a 'chemical' spark-plug for the incoming methanol charge. Certain problems were experienced with the injection system, due to the low lubricity, low vapour pressure and low viscosity of methanol. The lubricity of the methanol was improved by the addition of castor oil. Vapour locks created by the low vapour pressure were eliminated by the inclusion of a booster pump before the injector pumps.

The emission of pollutants was not investigated, but was believed to be considerably lower with DME/methanol fuelling than with diesel fuel.

The research reported in this thesis was carried out on the same engine, with the same fuels. These are diesel oil for baseline tests, and the methanol/DME combination as the alternative. However, the data acquisition system has been considerably upgraded and extended. The aim of the research has also been redefined to investigate the mechanism of combustion of the methanol/DME combination.

2.1.9 Conclusions

The literature survey on methanol as a fuel is by no means exhaustive. Conferences and symposia are held virtually every year, where researchers discuss their experience and findings when using methanol as a fuel. However, it is believed that the review is adequate to prove that methanol can be used as a fuel for compression ignition engines. It can not be used in its pure form, but as a solution, an emulsion, with an ignition promoter or with some engine modifications, it has its place as a substitute for diesel fuel.

The method of fuelling the engine, namely the injection of methanol and the aspiration of dimethyl ether (DME) as an ignition promoter, is by no means ideal, or practical. This method could be used for a constant speed, constant load application. Once the ratio of methanol to DME is selected, the engine could be run so whenever required. However, in the case of a variable load and speed situation a 'black box' approach would be better. Methanol would be simply supplied to a converter, where a certain fraction would change to DME and would be subsequently aspirated. The fraction converted would have to vary according to the prevailing conditions.

As discussed previously, the combustion of methanol and DME exhibit unusual features. It was therefore believed that it was of great importance to be able to control the quantities of methanol and DME both manually and independently. This would permit the flexibility to guide the research in a more meaningful direction, so as to understand the behaviour of this fuel combination.

To achieve this goal, certain analytical methods or techniques are essential. Some of the most widely used in the field of combustion are, amongst others, the rate of energy released by the fuel and the rate of heat transfer between the working fluid and the cylinder walls. Other considerations include temperature versus entropy, cylinder pressure versus volume and the derivative of pressure versus crank angle, to mention a few.

Therefore a further review of the literature was necessary to see what approaches were available with respect to energy release and heat transfer, in particular. This forms the subject of the next chapter, where these two aspects are discussed at length and in depth.

Chapter 3

LITERATURE SURVEY: ANALYTICAL METHODS

3.1 Energy Release

In order to assess the performance of a compression ignition engine, in terms of power, efficien y, starting behaviour, smoke and noise, the measured cyclic cylinder pressure is not sufficient. In addition, it is very important to know the rate at which energy is released. Energy release is basically a thermodynamic problem and can be determined by analysing the measured cylinder pressure diagram.

The rate of pressure rise during the combustion process of a compression ignition engine is the result of the rate at which energy is being released by the combustion of the fuel. This pressure rise then manifests itself in the form of work produced by the engine. Therefore the rate of energy release has a direct bearing on the power output, the mechanical loading and the efficiency of the engine.

The timing of the beginning of the energy release is in turn dependent *inter alia*, on, : the start of injection, the duration of injection, the prevailing temperature and pressure in the combustion chamber, the compression ratio, the injector pressure, the combustion chamber configuration and last but not least, the fuel used.

Therefore, a powerful means of evaluating and understanding the functioning of any alternative fuel to diesel, is to consider the energy release pattern of that fuel. Considerable research has been done into methods of evaluating the rate of energy release. There are simple models, based on many simplifying assumptions, to very complex ones taking into account the products of combustion, temperatures, compositions, mass flow rates, rates of heat transfer, *etc.*

A survey of the various methods of evaluating the rate of energy released has been conducted. A brief description of each authors work has been given, and in many cases a comparison between measured and calculated values is available.

3.1.1 Energy Release Models

The problem of predicting the rate of combustion of a liquid fuel spray injected into the combustion chamber of a compression ignition engine is a complex one. Contributing factors are the variety of size of the fuel in drops and the change of factors governing the combustion of each drop. Each drop has its own microclimate dictated by local temperature and pressure, swirl, *etc.* Tanasawa and Tesima (1968) established a simple theory as a standard for comparison with the actual phenomena. They concluded that the rate of change of combustion is only slightly affected by the size distribution of the drops, but strongly affected by the volume-surface mean diameter.

Lyn (1960) investigated the shape of the energy release versus crank angle diagram which would give as close an approach to the ideal cycle as is compatible with the acceptable maximum pressure. Consideration was also given to the relationship between fuel injection duration in degrees crank angle ($^{\circ}CA$) and the shape of the energy release diagram. The following conclusions were drawn : For a given heat-release duration, assuming some sort of triangular distribution, the indicated thermal efficiency depends on the peak cylinder pressure. The distributions of the energy release versus $^{\circ}CA$ as assumed by the author are shown in figure 3.1.

The rate of pressure rise depends on the shape of the energy release diagram, with preference given to a sloping rather than a steep front. The shorter the energy release period, the higher is the optimum peak pressure; $40^{\circ}CA$

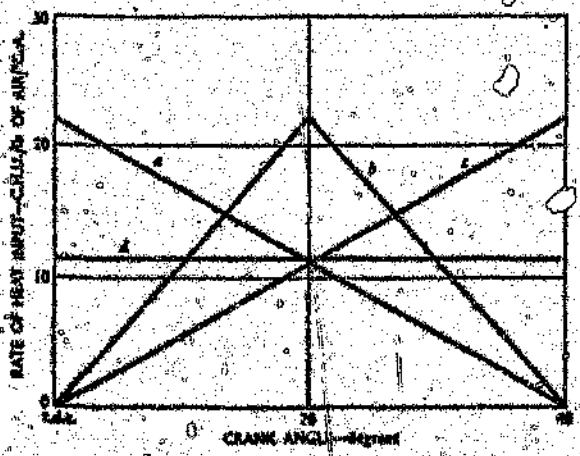

a—triangular distribution with peak at beginning
b—triangular distribution with peak at midway
c—triangular distribution with peak at the end
d—uniform distribution

Figure 3.1: Energy release diagrams (Lyn, 1960)

appeared to be a reasonable duration for combustion. It was suggested that the peak pressure for optimum efficiency gave a good indication of the actual energy release period. This could help to decide whether there could be room for improvement in combustion or fuel injection equipment. Finally the author considered that for a given peak cylinder pressure there was an optimum compression ratio for maximum efficiency and minimum rate of pressure rise. This was found to be at a compression pressure some 200 to 300 lb/in^2 (1,4 to 2,1 MPa) lower than the limiting pressure.

Austen and Lyn (1960) proposed that the rate of fuel injection can be related to the rate of energy release and hence the cylinder pressure versus CA diagram. Tests were carried out on a direct injection compression ignition engine to study the effects of load, speed and injection timing on the shape and duration of the injection and energy release diagrams.

The authors concluded that combustion proceeds in three distinguishable stages : immediately after ignition there is a short period of rapid burning of a premixed flame due to the burning of part of the fuel injected during the delay period. This is then followed by the main combustion period at a slower and gradually decreasing rate. In the final stage the burning rate is

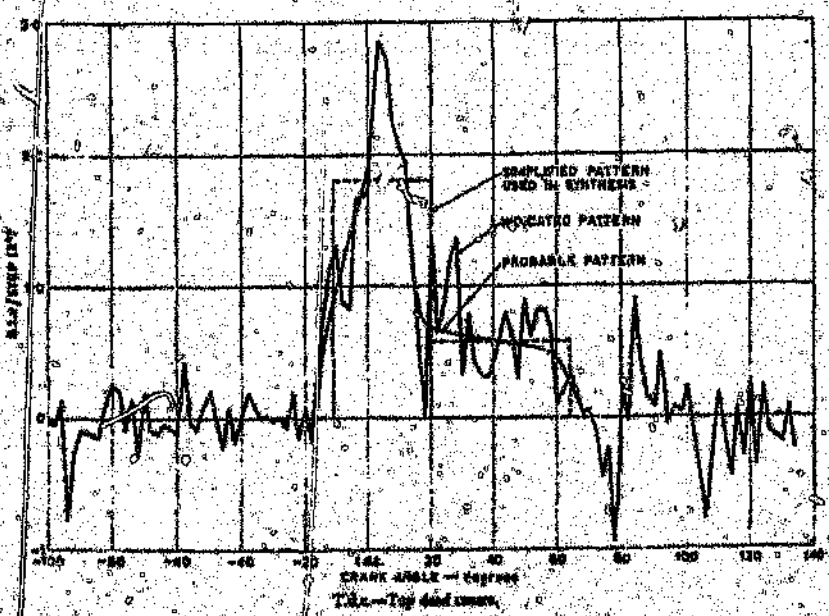

Figure 3.2: Rate of heat release (Whitehouse *et al*, 1962)

by ignition.

2. Fuel deposition on walls : negligible mixing takes place during the delay owing to limited evaporation. After ignition evaporation becomes rapid and its rate is controlled by access of hot gases to the droplet surfaces.

3. Fuel distributed near the wall : mixing proceeds during the delay period, but at a rate lower than in 1. After ignition, mixing is accelerated by the same mechanism as in 2.

Whitehouse *et al* (1962) developed a method of predicting some aspects of performance of a compression ignition engine. One such aspect was the energy release diagram. Since combustion in any given engine varies with changes in fuel injection characteristics or combustion chamber shape, the exact pattern could not be predicted. Therefore experimental indicator diagrams from developed engines were analysed by the authors to see what pattern of energy release could reasonably be expected. Figure 3.2 shows the predicted, indicated and probable patterns of the rate of energy release as found by the authors.

	Injection Timing °*ETDC*	Speed *rev/min*	*BMEP* lb/in^2
a	10	1500	77,5
b	10	2150	77,5
c	15	2150	83,9
d	15	2750	76,9

Table 3.1: Results of analysis (Bowden *et al*, 1969)

Whitehouse and Way concluded that for certain types of engines operating under normal conditions, energy release rates could be calculated based on a single zone model. Further advancement was dependent on evaluation of the variations of temperature and gas composition within the cylinder. These variations were caused by such factors as air movement and fuel injection characteristics. A two zone model was therefore suggested.

A model for the rate of energy release in high speed indirect injection compression ignition engines was proposed by Bowden *et al* (1969). As in the case of other researchers, the authors related the rate of injection to the rate of energy release.

The following model was proposed : the energy release diagram consists of two portions corresponding to combustion in the pre-chamber and in the main chamber. Combustion would initiate and proceed in the pre-chamber in a pattern similar to that in direct injection engines. As much energy as possible would be released here, with due regard to the limited availability of air in the pre-chamber, corresponding to the first portion in the energy release diagram. As the piston descends from TDC, further combustion occurs in the main chamber due to the availability of more air. This part of the combustion corresponds to the second portion in the energy release diagram. A typical such diagram is shown in figure 3.3.

For a given injection timing and irrespective of load, the amount of air utilization in the pre-chamber remained constant, provided that the injection characteristics remain the same. Hence the energy release in the main chamber would be reduced at lower loads, and eventually disappear if the

fuelling rate. This addition was supplemented by the main fuel charge in the normal way.

The authors found that the addition of a small quantity (usually not exceeding 6%) of the products of the slow oxidation reactions of an auxiliary fuel to the main charge of an engine, when running as a conventional engine, produced significant changes in performance. These changes were found to be either improvement or deterioration in performance depending upon reactor setting and engine load.

The ignition of a standard diesel fuel has been termed by the authors as a 'low-temperature' type where multi-stage pre-flame processes were involved. The presence of a fuel vapour uniformly dispersed at relatively low concentration could exert an influence on these processes, depending upon the nature, concentration and extent of reactivity of the fuel employed. Further, the presence of a partially reacted fuel, which could be itself undergoing exothermic reactions during the injection and pre-ignition of the main fuel would also play an important role in these processes. Normally the absorption of heat for fuel evaporation would exceed initially the energy liberated by reaction. Thus pre-flame processes for ignition of a liquid fuel would usually be accompanied by a pressure drop in comparison with the compression curve when operating with pure air. The presence of the auxiliary fuel, which could be undergoing exothermic reactions, would help to reduce the extent of such cooling. Such an energy release would be evenly dispersed, unlike that of the pre-ignition reactions of the main fuel charge.

The authors showed that the improvement in performance was not entirely due to the energy released by the auxiliary fuel during and towards the end of compression, thus conditioning the main charge. The chemical nature of these partially oxidized products appeared to play a part.

The combustion of the main fuel charge would be influenced thermally and chemically by any pre-reaction activity of the auxiliary fuel distributed over the chamber. It would also be affected by any enrichment of the system as a whole to areas where the flame could propagate more easily within the time available than it could in air of its own. If at the point of injection a relatively large amount of un-decomposed fuel was present, then the auxiliary fuel would simply pass to the exhaust almost unchanged. This would depend on the concentration of the auxiliary fuel.

The authors concluded that the most effective form for combustion improvement was given by the production of active intermediates within the combustion chamber 20 to 40°C*A* before the injection of the main fuel.

The problem of predicting the rate of energy release in turbo-charged compression ignition engines was considered by Grigg and Syed (1969). Their two models were based on the process of air entrainment into fuel sprays, turbulent mixing in fuel sprays and chemical kinetics. Constants were then chosen so that the predicted rate of energy release would fit experimental data.

The factors affecting the rate of energy release for the models were : ignition delay, nozzle hole diameter and number of holes, period of injection, rate of entrainment of air into the fuel spray, rate of turbulent mixing of fuel and air and the rate of reaction of fuel and air based on chemical kinetic theory.

The rate of entrainment of air into fuel sprays was based on two models. These were, the conical plume model and the doughnut model. In the former, the fuel spray is allowed to develop unimpeded as in an infinite atmosphere in a conical form. In the latter model, it is assumed that the doughnut cross-sectional area and circulating velocity relative to the surrounding air vary to conserve momentum.

Figure 3.4 shows a comparison between experiment and both air entrainment models for the rate of energy release.

The authors indicate that the curves of rate of entrainment could be regarded as the energy release that would have been obtained if there had been no ignition delay and the rate of turbulent mixing and chemical kinetic burning had been infinitely fast.

The comparison between the experimental energy release diagrams and the calculated results are given for the conical plane model only. One such case is shown in figure 3.5.

The authors concluded that the calculated curves were of the same general shape as the experimental curves. In general the plume model was found to be closer to the experimental results. Therefore the rate of energy release could be predicted from a model based on the rate of entrainment of air

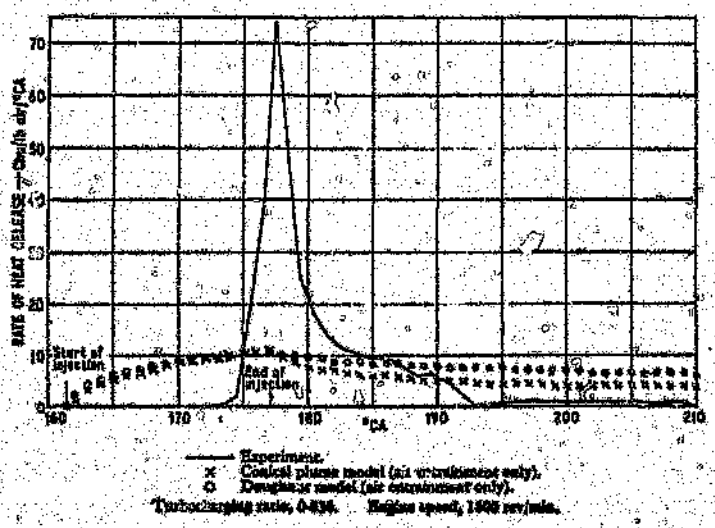

Figure 3.4: Comparison between experiment and both air entrainment models for rate of heat release (Grigg and Syed, 1969)

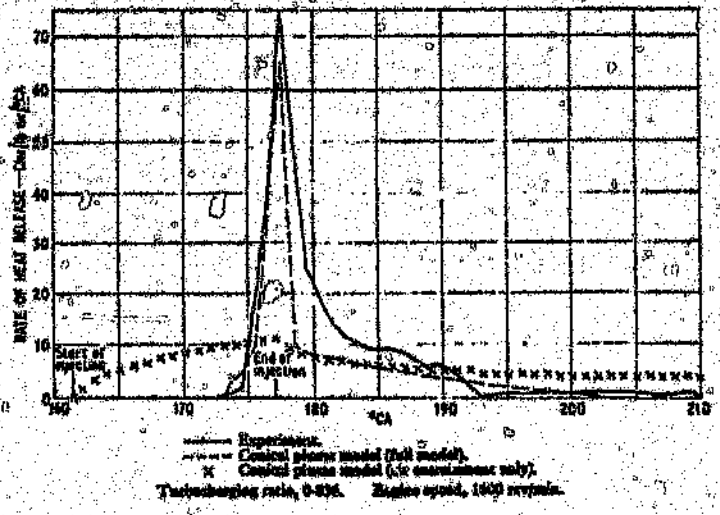

Figure 3.5: Comparison between experiment and conical plume model for rate of heat release (Grigg and Syed, 1969)

into the fuel sprays.

Woschni and Anisits (1974) approached the energy release problem from a different point of view. These authors obtained the energy release diagram and the rate of injection at one particular operating point from measurement. Then by means of correlations they were able to predict the energy release diagrams for any altered operating conditions.

A number of test runs were then carried out in which one parameter at a time was varied. These parameters were air-fuel ratio, boost air pressure, boost air temperature, start of fuel delivery and engine speed.

In order to bring the trends observed into a manageable analytical form, the authors introduced a substitute energy release diagram. This rate of energy release was defined in a way that, although simplified considerably in shape, would produce the same results in the cycle simulation as the actual rate of energy release with regard to the parameters of main interest. These were peak pressure, power and efficiency. An agreement of $\pm$ 2% between computation and measurement was achieved by the authors. Only the rate of pressure change could not be predicted within this accuracy.

Figure 3.6 shows the actual and substitute rate of energy release diagrams with variation in air-fuel ratio.

Although the relationships proposed by Woschni and Anisits were valid for large CI engines with Hesselmann type combustion chambers, good results were obtained with tests on other types of combustion chambers. The authors conducting this method did not aim to predict energy release diagrams for a new combustion process, but rather to describe the behaviour of a known process in terms of changed engine operating conditions.

Whitehouse and Abuga[illegible] (1975) developed a two-zone model taking into account the penetration and deflection of sprays in a compression ignition engine with swirl. In order to obtain values of swirl, a model cylinder simulating the engine used by the authors was built and used in a rig to measure swirl rates. The model was validated against experimental data.

The experimental programme explored the effects of swirl, the size and number of holes in the injector nozzle, boost pressure and load.

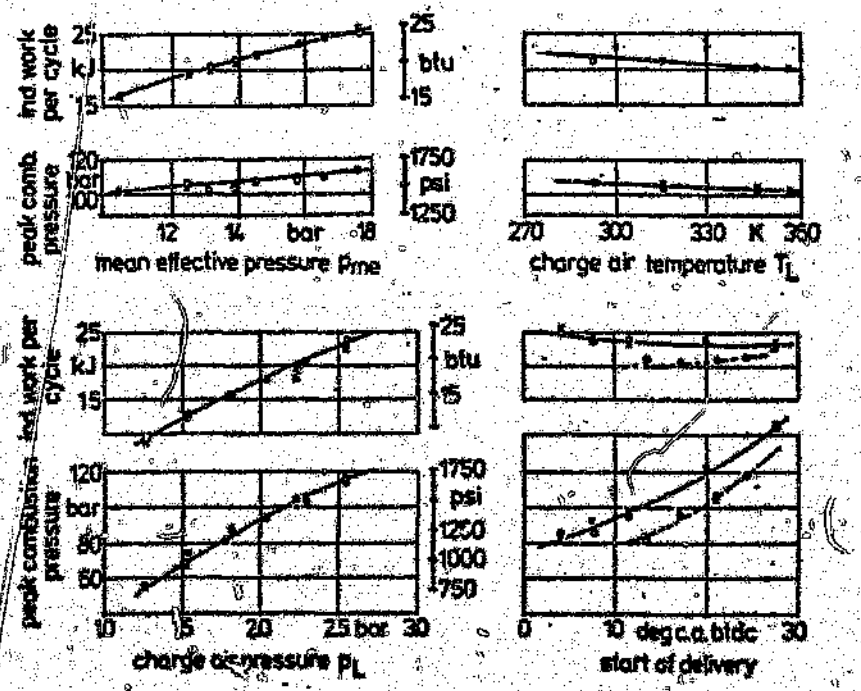

Figure 3.6: Actual and substitute rate of heat release dependent upon air-fuel equivalence ratio (Woschni and Anisits, 1974)

The authors reported that despite the similarity of the pressure diagrams, the energy release by analysis and that by calculation were appreciably different. This was believed to be primarily due to the different thermodynamic models used, ie, the two-zone model incorporated a high temperature zone with a non-linear increase in internal energy.

Furthermore at high load with very little excess air, the two zone model calculates inadequate combustion, as in the case of single zone models. The effects of the number of injector holes on efficiency have also been calculated - the efficiency decreases with the non-standard injector configurations. This was confirmed experimentally as well as by the two-zone model. This effect could not be recognized with the single-zone model.

Figure 3.7 shows the pressure and energy release diagrams for a standard 6-hole nozzle. The discrepancies as discussed by the authors are clearly shown.

The effects of experimental factors such as swirl, fuel injection period, number of fuel injector nozzle holes and initial fuel injection pressure on the

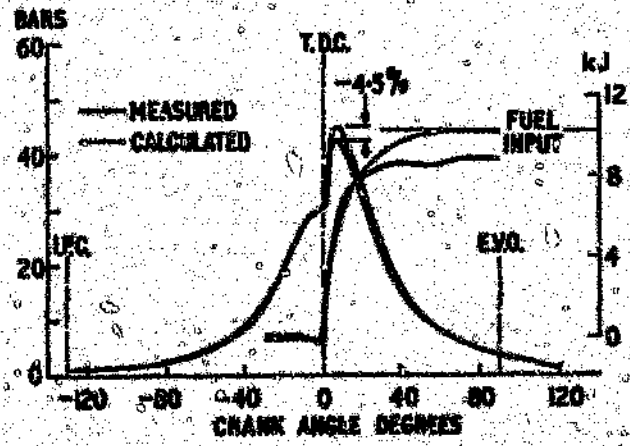

Figure 3.7: 6-Hole nozzle, low load, pressure and heat release diagrams (Whitehouse and Abughres, 1975)

energy release pattern were studied by Shimotsu and Endo (1982). The magnitude of the energy release rates were found to be strongly affected by the amount of residual fuel in the combustion chamber. Thus the combustion phenomena could not be analyzed by the energy release pattern only.

The authors therefore proposed an effective combustion rate Ke as an analysis coefficient, which would be unaffected by the quantity of residual fuel in the combustion chamber. Ke would be controlled by such factors as the combustion rate of a single droplet of fuel, distribution of the fuel, gas motion and degree of atomisation.

The energy release rate was calculated from the pressure pattern using the first law :

$$\frac{dQ}{d\theta} = \frac{\delta_v}{R} p \frac{dV}{d\theta} + \left(\frac{c_v}{R} - A\right) V \frac{dp}{d\theta}$$

where

Q = heat energy
θ = crank angle
c_p = specific heat at constant pressure
R = gas constant
p = pressure in the chamber
V = volume of the chamber
A = mechanical equivalent of energy.

This equation was re-arranged as follows :

$$K_e = \frac{4\frac{dQ}{d\theta}}{\pi \rho_s H_u D^2}$$

where

H_u = lower combustion energy of the fuel
K_e = effective combustion rates
ρ_s = fuel density
D = droplet diameter.

Using the above equation, the authors concluded the following :

1. The energy release pattern of a medium speed CI engine was dependent mainly on the fuel injection rate pattern.

2. For a high fuel injection rate, the burnt ratio Q_θ/Q_T in the early stages of combustion rose rapidly, but when the fuel injection was complete, the combustion rate slowed down (Q_θ is the integrated energy release from combustion initiation to a crank angle θ, Q_T is the total energy release for one cycle). The total fuel combustion period could not be shortened, even if the fuel injection duration was short. Thus there was an optimum fuel injection period required to achieve maximum thermal efficiency.

3. The effects of certain factors on combustion must be analyzed by means of the effective combustion rate Ke as defined above.

4. Swirl improved fuel distribution and raised the combustion velocity, an important factor in medium speed CI engine performance.

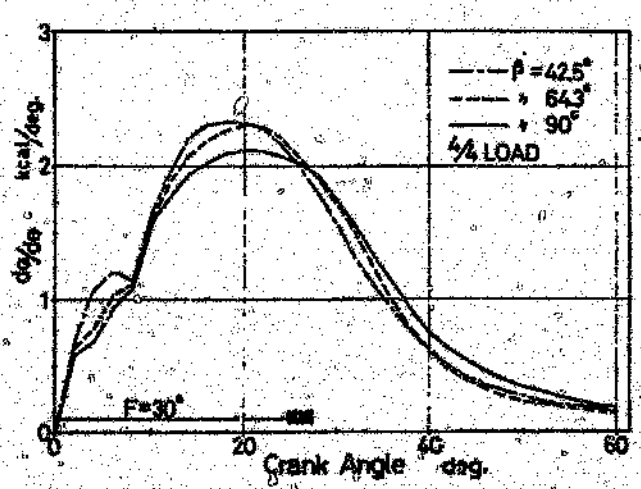

Figure 3.8: Change of $\frac{dQ}{d\theta}$ pattern with the change of swirl (Shimotsu and Erdo, 1982)

5. A strong swirl was essential when the fuel injection period was short, so as to ensure effective fuel distribution.

6. An increase in the number of nozzle holes improved the fuel distribution and atomization, while higher injector pressures increased fuel flow velocity at the nozzle and in turn atomization. These effects were more pronounced at low loads.

Figures 3.8 and 3.9 show the effect of swirl and fuel injection period on the rate of energy release.

Hsu (1984) extended the Otto and Diesel air standard cycle so as to establish some basic relationship between energy release, cycle efficiency and maximum cylinder pressure. An equivalent air standard cycle was used to analyze actual engine test data.

Using a single cylinder medium speed supercharged CI engine, this author studied the effects of changes in maximum cylinder pressure and injection timing on the rate of energy release.

Figures 3.10 and 3.11 show the results obtained by Hsu.

From the investigation, the following was concluded:

1. High cycle efficiency could only be achieved by energy released close

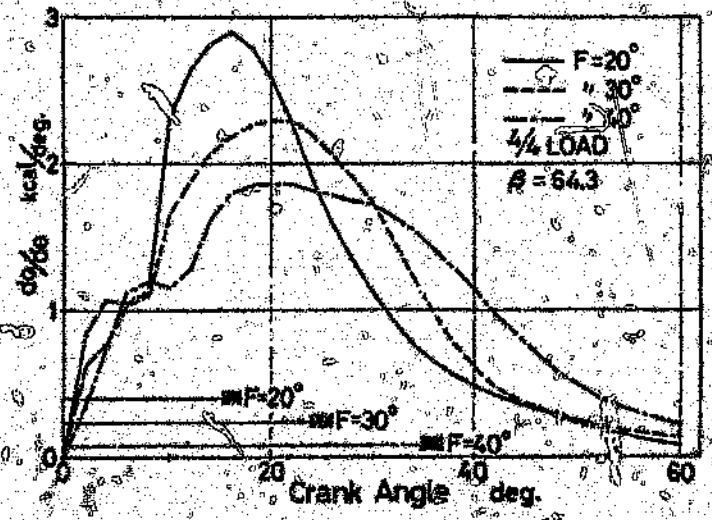

Figure 3.9: Change of $\frac{dQ}{d\theta}$ pattern with the change of fuel injection period (Shimotsu and Erdo, 1982).

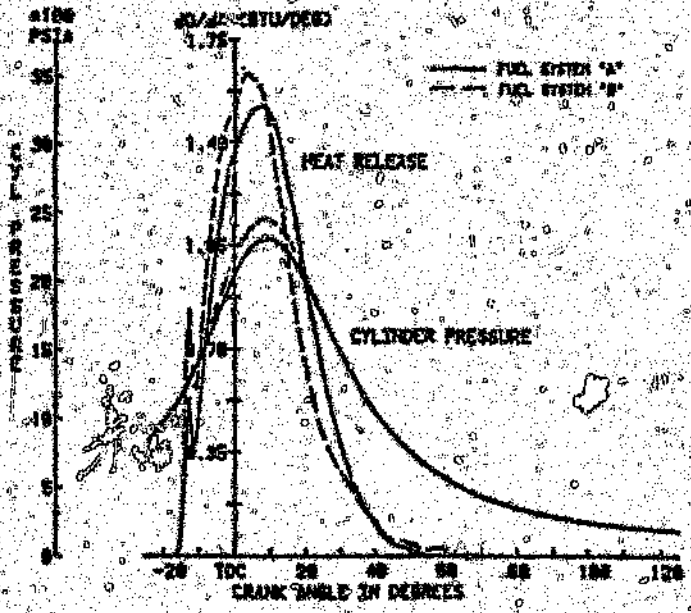

Figure 3.10: Heat release and cylinder pressure of two-fuel system (Hsu, 1984)

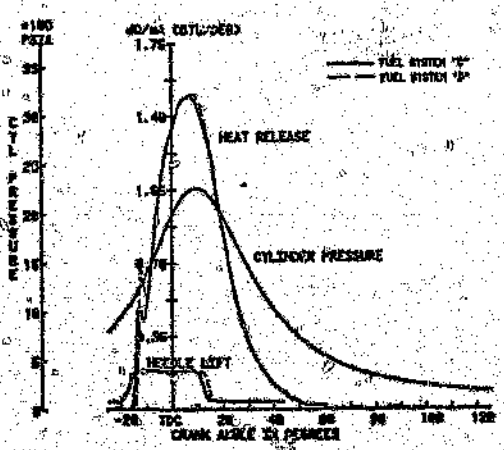

Figure 3.11: Heat release and cylinder pressure of two-fuel system at different injection timing (Hsu, 1984)

to TDC.

2. The energy released before TDC was slightly less efficient (effective) than that released at the same angle after TDC.

3. The energy released before TDC would cause higher maximum firing pressure than the same amount of energy released at the same angle after TDC.

4. The relative cycle efficiency could be used to compare the effects of different energy release curves on fuel consumption.

Faletti *et al* (1982) investigated the energy release patterns of hybrid fuels, to account for the increased brake thermal efficiency. Furthermore the effects of lower cetane numbers on the energy release rates were also investigated. Lastly the energy release characteristics of the hybrid fuels were compared.

The authors made use of the energy release model developed by Krieger and Borman to calculate the rates of energy release. This model requires engine pressure data as an input.

The results obtained indicated that the hybrid fuels had greater initial premixed burning levels and less diffusion flame burning. This trend increased as the diesel proportion in the hybrid fuel decreased, for all load conditions. Figures 3.12 and 3.13 show the burning rates for the full load case.

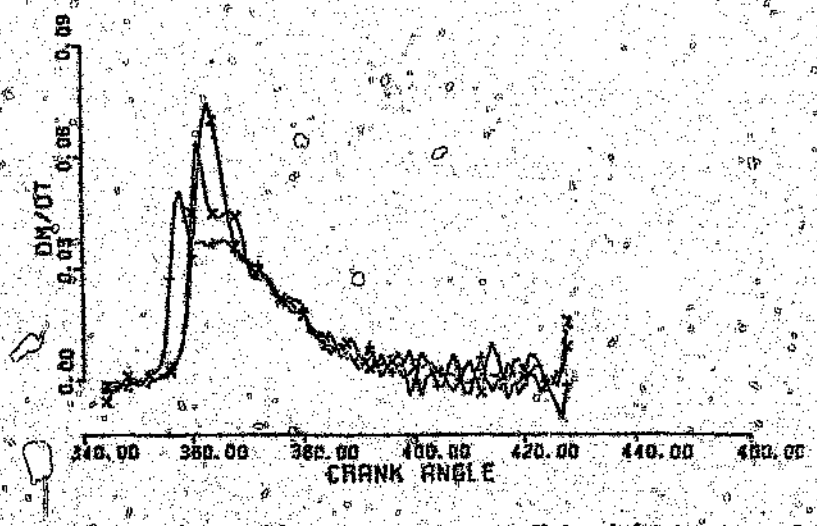

Figure 3.12: Comparison of burning rates at full load (Faletti *et al*, 1982)

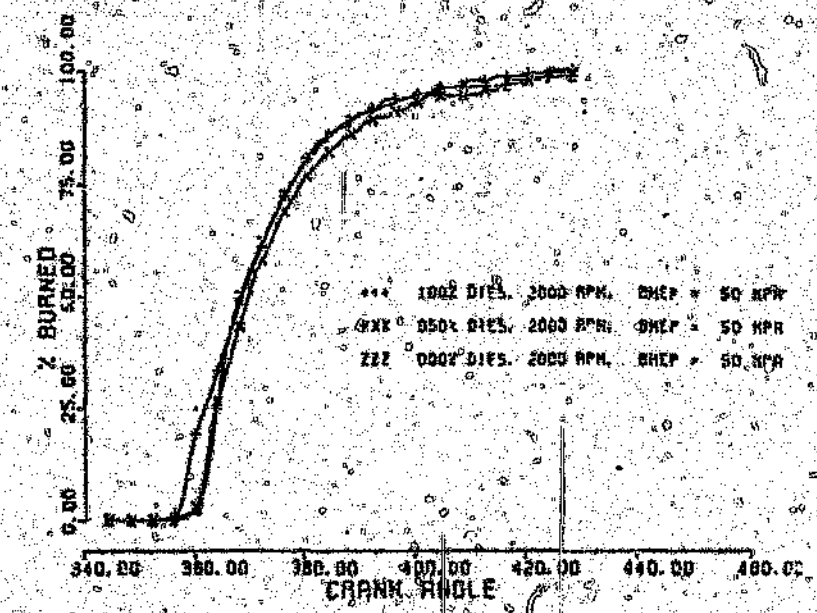

Figure 3.13: Comparison of cumulative energy release (Faletti *et al*, 1982)

Ignition delay, maximum cylinder pressure and maximum rate of pressure rise were all found to increase with a decrease in the proportion of diesel fuel in the mixture, as shown in figure 3.14.

The authors indicated that the longer ignition delays caused a larger percentage of the fuel to vaporize before ignition, and therefore leave a greater premixed energy release. The brake thermal efficiency gain with the hybrid fuel was caused by the higher premixed phase burning. Due to the longer ignition delay, the premixed portion of burning occurred closer to TDC, resulting in a larger percentage of the burning occurring at constant volume. This also resulted in higher peak cylinder pressures and rates of pressure rise during combustion.

Picken *et al* (1979) wrote a computer program to analyze the energy release from pressure-time diagrams for SI or CI engines, running on a single fuel or on a mixture of two fuels. The program calculates cylinder gas properties, instantaneous rate of burning of the fuel and the rate of energy release. It takes into account the variation in gas internal energy and the heat transferred between the gas and the cylinder wall. It could be used to study the effects of engine operating conditions on the combustion process and to provide a basis for testing the accuracy of any theoretical model of the combustion process in IC engines.

The calculations were based on the first law using a single zone model. The model was based on the following assumptions :

a) The gas within the cylinder is always a uniform mixture of air, gaseous fuel and combustion products from the previous cycle

b) The mixture is treated as air subject to the ideal gas relation.

c) The temperature and internal energy are considered constant throughout the mixture at any instant.

A comparison of the rate of heat release using the perfect gas theory and the program written by Picken *et al* is shown in figure 3.15.

Hayes *et al* (1986) presented a simplified energy release analysis technique for an approximate first look at the data quality. Comparisons were then

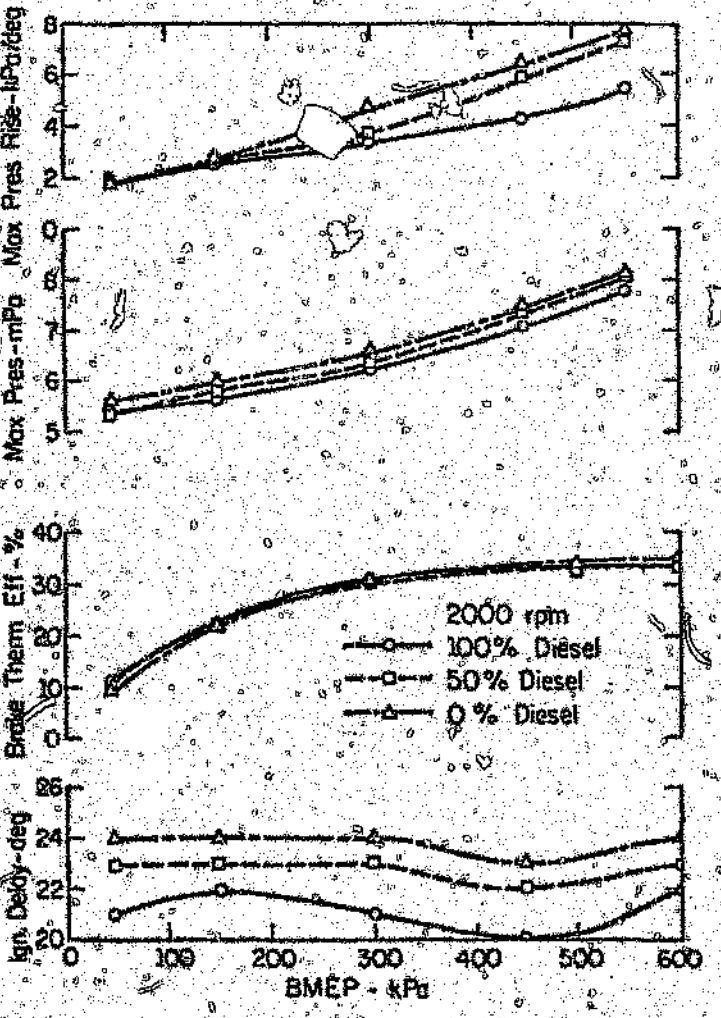

Figure 3.14: Ignition delay, brake thermal efficiency, peak cylinder pressure and maximum rate of pressure rise ; comparison at 2000 *rev/min* (Faletti *et al*, 1982)

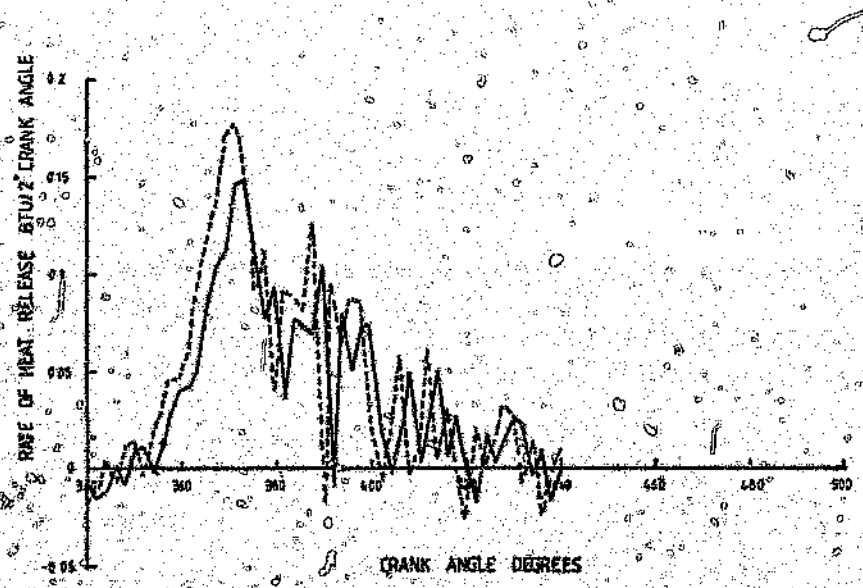

Figure 3.15: Comparison of heat release analysis achieved by : Perfect Gas Theory, (—) : Model (···) (Picken *et al*, 1979)

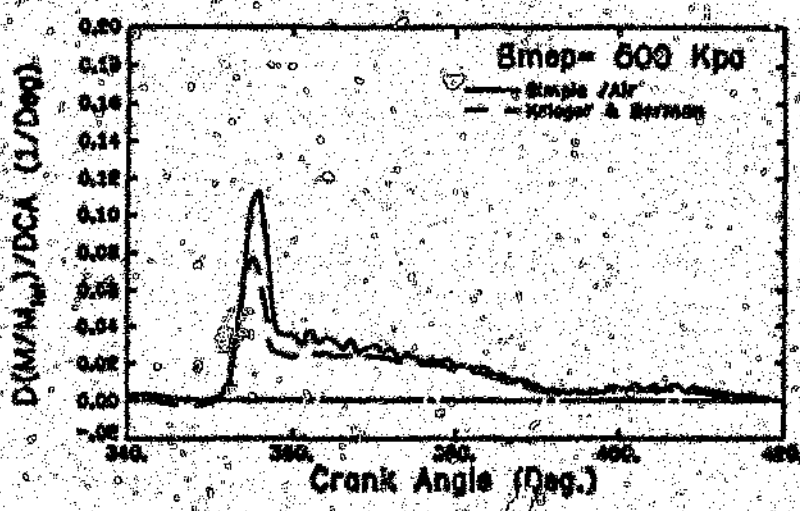

Figure 3.16: Comparison of normalized mass burning rates at a BMEP of 600kPa. The simple heat release model using an assumed initial mass (Hayes *et al*, 1986)

made between the results of their analysis and the Krieger-Borman energy release model which uses complete chemical equilibrium.

The apparent energy release was calculated using the first law of thermodynamics. The heat transfer to the combustion chamber surfaces was calculated using the Eichelberg correlation (1939).

Figure 3.16 shows one such outcome, where the simple model is compared to the Krieger-Borman model.

These authors concluded that qualitatively the simple model agrees well with the more comprehensive Krieger-Borman model. The simple model over-predicts the energy release rates for premixed combustion at all loads, and at loads of 300 and 600 *kPa* over-predicted the total energy released, as shown in figure 3.17.

The simple model did indicate the correct start of combustion as well as the effects of fuel vaporization.

The major difference between the models was in the estimate of the initial mass in the system. A rough estimate was used instead of an engine simulation as done in the more complex model.

Martin and Ahmad (1986) evaluated the combustion process in a wall-wetting direct injection compression ignition engine by calculating the apparent rate of energy release. As in the case of other researchers, use was made of the measured pressure history for several engine speeds, loads and start-of-combustion timings. The energy release characteristics of the engine were used to develop a conceptual model of the combustion process.

These authors considered the effects of varying combustion timing, speed and load on the rate of pressure rise and peak cylinder pressure. Advancing the timing start of combustion increased both the peak pressure and the maximum rate of pressure rise, as well as combustion noise. The pressures throughout the cycle were higher at the higher speeds because less time was available for heat transfer and blowby. In the case of varying loads, the peak pressures and the maximum rates of pressure rise were found to be similar. However, the pressure histories during expansion appeared to be diverging, indicating that combustion extended far into the expansion stroke for the heavier loads. This behaviour was believed to be typical for

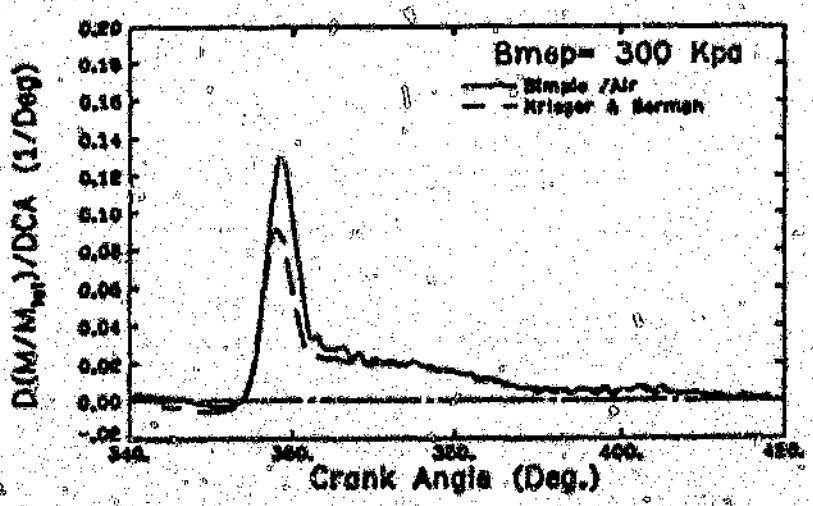

Figure 3.17: Comparison of normalized mass burning rates at a BMEP of 300 *kPa*. The simple heat release model using an assumed initial mass (Hayes *et al*, 1986).

diesel combustion systems.

The inputs required for the energy release calculations were: amount of fuel injected, initial mass in the cylinder, combustion chamber surface temperatures, heat-transfer coefficients and pressure history. The rate of energy released was then performed from a first l[illegible] analysis. These authors considered the rate of energy release for variation in timing, speed and load.

They concluded that as the injection timing was retarded, the premixed and airborne-diffusion portions of the burn seemed to decrease in significance as shown in figure 3.18. The accumulated energy release curves show that the higher rates of energy release associated with the advanced timings translate into shorter duration of energy released based on 90% fuel burned. The tails of the accumulated energy release curves had similar slopes as shown in figure 3.19. This indicated that the rate controlling process at the end of combustion was similar for each timing.

The effect of varying engine speed on the rate of energy release is shown in figure 3.20. As engine speed is increased the premixed portion of the energy release increases in duration. Ignition delays increased on a crank angle

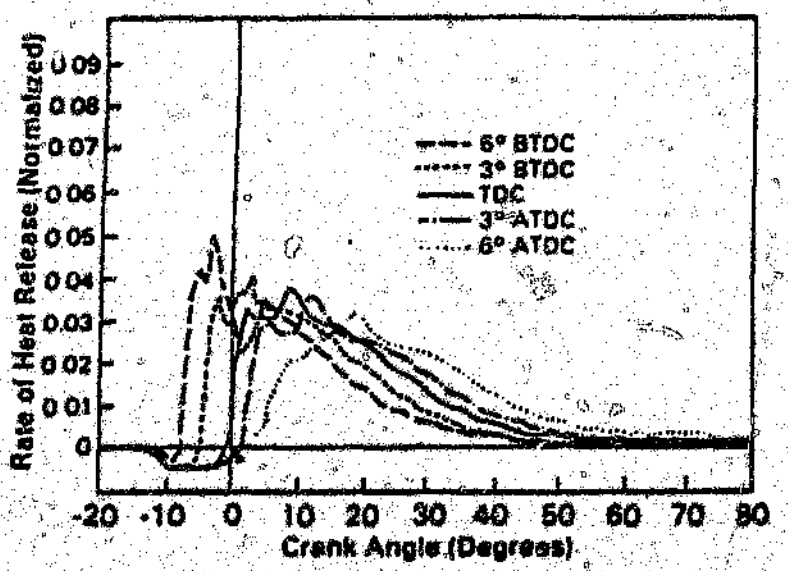

Figure 3.18: Rate of heat release for different SOC timings at 1500 *rev/min* and 45 :1 air-fuel ratio (Martin and Ahmad, 1986)

time scale, but decreased in real time as engine speed increased. However, the greater rate of injection at the higher speeds and faster mixing due to increased turbulence and bulk fluid motions caused a larger premixed energy release at the higher speeds.

Lastly the effects of the load on the rate of energy release are shown in figure 3.21. As the load was increased, the rate of energy release became smoother and the size of the premixed portion was reduced relative to that of the diffusion-controlled portion of the burn. The second peak in the rate of energy release was characterized by smaller gradients as the load was increased. The reason was that the rate of injection increased as the load increased, thus increasing the fuel momentum. This led to a higher percentage of the injected fuel impinging on the piston bowl surface, producing increased wall-burning.

Alkidas (1987) investigated the factors which influence the premixed combustion characteristics of a small high-speed direct injection compression ignition engine. He also evaluated the role of premixed combustion as a primary source of exhaust emissions.

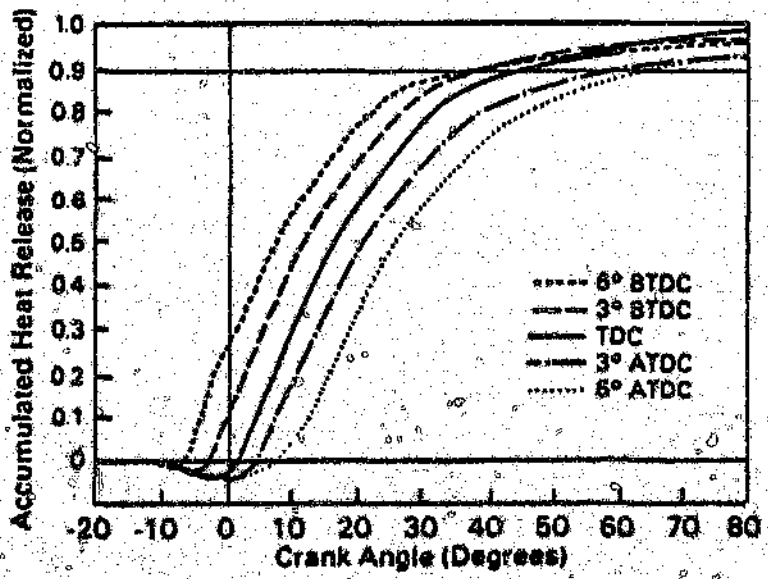

Figure 3.19: Cumulative heat release for different SDC timings at 1500 *rev/min* and 45 :1 air-fuel ratio (Martin and Ahmad, 1986)

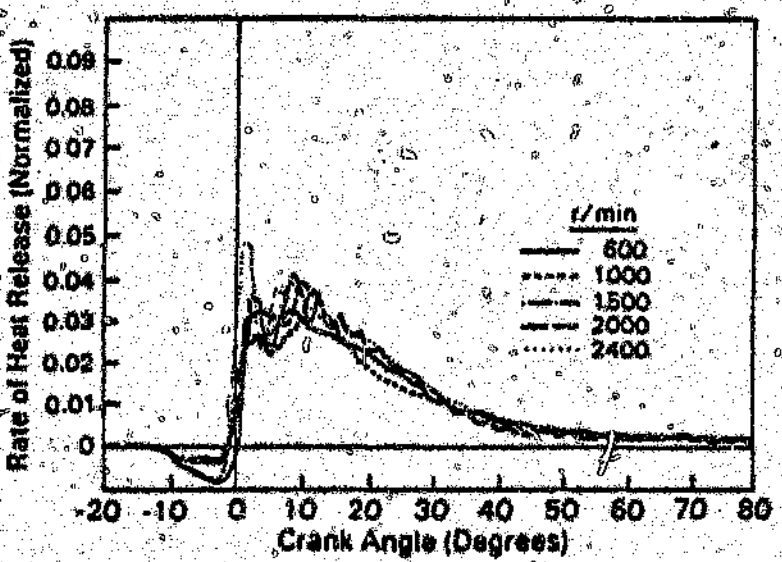

Figure 3.20: Rate of heat release for different speeds at 45 :1 air-fuel ratio and SDC timing at TDC (Martin and Ahmad, 1986)

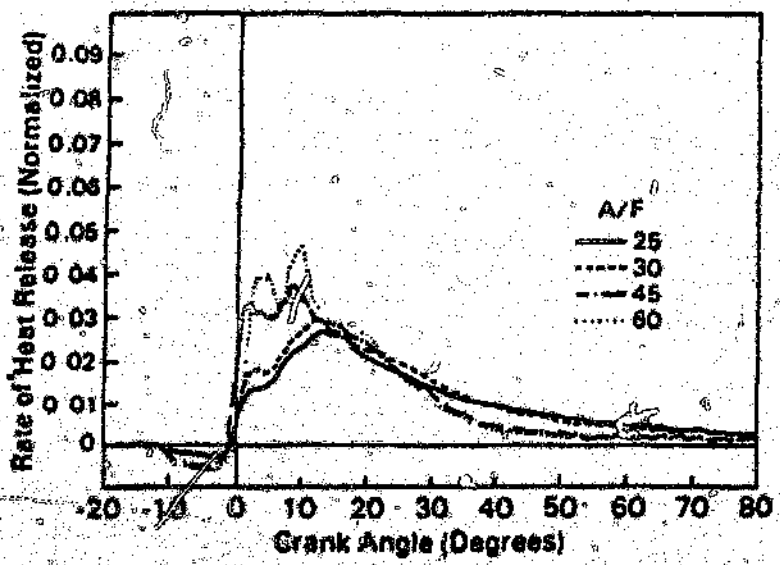

Figure 3.21: Rate of heat release for different air-fuel ratios at 1500 *rev/min* and SDC timing at TDC (Martin and Ahmad, 1986)

The combustion characteristics at various engine conditions were examined using a single-zone energy release model. The operational parameters examined were fuel-air ratio, engine speed and injection timing.

The instantaneous surface heat transfer was evaluated using

$$Q_w = h_g(\theta)\Sigma A_i(\theta)[(T_g(\theta) - T_{w,i})]$$

where
$T_g(\theta)$ and $h_g(\theta)$ are the gas temperature and convective heat transfer coefficient, respectively, at crank angle θ
A_i represents the surface areas of the cylinder head, piston and liner
$T_{w,i}$ represents their corresponding time-averaged temperatures.
The values of h were calculated from the empirical correlation developed by Woschni (1974).

Alkidas concluded the following :

1. The mass of fuel burned in the premixed mode of combustion was found to be essentially independent of the mass of fuel injected, and

increased linearly with the product of engine speed and ignition delay time.

2. The premixed-burned fraction increased with increasing engine speed, with decreasing fuel-air ratio, and with retarding injection timing.

3. The nitric oxide emissions were found to increase with decreasing premixed-burned fraction. This indicated that diffusion burning, rather than premixed burning, may have been the primary source of oxides of nitrogen emissions.

In another investigation Alkidas (1987a) analysed the energy release from a divided chamber compression ignition engine. The model used for both energy release and heat transfer, were the same as for the previous investigation. The parameters under investigation were engine speed, fuel air ratio and start of combustion. Based on the results of the investigation, the following conclusions were reached :

1. Increasing the fuel-air ratio increased the duration of combustion and, in general, the instantaneous fuel mass burned rate, which is linearly related to the energy release rate.

2. Increasing the engine speed, increased the fuel mass burned rate. Near the beginning and end of combustion this rate increased in direct proportion to engine speed. In the central part of the combustion duration, the rate was found to increase at a higher rate than engine speed. Thus the combustion duration in crank angle degree decreased with increasing engine speed.

3. Retarding the combustion timing significantly increased the combustion duration.

Alkidas (1987b) carried out a third investigation, but this time on an open-chamber compression ignition engine. The study investigated the influence of load and injection timing on :

- the premixed and diffusion peak energy release rates,

- the fraction of fuel burned in the premixed mode of combustion,
- the duration of energy release,
- and on the duration of premixed combustion.

Based on the results of this investigation, the following conclusions were reached :

1. Increasing the load decreased the amount of fuel burned in the premixed mode of combustion and correspondingly increased the amount of fuel burned in the diffusion mode of combustion.
2. During most of the diffusion combustion, the burning rate of the fuel appeared to vary almost linearly with the mass of fuel burned (rate of energy release).
3. Retarding the injection timing resulted in an increase in the premixed-burned fraction and a corresponding decrease in the diffusion-burned fraction.
4. The duration of energy release, in terms of degree crank angle increased with retarded injection timing. In general, the duration of energy release was found to vary linearly with load.

The effects of load and speed on the rate of energy release are shown in figures 3.22 and 3.23.

The effects of various combustion chamber configurations on the performance and energy release have been investigated by Ghojel (1982). The study investigates toroidal and cylindrical piston cavities with different fuel spray paths. This author reports that injection timing greatly affects rates of pressure rise and maximum cylinder pressures.

The indicated mean effective pressure (IMEP) was found to have an effect on the cumulative energy release. Increasing the IMEP lead to a slight decrease in the maximum value of cumulative energy release, and a sharp drop in the first peak of the rate of energy release.

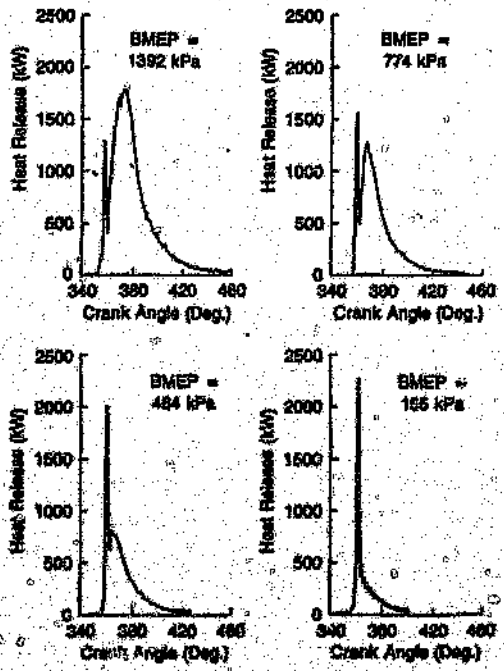

Figure 3.22: Heat release histories for various loads (1200 *rev/min*) (Alkidas, 1987b)

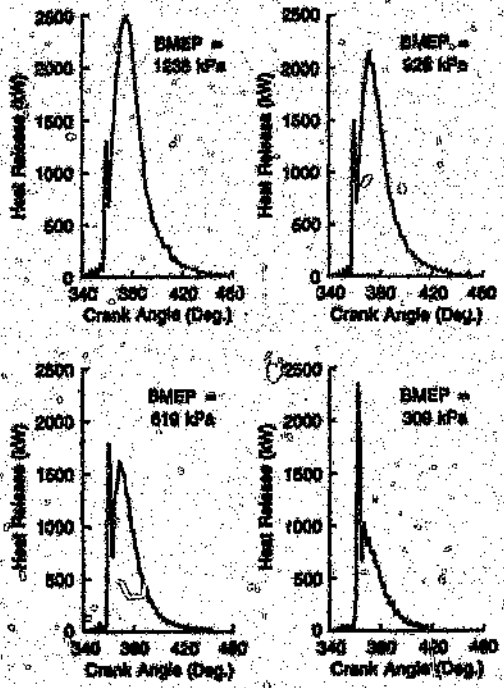

Figure 3.23: Heat release histories for various loads (1800 *rev/min*) (Alkidas, 1987b)

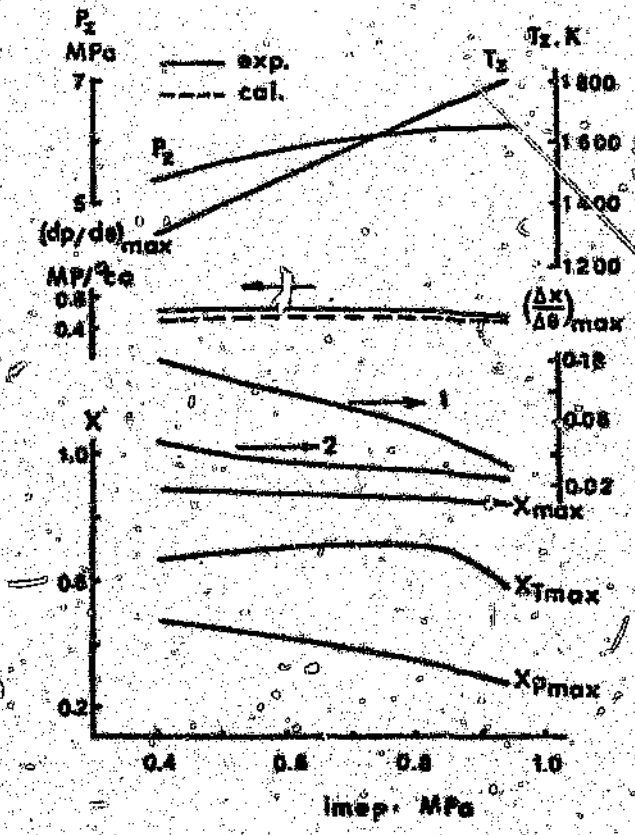

Figure 3.24: Heat release curves for arrangement D-2 at $n = 2200\ rev/min$, $\theta_{inj} = 24°$ CA BTDC (Ghojel, 1982)

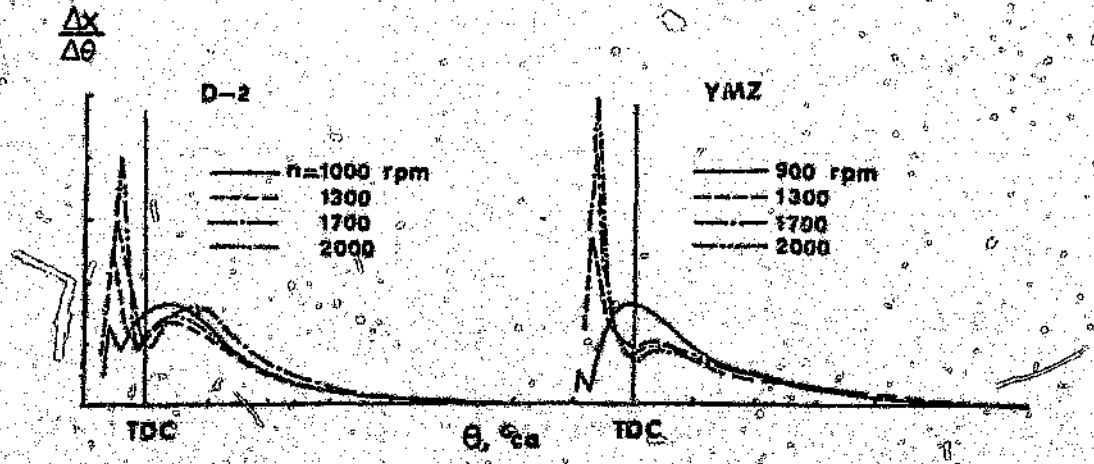

Figure 3.25: Effect of combustion arrangement and engine speed on rate of heat release at IMEP = 0.9 MPa (Ghojel, 1982)

This meant that the decrease of the first peak as a result of increasing IMEP was accompanied by a decrease of excess air coefficient with a net result of practically constant maximum rate of pressure rise.

Figures 3.24 and 3.25 show the effect of speed at constant IMEP on energy release parameters for both types of piston cavities.

At fixed injection timing, increasing engine speed led to the decrease of maximum cylinder pressure and the increase of maximum cycle temperature and of maximum cumulative energy release. This author reports that the increase in engine speed results in intensified burning during the stage of diffusive combustion.

Furthermore, by advancing injection timing, the beginning of combustion was also advanced and the magnitude of the first peak of energy release rate was increased. When the injection timing was set at its optimum for each speed, the energy released improved.

Figure 3.26 shows the effect of injection timing on energy release in a cylindrical piston cavity. Advancing injection timing resulted in the advancing of the beginning of combustion, and increased the magnitude of the first

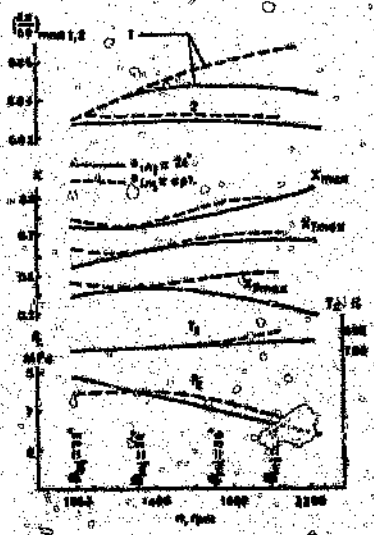

Figure 3.26: Effect of IMEP and injection timing on rate of heat release for arrangement D-2 at $n = 2000\ rev/min$. (Ghojel, 1982)

peak of the energy release rate. This was found to be more pronounced at high values of IMEP. The remainder of the rate of energy release remained virtually unaffected, supporting the idea that diffusive burning is independent of ignition delay, but is rather dependent on swirl.

Sorenson (1981) presented a simplified model for the simulation of the operation of internal combustion engines. This version was based on that of Shipinski (1967) which evolved from the study of the relation between the rate of fuel injection and the rate of apparent energy release in a direct injection, four-stroke compression ignition engine.

The energy release equation derived from the Weibe function has the following form:

$$(dQ/d\theta)_{app} = Ck_1(k_2+1)Y^{k2}\exp\left[-k_1Y^{k2+1}\right]$$

where

$$Y = (\theta - \theta_{ign})(\theta_z - \theta_{ign})$$

$$k_1 = 1/2AF$$

$$k_2 = 0,1496 - 0,2715 \ \ell n(PIBI)$$

$$c = [(mFA)/(1+FA)]\,(LHV)/(\theta_e - \theta_{ign})$$

and

$PIBI$ = % of fuel injected before ignition
AF = air-fuel ratio
m = total mass
θ = crank angle degree
θ_{ign} = crank angle degree at time of ignition
θ_e = crank angle degree at time of combustion.

Heat transfer in the engine was also accounted for by using Eichelberg's (1939) equation, as it was the simplest available.

The results obtained by this author to predict certain parameters at constant speed and part throttle are shown in figure 3.27.

The trends in the variation of fuel consumption, exhaust temperature, and IMEP as functions of air fuel ratio show that good predictions are possible. When predicting peak pressure, the model shows a slightly higher value for rich mixture, as it can not predict the multistage combustion process. Furthermore, at higher loads the combustion duration is longer and the initial combustion rates are reduced. This leads to slower initial rates of pressure rise. The pressures on the expansion stroke follow the correct trend and are higher as the load increases. Figure 3.28 shows simulated pressure-time diagrams.

3.1.2 Heat Transfer

Heat transfer from the cylinder gases to the walls of a compression ignition engine is a great importance. Heat transfer can be a limitation on engine ratings as imposed by thermal loading and its effects on engine performance. Although much published material is available on the subject, it is still a

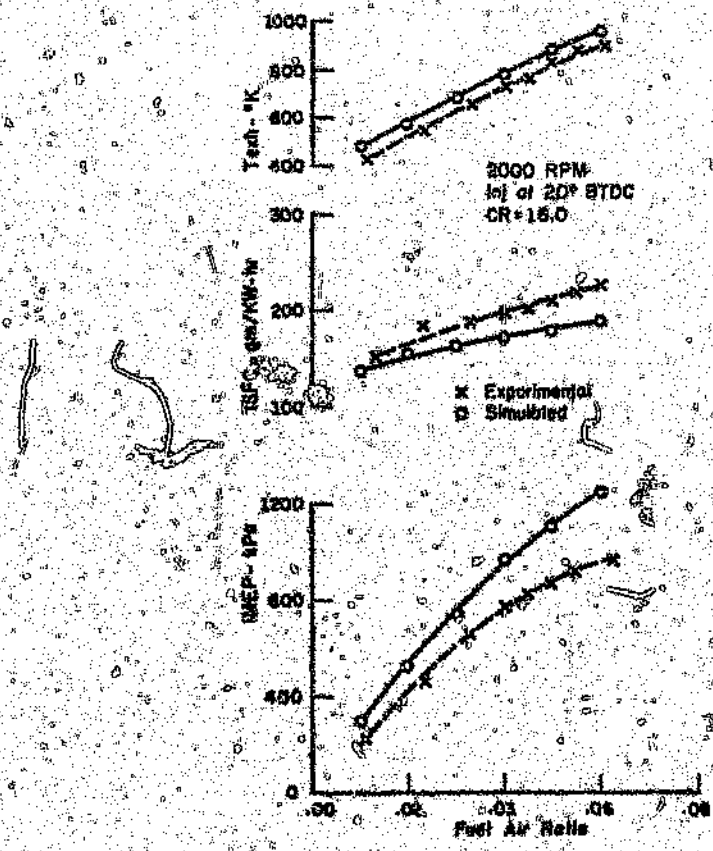

Figure 3.27: Comparison of experimental simulated results for the effect of fuel-air ratio on power, fuel consumption, and exhaust temperature in a diesel engine. (Sorenson, 1981)

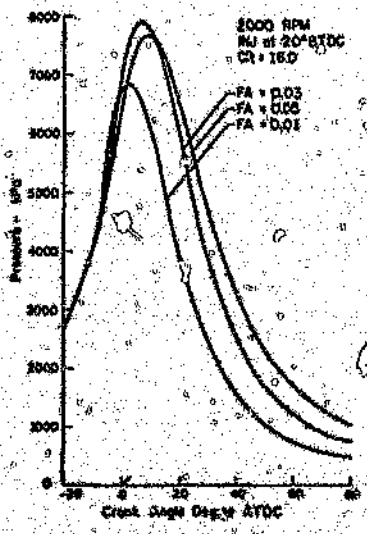

Figure 3.28: Simulated pressure-time diagrams showing the effect of fuel-air ratio in a diesel engine (Sorenson, 1981)

very difficult task to calculate the heat transfer rate for any engine under various conditions.

The methods generally available for calculating engine cycles are based upon simple single-zone models. These assume homogeneity throughout the combustion chamber, thus resulting in almost uniform instantaneous heat transfer rates to the exposed combustion chamber surfaces. The literature gives little comparison of these instantaneous heat transfer rates, but the effect of heat transfer on engine performance depends upon when in the cycle the heat transfer occurs.

In the literature survey that follows the development of the methods of calculating the heat transfer in an internal combustion engine will be discussed. Particular attention will be paid to compression ignition engines.

3.1.3 Heat Transfer Models

Engine heat transfer is a very complex problem, involving fast changes in gas pressure, velocity and temperature. In addition there are complexities of temperature and velocity distributions. Figure 3.29 shows a typical heat flux plot as measured by Le Feuvre *et al* (1969). The location of the ther-

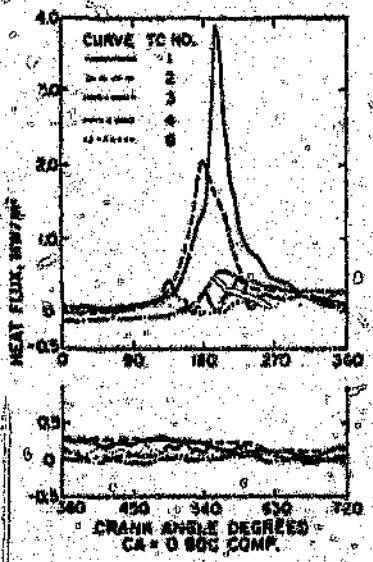

Figure 3.29: Heat flux calculated from data of figure 3.31 (Le Feuvre *et al*, 1969)

mocouples with the resulting surface temperature distribution over many cycles is shown in figures 3.30 and 3.31.

From these diagrams the large differences between surface temperatures and heat fluxes at various positions in the cylinder head and liner are quite evident. Large temperature differences on the cylinder head surface itself are noticeable, as shown by thermocouples numbers 1 and 2.

In principle, physical phenomena involved in engine heat transfer are functions of convection, diffusion, pressure, heat generated by combustion and radiation. The energy equation governs all these parameters, with the exception of radiation. However, the modelling of the engine heat transfer is made difficult due to the complexities of relating the above terms and the lack of information to solve the energy equation. Heat transfer modelling for engines began about sixty years ago, with considerable progress being made in both the experimental and theoretical analyses, yet a satisfactory predictive model has not been developed.

Many different approaches have been considered to analyze in-cylinder heat transfer. These may be classified into the following categories (Borman and

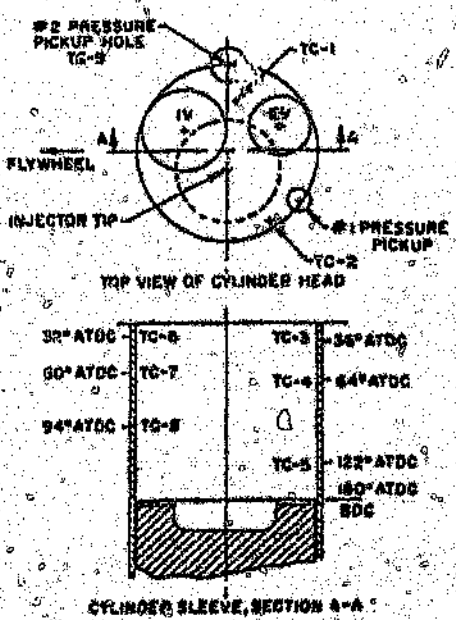

Figure 3.30: Thermocouple locations in the open-chamber diesel (Le Feuvre *et al*, 1969).

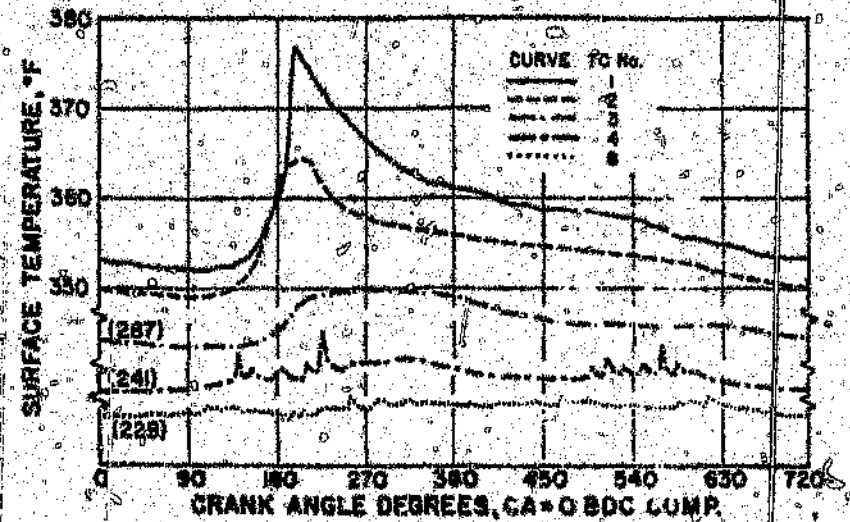

Figure 3.31: Surface temperature at five locations shown in figure 3.30. Supercharged at 2000 *rev/min* and 0.45 equivalence ratio (Le Feuvre *et al*, 1969)

Nishiwaki, 1987) :

1. Global (one zone) thermodynamic models.
2. Zonal (more than one zone) thermodynamic models.
3. One-dimensional analytical and numerical fluid-dynamic models.
4. Multi-dimensional numerical fluid-dynamic models.
5. Radiant heat transfer models.

Radiant heat transfer is included in the global models, sometimes lumped with the convective coefficient and sometimes as a separate term. Only global models will be discussed in this survey.

Global models deal with overall empirical heat transfer coefficients generally assumed for all heat transfer surfaces in the cylinder. A quasi-steady assumption is used as a basis for the model. This takes the form

$$q' = h(T - T_w)$$

where

q' = the heat flux
h = heat transfer coefficient
T = bulk mean gas temperature calculated from the equation of state for a given pressure
T_w = wall surface temperature.

The equation may be modified to account for local differences in wall surface temperature, by writing it as

$$q' = h \sum_{i=1}^{N} A_i (T - T_{w_i})$$

The combustion chamber surface is divided up into N uniform surface temperature areas, A_i.

The quasi-steady assumption presents a problem in that there is a phase shift between the flux and the temperature difference. This shift has been observed experimentally and supported by theoretical analysis. It is believed to be caused by the presence of extremum in the boundary layer temperature profile. The practical consequences of the shift are believed to be minor.

Global models are classified as empirical or semi-empirical correlations.

i) Empirical Correlations The first model for engine heat transfer ever presented was by Nusselt (1923). By relating experimental data in a spherical bomb and actual engine data, Nusselt put forward an overall heat transfer coefficient, h, as

$$h = h_c + h_r$$

where h_c is the convective component :

$$h_c = 5,41 + 1,24C_m)(p^2T)^{1/3} \qquad \left(\frac{J}{m^2K}\right)$$

and h_r is the radiant component :

$$h_r = \frac{4,21 \times 10^{-1}}{(1/\epsilon_g + 1/\epsilon_w - 1)} \frac{(T/100)^4 - (T_w/100)^4}{(T - T_w)} \qquad \left(\frac{J}{m^2K}\right)$$

where

C_m = mean piston speed (m/s)
p = pressure (N/m^2)
ϵ_g, ϵ_w = emissivities of gas and wall respectively.

The heat transfer coefficient has often been used to predict the instantaneous heat flux, because it is based upon instantaneous values of p and T.

Brilling (1958) (quoted by Chirkov and Stefanovski (1958)) modified Nusselt's coefficient by re-writing the mean piston speed term as $(3,5+0,185C_m)$

instead of $(1+1,24C_m)$. This was based upon data from his test engine. Van Tyen (1962) also modified the mean piston speed term to $(3,22+0,864C_m)$.

Eichelberg (1939) made the first measurement of the instantaneous heat flux. He took measurements on large naturally aspirated two stroke and four stroke compression ignition engines. Eichelberg put forward a heat transfer coefficient to predict the instantaneous heat transfer as :

$$h = 7,67(C_m)^{1/3}(pT)^{1/2} \qquad \left(\frac{J}{m^2sK}\right)$$

This coefficient does not explicitly include the radiation term. Based on this formula, he derived a time averaged heat-transfer coefficient. This formula has been and is still in use for low speed engines.

Pfaum (1961) modified Eichelberg's formula and carried out experiments using a pre-combustion chamber compression ignition engine. The effects of supercharging were taken into account by using different coefficients for the piston, cylinder head surface, and liner. The mean piston speed term was also revised.

Eichelberg's formula was also tested by Hensin (1965). Using a Lanova type compression ignition engine he showed that the formula gave a fair agreement with the experimental results during a compression stroke. However, a theoretically estimated instantaneous gas velocity value was used instead of the mean piston speed.

ii) Semi-Empirical Correlations A number of authors used dimensional analysis to assist them to formulate a more fundamental equation.

The simplified energy equation may be written in dimensionless form with certain assumptions. These are constant heat conductivity, constant specific heat, spatially uniform pressure, and treating chemical energy as a volume heat source. Also, the diffusion and convection of different species are neglected. The resulting equation as given by Borman and Nishiwaki is

$$\frac{\partial T^*}{\partial \tau} = \frac{1}{R_e P_r}\nabla^2 T^* - v^*\nabla T^* + \left(\frac{\gamma-1}{\gamma}\right)\frac{T^*}{p^*}\frac{dp^*}{d\tau} + q^*$$

where

$$
\begin{aligned}
p^* &= p/p_0 \\
T^* &= T/T_0 \\
v^* &= v/v_0 \\
q^* &= q/(c_p \rho T_0 v_0/D) \\
\tau &= tv_0/D \\
R_e &= \rho v_0 D/\mu \\
P_r &= c_p \mu/k \\
\gamma &= c_p/c_v
\end{aligned}
$$

The values of p_0, T_0, v_0, and D are the reference pressure, temperature, velocity, and length respectively.

The above equation, together with those of continuity and motion result in a correlation of Nusselt number in terms of the Reynolds and Prandtl numbers. Further terms due to the presence of p^* and q^* may also be of importance. The Reynolds number is based on the time-dependent density. Also the $dp^*/d\tau$ term can be quite large during combustion, and its coefficient is the reciprocal of density. Thus large variations can be expected through the boundary layer as well as with time. The result is that there is little hope that all the parameters can be incorporated in a universal global model. Thus many authors have opted for the simpler models of the general form,

$$N_u = CRe^n$$

to obtain correlations.

iii) Open Chamber Models Taylor (1960) showed in his early investigations that the exponent n, in the above equations, varied from 0,5 to 0,9 for time averaged heat fluxes. The value was dependent on engine type. Also, for the stated range, the Reynold's number was based on the cylinder bore and the mean mass flow rate through the engine. Oguri (1960 (a) and (b)) developed a more elaborate formula based on experiments with a spark ignition engine.

Annand (1963) reviewed all the existing formulae then available, and discussed the shortfall of each. The necessary theoretical ideas were set out

and used to establish criteria which had to be satisfied by any acceptable formula for instantaneous heat transfer rate. One group of the existing experimental data on instantaneous transfer rate was re-analysed and a new empirical formula was proposed to represent this information. The predictions made by this formulation were compared with some of the other published instantaneous rate data which themselves were not suitable for a full re-analysis.

Annand proposed the following instantaneous heat-flux formula :

$$q' = \frac{ak}{D} Re^{0,7} \times 10^3 (T - T_w) + b\sigma \times 10^3 (T^4 - T_q^4) \qquad \left(\frac{J}{m^2 s}\right)$$

where a is a constant ranging from 0,35 to 0,8, depending upon the intensity of charge motion. The value of b was suggested as $3,3 \times 10^{-11}$ for compression ignition engines.

This equation has a separate radiation heat flux as shown by the second term of the equation. The Reynolds number is based upon the cylinder bore and the mean piston speed and the gas properties were taken at the bulk mean temperature.

The formula was extended by Annand and Ma (1970) after examining experimental results obtained in a direct injection compression ignition engine using induction swirl. The proposed formula was :

$$q' = \frac{B}{D} Re^{0,7} \times 10^3 \left[a(T - T_w) + \frac{a'}{\omega} \frac{dT}{dt} \right] + b\sigma \times 10^3 \left(T^4 - T_w^4\right) \qquad \left(\frac{J}{m^2 s}\right)$$

where

ω	=	angular velocity of the engine crankshaft
σ	=	Stefan-Boltzman constant
a, a', b	=	constants obtained for the test engine and are dependent on engine speed and fuel-air ratio.

The difference between the two formulae is the presence of the time derivative of the bulk mean temperature, which is intended to compensate for

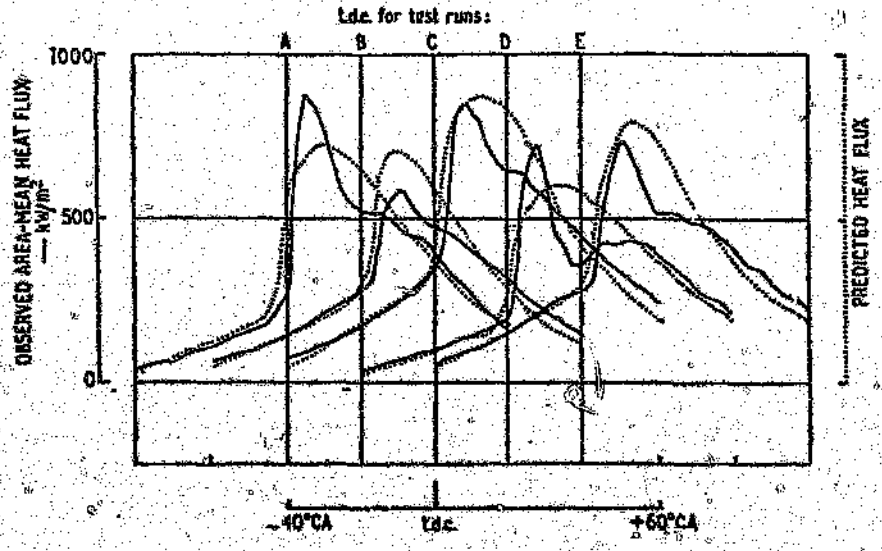

Figure 3.32: Comparison between measured area averaged heat flux and predictions (Annand and Ma, 1970)

the unsteady nature of the flow. For the reference velocity in the Reynolds number for the indirect injection engines, the authors adopted that proposed by Knight (1964). It was found to be suitable for well-mixed flow fields such as in combustion engines with a prechamber. The comparison between measured area-averaged heat flux and predictions from the above equations are shown in figure 3.32.

From these graphs the authors determined average values for the coefficients a, a' and b. These were :

$a = 0{,}12$
$a' = 0{,}2$
$b = 1{,}5$

Another widely used heat transfer coefficient is that proposed by Woschni (1967). He was not in favour of the experimental method using surface temperature because of the considerable scatter in the data. Instead, a heat balance was used to determine the total heat transferred to the combustion chamber walls for each process of a complete engine cycle. Woschni's proposed heat transfer coefficient was :

$$h = 0{,}820 \times 10^3 D^{-0{,}2} p^{0{,}8} W^{0{,}8} T^{-0{,}53} \qquad \left(\frac{J}{m^2 s K}\right)$$

where

$$W = \left[C_1 C_m + \frac{C_2 V_s T_1 (p - p_0)}{p_1 V_1}\right]$$

and

W	=	mean gas velocity
C_m	=	mean piston speed
C_1	=	6,28 and $C_2 = 0$ for the gas exchange process
C_1	=	2,28 and $C_2 = 0$ for the compression process
C_1	=	2,28 and $C_2 = 3{,}24 \times 10^{-3}$ for the combustion and expansion processes
p_0	=	pressure obtained for motoring (MPa)
V_s	=	displacement volume (m^3)

The subscript 1 indicates a specified time when the temperature and pressure are known. This could be inlet valve closure or beginning of combustion. The above heat transfer coefficient includes all the effects of convection and radiation in a lumped form. Figure 3.33 shows a comparison of various heat transfer coefficients as calculated by Woschni.

Woschni then added a swirl term by changing the coefficient C_1 for the gas exchange process to

$$C_1 = 6{,}18 + 0{,}417 \frac{C_u}{C_m}$$

and for the rest of the cycle to

$$C_1 = 2{,}28 + 0{,}308 \frac{C_u}{C_m}$$

where
$C_u = \pi D n_D, n_D$ was the rotation speed of the paddle wheel used in a steady-swirl test rig.

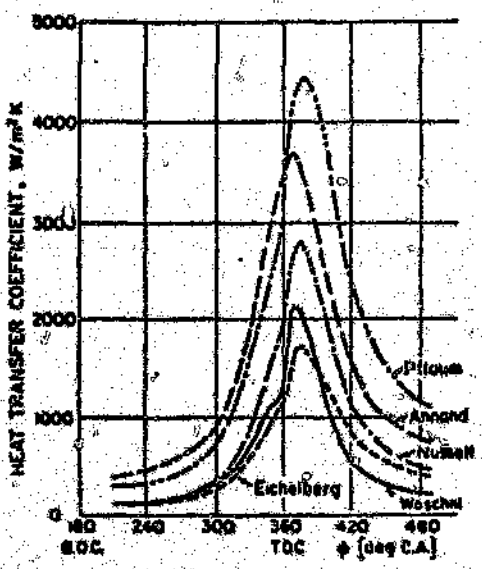

Figure 3.33: Comparison of heat-transfer coefficients calculated using different formulae for the same engine conditions (Woschni, 1967)

Woschni's formula was modified by Hohenberg (1979) so as to give a better prediction of time averaged-heat fluxes, obtained from one dimensional heat-flux probes. The instantaneous cylinder volume replaced the cylinder bore, and the exponent of the temperature term and the effective velocity W were changed.

Sitku and Ramanaiah (1972) also accepted Woschni's heat transfer coefficient. However, upon examining available data they proposed the following coefficient,

$$h = 2{,}36 \times 10^{-1}(1+b)\left(\frac{p^{0,7}C_m^{0,7}}{T^{0,3}(de)^{0,3}}\right) \qquad \left(\frac{J}{m^2sK}\right)$$

where

de = $4V/A$, which is an equivalent diameter
V = cylinder volume
A = heat absorbing area
b = dimensionless constant to take into account additional turbulent velocity, ranges from 0 to 0,35, depending upon the type of combustion chamber design.

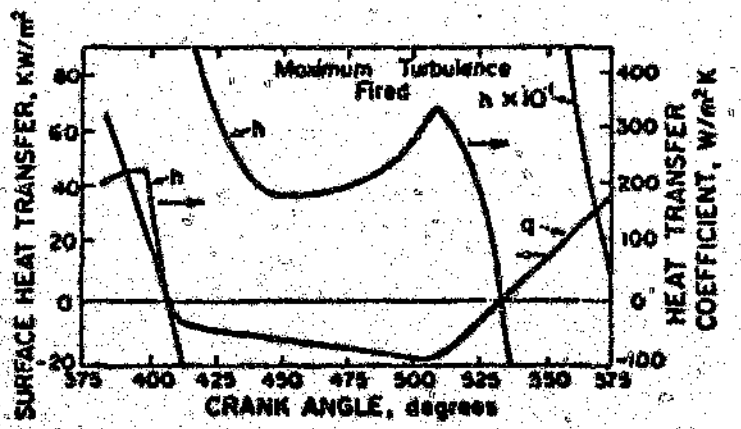

Figure 3.34: Heat flux data obtained using a CFR engine and calculated heat-transfer coefficients obtained by using measured wall and mass-averaged temperature differences (Overbye, 1961)

The unsteady nature of a thermal boundary layer presents a problem concerning the physical meaning of the heat transfer coefficient as defined by

$$q'' = h(T - T_w)$$

Overbye *et al* (1961) calculated the heat transfer coefficients using measured instantaneous heat flux and calculated bulk mean gas temperature based on pressure data. Figure 3.34 shows the results obtained.

The above figure shows the heat transfer coefficients taking on widely varying values, namely from infinity to negative values. This is believed to be due to the phase difference between the heat flux and the bulk temperature gradient. These authors proposed a dimensionless expression for instantaneous heat flux as a function of the Peclet number (Pe), (Pr) and dimensionless pressure (p^*). This was the result of examining the dimensionless form of the energy equation. The resulting equation is

$$q^* = 0,36\,[Pe\,(0,26p^* - 0,036) + 1000p^* - 200]$$

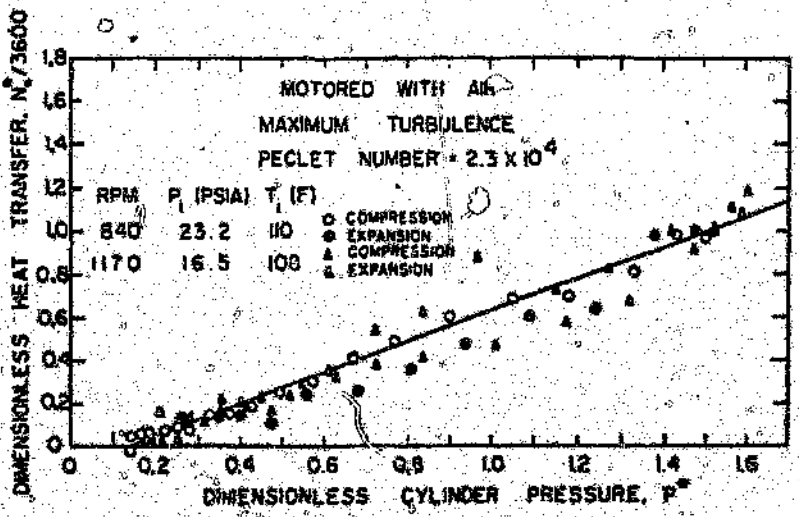

Figure 3.35: Dimensionless heat flux versus dimensionless cylinder pressure for a motored engine (Overbye, 1961)

where

q^* = $q''Lo/(kTo)$ = dimensionless heat transfer
To = gas temperature in the intake manifold
Lo = stroke
po = p/p^* = manifold pressure.

Figure 3.35 shows the dimensionless heat transfer coefficient against dimensionless cylinder pressure. The figure shows good agreement for the motored case, but not for the fired case. This was due to the uncertainties about other parameters affecting heat transfer in the fired case.

The quasi-steady turbulent heat-transfer model was also considered by Le Feuvre (1969), using instantaneous heat-flux data. The significant gas velocity was taken as the swirl velocity and used as the reference velocity in the Reynold's number. The instantaneous heat flux was given by :

$$q'' = a\frac{k}{r}Re^{0.8}Pr^{0.33}(T - T_w)$$

where

r = a radius at the test point on the cylinder head
Re = $r^2\omega/v$
ω = angular velocity of the cylinder gases
a = coefficient predicted to be 0,047 from motored data.

The above equation was applied to the motored case. The extent of agreement between the correlation and the data was found to depend upon the location of the thermocouple. The best agreement occurred when the thermocouple was placed between the inlet and exhaust valves. These authors then raised the question regarding the validity of the assumption of uniform gas temperature throughout the cylinder. The use of the mass-averaged temperature as a source temperature for surface heat flux was also in doubt.

Dent and Suliaman (1977) used a similar engine to that of Overbye *et al* and used the same Reynolds number in their study of heat transfer in compression ignition engines. They applied a steady turbulent convective heat transfer analysis for flow along a flat surface. The heat flux at radius r was given as :

$$q'' = 0{,}025\frac{k}{r}\left(\frac{r^2\omega}{v}\right)^{0,8}(T - T_w)$$

The angular speed ω of the air swirl in the above equation was evaluated from results of experimental studies done by Dent and Derham (1974). For the motoring case comparatively good agreement between predictions and measurements was achieved. Figure 3.36 shows comparisons for firing cases between the predicted and measured heat flux averaged over four locations on the combustion bowl surface.

From the diagram it can be seen that the equation underpredicts the peak heat flux levels, with the discrepancy increasing with engine load. The figure also shows the predictions attained with a two-temperature zone model. Here the assumption of complete mixing with a stoichiometric quantity of air and a combustion-enhanced swirl model was made. The heat-flux was based on the hot-zone temperature instead of the bulk mean temperature. The result is an improvement in the predicted heat-flux.

Whitehouse (1970) compared measured local heat fluxes using Annand's

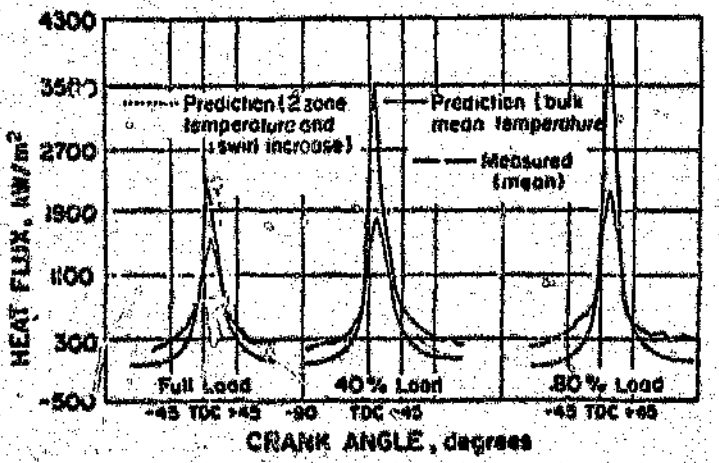

Figure 3.30: Measured surface heat flux in piston bowl and predicted flux using bulk mean and 2-zone model with swirl effect (Dent and Suliaman, 1977)

and Woschni's equations. In general the agreement between measured local heat flux and predictions by these models was found to be poor. In many cases the peak flux, and the cycle-averaged flux were found to be in error by a factor of more than two.

The effect of compression and expansion on instantaneous heat transfer in internal combustion engines was investigated by Lawton (1987). Tests were conducted on a motored compression ignition engine with the temperature being measured using a fast-response surface thermocouple fitted in the fuel injector pocket. Lawton reported that the observed heat flux was found to differ from that predicted by existing quasi-steady theories, namely those of Eichelberg, Woschni, and Annand. This was so even allowing some flexibility in the choice of constants. In particular, there was a significant heat-flux when the bulk gas and the wall temperatures were equal. This heat flux was positive during compression, that is from the gas to the wall, and negative during expansion. The maximum heat flux was found to occur about 8°BTDC. Also the heat flux during compression was larger than that occurring during expansion. In fact, this author found the heat flux to fall very quickly after top dead centre and attained a negative value

even though the gas was hotter than the wall. Quasi-steady analysis would need to interpret this as a negative heat transfer coefficient.

Lawton found Annand's quasi-steady equation to be accurate at TDC, and was therefore led to modify it to give a more useful non-steady equation. The recommended equation was then :

$$q_w = \frac{k}{d}\left[aRe^b\left(T_g - T_w\right) - 2,75LT_w\right] + c\sigma\left(T_g^4 - T_w^4\right)$$

The constants a, b, and c were as suggested by Annand. The non-steady term $2,75LT_w$ had a mean value of zero and thus the mean heat flux was not affected. The parameter L represents the compressibility number given by :

$$L = \frac{(\gamma - 1)Vt_o}{V}$$

where

γ	=	ratio of specific heats
t_o	=	time constant $= \left(\frac{d^2}{\alpha_0 \mu_p}\right)^{1/2}$
V	=	cylinder volume
d	=	cylinder bore
μ_p	=	mean piston speed
α_0	=	diffusivity of inlet air

3.2 Conclusion

As in the case of the literature survey on methanol as a fuel, this survey is not exhaustive. It is adequate to indicate what other researchers have formulated and subsequently used. Above all, this review clearly shows the difficulties one encounters when attempting to formulate a model for a given application. On the other hand, one could adapt an existing model, whether for energy release or heat transfer, using appropriate parameters.

The approach of using existing models was attempted in this research. However, these were found to be not satisfactory for the particular application.

In the case of the energy release, the models reviewed were either too simple or very complex. The simple ones, consider air only as the working fluid. Such models have been used and were found to be particularly good as a check on more advanced ones. The very complex models, such as the one put forward by Krieger and Borman (1966), are attractive, but are in their present form not capable of handling the presence of an aspirated ignition promoter such as DME. Extension to the Krieger Borman model are discussed in the next chapter.

Greater difficulties were encountered when searching for a heat transfer model. Although many of these models are referred to as 'universal', they all appear to suit the particular engine used by the researcher concerned. All heat transfer models have coefficients and exponents built into them. The values of some of these vary with prevailing engine conditions such as speed and air-fuel ratio. Difficulties were also encountered with the cylinder wall temperature, where some authors used a fixed value, whereas others used a variable temperature. The Eichelberg and Annand models were used in this research, but neither appeared to satisfy the prevailing conditions.

A decision was then made to formulate both energy release and heat transfer models appropriate to the engine and the fuels used. These models are not dissimilar to those of other researchers. A great deal was learned from the literature regarding the obstacles and difficulties encountered and the assumptions that had to be made by the various authors. This was found to be particularly so in the case of heat transfer. It is without doubt a vast and difficult topic, requiring sophisticated equipment for its measurement.

The development of the energy release and the heat transfer models ultimately used for this research are the topic of the next chapter. Other analytical methods believed to be of assistance in understanding the combustion are also discussed in the next chapter.

Chapter 4

THERMODYNAMIC ANALYSIS TECHNIQUES

This chapter is concerned with the development of thermodynamic analysis techniques necessary for the study of combustion in compression ignition engines. Some have been developed to facilitate the analysis of unusual combustion phenomena. These techniques have been divided into two types: general analysis and the energy release modelling and related techniques. They are complementary as they can be used as checks. Some are more informative in certain parts of the cycle. However, each has strengths and limitations, but when considering the overall picture, they go a long way in explaining combustion phenomena.

4.1 General Analysis Techniques

These analysis techniques use primarily recorded data, such as combustion chamber pressure, fuel line pressure and crank angle. The volume of the combustion chamber is calculated from the position of the piston. In some cases this data is manipulated mathematically so as to obtain derivatives or logarithms.

4.1.1 Combustion Chamber Pressure

The measurement of combustion chamber pressure is fundamental to most combustion studies. It is therefore, basic information which serves as input to most models in this field. It must be recorded as accurately as possible and the position of each reading relative to the crank angle is of utmost importance.

This data records events as they occur in the combustion chamber. The point of initial combustion is usually noticeable, as well as its position relative to TDC.

4.1.2 Derivative of Combustion Chamber Pressure

The purpose of evaluating the derivative of combustion chamber pressure is to locate the ignition point of the mixture. The search for the ignition point is restricted to the region from 340° to 360°CA. A three point moving average of the derivative is calculated in this region. If the value of the derivative at any point is twice that at the previous point then it is considered that the ignition point has been located.

The criterion of the slope change may be altered, and this was found to be necessary particularly in the case of the methanol/DME fuel system. The combustion was much smoother so that a sudden change in slope did not occur.

4.1.3 Combustion Chamber Pressure versus Volume

This is simply a plot of pressure against its corresponding combustion chamber volume. This diagram serves two functions: it permits the calculation of the amount of indicated work done in one cycle and it shows whether the combustion occurs predominantly at constant volume.

4.1.4 $\ell n\ (p/p_1)$ versus $\ell n(V/V_1)$

This is the natural logarithm of non-dimensional pressure (p/p_1) and non-dimensional volume (V/V_1), where p_1 and V_1 represent the combustion chamber pressure and volume at IVC respectively. These diagrams show the pumping loop as well as the power loop. The slope of the power loop at each data point represents the value of the polytropic index n.

4.1.5 Polytropic Index

As stated above, the value of the polytropic index is derived from the $\ell n\ (p/p_1)$ versus $\ell n\ (V/V_1)$ information. It finds its greatest use in the determination of the occurrence and direction of the heat flow. This heat includes that released from the fuel as well as that transferred to and from the trapped gas, resulting from temperature gradients between the gas and the exposed combustion chamber area. Preliminary tests have shown that in the vicinity of TDC, the values of n undergo enormous fluctuations due to this process occuring at almost constant volume. This results in a value of n tending to infinity. Thus the values of n are very informative from IVC to EVO, with the exception of a few degrees crank angle before and after TDC.

The usefulness of the polytropic index is enhanced when the value of the ratio of the principal specific thermal capacities γ is superimposed on the same diagram. The relative values of n and γ are used to determine the direction of the heat flow. The values of n are based on pressure and volume data and thus involve no modelling. The values of γ, on the other hand, have been arrived at from the energy release model, to be discussed in detail below.

4.1.6 Injector Line Pressure

A record of the variation of the fuel line pressure is used to determine the injection point. This point is located by determining where the derivative of the injector line pressure equals zero, after the initial steep pressure rise.

Once this point has been found, the line pressure drop indicates that fuel is being injected into the cylinder. The usefulness of this point is that the delay that occurs between injection and ignition, if it exists, can be easily identified. If these two points coincide then it indicates that the fuel burns as it is being injected.

4.2 Energy Release Modelling and Related Techniques

This section concerns itself with more advanced analysis techniques. These techniques are very much interrelated and are based on a number of assumptions.

The first technique to be developed is that for energy release. Various approaches are discussed, from a very simple model to a complex one taking into account heat transfer. The simple model is used as a guideline for the more complex models. The final discussions and analysis of the results are based on one model only, which accounts for products of combustion, heat transfer, and apparent mass burned, amongst others.

Related techniques concern the calculation of the gas temperature, entropy, apparent mass burned and the heat transfer model itself.

4.2.1 The Energy Release Model

The first law of thermodynamics is the basis of energy release modelling. The derivation given below is written in a form suitable for the method used to collect data.

The first law of thermodynamics for a closed system states that:

$$\delta q = \delta w + du$$

which for an ideal gas undergoing a reversible process reduces to :

$$\delta q = \frac{v\,dp}{(\gamma - 1)} + \frac{\gamma p\,dv}{(\gamma - 1)}$$

This equation can be written in incremental form with respect to crank angle:

$$\frac{\delta q}{d\theta} = \frac{v}{(\gamma - 1)}\frac{dp}{d\theta} + \frac{\gamma}{(\gamma - 1)}\frac{p\,dv}{d\theta}$$

or in a non-specific finite difference form:

$$\frac{\Delta Q}{\Delta\theta} = \frac{V}{(\gamma - 1)}\frac{\Delta p}{\Delta\theta} + \frac{\gamma}{(\gamma - 1)}p\frac{\Delta V}{\Delta\theta}$$

where, by definition

$$\gamma = \frac{c_p}{c_v}$$

and since

$$R = c_p - c_v$$

$$\gamma = \frac{c_p}{c_p - R}$$

where R is the specific gas constant.

The evaluation of c_p and R require particular attention.

4.2.2 The Determination of c_p and R

A number of methods are available for determining the values of c_p and R. These vary, as discussed above, from the simple approach, where the cylinder contents are assumed to consist of air only to the more complex method which assumes that certain species are present in the products of combustion.

When the more complex methods are used, the mole fractions of the species present in the products of combustion are evaluated. These are in turn used to determine the mean molecular mass of the products of combustion. The value of the specific gas constant R, is then calculated from:

$$R = \frac{R^*}{\bar{M}}$$

where R^* is the universal gas constant and $\bar{M}$ is the mean molecular mass of the products of combustion.

The development discussed below relates to four approaches studied in detail. These are:

(a) The Air Method

(b) The Perfect Combustion Method

(c) The 'CH Fuel System' Method

(d) The 'CHO Fuel System' Method

The air method is the simplest approach and applies from IVC to EVO, and is not dependent on the fuel type. The results obtained from this method are used as a guideline for the more complex approaches.

The remaining three methods are invoked once the ignition point has been found. Prior to this, the cylinder contents are assumed to be air only, when the engine is fuelled on diesel. However, when the engine is fuelled on methanol and DME, the 'CH fuel system' is not used, since it does not

account for the oxygen present in the DME. Methods (b) and (d) only are used. With these approaches, the mass of DME drawn into the cylinder is calculated and added to that of the air. Thus the presence of products of combustion is accounted for from IVC. Once the ignition point of methanol is found, its contribution to the products of combustion is also considered.

(a) The 'Air' Method

The underlying assumption in this method is that the working fluid in the cycle is air only. The composition of the fuel, the point of ignition, and the products of combustion are not accounted for in any way. It can thus be used for any fuel or fuel combination.

The air temperature at every point is calculated using the ideal gas equation. With this temperature, the value of c_p is calculated using an equation proposed by Zucrow and Hoffman (1976):

$$c_p = [3,6359 - \frac{1,333736T}{10^3} - \frac{3,294217T^2}{10^5}]R^* - [\frac{1,91142T^3}{10^9} - \frac{0,275462T^4}{10^{12}}]R^*$$

if the temperature is less than 1000 K, and

$$c_p = [3,04473 + \frac{1,338053T}{10^3} - \frac{0,488256T^2}{10^6}]R^* + [\frac{0,08554757T^3}{10^9} - \frac{0,00570132T^4}{10^{12}}]R^*$$

if the temperature is greater than or equal to 1000 K.

The units of c_p and of R^*, the universal gas constant, are $kJ/kmolK$.

(b) The 'Perfect Combustion' Method

This approach assumes that the products of combustion are H_2O, CO_2 and N_2, with excess air. It is applicable to any fuel or fuel combination.

The primary requirement is the carbon-hydrogen-oxygen ratio of the fuel. With this, the equation for the combustion of fuel with air can be set up and the mole fractions of the products can be evaluated.

In the case where the fuel was diesel, the carbon hydrogen ratio was constant. However, when methanol/DME was used, a different situation arose.

Since the proportion of DME to methanol varied in each test, the carbon-hydrogen-oxygen ratio had to be adjusted accordingly. A combined fuel formula was evaluated for each test, as follows:

From the recorded mass flowrate of the DME and methanol, the mole flow rate was calculated for each fuel. The $C-H-O$ ratio was based on the fraction of each fuel mole flow rate, to the total mole flow rate, multiplied by the number of atoms in each fuel. For example the ratio of carbon was:

$$n_C = \left[\frac{\dot{n}_{DME}}{\dot{n}_{Total}} \times 2\right] + \left[\frac{\dot{n}_{methanol}}{\dot{n}_{Total}} \times 1\right]$$

since there are 2 $C's$ in DME and 1 C in methanol. In the same way the ratio of H and O was evaluated.

With the mole fractions, the mean molecular mass of the air with the products of combustion was evaluated from ignition point to exhaust valve opening. The mean molecular mass was used in the calculation of the specific gas constant using the universal gas constant. The cylinder gas temperature was evaluated from the ideal gas relation, with the measured pressure, calculated volume and trapped mass consisting of air and fuel.

The value of c_p was then found at every $0,2°CA$ for each of the products of combustion. The polynomials used were those proposed by Campbell (1979). These are of the form:

$$c_p(T) = B + \frac{C}{T} \quad (kJ/kmolK)$$

where the coefficients B and C are functions of temperature. The temperature ranges were $400 \leq T \leq 1600\ K$ and $1600 \leq T \leq 3000\ K$.

(c) The 'CH Fuel System' Method

This method is based upon empirical formulae presented by Gulder (1988). These formulae predict the specific heat at constant pressure, and mean molecular mass of the combustion gases as functions of the atomic hydrogen to carbon ratio of the fuel, the equivalence ratio, and the gas temperature and pressure.

The proposed equations cover the following ranges:

fuel-air equivalence ratio ϕ from 0 to 1,0
pressure p from 10^5 to $7,5 \times 10^6 Pa$
temperature T from 300 to $2500K$
hydrogen-to-carbon ratio ω from 0,8 to 2,5

These ranges cover the conditions of interest in compression ignition engines, and the properties of conventional liquid hydrocarbon diesel fuels.

Gulder shows the dependence of the specific heat and molecular mass on the fuel type, equivalence ratio, pressure and temperature. Briefly, the effects are as follows:

The constant pressure heat capacity, c_p, of the combustion products varies slowly with the ω of the fuel; pressure does not affect c_p for $T \leq 1400K$, but the effect is quite significant above $1500K$; below $1500K$, the effect of temperature on c_p is small as compared to its effect above $1500K$; increasing temperature increases the effect of ϕ on c_p, but for $T \leq 1500K$, c_p varies almost linearly with ϕ.

The variation of the mean molecular mass of the combustion gases with ω, ϕ, temperature and pressure is as follows:

Molecular mass increases with decreasing π (dimensionless pressure $= p/p_o$ where p_o = reference pressure $101,3kPa$), and with ϕ; the dependence of molecular mass on temperature is complicated - however at a given pressure and ω, increasing gas temperature decreases the molecular mass for $T < 1500K$. Lower molecular mass at high temperatures is due to the increased extent of dissociation of triatomic and diatomic species into diatomic and monatomic ones.

The equations for specific heats and molecular masses were computed by using a chemical equilibrium code which considers 14 species in the products, namely: $H_2, H, O_2, N_2, N, OH, H_2O, O, NO, NO_2, N_2O, CO, CO_2$ and air.

Thermochemical data used by Gulder were taken from standard tables of Stull and Prophet's 1971 JANAF Thermochemical Tables.

A functional expression of the form shown below was adapted by Gulder to predict the specific heat and molecular mass of the combustion gases of complex hydrocarbon mixture-air systems. These expressions are functions of equivalence ratio, pressure, temperature and hydrogen to carbon ratio of the fuel:

$$\Omega_k = AS^{\alpha}\exp\left[\beta(\sigma+\lambda)^2\right]\pi^{\kappa}\theta^{\eta}\omega^{\nu}$$

For the temperature range $1500 \leq T \leq 2500K$

$$\Omega_1 = c_p$$

$$S = t = T$$

$$\theta = 1.2358 + \quad t^2 + 3.77256t^3 - 1.07368t^4$$

$$x = a_1 + b_1 t + c_1 t^2 \tag{4.1}$$

$$y = a_2 + b_2 t + c_2 t^2 \tag{4.2}$$

$$z = a_3 + b_3\sigma + c_3\sigma t \tag{4.3}$$

where

$$\sigma = \phi - 0.45$$

ω is the H/C atomic ratio of the fuel, and T is the absolute temperature in K.

For the temperature range $400 \leq T \leq 1500K$

$$\Omega_2 = c_p^{0.5}$$

$$S = \sigma = (\phi + 0.5)^2$$

In addition to the convective component of heat transfer, radiation was also calculated.

In the motoring cycles, the radiation component is ignored, since the emissivity of air is negligible. However, with combustion, radiation becomes more significant.

The resulting heat transfer model was put to the test with motoring cycles. The motoring cycle is taken immediately after a combustion cycle. When the cycle is recorded the engine returns to normal operation. The importance of this method of capturing cycles is that the temperatures during a motoring cycle can be considered as unchanged from a combustion cycle. Throughout the closed part of the cycle, the cumulative energy released with heat losses accounted for, must be zero.

The final model is satisfactory in that the cumulative energy released at exhaust valve opening (EVO) is close to zero. Figure 4.1 shows such a motoring curve. The lower graph is obtained from the recorded pressures and calculated volume, while the upper curve is the heat transfer correction. This diagram has been drawn on a very much enlarged scale. In a cycle where combustion has taken place, the cumulative energy released reaches values up to 1500J. The deviation from the zero cumulative energy release is thus not so pronounced.

4.2.9 Conclusions

The various analysis techniques outlined above were tested on experimental data obtained from actual tests. These tests were conducted on diesel oil, methanol/DME combination, methanol and DME separately, and on motoring tests.

With regard to the evaluation of c_p and the mean molecular mass, and hence R, for the products of combustion, close correlation was found using the different methods. This was very useful in that this served as a check that all methods were giving valid results. It was, however, decided to use the most comprehensive method, the 'CHO Fuel System', so as to achieve results as close to the actual process as possible.

$$x = a_1 + b_1\sigma + c_1\sigma^2 \tag{4.4}$$

$$y = a_2 + b_2\sigma + c_2\sigma^2 \tag{4.5}$$

$$z = a_3 + b_3\sigma + c_3\sigma^2 \tag{4.6}$$

and θ is the dimensionless temperature, i.e.,

$$\theta = T/300 \tag{4.7}$$

For the temperature range $300 \leq T \leq 1500K$

$\Omega_3 =$ molecular mass

$$\sigma = S = (\phi + 1)^2$$

and ϕ, y, z, and θ are the same as those given by equations (4.4) to (4.7).

For the temperature range $1500 \leq T \leq 2500K$

$\Omega_4 =$ molecular mass

$$\sigma = S = (\phi + 1)^2$$

and x, y, z and θ are the same as those given by equations (4.11) to (4.3) and (4.7).

A, d, β, a_j, b_j and c_j are constants, and their values are tabulated in table 4.1 for the two temperature ranges for both c_p and molecular mass.

	Specific Heat, c_p		Molecular Mass, M	
Const.	$400 \leq T \leq 1500$	$1500 < T \leq 2500$	$300 \leq T \leq 1500$	$1500 < T \leq 2800$
A	0.99318	0.91153	30.0346	0.20501
α	0.006	1	0.00266	-0.01537
β	0.00098	0.02103	-0.00121	0.000091
λ	-0.56978	1.8395	-6.48722	232.731
a_1	0	-0.33224	0	0.000013
b_1	0	0.3948	0	0.00112
c_1	0	-0.11764	0	-0.000029
a_2	0.06712	0.27269	0	-0.00435
b_2	0.01452	-0.57967	0	-0.00643
c_2	-0.00282	0.15654	0	-0.00176
a_3	-0.00405	0.02401	0.02478	0.02502
b_3	0.01853	-0.58774	-0.2762	-0.2809
c_3	-0.00246	0.329	0.00219	0.00232

Table 4.1: Constants for c_p and M equations (Gulder, 1988)

(d) The 'CHO Fuel System' Method

This is a more general approach, in that fuels containing oxygen can be accounted for. However, the actual calculation procedure is more complex. This approach requires the mole ratios of the product species and the specific heat to be calculated from two separate sources. The mole ratios are found using a subroutine listed in Strehlow (1984) based on a technique described by Weinberg (1957) and the specific heats from polynomials presented by Prothero (1969), as described below.

(i) Multispecies equilibrium calculations

The approach given here has been quoted from Strehlow (1984).

'In a system that contains s species and c component elements the calculations of an equilibrium composition usually becomes difficult when $s-c > 3$. A good practical example is the calculation of the high-temperature equilibrium composition of the products of combustion of a hydrocarbon-air mixture at some specified temperature and pressure. The problem is to cal-

culate the gas phase equilibrium composition of a general $C-H-O-N-I$ system where I is an inert gas such as argon'.

'The species composition of the initial mixture allows for the calculation of the ratios $n_{C/0}, n_{H/0}, n_{N/0}$ and $n_{I/0}$, where n is the atomic ratio of the species as listed. The calculation of the mole ratios is given in the next section. This information, the specified equilibrium pressure and temperature, the list of the species present at equilibrium and the assumption that the gas is an ideal gas are the required inputs to perform an equilibrium calculation'.

'The very general case in which the 14 species $O_2, N_2, H_2, CO_2, CO, H_20, OH, NO, NO_2, O, N, H, CH_4$ and A_r, are present at equilibrium will be considered'.

'To solve for the species composition a technique described by Weinberg is followed. The atomic ratios which specify the fixed atomic composition can be written in terms of partial pressures as follows':

$$n_{C/O} = \frac{\beta_C}{\beta_O}; \quad n_{H/O} = \frac{\beta_H}{\beta_O}; \quad n_{N/O} = \frac{\beta_N}{\beta_O}; \quad \text{and} \quad n_{I/O} = \frac{\beta_I}{\beta_O} \tag{4.8}$$

where

$$\begin{aligned}
\beta_C &= p_{CO} + p_{CO} + p_{CH_4} \\
\beta_O &= 2p_{O_2} + 2p_{CO_2} + p_{CO} + p_{H_2O} + p_{OH} + p_{NO} + 2p_{NO} + p_O \\
\beta_H &= 2p_{H_2} + 2p_{H_2O} + p_{OH} + p_H + 4p_{CH_4} \\
\beta_N &= 2p_{N_2} + p_{NO} + p_{NO_2} + p_N \\
\beta_I &= p_I
\end{aligned} \tag{4.9}$$

with the added equation that the specified pressure of the system is the sum of the partial pressures

$$p = \sum_{i=1}^{4} p_i \tag{4.10}$$

'At this point there are 14 unknowns (the $p_i's$) and only five equations (4.8) to (4.10). Thus nine independent equilibrium equations are needed to solve for the equilibrium composition. The choice is arbitrary and the following independent equations are used':

1. Carbon dioxide dissociation: $CO_2 = CO + \frac{1}{2}O_2$.
$$K_{p1} = \frac{p_{CO} p_{O_2}^{1/2}}{p_{CO_2}}$$

2. The dissociation of water: $H_2O = H_2 + \frac{1}{2}O_2$
$$K_{p2} = \frac{p_{H_2} p_{O_2}^{1/2}}{p_{H_2O}}$$

3. The formation of hydroxyl radicals: $H_2O = \frac{1}{2}H_2 + OH$
$$K_{p3} = \frac{p_{H_2}^{1/2} p_{OH}}{p_{H_2O}}$$

4. The dissociation of hydrogen: $\frac{1}{2}H_2 = H$
$$K_{p4} = \frac{p_H}{p_{H_2}^{1/2}}$$

5. The dissociation of oxygen: $\frac{1}{2}O_2 = O$
$$K_{p5} = \frac{p_O}{p_{O_2}^{1/2}}$$

6. The formation of methane: $4H_2 + CO_2 = CH_4 + 2H_2O$
$$K_{p6} = \frac{p_{CH_4} p_{H_2O}^2}{p_{H_2}^4 p_{CO_2}}$$

7. The formation of nitrogen atoms: $\frac{1}{2}N_2 = N$
$$K_{p7} = \frac{p_N}{p_{N_2}^{1/2}}$$

8. The formation of nitric oxide: $\frac{1}{2}N_2 + \frac{1}{2}O_2 = NO$
$$K_{p8} = \frac{p_{NO}}{p_{N_2}^{1/2} p_{O_2}^{1/2}}$$

9. The formation of nitrogen dioxide: $\frac{1}{2}N_2 + O_2 = NO_2$
$$K_{p9} = \frac{p_{NO_2}}{p_{N_2}^{1/2} p_{O_2}}$$

'The solution of this set of equations can be rendered tractable by noting that the partial pressures of the species N, NO, and NO_2 will always be rather small and that they can be calculated by an 'add-on technique'. This reduces the main calculation to the determination of the composition of a system containing only the three active components C, H and O'.

'To do this one only need assume the partial pressures of three species that independently contain the component elements. Any set that satisfies this requirement may be chosen, such as $p'_{CO_2}, p'_{H_2}, p'_{O_2}$ or $p'_{CO_2}, p'_{H_2O}, p'_{O_2}$ etc, where the primes indicate that the partial pressure is a guess. Using this guess the (incorrect) partial pressures of the remaining species, p'_i, may be calculated using the equilibrium constants. The three mass-conservation equations (4.8) (4.9) and (4.10) are then written by substituting $p_i = p'_i \delta_i$, where δ_i is the correction to the partial pressure which is an unknown. However, the equilibrium relations written in terms of $p_i = p'_i + \epsilon_i$ can be differentiated to yield an expression for each of the remaining $\delta'_i s$ in terms of the guessed species $\delta'_i s$'.

'When these are substituted into the mass-balance set one obtains three equations for the three unknown correction factors, one for each of the three guessed species. Since these equations are linear they are easily solved in determinant form'.

'The calculation converges rapidly if the initial guesses of partial pressures are reasonable and if the guessed species have a relatively large partial pressure at equilibrium'.

'The nitrogen-containing species and the inerts are included in the calculation as 'add-on' species at each step by writing

$$p_{calc} = p - p_N - p_{NO} - p_{NO_2} - p_I$$

where f is calculated from $n_{I/O}$ and the properly weighted partial pressures of the oxygen containing species (equation (4.9)) and the p_N, p_{NO}, p_{NO_2} are calculated from the values of p_{N_2} and p_{O_2} and the appropriate equilibrium constants.'

(ii) Determination of c_p and molecular mass

The specific heat capacity for each of the 14 species listed above was calculated using polynomials derived by Prothero (1969).

The coefficients in each polynomial were based on JANAF thermochemical data and are functions of temperature. The temperature range covered was made up of two parts: from 300 to 2000 K and from 2000 to 6000 K. Each range had its polynomial for each specie.

The accuracy of the polynomials was checked with tabulated data by Prothero. An accuracy comparable to the number of significant figures given in the tabulated values was achieved.

Having calculated the mole ratios of the products of combustion as proposed by Strehlow, the value of c_p was found from:

$$c_p = \sum_{i=1}^{14} n_i c_{pi}$$

where n is the mole ratio and i refers to the i*th* specie.

Similarly the mean molecular mass of the products of combustion was evaluated from:

$$\bar{M} = \sum_{i=1}^{14} n_i M_i$$

from which the mean gas constant was found:

$$R = \frac{R^*}{\bar{M}}$$

The cylinder gas temperature was then calculated at each point using the appropriate R, and the c_p for the cylinder contents.

4.2.3 Gas Temperature

The value of the mean gas temperature at each recorded crank angle point is determined from the ideal gas equation, $pV = mRT$. The evaluation of each of these variables is outlined below.

The values of p are those recorded by the combustion chamber pressure transducer, and represent data in its original form. The pressure recorded by the transducer at IVC was found to be up to 1,5 times atmospheric pressure. In practice, this pressure is close to atmospheric, as confirmed by Obert (1973). The reason for this occurrence is that the pressure transducer measures relative rather than absolute pressure. Therefore the combustion chamber pressure at IVC was set to atmospheric, and all subsequent readings were adjusted accordingly.

The values of V, the volume of the combustion chamber are calculated at each crank angle point according to the position of the piston.

The evaluation of m, the mass of the contents enclosed in the combustion chamber at IVC is dependent on the fuelling system used. When the engine is fuelled on diesel oil, the mass of [illegible]tially enclosed in the cylinder is calculated from the air flowrate. When the engine is fuelled on the methanol/DME combination, DME is drawn into the cylinder with the intake air. This mass is also calculated from the DME flowrate, and is then added to that of the air. With both fuelling systems, the mass calculated at IVC remains constant up to the ignition point. Once the ignition point has been located, the calculation of m is a much more involved procedure, as the full energy release model is invoked. Once the combustion process is initiated, the fuel is assumed to burn in discrete steps. The mass of fuel burnt is calculated by dividing the energy released with heat transfer adjustment, at each crank angle step, by the calorific value of the appropriate fuel. This mass is then added to that of the cylinder contents, and the temperature at the next crank angle point is evaluated. This temperature serves as the new temperature for the calculations of the species present in the products of combustion. This procedure is continued until the mass of the fuel burned is equal to that injected. Once this point has been reached, the value of temperature is based on a frozen composition of the products of combustion, and is then dependent on the combustion chamber pressure only, up to EVO.

Lastly, the value of R, the specific gas constant, is calculated as detailed above. It is also calculated at each crank angle point.

4.2.4 Compression of DME and Air

The method of accounting for the presence of DME in the cylinder has been discussed above. However, some finer points need to be considered here.

DME is drawn into the cylinder with the intake air. When the inlet valve closes, the mixture of air and DME is compressed. However, the assumption made is that DME is converted to products immediately. The mole fraction of the species present is then a function of pressure. On analysing the cumulative energy release curves for DME, two distinct 'steps' are evident. Thus it is assumed that DME is converted to products at IVC, and the energy is 'stored' in the system and released in two stages prior to the methanol injection. When methanol is injected, a short delay occurs before burning starts, or in certain cases, methanol burns at the injector as it is being injected. These events will be discussed in detail in Chapter-6, when the results are analysed.

4.2.5 Calculation of Apparent Mass Burned

The method of calculating the apparent mass of fuel burned has been outlined above. However, some of the assumptions on which these calculations have been based are discussed here.

The approach used in calculating the apparent mass of fuel burned has been based on that suggested by Krieger and Borman (1966). The fuel is assumed to burn to completion and at equilibrium at each crank angle step. The mass of fuel burned is calculated by dividing the energy released, with heat transfer adjustment, in each crank angle step by the calorific value of the appropriate fuel. This mass is then added to that in the cylinder and the new temperature is calculated, as described above. However, one important aspect needs clarification.

The primary input for the energy release model is combustion chamber

pressure. This pressure, sometimes undergoes fluctuations, as a result of knock or the 'organ pipe' effect due to the narrow passage connecting the combustion chamber to the transducer diaghram. The result is that the energy release calculated per step sometime becomes negative, and consequently the mass burned is also negative. This mass, whether positive or negative, is left unchanged throughout the calculations, except where the atomic ratio is required for the determination of the mole fraction of the species present in the products of combustion.

4.2.6 Entropy

The value of the change in entropy for each crank angle step is calculated from the relation

$$\Delta s = \Delta q / T$$

where Δq is the energy released, with heat transfer adjustment, for each crank angle step. The temperature T is the mean cylinder gas temperature at the appropriate interval as calculated above.

The resulting $T - s$ diagram is another useful technique which, when used in conjunction with the other techniques, helps in the understanding of combustion phenomena.

4.2.7 Heat Transfer in the Engine

In order for the energy release model to represent the real situation as closely as possible, the heat transfer in the engine has also been modelled.

The first approach was to adapt the equations developed by Annand and Ma (1970) because these were derived for an engine similar to the one used in the present research. However, these equations were found to be not adequate. When applied to a motoring curve (section 5.3.1), the compression/expansion process was found not to be adiabatic (which it should be

if heat transfer is correctly accounted for) but indicated a net heat loss throughout.

It was then decided to derive an equation for heat transfer for this engine in particular.

4.2.8 Basis of the Heat Transfer Equation

The starting point for a convective heat transfer equation for internal combustion engine work is:

$$Nu = C_1 Re^n Pr^m$$

where C_1, m and n are constants. From this equation, the convective heat transfer coefficient can be calculated.

The Reynolds number used is that for pipe flow, where the characteristic length is the cylinder bore, and the velocity is the mean piston speed.

If the mean piston speed is used, then Re varies with density and viscosity. However when the instantaneous piston speed is used, Re fluctuates with speed. This means that at TDC, Re is zero so that no heat transfer takes place. This is of course not true.

The heat transfer model was then refined by adding two further components. These were the radial velocity of the air into the piston bowl and a swirl component resulting from the inlet valve geometry.

Both these velocity components were calculated using equations derived by Dent and Derham (1974). These authors studied the air motion in a motored four-stroke compression ignition engine. They put forward a mathematical model for the mean air swirl motion during induction and compression periods. A model for the inward radial component flow that is spiralling towards the combustion bowl was also proposed.

The details of the relevant equations are given in Appendix A.

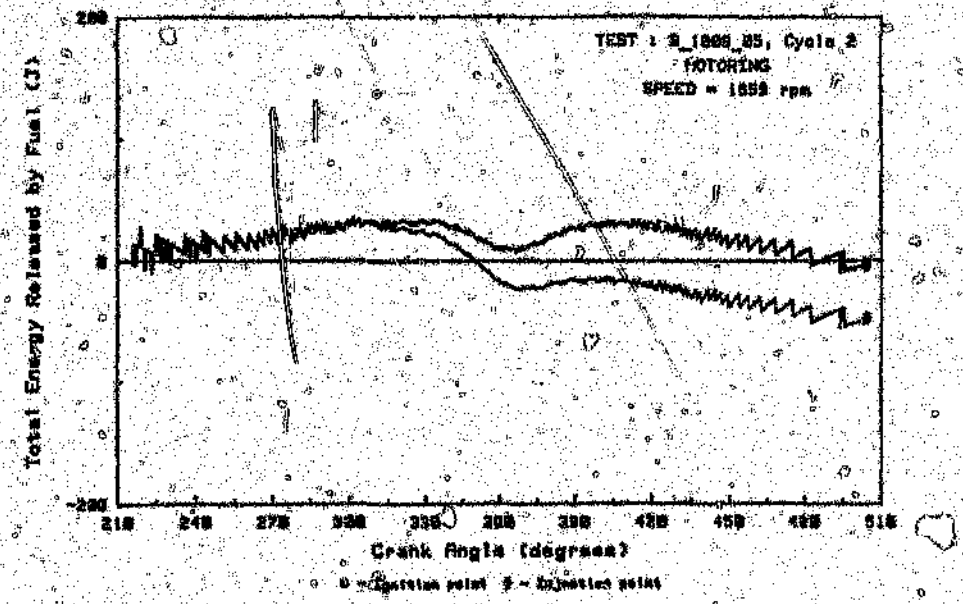

Figure 4.1: Cumulative energy released versus crank angle for a motoring cycle

The heat transfer model is believed to be a comprehensive one, in so far as various velocity components are considered. Instantaneous values of gas velocities, density, viscosity and exposed combustion chamber area are calculated at each crank angle step and used to calculate the corresponding heat transfer. Although the heat transfer model is not perfect throughout the cycle, it serves its purpose adequately, as will be shown in the discussions of the results.

The model has been calibrated with a motoring cycle in an effort to make it as realistic as possible.

Each method of analysis conveys information on certain parts of a cycle. When this information is put together, a comprehensive 'picture' of the combustion is obtained. This will become clearer when actual results are discussed.

The energy release and heat transfer models are not believed to be faultless, as continuous improvements and refinements are being made. However, these models serve their purpose well in understanding unusual combustion phenomena as in the case of the methanol/DME fuel system.

Chapter 5

EXPERIMENTAL EQUIPMENT AND PROCEDURE

A short description of the equipment and instrumentation used for the research is given below. The detailed specifications are given in Appendix 1.

The experimental procedure considers the preparations required for the engine and equipment so as to formulate a meaningful testing sequence. The testing procedure ultimately followed was arrived at after many trial runs. The data captured was analyzed in detail to assist in deciding where and how improvements could be made. The system whereby a methanol/DME combustion cycle was immediately followed by a motoring, a methanol only or a DME only cycle is believed to be novel in compression ignition engine work. Depending upon the engine speed, one or two such cycles would follow the combustion cycle, after which both fuels would be reinstated. The information gained this way was of great value when consecutive cycles were compared. The effect of the single fuel, for example, could be clearly seen.

5.1 Experimental Equipment

5.1.1 The Engine and Fuel System

The engine used for the research programme was a direct injection two cylinder, four stroke, water cooled Petter type PH2W of 1330 cm^3 capacity. The fuel setting of the injectors was achieved by the manual simultaneous adjustment of the control racks on the injector pumps. The racks were linked together rigidly to ensure equal displacement on each pump.

The fuel supply to each pump was controlled separately. The engine could be run on one cylinder while motoring the other. An electrically operated solenoid trip switch was linked to the pump so that the fuel could be cut off instantaneously to capture a motoring or a DME only combustion cycle. The factory fitted governor was disconnected and an over-speed safety trip system was installed in its place. Should the engine speed exceed 2100 *rev/min*, the fuel supply to the pump would be instantaneously shut off. This system allowed the engine to run at any desired speed in the range of 1100 to 2000 *rev/min*, and at any load.

5.1.2 The Dynamometer

The engine was loaded by means of a water cooled eddy current dynamometer coupled to the output shaft. Engine speed was monitored by a tachogenerator mounted at the free end of the dynamometer. The load applied to the dynamometer was measured by a strain gauge glued on to a load cell. The load cell was firmly bolted onto the frame of the dynamometer under the calibration arm. Both the tachogenerator and the load cell were calibrated appropriately.

5.2 Instrumentation

The engine's performance was evaluated by monitoring a number of parameters. These may be classified as steady or transient.

The steady state parameters remained, as the name implies, reasonably steady as long as engine conditions did not change. The outputs of the instruments used for these parameters were all recorded by a data logger. These were:

- temperatures
- atmospheric pressure
- air flow
- engine speed
- torque
- fuel flow rate

The transient type parameters were recorded by an eight-channel data transient recorder. These were:

- cylinder pressure
- injector pressure
- injector needle lift
- degree crank angle ($^{\circ}CA$)
- top dead centre (TDC)

A number of other parameters were recorded manually and fed into the computer program as required. These were:

- dimethyl ether flow rate
- smoke when the engine was fuelled on diesel.

5.2.1 Steady State Parameters

These were measured as follows:

Temperatures: iron-constantan thermocouples were used for this purpose.

Atmospheric pressure: a pressure transducer with a built-in amplifier was made up in the laboratory. The sensitivity of the device was 1 $mbar/mV$.

Air Flow: an orifice plate designed according to BS 1042:1984 was used to measure the amount of air required by the engine. The pressure difference across the orifice plate was read off an electronic micromanometer.

Engine speed: use was made of a tachogenerator mounted on the end shaft of the dynamometer.

Torque: this was measured by strain gauges glued onto a load cell, forming a four active arm Wheatstone bridge.

Fuel flow rate: this was monitored by a positive type flow detector with digital and analog read-outs. A positive displacement pump was fitted in the line before the flow meter to prevent the formation of vapour lock in the fuel line. This was particularly necessary in the case of methanol.

5.2.2 Transient Parameters

Transient type parameters were measured as follows:

Cylinder pressure: variations in cylinder pressure were measured on the cylinder closest to the engine's front output shaft. To achieve this, a passage was drilled through webs in the cylinder head, taking the shortest possible route to the cylinder.

Although a high temperature piezo-electric pressure transducer was used, it was considered safer to maintain the transducer body and diaphragm as cool as possible, to avoid damage. To this end, a purpose made brass

water cooled housing to receive the transducer, was built. This housing was mounted on the outside of the cylinder head, in line with the passage. Inlet and outlet water connections were made, to ensure a continuous supply of cold water through the housing.

The output signal of the pressure transducer was fed to a charge amplifier before being recorded.

Injector lift: the displacement of the injector needle was measured by means of a linear variable differential transformer. The transformer was mounted in a purpose made brass holder fixed by means of grub screws onto the injector body. The injector spindle was extended through the back of the injector body so that its end was about half way into the cylindrical passage of the transformer.

°CA and TDC: these were monitored using an optical marker with a 0,1 ° resolution. The unit was mounted on a flange at the front end of the output shaft of the engine. The *°CA* and TDC signals were recorded on two separate channels of the transient recorder.

5.2.3 Manual Inputs

The parameters which were manually recorded were measured as follows:

DME flow rate: A bottle of DME was mounted with its outlet pointing down. This ensured a consistent composition as liquid was extracted. The bottle's outlet was connected to two rotameters, one for each cylinder. The gas was admitted into the engine manifold as close as possible to the inlet valve of each cylinder. The inlet pipe was cut off at a 45° angle facing the valve, so as to prevent cross flow between the cylinders. Furthermore, an electrically operated solenoid valve was put in the DME line on the test cylinder as close to the manifold as possible. The DME flow could then be cut off instantaneously to capture a motoring cycle, or a methanol only cycle.

Smoke emission: engine exhaust gases were extracted some distance away from the exhaust manifold and passed through a smoke-meter. The arrangement was such that the required quantity of smoke would flow through the meter when readings were being taken. The excess was exhausted to

the atmosphere, through the smokemeter's relief valve.

5.3 Preliminary Tests

Before any experimental procedure could be drawn up, many exploratory tests were run on diesel oil. In this way, the engine, the auxiliary equipment, the instrumentation and the controlling computer programs could be tested to ensure proper functioning. As these tests were run and the data analyzed, improvements were made wherever necessary.

The description given below relates to the development of the most significant aspects of the preliminary tests.

5.3.1 Location of Top Dead Centre

The first method used to generate degree crank angle and the TDC markers was by the toothed disc method. Slots of equal width were cut along the circumference of a steel disc, with one slot per degree crank angle. A second disc with a single slot was used to indicate the position of TDC. Both these discs were mounted on the front end of the output shaft of the engine. A photo cell was mounted across the slots of each disc. A circuit was built so that the TDC was used to trigger the transient recorder, once armed.

However, a number of problems were encountered with this system. The two major ones were that the slots could only be machined every one degree crank angle and the photocells were very sensitive to other sources of light. A completely sealed system was required.

It was then decided to acquire an optical crank angle marker, manufactured by AVL. It generates a pulse very 0,2° crank angle on one disc and has a trigger marker on a second disc. The trigger marker was aligned with TDC of the test cylinder as accurately as possible. After a few tests, fine adjustments were made by rotating the trigger disc in the appropriate direction. The following method was used to ensure that the alignment was within specification.

The test cylinder was motored over the speed range from 1000 to about 2000 *rev/min*. Measurement of pressure at every 0,2°*CA* and the TDC marker were recorded. A large number of tests were performed over the entire speed range, with many at essentially the same speed so as to ensure repeatability. The pressure versus crank angle data was processed to calculate the first derivative, $dp/d\theta$, particularly in the region 355° to 365°*CA*. The value of $dp/d\theta$ was plotted against crank angle. Theoretically, then, at 360°*CA*, $dp/d\theta$ should be zero. However this was not the case with many tests. The distance between the point of zero $dp/d\theta$ and the 360°*CA* was measured and converted to degrees. These offsets were then plotted against speed and the general trend that emerged was a straight line. The amount of offset was less as the speed increased because of a reduction in leakage. Using linear regression, a straight line was fitted to the data. The scatter about the line indicated that TDC was located within +0,21°*CA* as compared to +0,2°*CA* specified by the manufacturers. This regression equation was built into the software so that the data would always be adjusted according to speed.

5.3.2 Optimization of Injection Timing

It was essential that, for comparative purposes, the engine timing be set at its optimum. This could only be achieved by varying the injection timing and then analysing the performance curves.

The injection timing was checked and set by the spill method at 28°BTDC, as recommended by the manufacturers.

Having done this, injection timing can be advanced or retarded further by adjusting the fuel pump rocker. However, for experimental purposes, it was imperative to ensure that any particular timing could be repeated. In order to ensure repeatability, injection timing was retarded by adding an equal number of shims under each pump body. The shim thickness was 0,25 mm. The effect of this was to raise the pump so that the pump cam would come in contact with the pump later. As it happened it was found necessary to advance the timing from its 28° BTDC position.

The injector opening pressure was also checked and adjusted to 200 *bar*, as per specifications.

A number of tests were then carried out to locate optimum injection timing.

Starting at 28° BTDC, and with three fuel settings referred to as minimum, middle and maximum, data was captured to cover the entire speed range. The speed interval was approximately 100 *rev/min*.

From the data gathered, the performance characteristics were evaluated and plotted against speed. These were:

- Torque
- Power
- Brake specific fuel consumption
- Brake thermal efficiency
- Brake mean effective pressure
- Smoke

Some combustion parameters were also calculated and plotted against speed, as follows:

- Start of injection
- Start of combustion
- Ignition delay

Ignition timing was retarded by inserting 1 shim beneath each pump body and the above procedure was repeated. This process was continued until the fuel pumps were raised by three shims each.

Each of the above parameters were plotted for all three fuel settings. In this way, the effect of fuel injection timing could be determined.

The fuel setting for optimum torque, and therefore power was achieved by retarding injection with two shims. The start of the injection process was thus now at 17° BTDC.

The brake thermal efficiency was lower at maximum fuel setting, but was more or less the same for both minimum and middle fuel settings.

Smoke level was measured for every test using the Hartridge Smoke Meter. On the minimum fuel setting the smoke emitted was overall lower across the entire speed range with two shims. At the highest speed a maximum of 48 Hartridge Smoke units (HSU) was obtained against 60 HSU with original timing (no shims). With middle fuel setting, the maximum smoke reading was 75 HSU versus 86 HSU. However, in the case of maximum fuel setting, the position was reversed. Original timing produced a maximum of 85 HSU while with two shims 99 HSU were emitted. Generally speaking, maximum fuel setting produced heavy smoke at all timings.

The start of injection was determined from the plot of the first derivative of the injector pressure. The injector pressure diagram, figure 5.1 shows the pressure variation in the fuel line. The position at which the maximum fuel line pressure occurred, was taken to be the point where the injector needle started lifting and hence the start of injection. This position was located on the injector pressure derivative plot where the value of the derivative was equal to zero.

The start of combustion was found from the plot of the first derivative of the cylinder pressure. This was taken as the point where the derivative showed a sudden and very steep rate of pressure rise as shown in figure 5.2. This point was not so easily determined from the pressure trace itself.

With the values of crank angle at which the start of injection and the start of combustion available, the ignition delay in degrees crank angle was found. Since the ignition delay is a function of speed, it was converted to real time in seconds. Values of ignition delay versus speed were plotted for each setting.

The general pattern was quite clear, that the ignition delay decreased in real time with an increase in engine speed. For any fuel setting, the longest delay occurred with the injection timing as recommended by the manufacturers. As the injection timing was progressively retarded, the ignition delay was reduced. This was found to be the case with all fuel settings. The shortest ignition delay occurred between the two and three shims. However, coupling this with the torque curves, the two shims timing was still

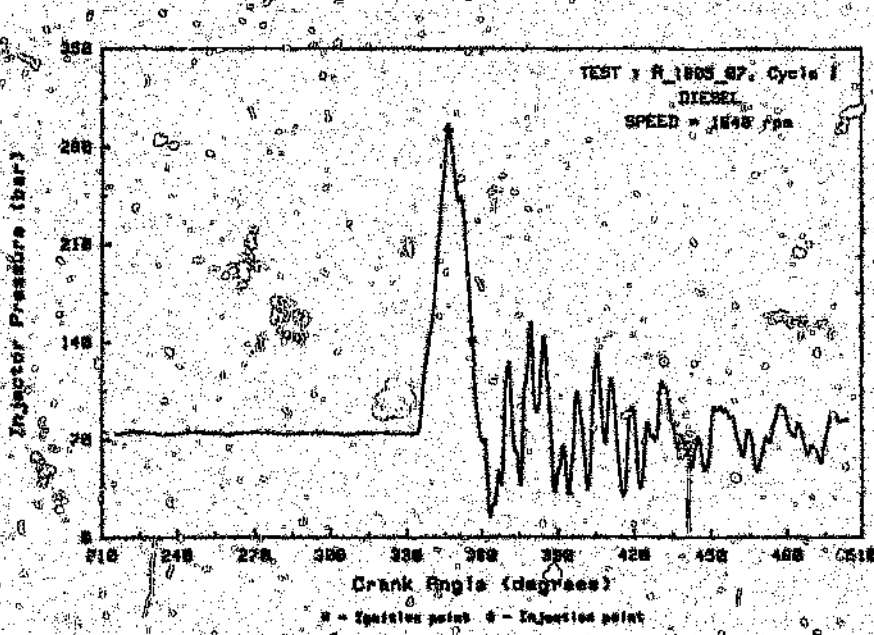

Figure 5.1: Injector pressure versus crank angle

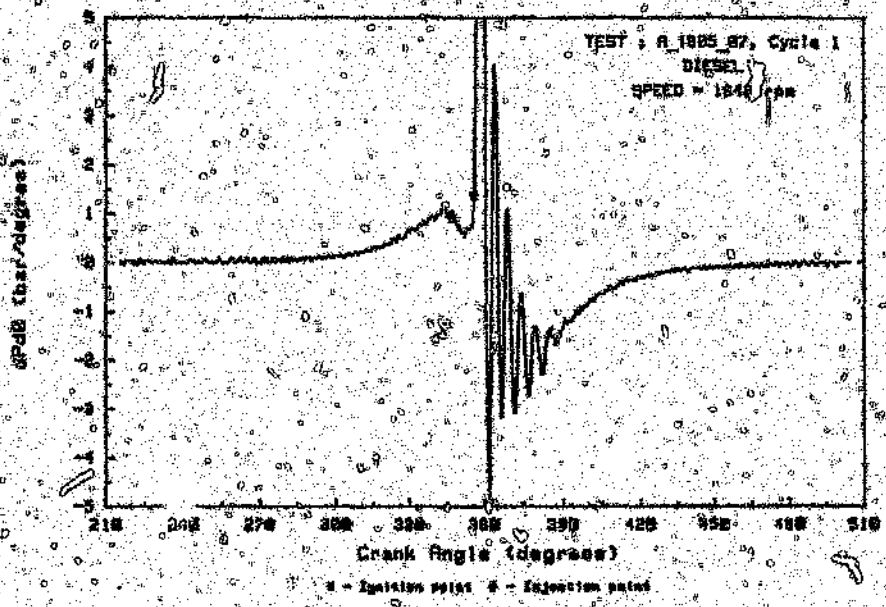

Figure 5.2: Derivative of cylinder pressure versus crank angle

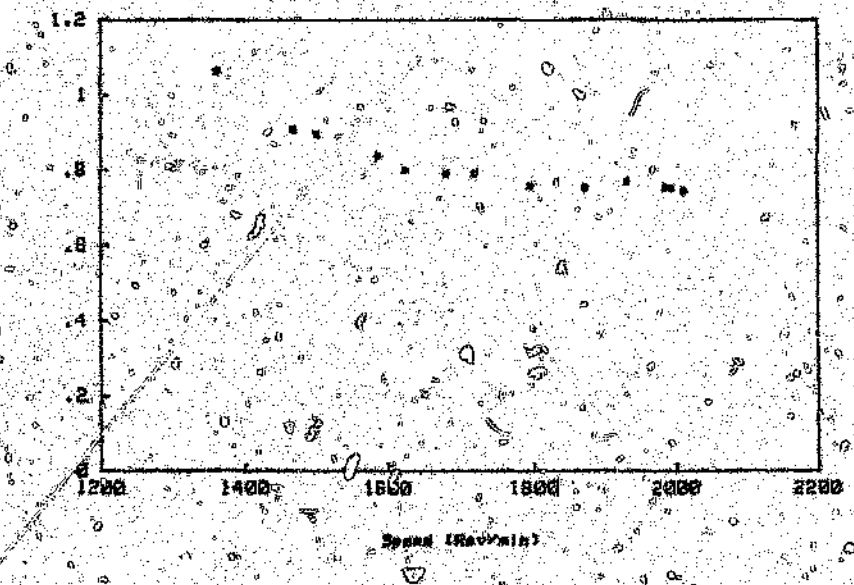

Figure 5.3: Ignition delay versus speed

preferable. Figure 5.3 shows the ignition delay variation for one fuel setting.

The other parameter, namely start of combustion to TDC in $^{\circ}CA$, was determined to locate the position of TDC relative to peak pressure. If the steep rate of pressure rise and the peak pressure occur before TDC, then a substantial amount of negative work is done. Retarding the injection timing therefore reduces the net output of the engine but the start of combustion would naturally approach TDC. The general trend that emerged was that for any given timing the start of combustion approached TDC as the speed increased. This was to be expected. Furthermore as the number of shims increased, the start of combustion was closer to TDC. In the case of the three shims, the ignition of the fuel occurred partly before and partly after

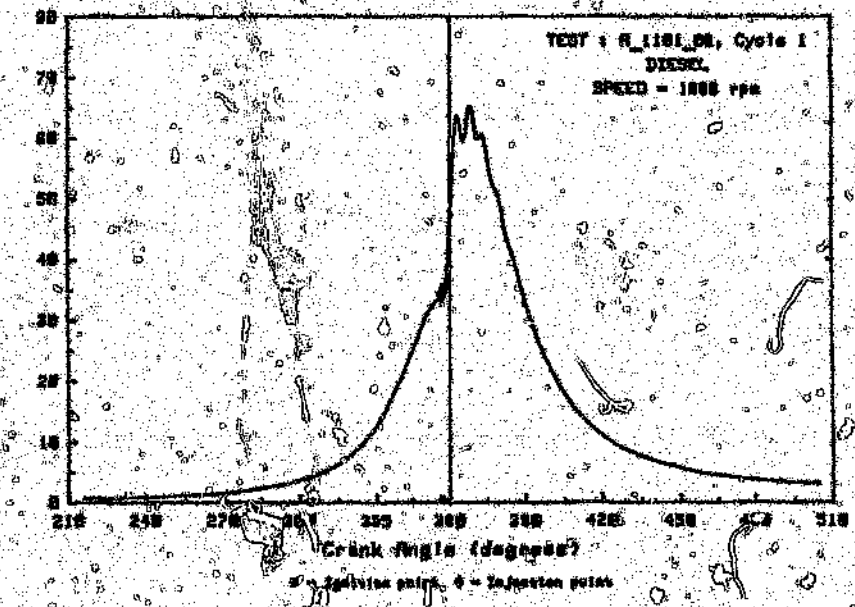

Figure 5.4: Cylinder pressure versus crank angle

TDC as shown in figure 5.4. However, a reduction in power output was evident.

5.3.3 Supplying DME to the Engine

The supply of a new fuel to an engine always presents hazards. Therefore, this exercise must be approached with great caution.

The DME container was fixed to a nearby wall by means of brackets, in an upside down position. The purpose of this was to draw liquid from the bottle as opposed to a liquid/vapour mixture.

The liquid was then fed to a rotameter so that the mass flowrate supplied to the engine could be measured. On leaving the rotameter the liquid was throttled through a fractionally opened needle valve so as to convert it to the gaseous phase. From the valve the gas was directed to the centre of the air intake pipe approximately 150 *mm* above the inlet manifold. The pipe feeding the DME to the engine was placed perpendicularly to the air flow with holes facing the incoming air stream. This was done to allow the mixing of the incoming air with the DME, before diverting to the cylinders.

A technique now had to be developed to ensure smooth starting on DME. In the first attempts, the fuel lines, pumps and injectors were flushed with methanol until all the diesel was purged out. The rotameter was opened fractionally while the engine was motored with the starter. Once combustion occurred, the amount of DME was increased until the speed was about 1000 *rev/min*. The fuel pumps were then opened until the required amount of methanol was reached. The rotameter was also opened up slowly and the load on the dynamometer was increased until a desired running condition was achieved.

Various tests were conducted where the mass flowrate of the fuels, the load and speed were changed individually. These tests were all recorded and analyzed so as to assist in the formulation of a testing procedure. It also served the purpose of observing the behaviour of the engine with varying amounts of DME.

Having analyzed these tests, it was decided to improve the method of supplying DME to the engine, namely to feed each cylinder independently, as described in Section 5.2.3. The method of recording the data was modified to account for this change. This is described in Section 5.3.5.

5.3.4 Heating and Cooling the Inlet Air

The analysis of the DME/methanol pressure crank angle diagrams revealed a slight hump shortly before the start of combustion. When the first derivative of pressure was plotted, a sudden change of slope was found to correspond with the hump on the pressure trace.

It was therefore decided to see what effects an increase or decrease in inlet

air temperature would have on the position of this hump.

Cooling of the inlet air was achieved as follows:

A 5 m long copper tube of internal diameter 10 mm was wound into a coil of internal diameter 200 mm. One end of the copper coil was connected to an air supply, and the other to the air intake of the engine. The coil itself was placed in an insulated plastic container filled with liquid nitrogen. The inlet air temperature was measured in the intake manifold, by means of a digital voltmeter with a thermocouple module reading in degrees Celsius. The lowest temperature reached was -5,5°C.

Heating was achieved by means of a 2 kW electric heater installed just above the air intake manifold. A maximum temperature of 41,8°C was reached before the engine stalled.

An analysis of the pressure trace and its derivative indicated that the position of the hump shifted with a change in temperature. A decrease in temperature was found to delay the DME humps whereas an increase in temperature had the opposite effect.

The inlet air temperature for all subsequent tests was left at ambient.

5.3.5 Data Acquisition Triggering System

The data acquisition system, namely the transient recorder, was originally set up to capture single cycles. The starting point of the cycle was the TDC of the induction stroke, and the end point the TDC of the exhaust stroke. Thus data would be considered acceptable if the above points were included.

The transient recorder and data logger data was recorded on disc. It was then processed to plot the parameters of interest and perform all the relevant calculations.

This system worked very well for a single cycle and was found to be well suited for a single fuel, such as diesel oil. However, when the same system was used on methanol and DME, other considerations arose.

When analyzing, for example, a pressure trace or a cumulative energy release diagram for two fuels, it is not possible to distinguish the contribution effect of each fuel. The solution was to have one cycle with both fuels, and one cycle with, say, DME only. However, for any comparison to be drawn, ideally all other conditions should be essentially identical.

The number of cycles read by the transient recorder depends upon the sampling rate. This number increases with the sampling rate. However, this is accompanied by a decrease in resolution. It was decided to adjust the rate so as to acquire two or three cycles per test, depending on engine speed.

A control system was built so as to capture multicycles, where the first was a dual fuel cycle and the subsequent ones, a single fuel. A triggering device was made up so that the test cylinder could run on both fuels, DME only or methanol only, or could be motored.

The device consisted of three toggle switches. The interruption of any one, would send a signal to the transient recorder to initialize reading of data. The pressure traces were displayed on the oscilloscope, and if full cycles were not captured, the transient recorder was triggered again. This was repeated until the pressure traces were satisfactory. One toggle switch controlled the solenoid valves on both fuels, one the DME only and one methanol only. The on-off action of the solenoid was sufficiently fast to allow the reading of the first cycle on both fuel, the second and third on single fuel or no fuel. The fourth cycle was once again on both fuels, but was not recorded. This was confirmed by increasing the sample rate and observing the injector needle lift trace.

The comparison of the first and second cycle was now a possibility, since engine conditions were virtually unchanged between cycles.

The method of acquiring two consecutive cycles, a dual fuel combustion cycle followed by a single fuel or motoring cycle is believed to be novel. This is with particular reference to compression ignition engine work. This approach has not been encountered in the literature reviewed, nor has it been considered by engine testing equipment manufacturers such as AVL. This was confirmed with AVL.

5.3.6 Computer Programs

This research programme consisted of two components: the acquisition of data, and the subsequent analysis. Consequently software programs were written for each component.

The data acquisition program was developed to control the sequence of reading of the data. The data was then stored on disc, and a printout listing test code, speed, performance parameters, mass flow rate of fuels, and temperatures was available for each test. The same program was used for single or multi cycle tests, as well as for diesel and methanol and DME. The fuel type was designated in the test code so that the correct fuel properties were used.

This data was then used as input for the analysis program. It recognised the number of cycles in a test by the number of TDC marks recorded, and the type of fuel for each cycle.

5.4 Experimental Procedure

Having completed the preliminary tests and the setting up of the instrumentation and equipment, the total system was tested and found to run very well. The relevant instrumentation was calibrated, after which single and multi-cycle tests were conducted.

5.4.1 Testing Procedure

Various instruments required calibration before being put into operation. These included, the cylinder pressure transducer, fuel line pressure transducer, injector needle lift, rotameter, fuel meter, tachometer, load cell and airflow meter. The calibrations were repeated at regular intervals, to ensure consistency of the results. The various calibration equations were included in the data capture programme. The calibration procedure and a typical set of results for each is given in Appendix C.

Having carried out the preliminary tests to ensure the optimum timing of the engine, tests with methanol and DME were undertaken.

Some preliminary tests were carried out to see the effects of varying certain parameters such as: load, speed, fuel mass flowrate and DME mass flowrate. These tests were analyzed mainly in terms of energy release. From these results the testing procedure, required to emphasize certain aspects of the energy release, was decided upon.

Starting with optimum timing, as found for diesel fuel, three load conditions were chosen. These were termed high, medium and low. With each of these loads the mass flowrate of methanol was decreased gradually while that of DME was increased so as to keep the speed approximately constant. These fuels were varied until the engine was unable to keep up the desired speed. Fo each setting two tests were recorded to ensure repeatability.

The same procedure was repeated with the injection timing advanced and retarded.

All these tests were recorded in the multi-cycle mode so that the first cycle was a dual fuel, while the second and third were DME only.

Chapter 6

RESULTS AND DISCUSSION

Two sets of results are presented and analysed in this chapter. The first deals with diesel oil fuelling and the second with the methanol/DME combination.

The examination of diesel fuelling serves three purposes. First, in dealing with a known situation, it provided a check on the correct functioning of the instrumentation and the absence of software errors. Secondly, it permits the demonstration of the capabilities of the techniques that were developed, particularly with regard to their mutually corroborative and complementary nature. Finally, it provides the baseline information that allows unusual features of the combustion of methanol/DME to be recognized.

The results on methanol/DME fuelling are in turn, presented in two sections, the first dealing with engine performance, and the second with combustion characteristics.

The first aspect is dealt with briefly, since the assessment of performance on alternative fuelling is not the primary aim of their study. Sufficient detail is, however, provided to permit some evaluation of the practical aspects of methanol/DME fuelling. Of greater importance is that engine performance is the macroscopic manifestation of combustion characteristics the study of

which is the focus of this thesis. The combustion of methanol/DME is thus treated in detail and the insight thereby gained is used to explain the observed performance data. Results are given for two levels of load, both at the same constant speed, with a range of ratios of methanol to DME for each load (power). Additionally, for each test point on such a dual fuelling, a single combustion cycle on fuelling with DME alone, at otherwise identical conditions, is reported and analysed.

6.1 Diesel Fuelling

6.1.1 Test Conditions

As discussed in Chapter 5, injection timing was adjusted to the 'best average' value for maximum power, over the speed and load range of the engine. This injection timing was unaltered throughout the tests on diesel oil and on the methanol/DME fuel combination that are reported in this study.

For diesel oil two fuel settings were chosen: the minimum that the engine could sustain over a reasonable range of speeds and the maximum corresponding to the highest permissible smoke emissions. One test has been selected from each setting for presentation here. The speed for the test at minimum fuel setting was the closest available to the mean speed of that of the methanol/DME tests.

The overall test conditions are shown in Table 6.1

Fuel Setting	Speed *rev/min*	Brake Power *kW*	Fuel Flowrate *kg/hr*	Equivalence Ratio ϕ
'minimum'	1866	7,88	2,413	0,6423
'maximum'	1466	8,55	2,627	0,8698

Table 6.1: Test conditions, diesel fuelling

Although the brake power for the two cases does not differ greatly, the

speed does and certain aspects of combustion (to be discussed below) exhibit sufficient differences to make presentation of both desirable. Mixture strength is in both cases lower than stoichiometric (lean $\phi < 1$) which is a requirement for the validity of the method of calculating equilibrium compositions.

6.1.2 Analysis and Discussion

The thermodynamic analysis techniques described in previous chapters are now applied to the above tests on diesel fuelling.

Typical pressure versus crank angle diagrams for each fuel setting are shown in figures 6.1 and 6.2. These diagrams give data as collected and not smoothed. Table 6.2 summarizes some of the important features. The near-identical crank angle positions for maximum pressure are co-incidental, and result from pressure oscillations after TDC. These oscillations are believed not to be associated with knock, but rather the result of the initial steep pressure rise and possible amplification in the passage between the combustion chamber and the transducer diaphragm.

Figure Number	Fuel Setting	Peak Pressure		Injection	Ignition
		bar	*°CA*	*°CA*	*°CA*
6.1	'minimum'	71,12	363,2	348,4	358,2
6.2	'maximum'	74,64	363,8	345,6	355,0

Table 6.2: Summary from pressure crank angle diagram

Taking ignition lag as a first approximation to be constant with respect to time, it is clear that a reduction in speed results in the advancement of the crank angle ignition point. Thus figure 6.2 (lower speed) shows ignition to have occurred 'too early' with the pressure rise completed before TDC, thus leading to an increase in 'negative work'. Figure 6.1 (higher speed) shows a more favourable, later ignition and a combustion pressure rise that optimizes the net work output. Thus the supposedly 'best average'

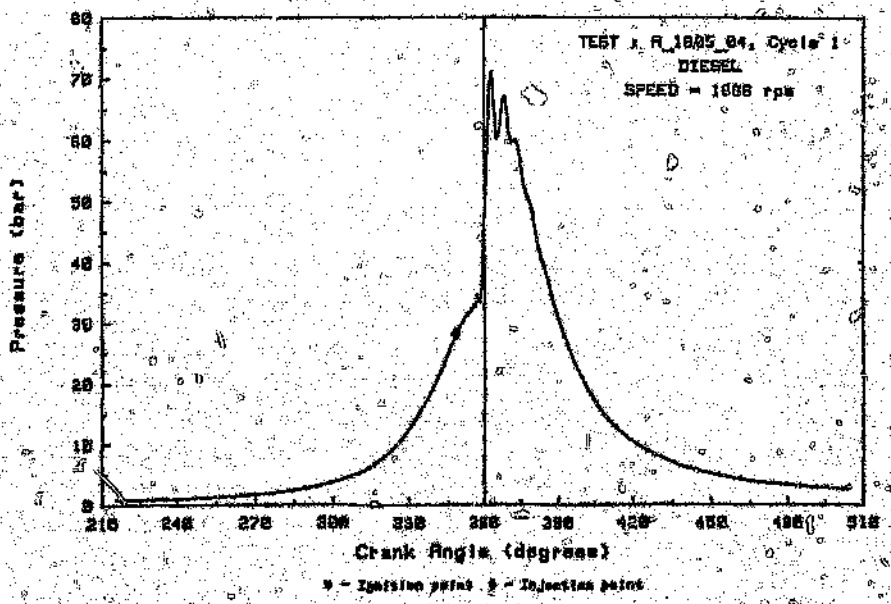

Figure 6.1: Combustion chamber pressure versus crank angle for minimum diesel fuelling

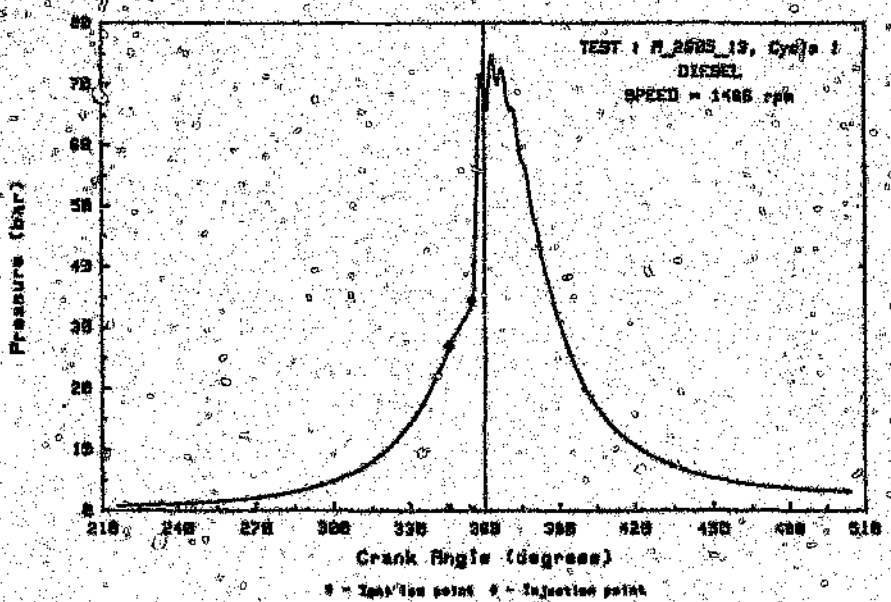

Figure 6.2: Combustion chamber pressure versus crank angle for maximum diesel fuelling

injection timing was in fact optimized for higher speeds. Examination of these figures suggests that in both cases a slight decrease in the rate of pressure rise occurs between the injection and ignition points. As will be shown later, this is the result of the vaporization of the fuel. This effect is very distinct in some of the other plots, for the same cycle, to follow, and less so in others.

It is useful to recall how the injection and ignition points were found. Figure 6.3 shows the injector line pressure versus crank angle, for the maximum fuel setting. The injection point indicated on the diagram was taken to correspond to the position of maximum line pressure. This was the position where the derivative of the line pressure versus crank angle, was zero, after the initial steep pressure rise. The ignition point was found numerically from the pressure versus crank angle records, its position corresponding to the onset of the steep pressure rise.

The combustion chamber pressure versus volume diagrams are shown in figures 6.4 and 6.5. The volume was calculated at every 0,2°CA and plotted against the appropriate pressure reading. In both instances the initial combustion of the fuel occurs almost at constant volume. The quenching effect of the fuel is again discernible between the injection and ignition points.

Figures 6.6 and 6.7 show the same experimental data as in figures 6.4 and 6.5, but as the natural logarithms of non-dimensional pressure, p/p_1, and non-dimensional volume, V/V_1 (p_1 and V_1 being the values at IVC).

The data has, however, been subjected to mild four point moving average smoothing. This was necessary since the transformation of p to $ln(p/p_1)$ magnifies the fluctuations present in the original data to the point of causing confusion. The pumping loops in these figures should be ignored; their irregular appearance (despite smoothing) is due to the limited resolution of the transient recorder. The slopes of the power loops represent the polytropic index, n, to be discussed below. The effect of fuel vaporization is again just discernible and initial combustion is seen to have occurred at nearly constant volume.

The variation of the polytropic index with crank angle is given in figures 6.8 and 6.9. The data results from the numerical differentiation of the

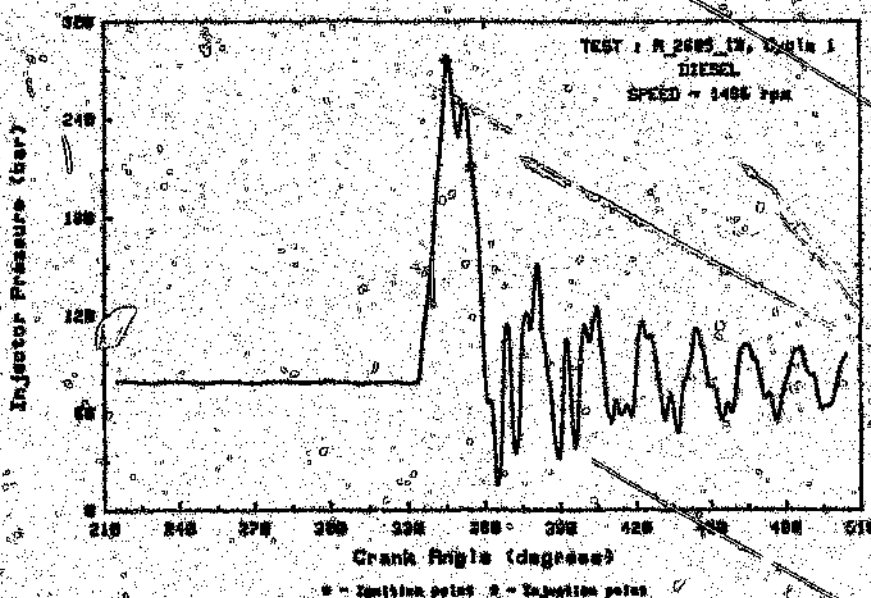

Figure 6.3: Injector line pressure versus crank angle for maximum diesel fuelling

data of figures 6.7 and 6.8 and are thus purely experimental, except for the smoothing previously discussed. In the region from 355° to 370°CA, n shows very large fluctuations resulting from those shown in the pressure diagrams of figures 6.1 and 6.2 and from the fact that for a constant volume process, $n = \pm\infty$.

The values of the ratio of the principal specific thermal capacities, $\gamma = c_p/c_v$, are superimposed on these diagrams. These values were calculated using the energy release model, as described in the previous chapters. Having both n and γ on the same diagram is of assistance in the determination of the occurrence and direction of the heat flow. In the present context 'heat flow' includes both heat transfer in the normal sense to and from the trapped gas and energy release (or absorption) due to combustion.

During the compression stroke, the polytropic index shows a downwards trend, for both fuel settings. The mean value of n starts slightly above that of γ at 290°CA and then decreases to less than γ at the start of the vaporization dip. Thus where $n > \gamma$, the temperature of the gases is increasing, over and above that due to adiabatic compression because of heat transfer from the cylinder walls. At the instant $n = \gamma$, the process is adiabatic with the temperature rise being only due to compression. In the region where $1 < n < \gamma$ the gas temperature is *rising* (due to compression) but heat transfer takes place from the gas to the walls of the cylinder.

Thus the principal areas of interest here are from about 290° to 355°CA and from 380° to 450°CA. The effect of the vaporization of the fuel is very clear in these figures, as shown by a large drop in the value of n just before the steep fluctuations around TDC.

It should be noted that in both figures 6.8 and 6.9, n drops to a minimum value of 0,85 during the 'vaporization dip'. Values of $0 > n > 1$ (during compression) indicate heat extraction accompanied by a falling temperature. The presence of this temperature drop will be confirmed on examination of the temperature versus crank angle diagram.

During the expansion stroke (in the analyzable region beyond 380°CA) the polytropic index rises in the range $1 < n < \gamma$ and appears to asymptote to approximately γ. This implies a net heat supply to the system, asymptoting to zero, while the temperature falls. As stated earlier, this 'net heat'

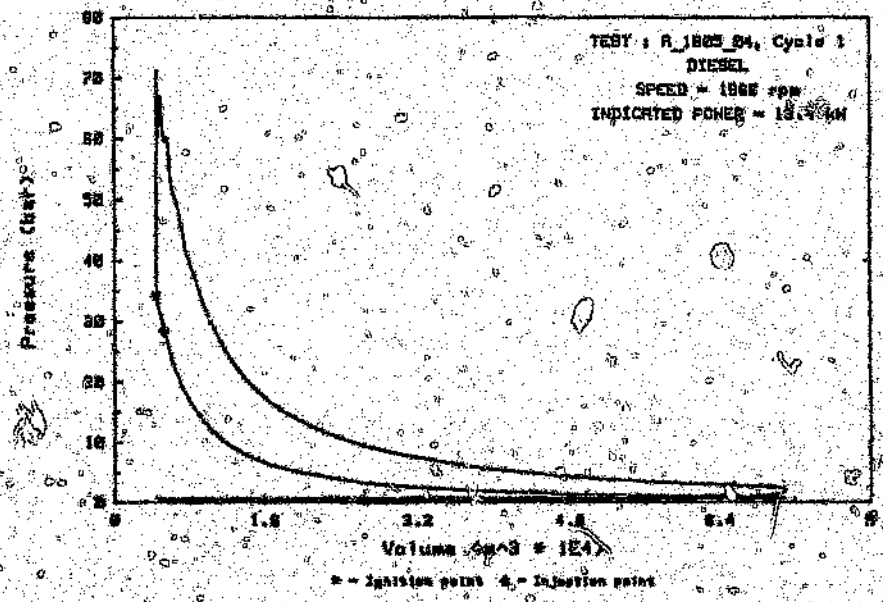

Figure 6.4: Combustion chamber pressure versus volume for minimum diesel fuelling

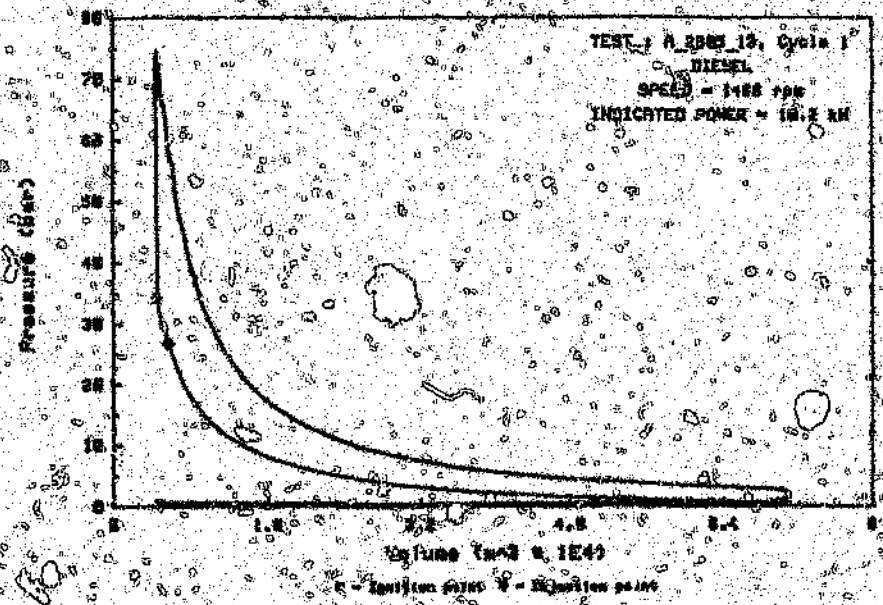

Figure 6.5: Combustion chamber pressure versus volume for maximum diesel fuelling

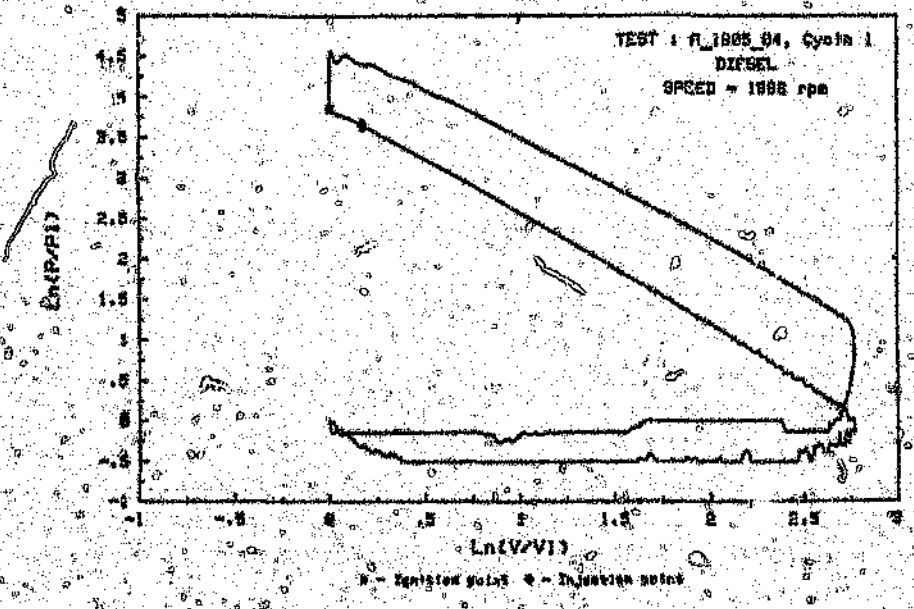

Figure 6.6: $ln(p/p_1)$ versus $ln(V/V_1)$ for minimum diesel fuelling

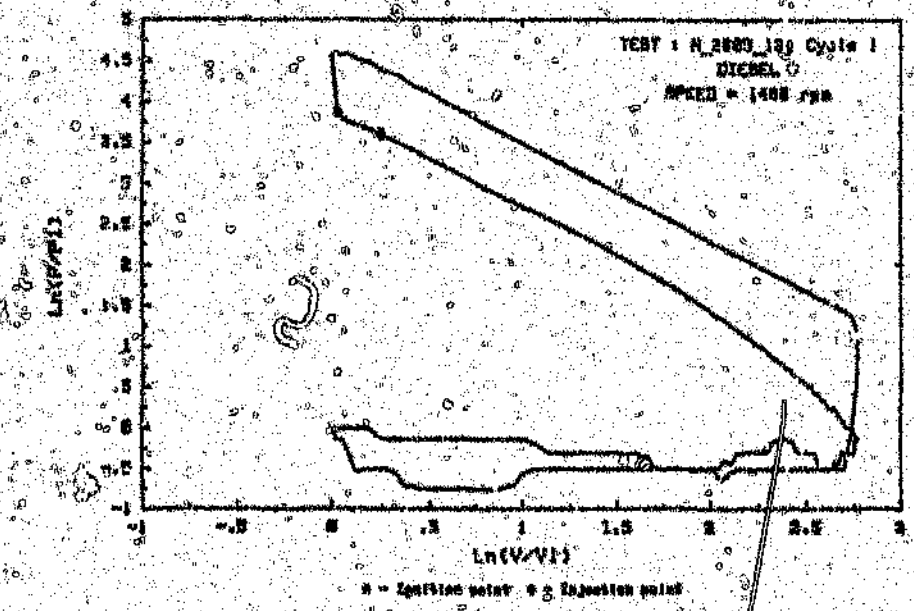

Figure 6.7: $ln(p/p_1)$ versus $ln(V/V_1)$ for maximum diesel fuelling

cannot at present be separated into the effects of combustion, dissociation, reassociation and heat transfer.

The variation of gas temperature with crank angle is shown in figures 6.10 and 6.11. It will be recalled that the temperatures were calculated using the ideal gas equation $pV = mRT$, where both the mass and the specific gas constant were recalculated at every incremental data point after ignition to take account of the products of combustion (see Chapter 4). The temperature data thus incorporate the full energy release model including the heat transfer correction. The temperature dip after injection, discussed above, is clearly discernible. In general, the shapes of the temperature versus crank angle diagrams mirror those of the pressure versus crank angle diagrams. Thus the steep temperature rise after ignition occurs largely before TDC for the case of maximum fuelling. The temperature fluctuation after TDC are reflections of the corresponding pressure oscillations, discussed above. Peak temperature is 2283,2K, and at EVO 1302,8K, which is to be expected owing to the greater loading. Finally since the information in figures 6.10 and 6.11 contains the effects of heat transfer, the compression curve should both be adiabatic and thus geometrically similar. This is not the case, for reasons that will be clearer on examining the remaining figures.

Figures 6.12 and 6.13 show the cumulative energy release versus crank angle diagrams. In each diagram, there are two curves. One curve represents the apparent cumulative energy release with no heat transfer adjustment, while the other is the total cumulative energy released with heat transfer correction.

During the compression part of the cycle, it is difficult to detect the difference between the two curves. After TDC the upper curve represents the cumulative energy release with heat transfer correction. If the compression part is enlarged or the curves are plotted in different colours, it is possible to see that these two curves cross over one another in the region from 300° to 320°CA. The trapped mass initially gains heat and then loses heat to the cylinder walls. Comparing the cumulative energy released at IVC and at injection, it is noted that these are both zero as they should be. During compression the total cumulative energy release curve should be horizontal. This is the case in figure 6.12. Figure 6.13, however, suggest a gradual energy release and re-absorption. The difference between these two cases was already noted on examination of the temperature versus crank angle

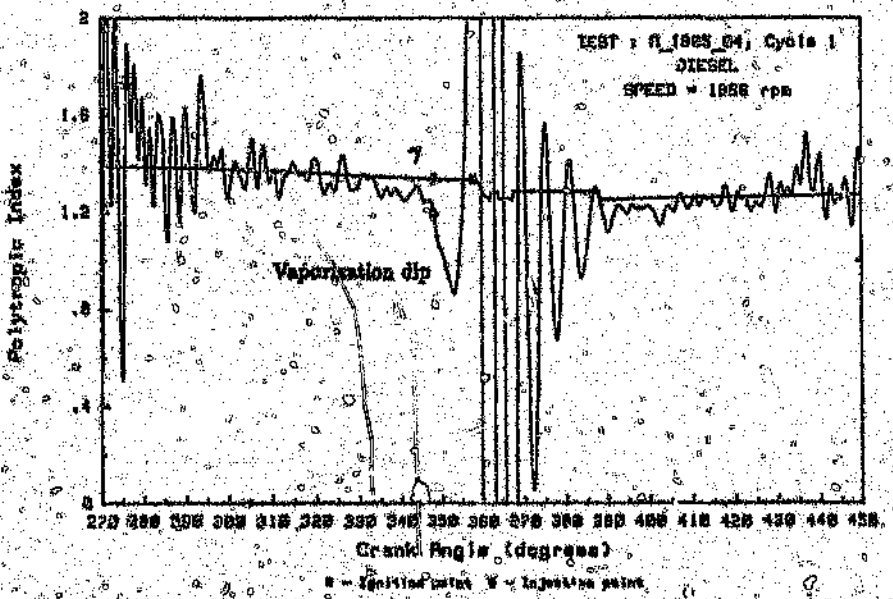

Figure 6.8: Polytropic index and gamma versus crank angle for minimum diesel fuelling

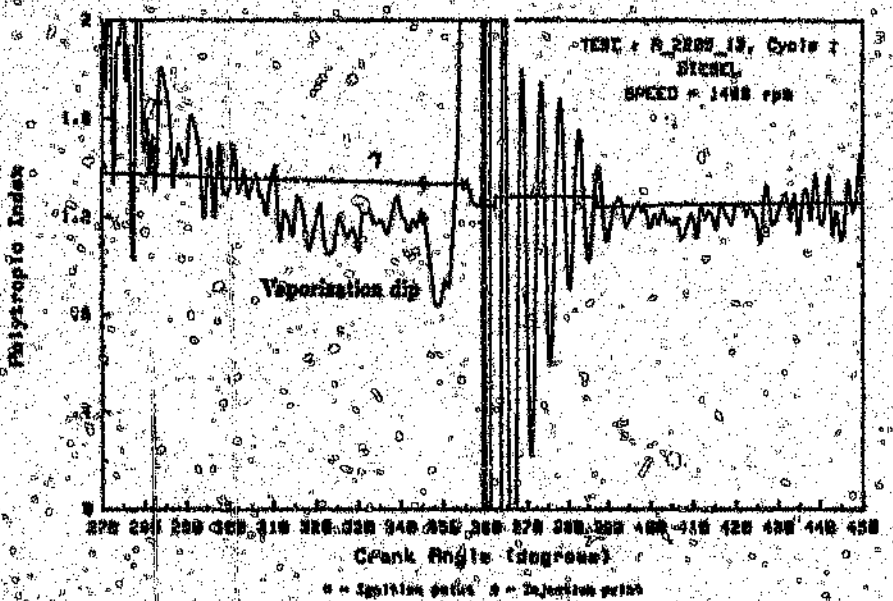

Figure 6.9: Polytropic index and gamma versus crank angle for maximum diesel fuelling

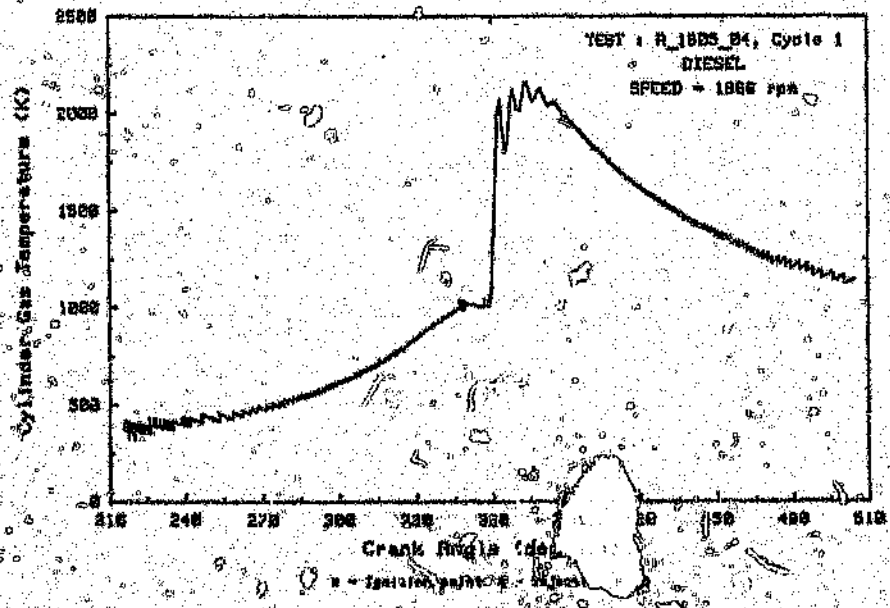

Figure 6.10: Gas temperature versus crank angle for minimum diesel fuelling

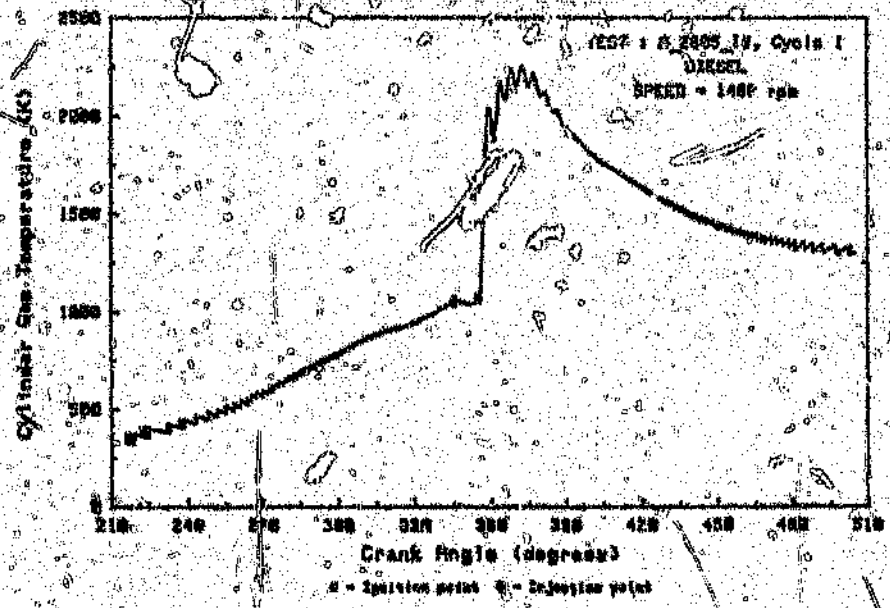

Figure 6.11: Gas temperature versus crank angle for maximum diesel fuelling

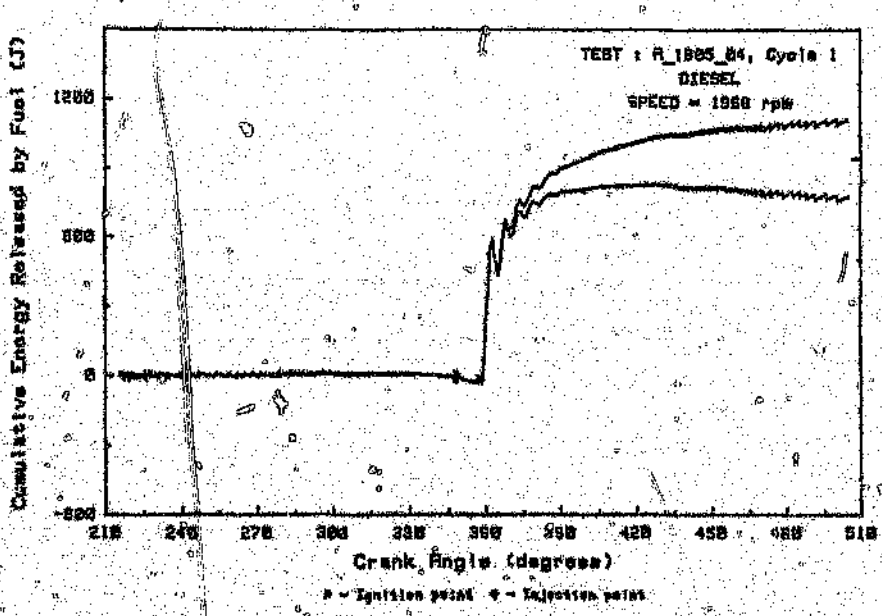

Figure 6.12: Cumulative energy release versus crank angle for minimum diesel fuelling

diagram. In view of the general magnitudes of the heat transfer corrections during compression and expansion, it can only be concluded that the rise in the cumulative energy release is not a result of the heat transfer model, but it is inherent in the original data. It must be emphasised that these diagrams represent single cycles and may display peculiarities which are not necessarily representative of normal occurrence. Had a large number of cycles been captured and averaged, such anomalies might have been smoothed out.

The region between injection and ignition once again shows the vaporization dip, as discussed previously.

This dip is followed by a substantial energy release. In figure 6.12 this energy release is satisfactory, as discussed previously; the energy is released partly before and partly after TDC. In figure 6.13, the energy is released largely before TDC, leading to 'negative work' as noted in the pressure versus crank angle diagram, shown in figure 6.2. The oscillations in the cumulative energy release diagrams merely reflect those observed in the pressure versus crank angle diagrams.

During the remaining portion of the expansion stroke, the process tends to

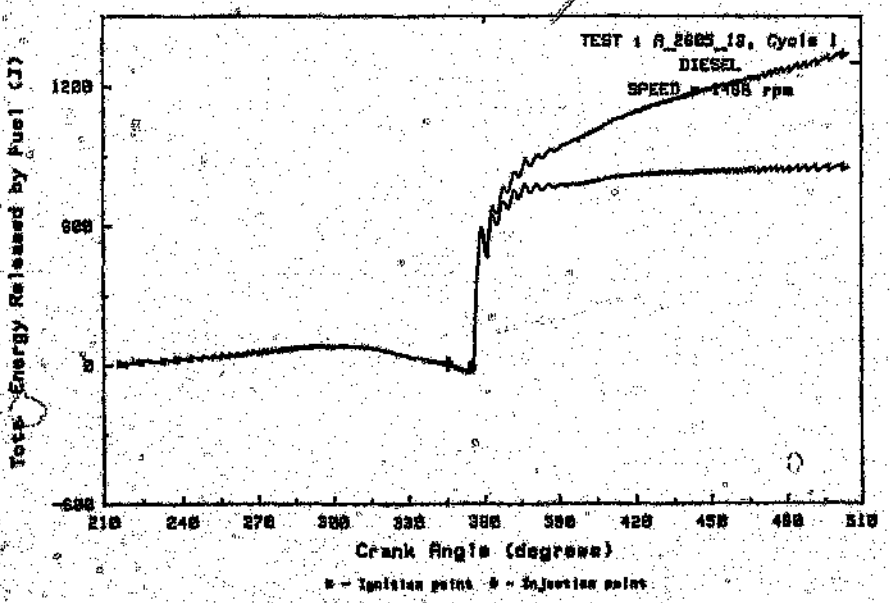

Figure 6.13: Cumulative energy release versus crank angle for maximum diesel fuelling

adiabatic as shown by the consistency of the apparent cumulative energy release in figure 6.12. This trend was noted in the value of the polytropic index n, as shown in figure 6.8. Although the total cumulative energy release (with heat transfer adjustment) rises over the same period, it does so very gently, at a decreasing rate. In figure 6.13, the situation is rather different. The apparent cumulative energy release continues to rise, although gradually. The total cumulative energy release however shows a steep rise up to EVO. This is believed to be a consequence of the heat transfer model, which appears to underpredict the amount of heat transfer in the vicinity of TDC, and overpredicts during the expansion stroke. The events depicted during the expansion stroke in figure 6.13 are thus not entirely realistic.

The upper mark on the right hand ordinate in each energy release diagram represents the total energy supplied by the fuel. This is determined from the steady state measurement of mass flow rate of fuel. In figure 6.12 the modelled cumulative energy release at EVO exceeds the measured energy supplied by some 18%. In figure 6.13, however, the corresponding two figures agree quite well. This behaviour may be due to the fact that single engine cycle were recorded for which the averaged fuel supplied might not apply exactly.

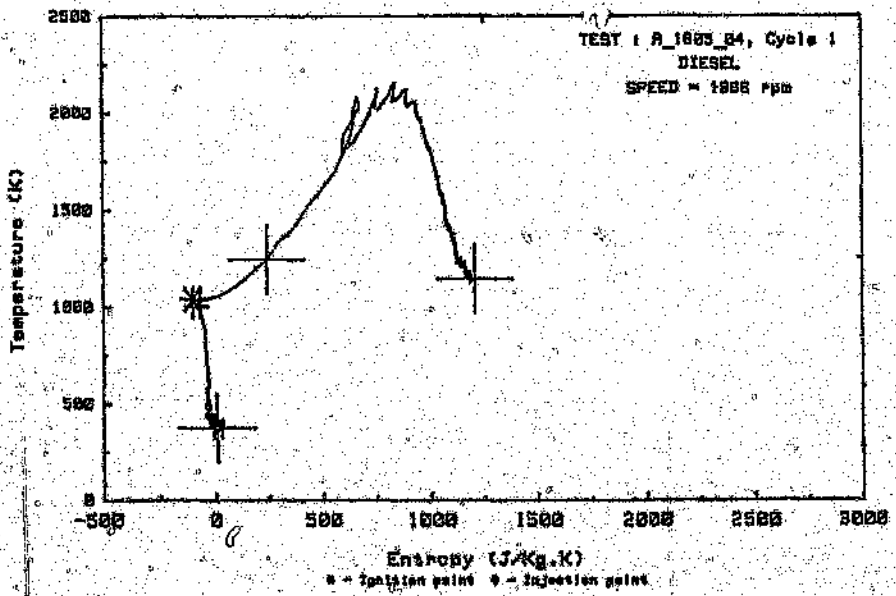

Figure 6.14: Gas temperature versus entropy for minimum diesel fuelling

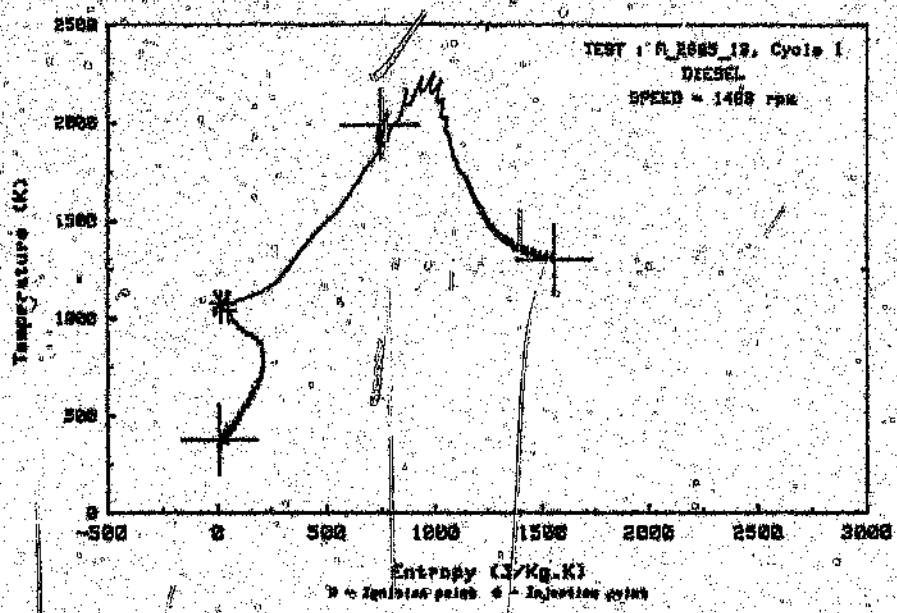

Figure 6.15: Gas temperature versus entropy for maximum diesel fuelling

Returning to the subject of continuously increasing cumulative energy release up to EVO it would seem logical to examine the products of combustion during this part of the cycle. Unfortunately no useful answers can be obtained by this approach. The reason for this is that owing to numerical difficulties detailed in Chapter 4, the gas composition reflects a much earlier end to combustion than that which in reality occurs. This inadequacy of the program does not greatly affect the energy release, but only the physical properties of the trapped mass which in any event consists mainly of air. This is confirmed in figures 6.8 and 6.9 which show γ to be nearly constant throughout the expansion stroke.

The temperature versus entropy diagrams are given in figures 6.14 and 6.15. The points indicated by a '+' represent IVC, TDC and EVO in this sequence. The injection and ignition points denoted by '#' and '*' respectively are seen to nearly coincide owing to the transformation of the ordinate from crank angle to entropy co-ordinates. The vaporization dip is therefore hidden. For the same reason these figures expand the region in the vicinity of TDC, where very rapid changes occur in the cumulative energy release diagram. Thus the satisfactory energy release largely after TDC is shown with clarity in figure 6.14 as is the reverse in the case of figure 6.15.

Portion of the compression stroke from IVC to the injection point is close to adiabatic in the case of figure 6.14, whereas figure 6.15 shows the anomalies previously discussed.

Similarly the expansion part after maximum temperature shows a slightly increasing entropy in figure 6.14 and figure 6.15 again shows the anomalous late energy release.

The temperature at the point of injection/ignition is approximately the same in both cases. Maximum cycle temperatures are 2157 K in figure 6.14 and 2253 K in figure 6.15, as expected in view of the higher load in the latter case. Temperatures at EVO are approximately 1139,0 K in figure 6.14 and 1305,6 K in figure 6.15. The latter corresponding to the case of higher load, might be higher than actual owing to the anomalous late energy release.

In general therefore, the temperature versus entropy diagrams confirm the events previously noted but provide an additional technique particularly in

the study of the region of rapid energy release.

6.1.3 Interim Conclusions

The techniques outlinad above range from straightforward and purely experimental, namely combustion chamber pressure versus crank angle, to comprehensive energy release modelling with heat transfer corrections. When viewed collectively these techniques are mutually corroborative and complementary. Each tells essentially the same story thus indicating the absence of gross errors, but with different emphasis. Thus, for example a comparison of n and γ gives an indication of the occurrence and direction of the net energy transfer, but fails to be informative in the region of TDC. The full energy release diagram separates the effects of heat transfer and energy flows that are due to the fuel. But this information is very compressed in the region of TDC. The temperature versus entropy diagram gives the same information in transformed co-ordinates, thus expanding the region of TDC.

It is clear that this modelling of heat transfer requires further refinement. For the purpose of the present study, however, it is sufficiently effective so as not to hide unusual features of combustion. This will be confirmed on examining combustion of the methanol/DME combination.

Finally the technique of capturing single cycles holds some dangers in that the particular cycle might not necessarily be representative of 'typical' behaviour. The case of maximum fuelling, which shows the ostensible energy release during compression of air appears to a case in point.

6.2 Methanol/DME Fuelling

The tests to be reported below were performed at the same injection timing as for diesel fuelling. Initially three engine loading conditions were chosen. These were termed low, medium and high. The speed was essentially the same for each loading condition. At each loading condition the mass flowrate of DME was the lowest possible corresponding to the onset of

mishre; the flowrate of DME was increased gradually and that of methanol decreased such that the load and speed were maintained essentially constant; the procedure was continued until the onset of knock or the selected speed could no longer be maintained. Thus for each load setting a number of tests at constant power were conducted with varying ratios of methanol to DME fuel. On analysis the medium load tests were found to give results rather close to those of low load and are therefore not reported.

The overall test conditions are shown in table 6.3. It will be noted that at each load the reported conditions were constant to within ± 4%. This was the best that could have been achieved with the equipment available.

Load Setting	Speed *rev/min*	Torque *Nm*	Brake Power *kW*	BMEP *kPa*
'Low'	1853 ± 22	22,60 ± 0,40	4,41 ± 0,10	211,16 ± 3,61
'High'	1842 ± 28	33,71 ± 0,85	6,49 ± 0,24	314,94 ± 7,71

Table 6.3: Test conditions, methanol/DME fuelling

Table 6.4 gives the range of fuelling conditions that were covered. For each load setting the minimum and maximum contribution of DME to total fuelling are reported; these correspond to the onset of misfire and knock discussed above. Also shown are the corresponding methanol mass flowrates and two equivalence ratios. The first, ϕ_{DME}, is the ratio of stoichiometric

Load Setting	DME Contribution to total fuel	DME Flowrate *kg/h*	Methanol Flowrate *kg/h*	ϕ_{DME}	ϕ_{TOTAL}
'Low'	min	1,016	2,422	0,155	0,420
	max	1,693	1,609	0,262	0,452
'High'	min	0,953	3,001	0,153	0,492
	max	2,425	2,084	0,395	0,637

Table 6.4: Fuelling conditions

to the actual air DME ratio. It is thus a measure of 'richness' with regard to DME. The second is the overall equivalence ratio referred to the combined methanol and DME fuels. All tests were thus conducted with mixtures that were lean overall.

A brief report on engine performance is given first. This is followed by a more detailed analysis and discussion of combustion characteristics. The latter refer to the limiting fuelling cases reported in Table 6.4.

6.2.1 Engine Performance Characteristics

The parameters discussed below are brake thermal efficiency, indicated power, indicated thermal efficiency and mechanical efficiency all as a function of ϕ_{DME}. It should be emphasized that the tests at each load level are essentially at constant brake power (and speed).

In defining the above thermal efficiencies the energy input to the engine was calculated on the basis that methanol and DME are separate fuels. In practical implementation of this fuelling method, however, the engine/catalytic converter system would be externally supplied with a single fuel, namely methanol. The DME would be generated internally using exhaust gas energy. It is thus important to ascertain whether the catalytic conversion is 'regenerative' ie, accompanied by a net fuel energy gain. The relevant reaction is:

$$2CH_3OH \longrightarrow CH_3OCH_3 + H_2O$$

The enthalpies of combustion are 638,4 $MJ/kmol$ for methanol and 1328 $MJ/kmol$ for DME. Thus the energy gain ratio or 'regeneration factor' associated with the conversion reaction is $1328/((2)(638,4)) = 1{,}040$. The energy gain is thus a mere 4%. In view of this [illegible] thermal efficiencies, based on separate fuels, apply approximately also [illegible] practical situation with regeneration.

Brake thermal efficiency, the ratio of brake power to the rate of supply of fuel energy is shown in figure 6.16. At both loads, this efficiency decreases

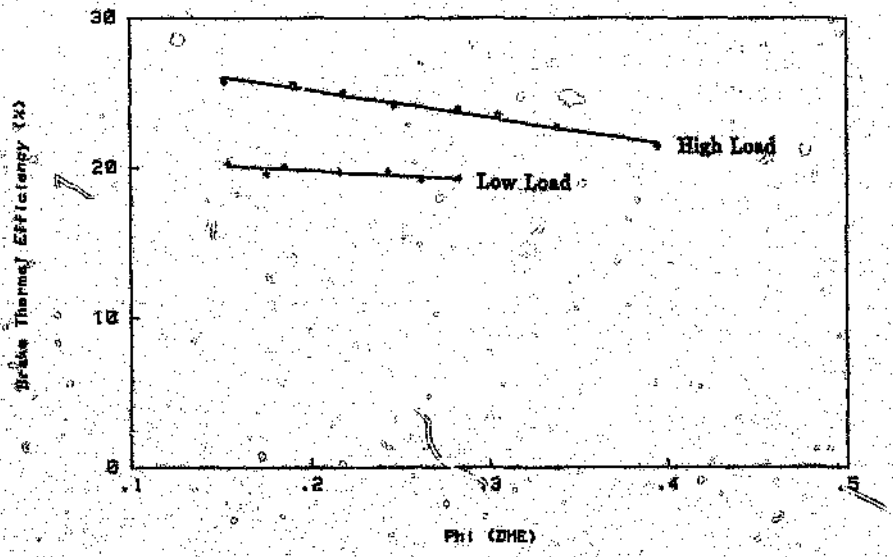

Figure 6.16: Brake thermal efficiency versus ϕ_{DME} for low and high loads, methanol / DME fuelling

with increasing DME content of fuel. This means that with increasing ϕ_{DME} more total fuel needs to be supplied to achieve the same brake power.

Since DME is supplied in gaseous form an increase in the DME proportion of the total fuel results in a reduction in the air breathing capacity of the engine. Thus a reduction in brake thermal efficiency is to be expected. However, the reduction in air flow rate from minimum to maximum DME fuelling was a mere 0,7% and 1,6% for low and high loads respectively. The corresponding reduction in brake thermal efficiency were of the order of 0,01 in 0,20 i.e. 5% and 0,044 in 0,26, i.e. 17%. The displacement of air by aspirated DME is thus not sufficient to explain the reduction in brake thermal efficiency. The reason for this behaviour is thus likely to lie in the combustion process.

Figure 6.17 shows indicated power versus ϕ_{DME}. For both loading situations, indicated power falls with increasing DME contribution. The reductions are of the order of 20% and 10% for the low and high loads respectively. The difference between these trends and those shown by the brake thermal efficiency, must be due to differences in mechanical efficiency to be discussed shortly. The 'hump' shown in the high load data is believed

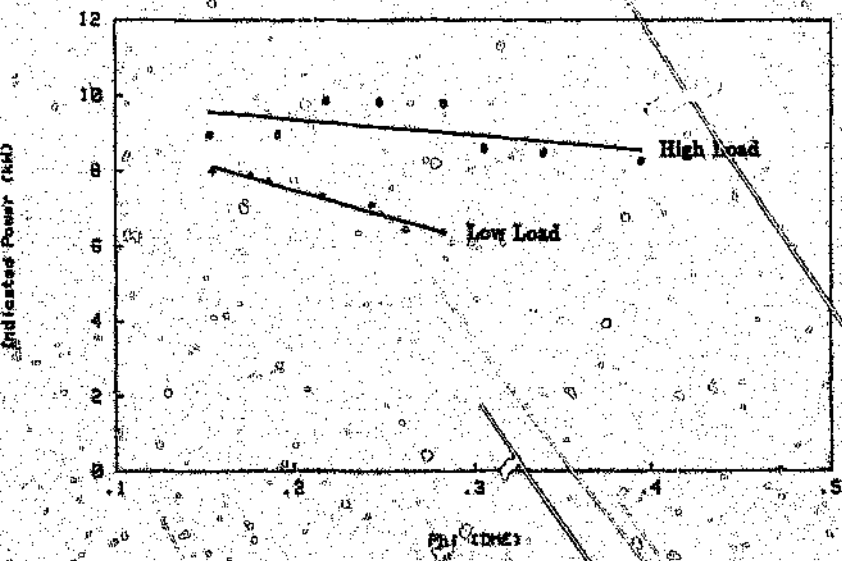

Figure 6.17: Indicated power versus ϕ_{DME} for low and high loads, methanol/DME fuelling

to be scatter, due to the sampling of single cycles, that are not necessarily typical. (The information in figure 6.16, by contrast, derives from averaged measurements).

Figure 6.18 shows indicated thermal efficiency versus ϕ_{DME}. This information merely reflects that given in the previous figure.

Figure 6.19 shows mechanical efficiency versus DME contribution of fuel. It will be noted that the efficiency is generally higher at higher loads and increases with increasing ϕ_{DME}. The reason for these trends are as follows. Mechanical friction and gas pumping work are speed dependent (Obert, 1968), and thus are approximately constant in these tests. Since tests at higher loads produce more net work output, the constant frictional and pumping losses represent a smaller proportion of the gross work done by the engine thus leading to higher mechanical efficiency.

As ϕ_{DME} increases, the mass flowrate of methanol decreases. Thus the work required to drive the fuel pumps (losses) also decreases. This explains the increasing trend in mechanical efficiency with ϕ_{DME} for both loads.

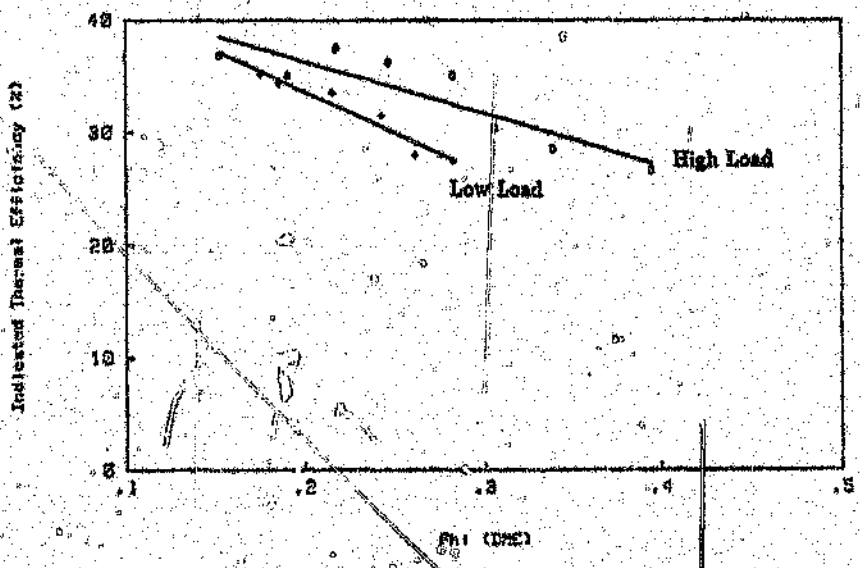

Figure 6.18: Indicated thermal efficiency, versus ϕ_{DME} for low and high loads, methanol/DME fuelling

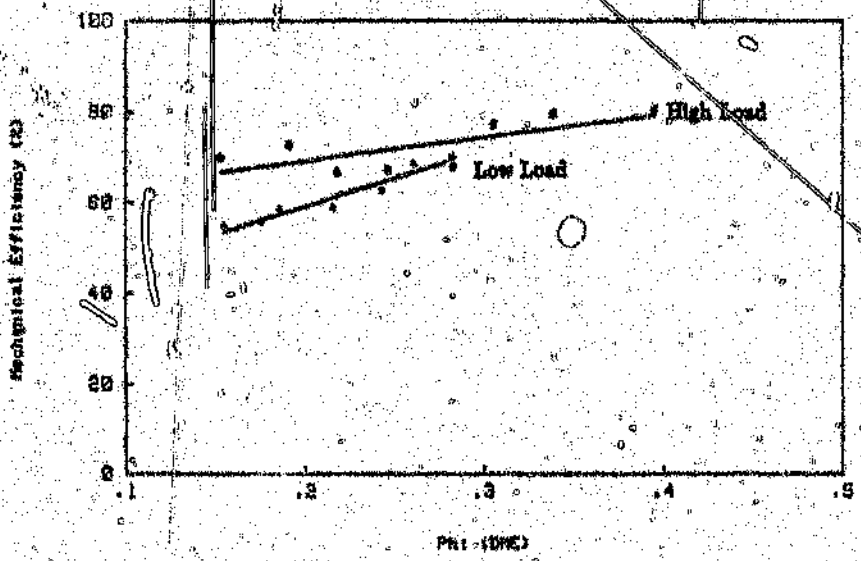

Figure 6.19: Mechanical efficiency versus ϕ_{DME} for low and high loads, methanol/DME fuelling

6.2.2 Combustion Characteristics

(a) Combustion Chamber Pressure versus Crank Angle

Figure 6.20 shows combustion chamber pressure versus crank angle for the case of low load with low DME fuel contribution. Three curves are shown. The upper refers to fuelling on methanol and DME (referred to as cycle 1), the middle to fuelling on DME alone (referred to as cycle 2) at otherwise identical conditions and recorded immediately after cycle 1. The lowest is an air motoring curve. The latter was not recorded during the same test run and was subsequently scaled down so as to coincide with the early portion of the compression curve of cycles 1 and 2. It is thus a 'generated' motoring curve intended to serve as a basis for comparison with the combustion curve. The generation procedure seems not unreasonable since the mass fraction of DME to air is only some 2% and the values of $\gamma = c_p/c_v$ are approximately 1,11 and 1,4 for the two gases respectively.

As in the case of diesel fuelling, the pressure versus crank angle curves are not smoothed. As previously the oscillations in the region of maximum pressure are believed not to be an indication of knock but probably due to an 'organ pipe' effect in the passage connecting the cylinder to the transducer. The injection and ignition points (marked by '#' and '*' respectively) refer to methanol. It will be noted that before methanol injection, cycles 1 and 2 are coincident. This is most gratifying and demonstrates the degree of repeatability that is achieved by the single cycle technique. This holds also for the pressure traces given in figures 6.21, 6.22 and 6.23. It should be pointed out that the tests shown in figures 6.20 to 6.23 were not specifically selected but that the remarkable repeatability of the DME portion of the curves was noted only in the late stage of the analysis.

Returning to figure 6.20, attention is focused on the point of breakaway of the fuelled curve from the motoring curve. The slight 'hump' (marked by an arrow) would seem to indicate an early energy release on the part of DME, which subsequently dies away in the region of 340°CA. This is followed by a second sharper pressure rise which would indicate a second stage of energy release by the DME air system. This is more clearly seen in figures 6.21 and 6.23 which refer to the cases of high DME fraction of the total fuel.

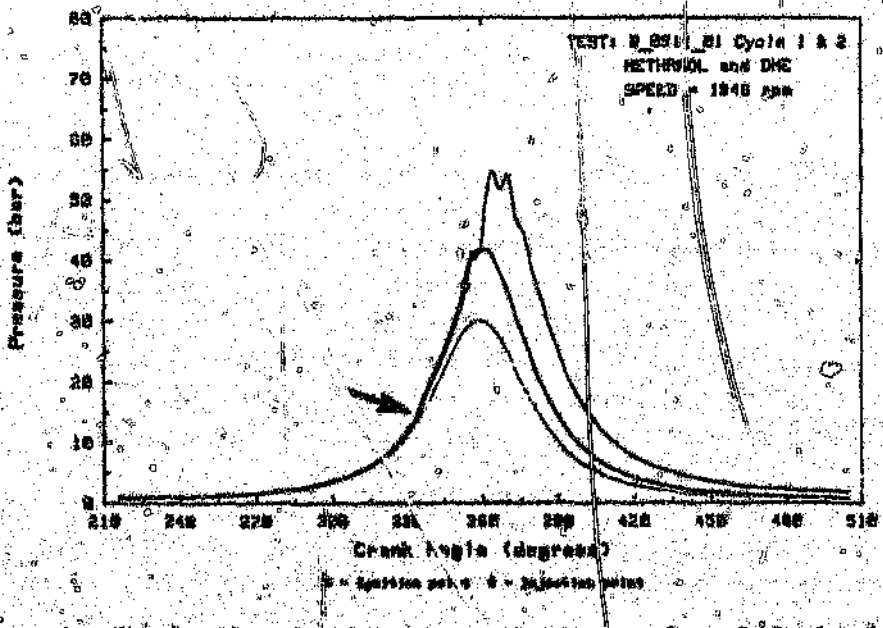

Figure 6.20: Combustion chamber pressure versus crank angle for low load, low DME fuel contribution

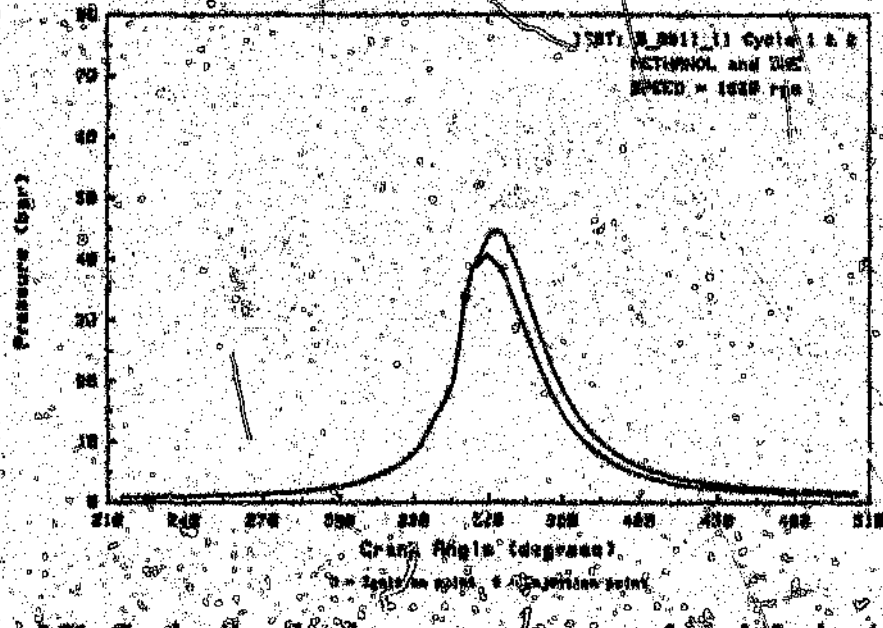

Figure 6.21: Combustion chamber pressure versus crank angle for low load, high DME fuel contribution

In all cases, figures 6.20 to 6.23, maximum pressure on DME combustion only (cycle 2) is reached approximately at TDC. This indicates that DME is burned essentially entirely before TDC, thus leading to negative work.

In no case is a vaporization 'dip' noticeable. At this point it is necessary to distinguish between the cases of low and high DME contributions to the total fuel. In the former case, figures 6.20 and 6.22, a methanol ignition lag exists, though the vaporization 'dip' is not discernible, presumably swamped by the continuing energy release of DME. It should be remembered that these tests were conducted with a DME contribution just above the threshold of misfire. Thus had the DME contribution been slightly less, the methanol would have quenched the DME combustion altogether. In the cases of high DME contribution, figures 6.21 and 6.23, the injection and ignition points coincide. (This will be confirmed on examination of the energy release diagram). It would appear therefore, that in these cases the DME combustion is sufficiently vigorous for the injected methanol, which is smaller in quantity than in the above cases, to ignite immediately and to burn at the nozzle.

Attention is now drawn to the methanol combustion in figures 6.20 and 6.21. In the former case (low DME and high methanol) essentially no simultaneous burning of both fuels occurs and the pressure rise on combustion of methanol is relatively steep. In the latter case (high DME and low methanol), the methanol ignites on injection and evidently well before the DME combustion is completed. The subsequent pressure rise (methanol burning alone) is low both in rate and amplitude, the latter reflecting the small quantity of methanol supplied. Thus the larger the DME proportion of the fuel, the slower the combustion of methanol. This point will be taken up in the discussion of energy release.

The same effects may be observed in the high load (and power) tests, figures 6.22 and 6.23, but with higher peak pressures. Additionally figure 6.23 (high load, high DME contribution) demonstrates the presence of knock on combustion of DME. A parallel may be drawn from knock on diesel fuelling where the presence of a large quantity of combustibles auto-igniting leads to excessive pressure rise and dissipative oscillations. Both the latter effects are strikingly demonstrated in

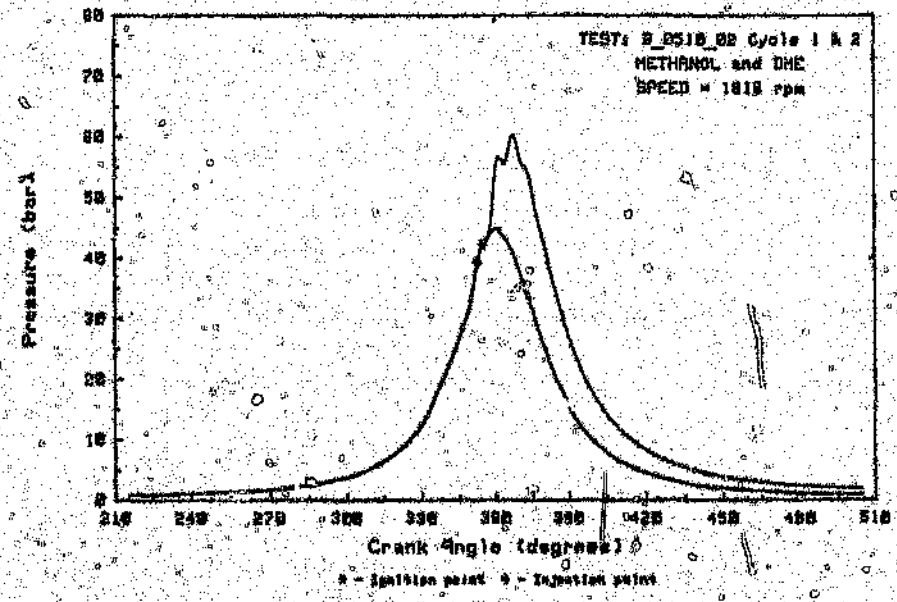

Figure 6.22: Combustion chamber pressure versus crank angle for high load, low DME fuel contribution

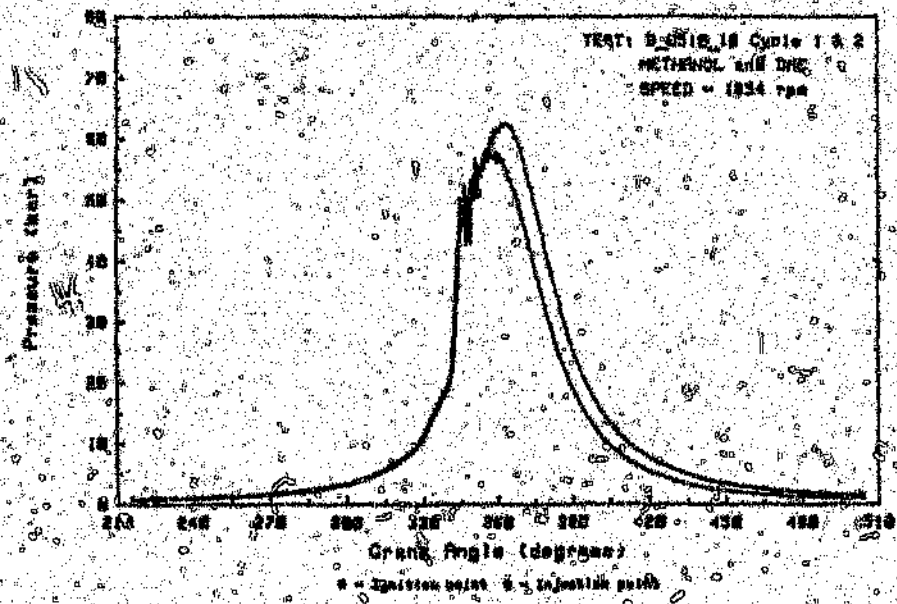

Figure 6.23: Combustion chamber pressure versus crank angle for high load, high DME fuel contribution

figure 6.23. The injection of methanol appears to attenuate but not eliminate the knock, thus resulting in inefficient combustion of both fuels.

(b) Combustion Chamber Pressure versus Volume

Combustion chamber pressure versus volume diagrams are shown in figures 6.24 to 6.27 for the cases of low and high load each with low and high DME fuel contribution. In all cases cycles 1 (methanol and DME) and 2 (DME only) are superimposed. As noted in the previous four figures, the compression portion of the curves coincide. For the expansion portion, the upper curve corresponds to cycle 1 and the lower to cycle 2. Thus the area of the outer envelope corresponds to the indicated work obtained with both fuels and the area of the inner lower loop to that of DME only. In both the low load and high load case, the area of the outer envelope is noticeably smaller for the high DME fuel contribution. This means that at both high and low load, the indicated work falls with increasing DME contribution even though both sets of tests were conducted at constant brake power and speed. The findings summarized in figures 6.17 and 6.18 (indicated power and thermal efficiency, both versus ϕ_{DME}) are visibly demonstrated.

In all cases the 'hump' in the compression curve, indicated by an arrow, signals the first stage of DME energy release. Since this reduces the enclosed area, it results in a reduction of net indicated work. The second energy release is fairly gradual in the case of figures 6.24 and 6.26 (low DME), rapid in figure 6.25 (low load, high DME) and extremely rapid in figure 6.27 (high load, high DME). In the last case this leads to knock. The more rapid this pressure rise before TDC, the greater the proportion of negative work.

The confusing appearance near TDC in figure 6.27 (high load, high DME) is caused by rapid pressure fluctuations associated with knock. These are also responsible for the diagram 'looping over itself' in this region, for both cycles, and lead to computational difficulties in the energy release model.

(c) $\ell n\ (P/P_1)$ versus $\ell n\ (V/V_1)$

The natural logarithm of dimensionless pressure versus natural logarithm of dimensionless volume for the four cases under discussion are

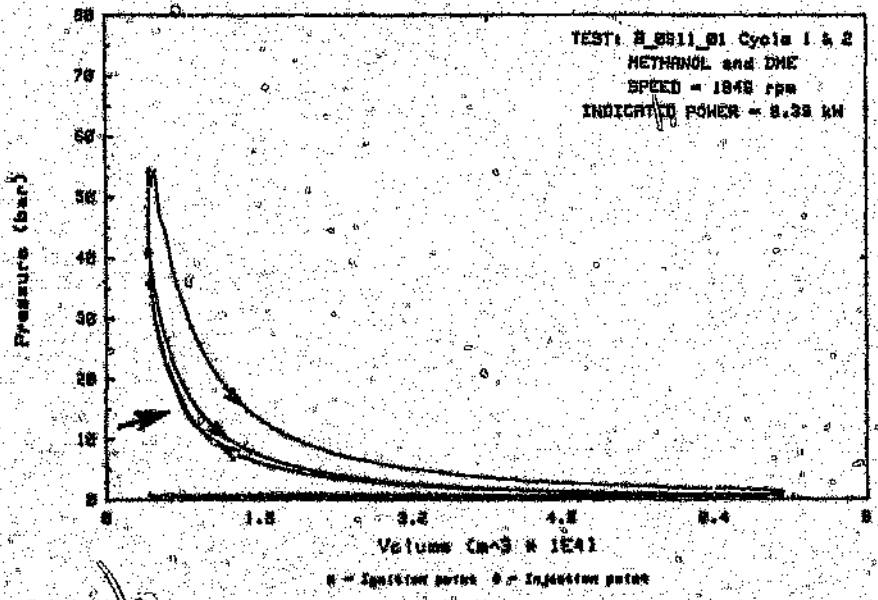

Figure 6.24: Combustion chamber pressure versus volume for low load, low DME fuel contribution

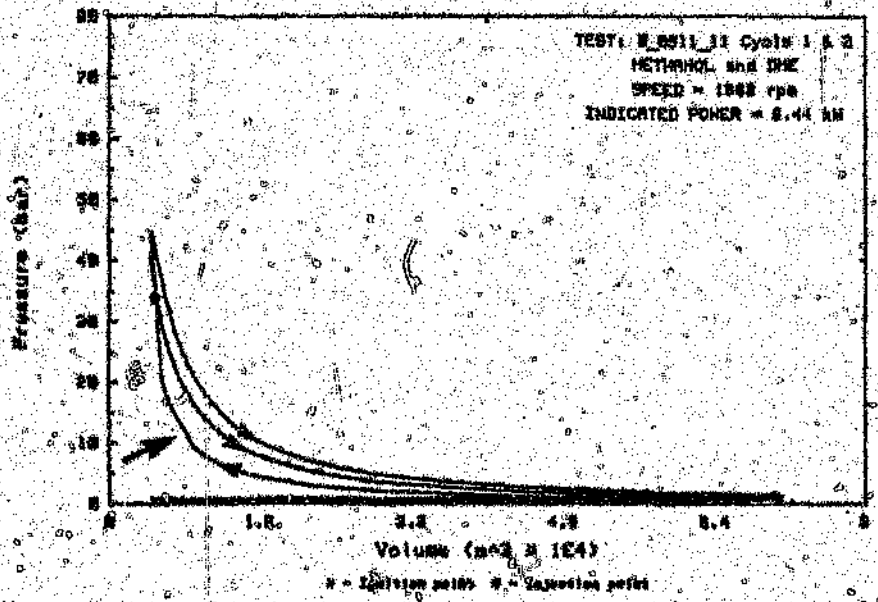

Figure 6.25: Combustion chamber pressure versus volume for low load, high DME fuel contribution

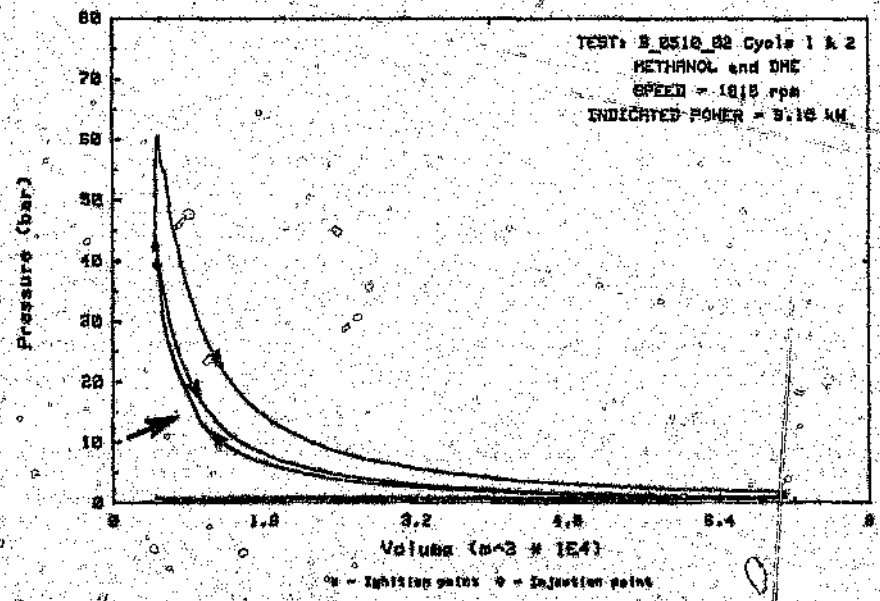

Figure 6.26: Combustion chamber pressure versus volume for high load, low DME fuel contribution

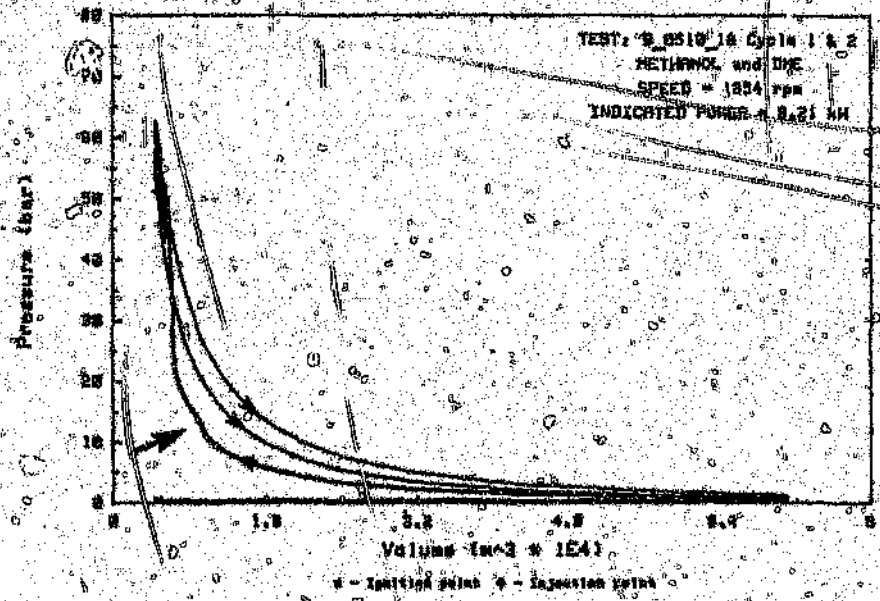

Figure 6.27: Combustion chamber pressure versus volume for high load, high DME fuel contribution

shown in figures 6.28 to 6.31. As in the case of diesel fuelling and for the same reason, the data has been subjected to four point moving average smoothing. As in figures 6.24 to 6.27, cycles 1 and 2 for each case are shown in the same diagram. The pumping loop should be ignored for reasons given in Section 6.1.2. The compression curves for cycles 1 and 2 coincide in figures 6.28 to 6.30, but are separate in figure 6.31. This would seem to contradict information given in figures 6.23 and 6.27. Closer inspection of the combustion chamber pressure versus crank angle diagram, figure 6.23, however, shows the compression curve to be rather thick. When this diagram was plotted at greater magnification, and in two colours, it was noted that cycle 2 consistently lay below the curve for cycle 1. The clearly separate lines in figure 6.31 result from the fact that the logarithm transformation magnifies differences at low values (in the early part of the compression curve) and that at higher values and a steeper pressure rise, pressure differences at a particular crank angle are quite large.

Focussing attention on the compression curves, the first stage of energy release of DME is clearly discernible as the 'hump' marked by a short arrow. This is followed by the second stage of energy release indicated by an increasingly negative slope (marked by a long arrow) which is mild in the case of low DME and sharp with high DME fuel contribution.

After the onset of combustion of methanol marked by '*' the pressure rise is fairly steep in the cases of low DME contribution, figures 6.28 and 6.30, approximately to constant volume combustion in the former case. In the cases of high DME contributions the methanol combustion is evidently very slow as indicated by the tail-like protrusion in the top left hand part of figures 6.29 and 6.31. In the latter case, the smoothing in this region, which is known to exhibit knock, may have resulted in some distortion, so that the methanol ignition point appears to be displaced to the left. The computational difficulties associated with the combustion of DME alone in the presence of knock is presumably responsible for the 'loop' in this region of cycle 2.

The slopes of the power loops in these figures represent the polytropic index to be discussed below.

(d) Polytropic Index versus Crank Angle

The variation of the polytropic index versus crank angle is given in

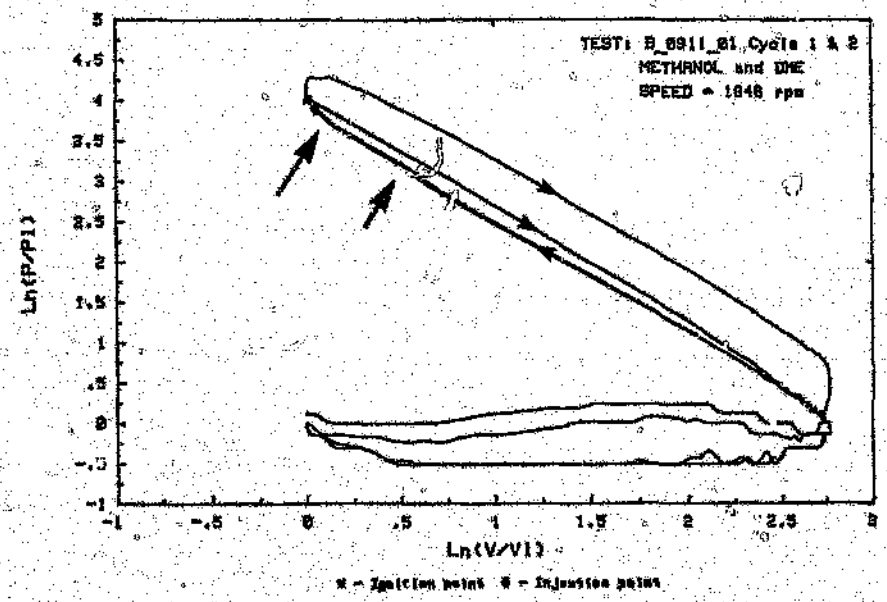

Figure 6.28: $Ln(P/P_1)$ versus $Ln(V/V_1)$ for low load, low DME fuel contribution

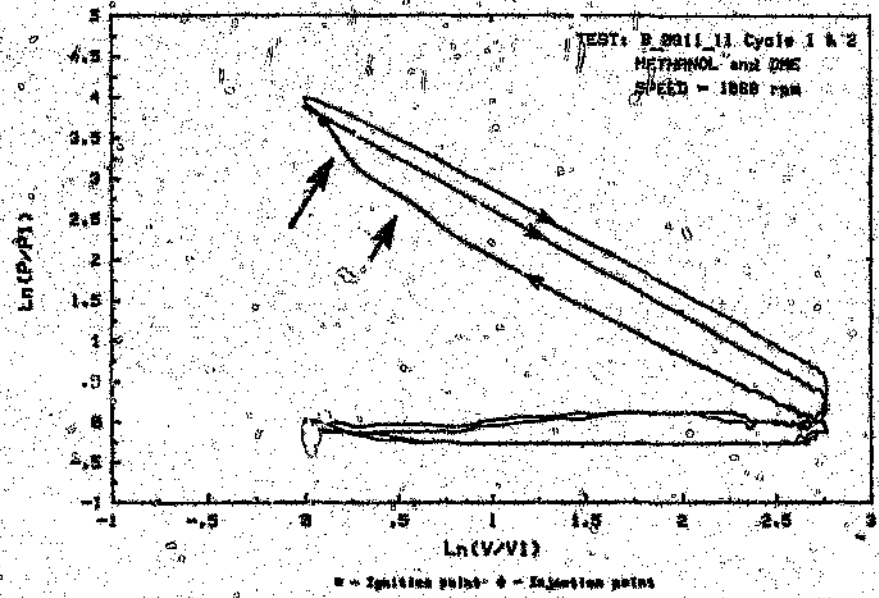

Figure 6.29: $Ln(P/P_1)$ versus $Ln(V/V_1)$ for low load, high DME fuel contribution

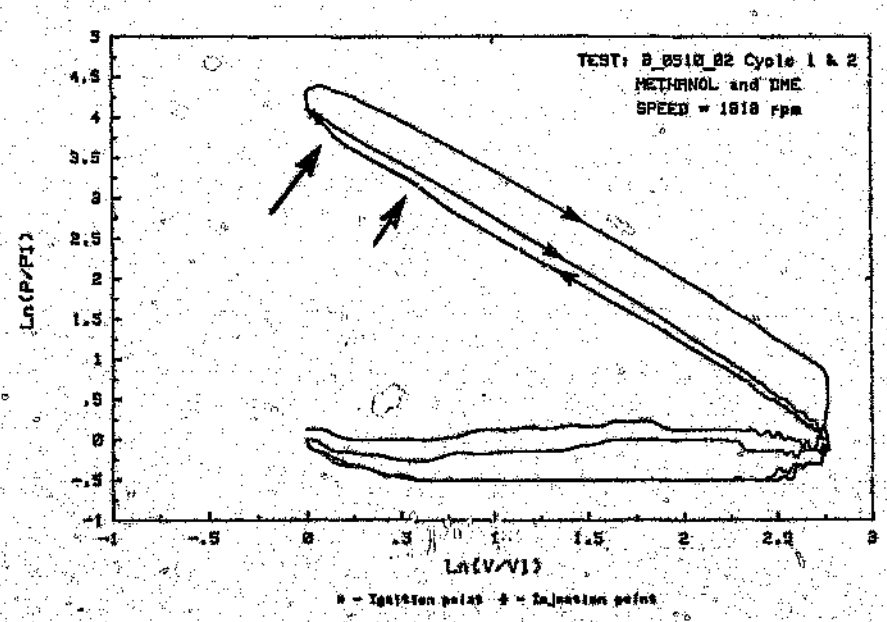

Figure 6.30: $ln(P/P_1)$ **versus** $ln(V/V_1)$ **for high load, low DME fuel contribution**

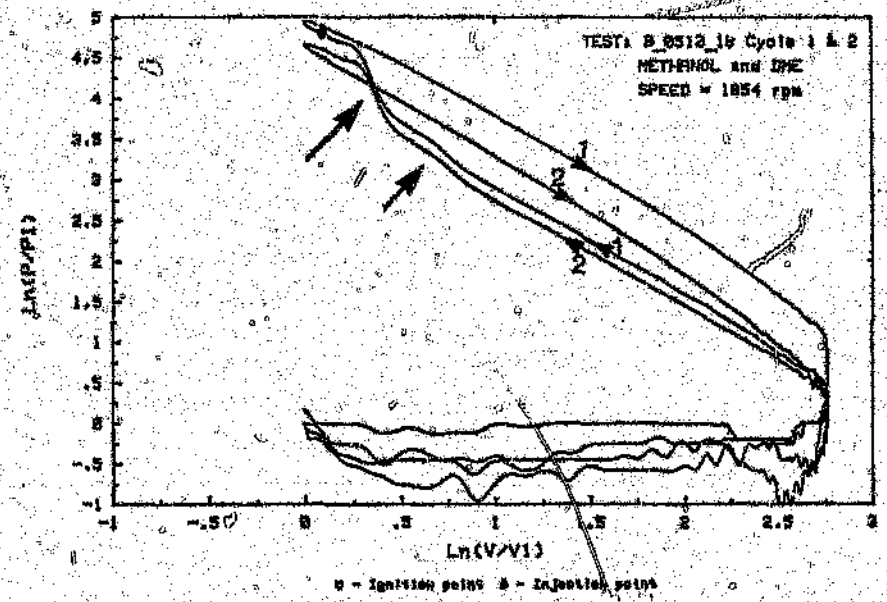

Figure 6.31: $ln(P/P_1)$ **versus** $ln(V/V_1)$ **for high load, high DME fuel contribution**

figures 6.32 to 6.35, for the four cases discussed above. The figures refer to cycle 1 (both fuels). Cycle 2 (DME only) has not been superimposed on these since the combined diagram does not allow the two cycles to be readily distinguished, (without resorting to colour) and a more complete interpretation in any event emerges in the energy release analysis.

As in the case of diesel fuelling, the data in figures 6.32 to 6.35 results from the numeric differentiation of the $\ell n(P/P_1)$ versus $\ell n(V/V_1)$ diagram. They are thus purely experimental except for the smoothing previously discussed. The values of $\gamma = c_p/c_v$ (calculated from the full energy release model) are superimposed on these diagrams.

Comparison of figures 6.32 to 6.35 with figures 6.8 and 6.9 (diesel fuelling) shows the former to be noticeably less 'spikey'. This is due to the reduced sampling rate on methanol/DME fuelling necessitated by the capture of three as opposed to one cycle per test. Thus a data point was captured every 0,6°CA in the case of methanol/DME and every 0,2°CA in the case of diesel.

Regarding the compression curves, it would appear that in figures 6.32, 6.34 and 6.35, these are approximately adiabatic, up to some 330°CA, the heat transfer correction prior to ignition being small (see figures 6.12 and 6.13). In figure 6.33 the polytropic index rises in the range $1 < n < \gamma$, which indicates a decreasing energy absorption in the same region of compression. This point will be taken up in the discussion of the relevant energy release diagram.

In all four figures, a spike in n with $n < \gamma$, occurs starting in the region of 325° to 330°CA and ending at about 335° to 340°CA. This clearly corresponds to the first stage of DME energy release. This is followed by a second spike, (the top of which is in all cases off-scale) which corresponds to the second stage of energy release. The main value, in the present context, of a diagram of the type shown in figures 6.32 to 6.35 is that the onset of these stages of energy release can be located with particular ease.

The double spike with $n < \gamma$ in the region of 350°CA in figure 6.35, is associated with the pressure fluctuations that result from knock.

In the expansion portion of the cycle beyond approximately 380°CA, in all four diagrams, n rises to greater than γ, with a final value of approximately 1.5 at 450°CA. This indicates an initial net energy

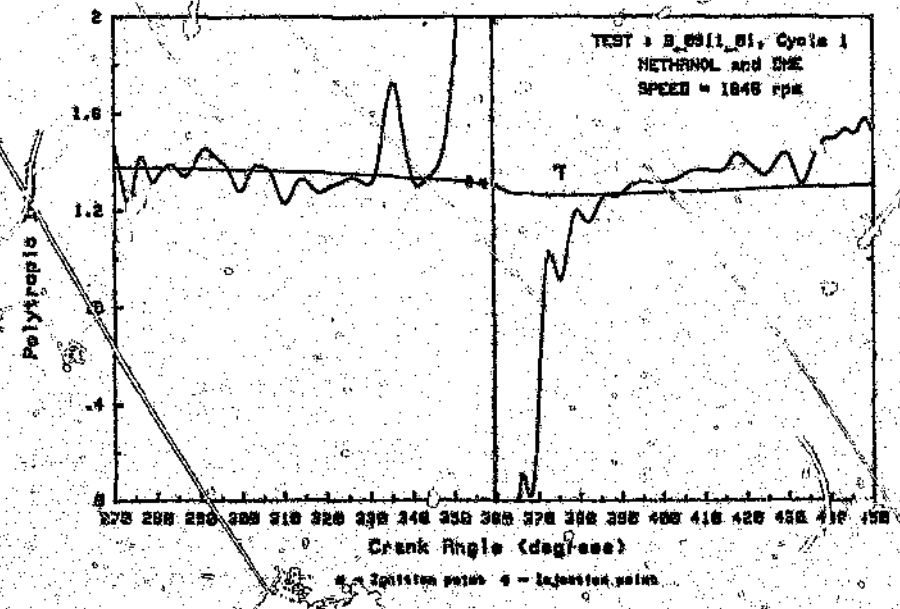

Figure 6.32: Polytr s crank angle for low load, low DME fuel contribution

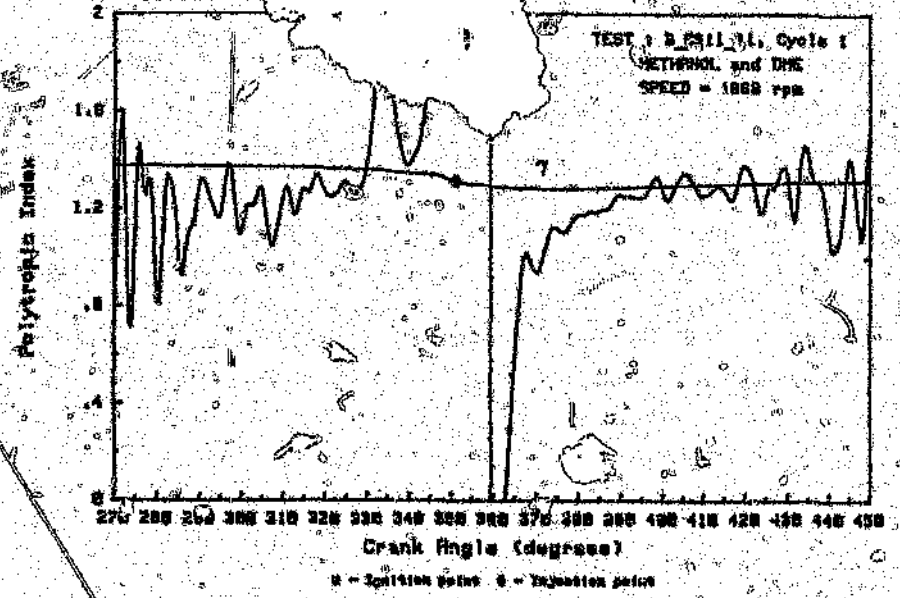

Figure 6.33: Polytropic index versus crank angle for low load, high DME fuel contribution

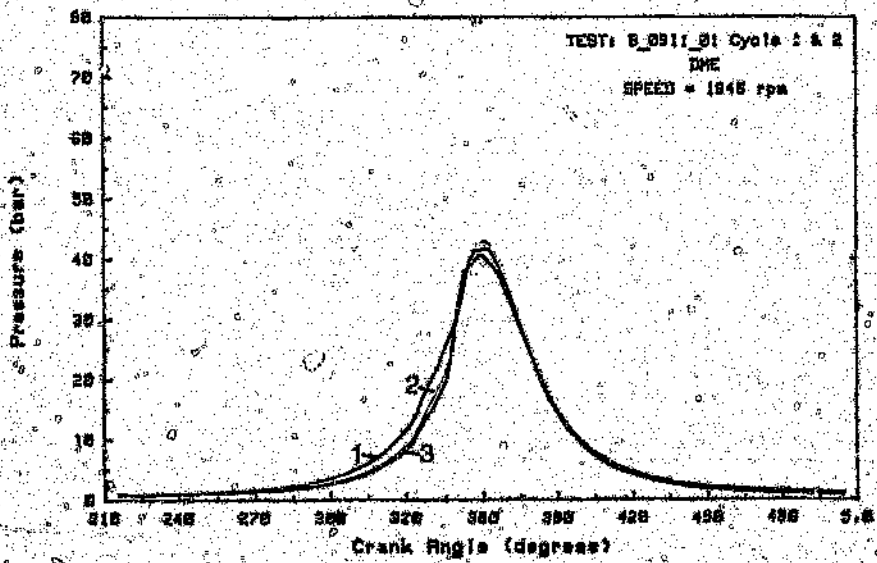

Figure 6.45: Combustion chamber pressure versus crank angle for low load at three different DME fuel contributions

A certain amount of scatter is evident in this figure. This is partly the result of the fact that the values of Q_a were measured off the energy release diagram which contains a certain amount of 'noise' and that Q_a is a small quantity compared with the total energy release. Despite the scatter two clear trends emerge.

The first is that Q_a becomes increasingly negative with increasing ϕ_{DME}. Table 6.5 shows Q_f to occur at essentially constant crank angle, i.e. at constant time after IVC. Thus during this period, the larger the amount of DME present, the larger the energy absorption. It would appear that the energy absorption Q_a is a measure of the degree of endothermic pre-reaction to the first energy release Q_1. Thus the more DME is present, the more mixture pre-reacts during a fixed time interval. (The apparent discrepancy regarding the origin of Q_a – some data points being positive and some negative – will be discussed shortly).

The second trend is the reduction in Q_a in going from low load to high load. The most likely reason for this would seem to be a difference in heat transfer effects, between the two cases.

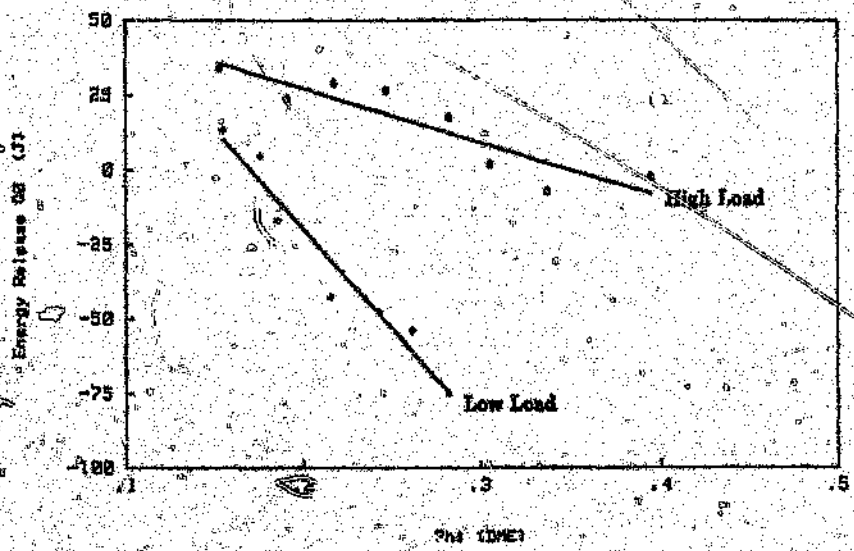

Figure 6.46: Energy release Q_o versus ϕ_{DMB} for low and high loads

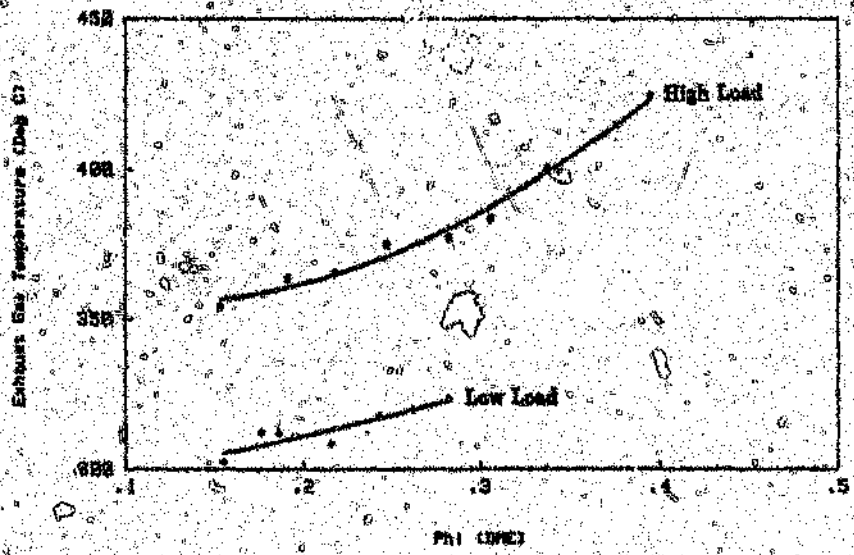

Figure 6.47: Exhaust gas manifold temperatures versus ϕ_{DMB} for low and high loads

supply to the trapped mass up to $n = \gamma$, followed by a net energy loss with the temperature falling throughout. In the case of figure 6.33, n appears to asymptote to γ at $450°CA$, thus indicating a net energy supply with falling temperature. In this region the heat transfer effects are large and can not be separated from the energy release by the fuel. The matter is thus more profitably discussed after examination of the full energy release diagram.

(e) **Combustion Chamber Gas Temperature versus Crank Angle**

The variation of combustion chamber gas temperature with crank angle is shown in figures 6.36 to 6.39. In each case, cycle 1 (both fuels) and cycle 2 (DME alone) have been superimposed.

Before ignition of methanol the two cycles nearly coincide. Where divergence in this region occurs the upper curve refers to cycle 2. This divergence is significant only in figure 6.39, and is due to reasons previously discussed. After TDC, the upper curve in each case refers to cycle 1. As discussed in Chapter 4 and section 6.1.2, the temperature data incorporates the full energy release model, including the heat transfer corrections. In all four figures the first energy release of DME is quite clearly noticeable. This is followed by the second energy release of DME which is fairly gradual in the case of figures 6.36 and 6.38 (low DME) and is steep in figures 6.37 and 6.39 as previously discussed.

In comparing figures 6.36 and 6.37, the compression curve of the latter would appear to be anomalous with too low a rate of temperature rise. This matter will be taken up in the corresponding energy release diagram. Regarding the combustion of methanol in the two cases, the temperature data confirms the remarks made on the discussion of the relevant pressure versus crank angle diagram (sub-section (a) above). The slow combustion of methanol in the presence of large quantities of products of combustion of DME, figure 6.37, leads to a very low peak cycle temperature of approximately 1399 K. Gas temperatures at EVO are of the order of 700 K in both cases for cycle 1, reflecting the low load. The temperature at EVO for cycle 2 is of the order of 400 K, which is approximately the same value at IVC, in figure 6.36. The same holds for figures 6.38 and 6.39. This would appear to indicate that the modelling of energy release of the DME is imperfect (see next sub-heading). In figures 6.38 and 6.39, the gas temperature

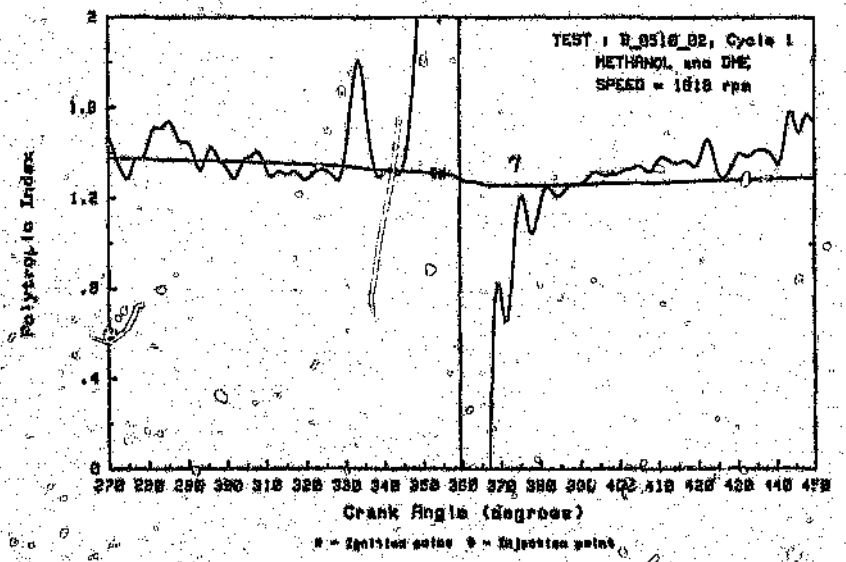

Figure 6.34: Polytropic index versus crank angle for high load, low DME fuel contribution

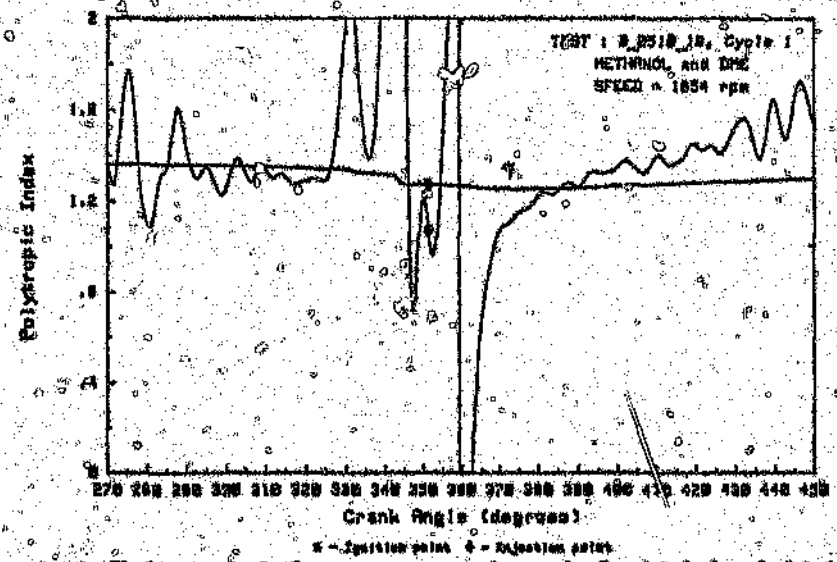

Figure 6.35: Polytropic index versus crank angle for high load, high DME fuel contribution

at EVO is of the order of 800 K in the former case, which makes sense in view of the higher load. In the latter case, however, this temperature is 600 K which may well be due to the dissipative losses associated with knock.

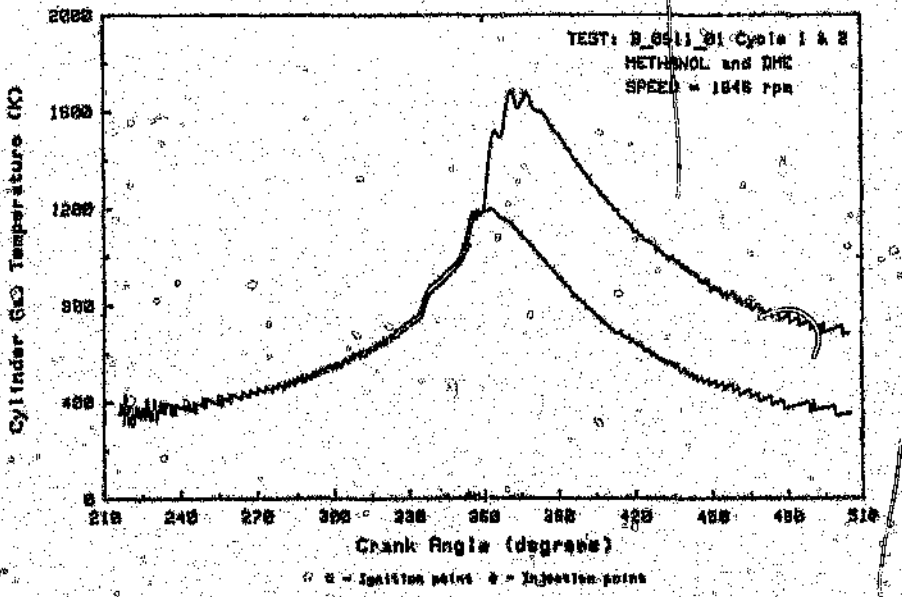

Figure 6.36: Combustion chamber gas temperature versus crank angle for low load, low DME fuel contribution

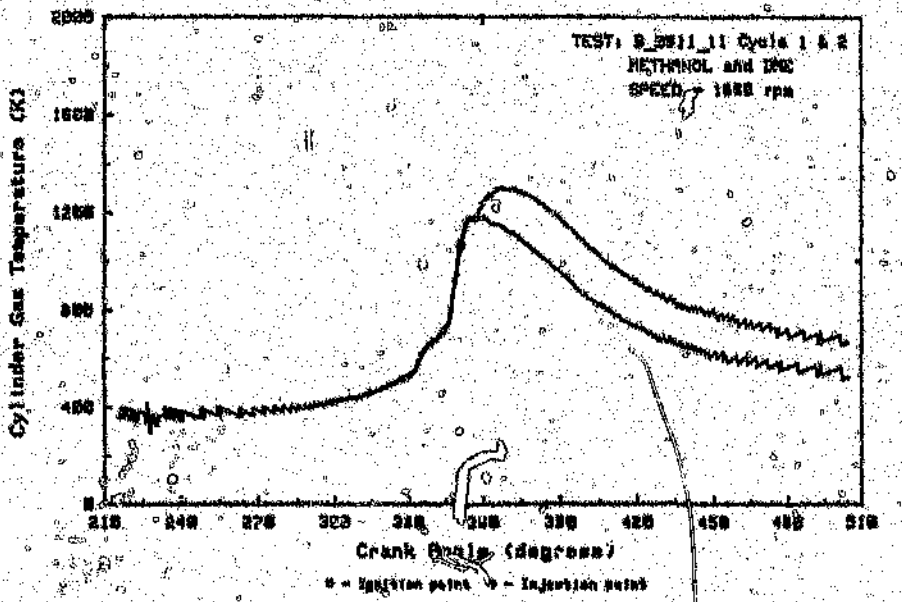

Figure 6.37: Combustion chamber gas temperature versus crank angle for low load, high DME fuel contribution

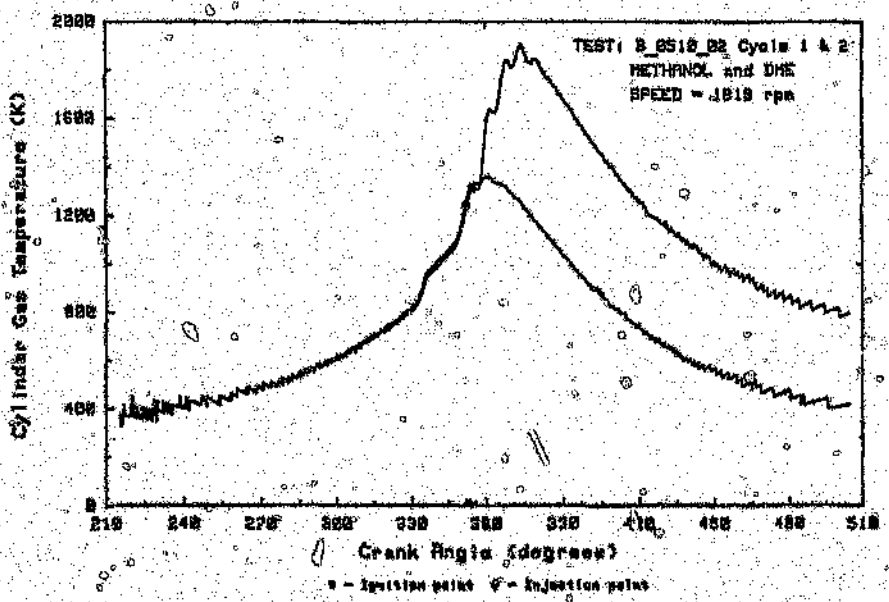

Figure 6.38: Combustion chamber gas temperature versus crank angle for high load, low DME fuel contribution

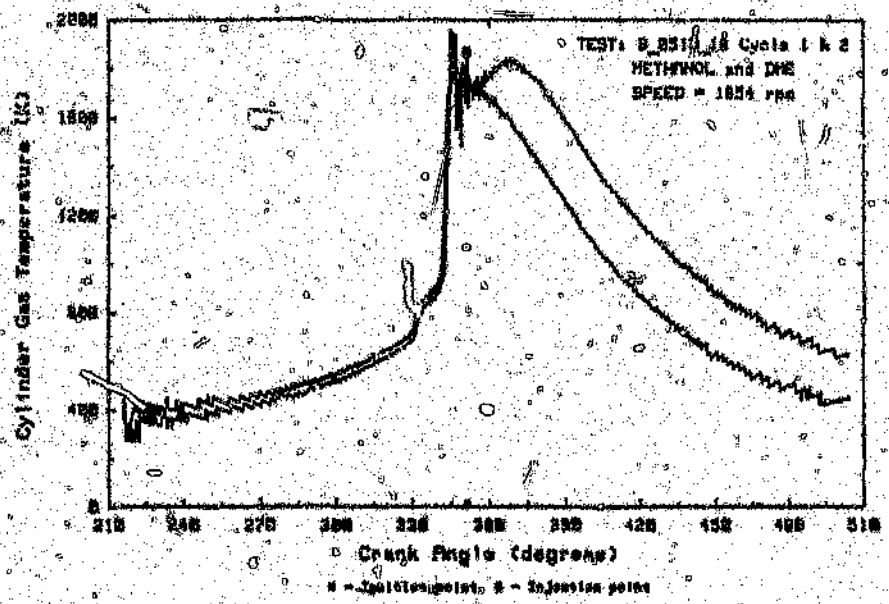

Figure 6.39: Combustion chamber gas temperature versus crank angle for high load, high DME fuel contribution

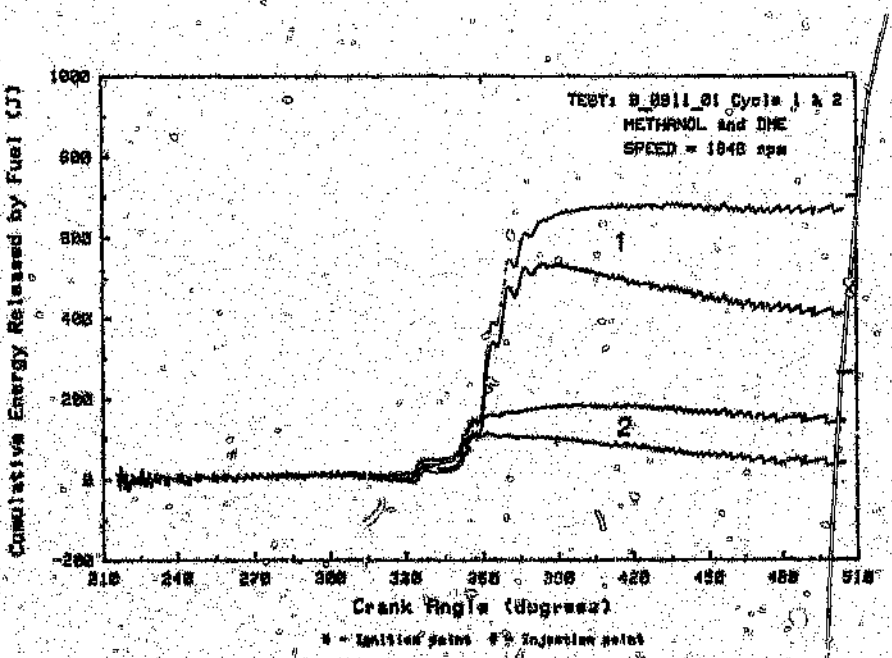

Figure 6.40: Cumulative energy release versus crank angle for low load, low DME fuel contribution

(f) Cumulative Energy Release versus Crank Angle

Figures 6.40 to 6.43 show the cumulative energy release diagrams for the four cases under discussion. In each figure cycle 1 and cycle 2 are superimposed, and each is rendered with and without heat transfer correction. In the expansion portion of the diagram the two top curves refer to cycle 1 and the two lower ones to cycle 2, the higher in each case depicting the energy release with heat transfer correction.

In the region of VC to approximately 300°CA the four curves coincide in all cases. In the region from 300° to approximately 350°CA, the cycle 2 curves lie slightly above those of cycle 1 in figures 6.40 and 6.42 and are essentially indistinguishable in figures 6.41 and 6.43. The two marks which appear on the right hand ordinates refer to the energy supplied during a cycle, the upper mark being that for cycle 1 and the lower for cycle 2. In the case of figure 6.43 the upper mark coincides with the upper frame of the diagram.

Before initiating the detailed discussion of energy release, the features of figures 6.40 to 6.43 will be noted in broad outline. These are: compression up to approximately 330°CA appears roughly adiabatic, as

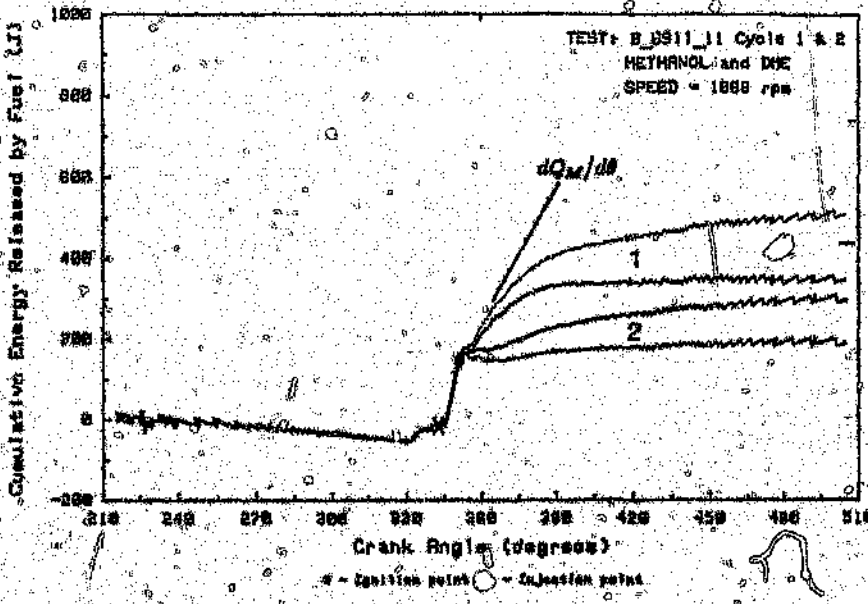

Figure 6.41: Cumulative energy release versus crank angle for low load, high DME fuel contribution

expected, in figures 6.40, 6.42 and 6.43. In figure 6.41 however, (low load, high DME) a negative energy release in this region appears to be indicated. The first energy release in all cases occurs at approximately 330°CA, and appears to be of roughly constant magnitude. The second energy release starts at some 345°CA, its amplitude increasing with the amount of DME supplied. In the case of figure 6.43 (high load, high DME) the latter energy release is rapid and results in knock. The rate of pressure rise associated with the initial combustion of methanol decreases with increasing DME fuel contribution. In general the modelled energy release (inclusive of heat transfer) accounts imperfectly for the fuel energy supplied, particularly for cycles 2 (DME only).

To facilitate detailed discussion, the magnitude of the first stage of energy release will be referred to as Q_1, and that of the second stage as Q_2, as shown in figure 6.44.

The first aspect of energy release to be considered is the apparent negative energy release that precedes Q_1, as indicated for example in figure 6.41. The first reaction to this finding was that it was due to

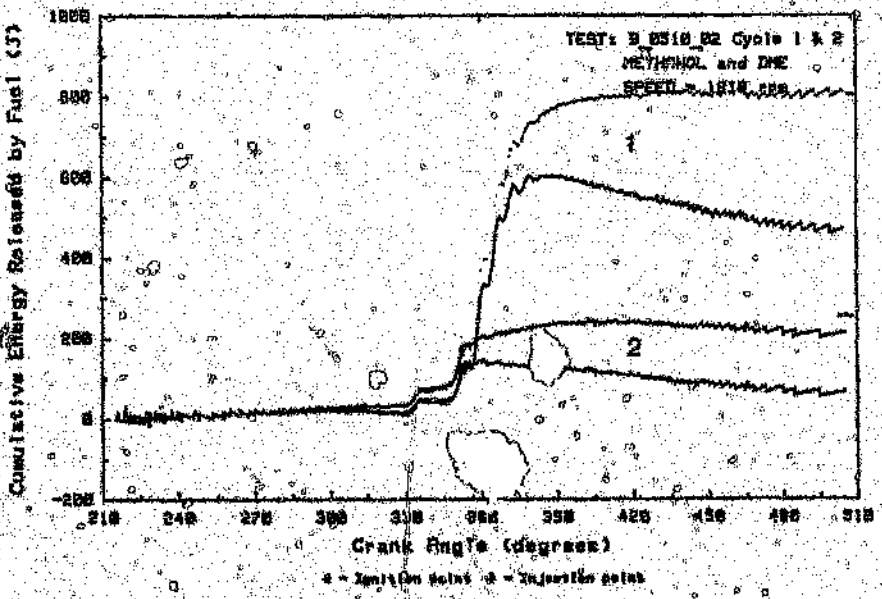

Figure 6.42: Cumulative energy release versus crank angle for high load, low DME fuel contribution

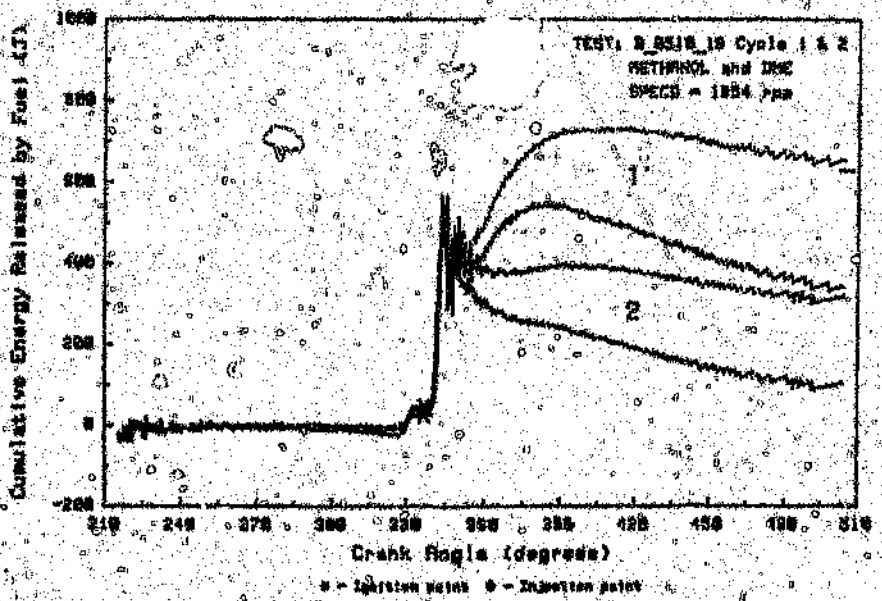

Figure 6.43: Cumulative energy release versus crank angle for high load, high DME fuel contribution

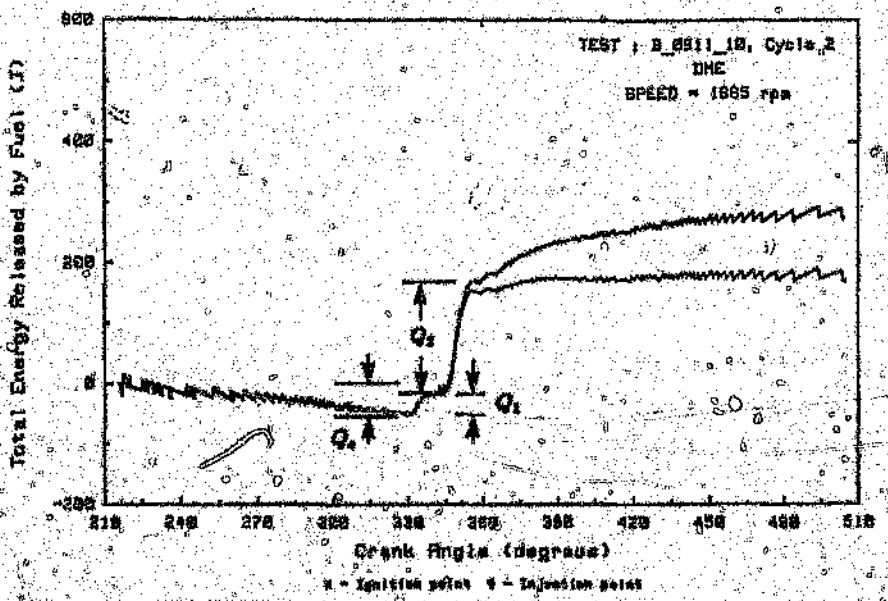

Figure 6.44: Cumulative energy release versus crank angle showing where Q_1 and Q_2 are measured

a computational error or that the particular test was atypical.

In order to examine the first aspect the raw pressure versus crank angle data was re-analysed for indications of such energy absorption. Figure 6.45 shows three pressure versus crank angle records superimposed for cycle 2 and low load for the cases of (1) $\phi_{DME} = 0{,}155$, (2) $\phi_{DME} = 0{,}186$ and (3) $\phi_{DME} = 0{,}235$. It will be noted that in the region preceding Q_1, the pressure at a particular crank angle falls with increasing ϕ_{DME}. Evidence for energy absorption during the early compression of the air DME mixture is thus inherent in the unprocessed data. The magnitude of this 'energy release' will be termed Q_n, and will be negative for the case of absorption.

In order to examine whether the data shown in figure 6.41 is atypical or is part of a general pattern, figure 6.46 shows Q_n versus ϕ_{DME} for all tests at both high and low load. (See also table 6.5). Each DME data point is the mean of cycles 1 and 2. Further in all but two cases both cycles 1 and 2 were recorded twice under the same conditions. Thus each data point is the mean of four cycles excepting for two points in which two cycles were averaged.

ϕ_{DME}	Q_e J	θ_1 °CA	Q_1 J	T_1 K	θ_2 °CA	Q_2 J	T_2 K
LOW LOAD							
0,155	13,1	332,7	35,7	741,3	346,5	101,0	943,5
0,176	4,5	332,5	38,0	72[illegible]4	346,9	121,2	941,8
0,186	-17,1	332,8	37,9	652,1	345,9	127,6	832,7
0,216	-42,7	331,2	36,5	583,8	343,5	158,7	771,2
0,243	-47,8	330,8	34,4	554,2	343,5	189,1	732,4
0,262	-53,9	330,1	36,1	535,1	342,9	197,4	708,0
0,283	-75,2	330,2	30,6	468,8	343,7	207,0	618,6
HIGH LOAD							
0,153	34,1	330,5	38,7	795,9	344,9	108,6	1007,6
0,191	23,5	330,7	39,8	772,1	344,1	133,0	985,2
0,218	28,9	329,8	47,5	801,0	343,2	180,4	1030,9
0,247	26,6	329,5	49,2	777,1	342,3	241,6	1003,0
0,283	17,4	330,0	47,2	744,6	341,0	286,6	952,0
0,306	1,5	329,5	41,7	679,3	340,9	325,4	872,4
0,339	-7,3	329,6	46,4	673,1	340,3	340,2	875,6
0,395	-2,5	328,8	46,3	684,2	339,2	377,5	890,8

Table 6.5: Stages of energy release of DME

Figure 6.47 shows exhaust temperatures measured in the exhaust manifold for the high and low load cases. The exhaust temperatures are seen to be higher for the high load case than for the low load, and further to increase with ϕ_{DME} in both instances. In an attempt to explain the higher exhaust temperatures at higher load, two factors are considered. The first concerns residuals. A simplified analysis given in appendix D shows however that the temperature of the mixture of fresh charge and residuals, on the basis of pure mixing (ignoring heat transfer from the walls) is approximately independent of load.

Of greater importance would appear to be the higher combustion chamber wall temperature in the case of higher load. Attempts were made to keep the cooling water temperature constant, this, however, does not change the fact that the higher the energy release (load)

the higher the mean internal wall temperature. The increasing wall temperature with increasing ϕ_{DME} for both high and low load is very likely to be due to the increasingly slow burning of methanol (see section (a) above, and below). Thus the heat transfer to the trapped mass is higher for high load than for low load and in each case increasing with increasing DME content of the mixture. The overall model assumed constant wall temperature in all cases.

The above effects can explain the information regarding Q_o shown in figure 6.46. The higher wall-to-gas heat transfer in the higher load case is clearly not correctly accounted for in the model, thus partially 'swamping' the energy absorption Q_o. This swamping effect is overall less pronounced at low load, that is, at low mean wall temperature. It is postulated that a pre-reaction energy absorption occurs in all cases and that Q_o should always be negative (and become more so with increasing ϕ_{DME}). The inadequacies of the heat transfer model would appear to have resulted in a displacement of the Q_o curve in a positive direction. These wall temperature effects also explain the flatter slope of the Q_o curves at high load: the steeper slope of the high load exhaust gas temperature curve would suggest a more rapid increase in wall temperature with ϕ_{DME} than for low load.

Having discussed the temperature dependence of the amplitude of Q_o, it is of interest to examine the duration of this pre-reaction. It was stated earlier that the onset of Q_1, in other words the end of the pre-reaction, occurred at essentially constant crank angle, that is, at a constant time after IVC (the tests having been conducted at constant speed). On closer examination of table 6.5, and on plotting crank angles corresponding to the onset of Q_1, referred to as θ_1 (see figure 6.45), two trends emerge. First, the values of θ_1 are generally lower at high load than at low load and secondly in both cases fall with increasing ϕ_{DME}. In view of the foregoing discussion it would appear, at first sight, that the duration of the pre-reaction Q_o (measured from IVC) is wall temperature dependent, decreasing with increasing temperature.

The calculated gas temperatures at θ_1, that is, T_1, however fall with ϕ_{DME} and more drastically at low load than at high load (see figure 6.50). This might suggest that the duration of Q_o decreases with increasing wall-to-gas temperature difference. Since the wall temper-

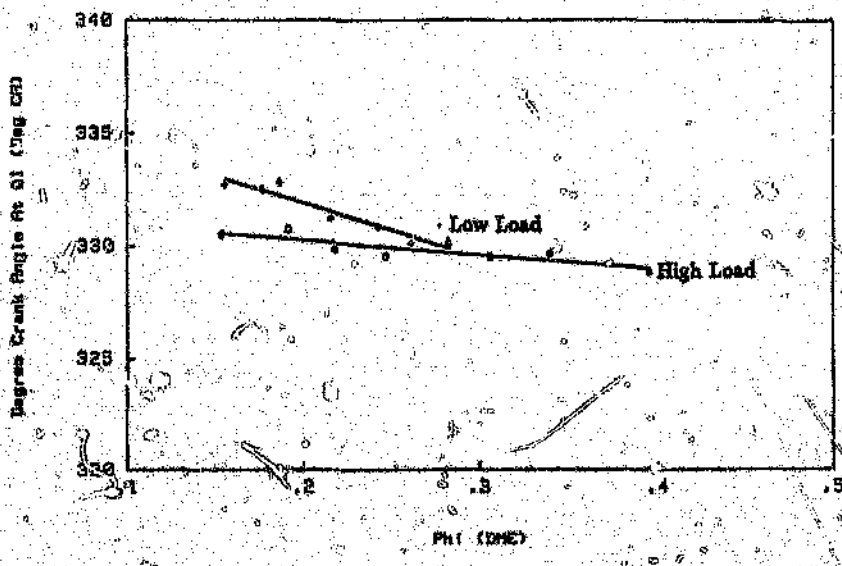

Figure 6.48: Degree crank angle at Q_1 versus ϕ_{DMY} for low and high loads

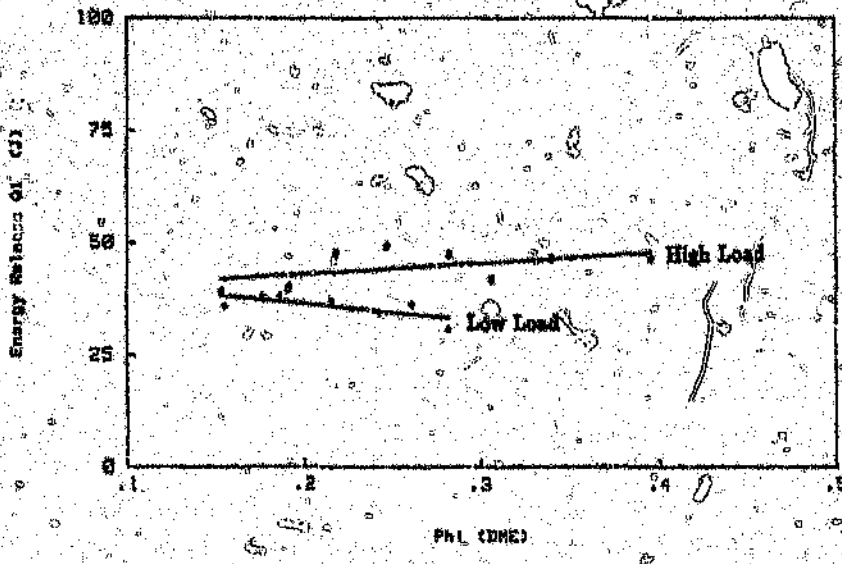

Figure 6.49: Energy release Q_1 versus ϕ_{DMX} for low and high loads

ature, however, is not known this possible explanation can not be further explored.

A further difficulty in this connection arises from the preliminary tests (chapter 5, section 5.3.5) in which the inlet air was heated and cooled. These tests were conducted on an incompletely instrumented test rig, which did not permit the comprehennive recording of data. However, at an approximate engine speed of 1510 rev/min, the varying of air/DME mixture from -5,5°C to 41,8°C led to a change of θ_1 from 118,8° to 112,4°CA from IVC. This corresponds to a difference in pre-reaction duration measured from IVC of 0,71 ms. The time scale in figure 6.48 is 0,45 ms for 5°CA. Thus the difference between the shortest and the longest pre-reaction is 0,35 ms. The important point is that in these preliminary tests θ_1, moved in the opposite direction with gas temperature than in the main tests discussed above. The wall temperature in the preliminary tests is again unknown. The duration of the pre-reaction, that is, the magnitude of θ_1, would appear to require study by techniques other than those available on the present test rig.

Clearly the presence of the endothermic pre-reaction, in effect cooling during compression, is by itself favourable to engine performance. The combustion of DME however, exhibits other complicating features, which require prior analysis before the overall effect on performance can be discussed.

The next item to receive attention is the magnitude of the first energy release, Q_1. This is given in table 6.5 and figure 6.49. (The majority of data points, as in previous figures, are the mean of four tests). The magnitude for both high and low loads appear to be essentially independent of ϕ_{DME} and to be of the order of 44 J and 36 J respectively.

Figure 6.50 shows the calculated gas temperature at the start of the energy release Q_1. The variations in temperature are clearly the result of the cumulative energy absorption Q_a, as borne out by the geometric similarity of figures 6.46 and 6.50. Evidently the magnitude of the energy release Q_1 is essentially independent of temperature. The observed effects could be explained as follows: the energy release Q_1 is associated with a preparation reaction for the second energy release Q_2. The latter reaction starts, though preceded by an induction pe-

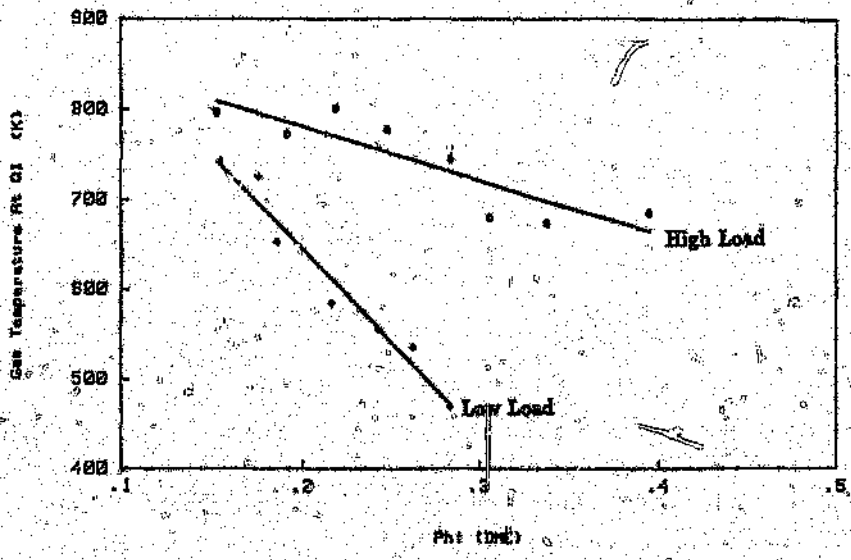

Figure 6.50: Calculated gas temperature at the start of Q_1 versus ϕ_{DME} for low and high loads

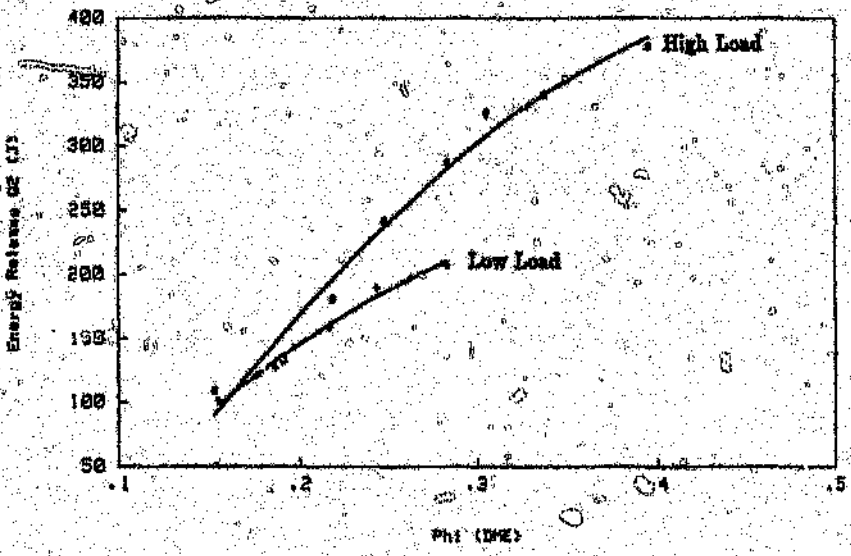

Figure 6.51: Energy release Q_1 versus ϕ_{DME} for low and high loads

riod, when a certain fixed concentration of products of the reaction Q_1 is attained in the mixture. The above interpretation suggests the possibility that the magnitude of Q_1 is an overall constant and that the small difference between high and low loads is due to an error in the heat transfer model. This suggests that Q_1 has a constant value of about 40 J overall. The trapped air/DME mixture per cycle amounted to a mean of (18,29 $\pm$ 0,33) (10^{-6}) *kmol* over all reported tests. Thus the energy release Q_1 is estimated at 2,19 $\times 10^6$ $J/kmol$ of ignitable air/DME mixture.

The measurement of the magnitude of the second energy release Q_2 presents a number of problems. First, in attempting to extract these values from the energy release diagrams for cycles 1, it was difficult to detect the end of this energy release (particularly in the cases of high DME). The reason for this is that the methanol ignites immediately on injection. Thus all the data pertaining to Q_2 in table 6.5, and the figures to be discussed below refer to cycle 2. (The majority of these data points are the means of two tests). Even in the case of cycle 2, however, the definition of the termination of Q_2 presents difficulties. Figures 6.40 to 6.43 generally show a steep energy release before TDC, followed by what appears to be additional slower burning. Since the main concern here is with aspects of negative work associated with Q_2, the end of the energy release was defined as the end of the steep energy release as shown in figure 6.44.

The magnitude of Q_2 thus defined is shown in figure 6.51. Two features are to be noted. First, and not surprising, the more DME is present, the greater the associated energy release. Secondly, at a particular ϕ_{DME} the energy release at high load is greater than at low load. The latter effect is not easy to explain. It should be noted however, that the engine ran hotter at high load than at low load and that the model assumes the same wall temperature distribution throughout.

The crank angles (times) corresponding to the onset of Q_2, ie θ_2, are shown in figure 6.52. This figure is similar in appearance to figure 6.48 (θ_1 versus ϕ_{DME}) but steeper in slope. The explanation of these variations presents the same problems as those associated with θ_1, and similarly requires further study.

The calculated gas temperature corresponding to the onset of Q_2, ie

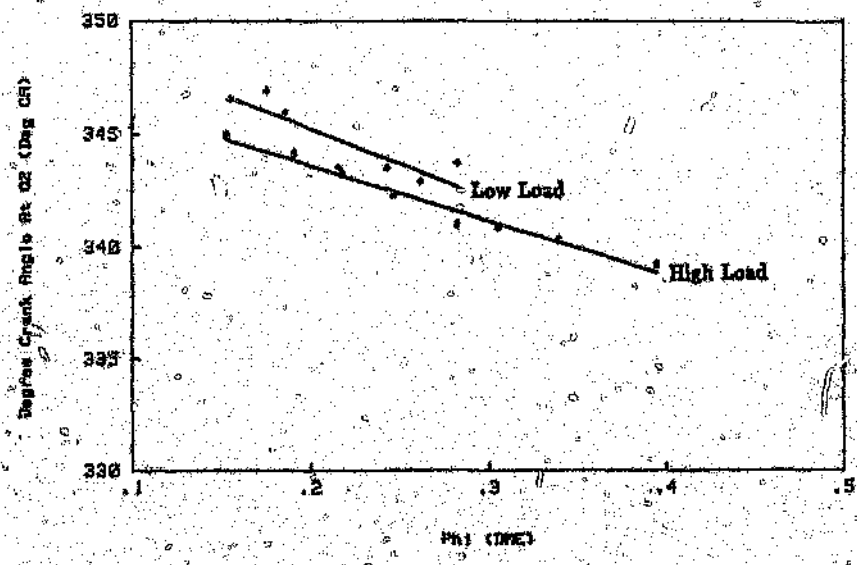

Figure 6.52: Degree crank angle at Q_2 versus ϕ_{DME} for low and high loads

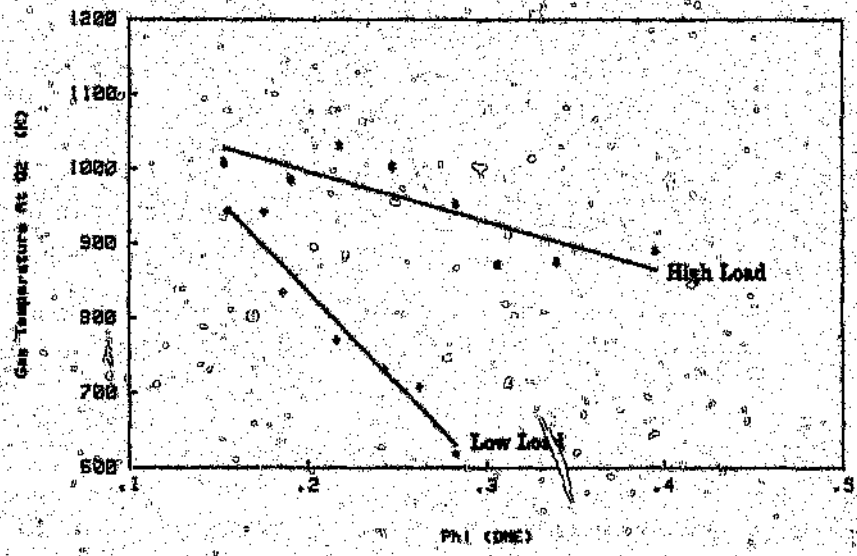

Figure 6.53: Calculated gas temperature at the start of Q_2 versus ϕ_{DME} for low and high loads

T_2, is shown in figure 6.53. This figure is essentially identical to figure 6.50 (T_1 versus ϕ_{DME}) but displaced upwards by approximately 200 K. This is clearly the result of an essentially constant energy release namely Q_1, together with normal compression, that has occurred between θ_1 and θ_2.

Clearly the chemistry of oxidation of DME is complex and deserving of detailed study. The postulation of and the testing for the reaction mechanisms and the study of the associated kinetics, falls outside the field of mechanical engineering thermodynamics. No speculation regarding these matters are offered in the present study. Engine performance, however, can and will be explained below in terms of the three stages of reaction of the air/DME mixture that have been identified.

Consideration is given first to the combustion of DME as the sole fuel. The maghitude of the pre-reaction Q_0 increases with increasing DME proportions of the fuel thus causing increasing cooling during compression and thus progressive reduction in negative work. The energy release Q_1 is of approximately constant magnitude, but occurs at increasingly earlier crank angle with increasing ϕ_{DME}. The energy release Q_2 increases in magnitude with increasing ϕ_{DME} and occurs at progressively earlier crank angle (all before TDC). The latter two effects cause an increase in negative work with increasing proportions of DME in the fuel. Figure 6.54 shows the indicated thermal efficiency for cycle 2 (DME alone) for both low and high loads as a function of ϕ_{DME}. It would seem that the cooling effect of Q_0 predominates up to approximately $\phi_{DME} = 0{,}25$ and is thereafter swamped by the unfavourable effects of Q_1 and Q_2.

It will be re-called that in considering engine performance of methanol/DME dual fuelling, the indicated thermal efficiency was found to decrease consistently with ϕ_{DME} at both low and high loads, (see figure 6.18). Clearly the favourable effect of increasing concentrations of DME in the range $\phi_{DME} < 0{,}25$, (figure 6.54) are overridden by poor burning of methanol. It has previously been noted, section 6.2.2 (a), that an increasing ϕ_{DME} leads to a reduction in the rate of pressure rise on combustion of methanol. Figure 6.55 shows the initial rate of energy release of methanol $dQm/d\theta$ (measured as indicated in figure 6.41) to fall with ϕ_{DME} for both low and high loads, the

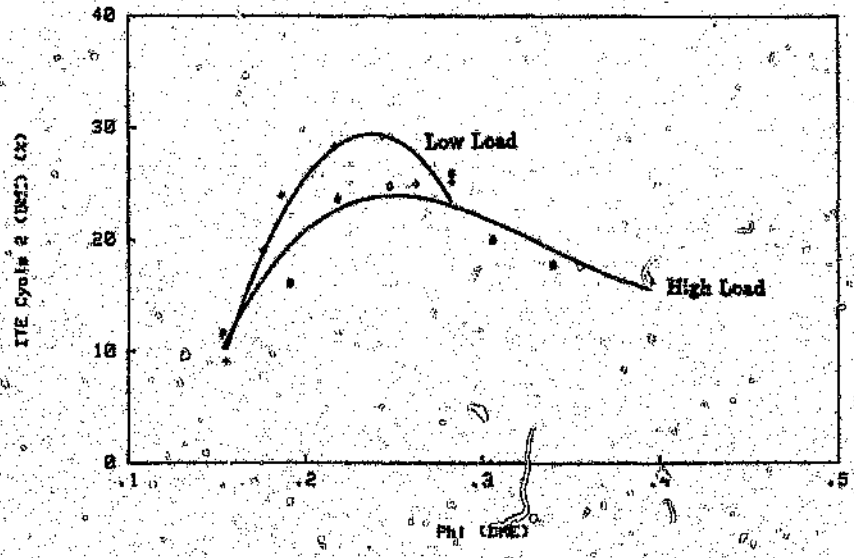

Figure 6.54: Indicated thermal efficiency for cycle 2 (DME only) versus ϕ_{DME} for low and high loads

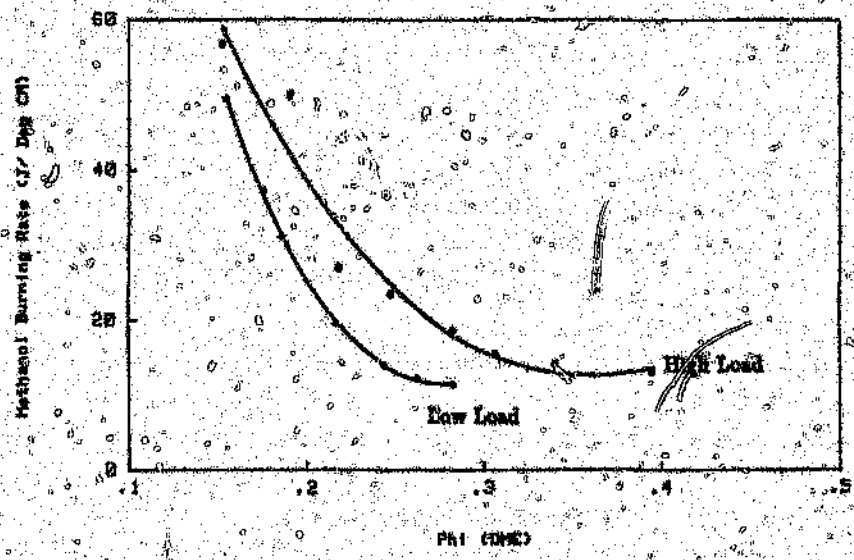

Figure 6.55: Initial rate of energy release of methanol versus ϕ_{DME} for low and high loads

decrease being drastic at low ϕ_{DME}. The reason for this behaviour would appear to be that methanol is injected at a point when the combustion of DME is completed, or nearly so. This means that with increasing ϕ_{DME}, methanol burns in an environment containing increasingly large pre-existing concentration of carbon dioxide and water. (Considerations concerning the progressively decreasing concentration of oxygen are not to the point, since $\phi_{TOTAL} < 1$, that is, overall mixtures were lean in all tests). Figure 6.56 shows the concentrations of carbon dioxide and water (calculated by the energy release model) which result from the complete combustion of DME in all tests versus ϕ_{DME}.

The addition of CO_2 to gaseous fuel/oxidant mixtures has been noted to lead to drastic reduction in laminar burning velocity (Lewis and Von Elbe, 1951). Jawurek *et al* (1987), on testing of a spark ignition engine fuelled with simulated raw biogas, that is, mixtures of methane and carbon dioxide, found increasingly poor burning of methane (low rate of pressure rise, peak pressure low in amplitude and retarded in crank angle position) with increasing carbon dioxide content in the gas.

It will be noted that the decrease in the initial rate of energy release of methanol, $dQ_m/d\theta$, is particularly sharp in the region $\phi_{DME} <$ 0,25 (figure 6.55). It is in this same range of concentration that the indicated thermal efficiency of DME burning by itself increases with increasing ϕ_{DME} (figure 6.54). The combination of these two effects leads to an indicated thermal efficiency for combined methanol/DME fuelling that falls throughout the entire range of DME concentrations (figure 6.18). The most favourable concentration of DME is thus the minimum above the onset of misfire.

It was mentioned at the beginning of this subsection that the modelled energy release accounts imperfectly for the supplied fuel energy. Table 6.6 shows the ratio of the modelled energy release at EVO, Q_{EVO}, to the energy supplied by the fuel, Q_{FUEL}. The ratios in all cases except one are less than unity. In general, Q_{FUEL} is accounted for more completely in the case of high load than low load. This is particularly the case if the last three sets of tests below the dotted line in table 6.6 (high load portion) are disregarded. In this region there was evidence of knock, the dissipative losses of which the energy release model did not consider.

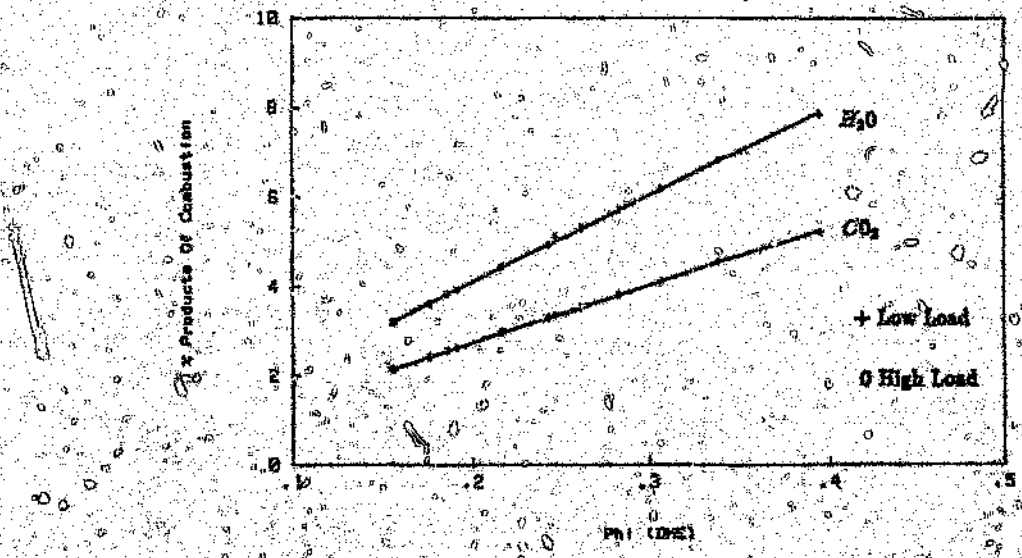

Figure 6.56: Concentrations of CO_2 and H_2O resulting from the complete combustion of DME versus ϕ_{DME} for all tests

Clearly the energy release model and in particular the heat transfer effects are better 'tuned' for the high load (higher engine temperature) than for low load. An improvement in the ratio Q_{EVO}/Q_{FUEL} could be brought about by assigning a lower wall temperature distribution to this case. This however would not be sufficient to account for the falling trend Q_{EVO}/Q_{FUEL} for cycle 1 with increasing ϕ_{DME}. Despite these imperfections the energy release model has permitted a substantial amount of information on this complex fuelling system to emerge.

(g) Temperature versus entropy

Figures 6.57 to 6.60 show the temperature versus entropy diagrams (mildly smoothed) for cycle 1 (both fuels) corresponding to the energy release diagrams, figures 6.40 to 6.43. In general the temperature entropy diagrams confirm the events previously discussed but the details of DME combustion are a little more difficult to recognise.

Shown on all figures are temperatures T_1 and T_2 which mark the start of Q_1 and Q_2 respectively. These temperatures are taken from table

ϕ_{DME}	CYCLE 1			CYCLE 2		
	Q_{EVO} J	Q_{FUEL} J	$\frac{Q_{EVO}}{Q_{FUEL}}$ %	Q_{EVO} J	Q_{FUEL} J	$\frac{Q_{EVO}}{Q_{FUEL}}$ %
LOW LOAD						
0,155	652,6	705,1	92,6	160,0	264,6	60,5
0,176	644,5	719,4	89,6	213,5	293,7	72,7
0,186	605,7	719,7	84,2	234,0	318,0	73,6
0,216	550,2	709,3	77,6	265,4	356,3	74,5
0,243	524,4	721,1	72,7	341,0	397,4	85,8
0,262	516,7	738,1	70,0	290,0	433,2	66,9
0,283	447,8	742,2	60,2	257,7	469,7	54,9
HIGH LOAD						
0,153	768,9	800,8	96,0	211,0	251,1	84,0
0,191	761,9	839,5	90,8	249,8	317,4	78,7
0,218	878,7	847,6	103,7	339,2	346,5	97,9
0,247	862,2	873,8	98,7	377,5	398,6	94,7
0,283	351,4	895,4	95,1	406,2	452,1	89,8
0,306	686,3	912,7	75,2	314,4	492,2	63,9
0,339	635,6	955,9	66,5	299,5	546,5	54,8
0,395	640,6	1001,8	63,9	453,6	625,9	72,5

Table 6.6: Modelled energy release and supplied fuel energy

6.5, where the tabulated values are generally the means of four tests and were read from the cumulative energy release and temperature versus crank angle diagrams. It is for this reason that the indicated temperatures do not in all cases coincide exactly with the 'kinks' in the T versus s curves. It would have been possible and perhaps preferable to read these temperatures from the temperature entropy diagrams, and to average in each case for the (usually) four tests. The level of agreement between the 'kinks' and the indicated temperatures obtained by the methods attained above, is in any event gratifying. The end of the energy release Q_2 is quite difficult to detect in all four figures. However an estimate of its position is shown in figure 6.58 for purposes of illustration. The figure also shows the entropy intervals corresponding to Q_1 and to the endothermic pre-reaction Q_v. As was the case in the energy release diagram, Q_v is 'masked' in the other three figures. The unusual appearance of the compression curve in figure 6.60 (high load, high DME) is due to the large energy release Q_2 before TDC.

Not too much importance should be attached to the falling temperature portion of the expansion curves. In the case of figures 6.57 and 6.59 (low DME) these appear approximately adiabatic as also shown in the energy release diagrams. Figure 6.58 (low load, high DME) indicates energy release up to EVO. It is doubtful whether this effect is real; on the other hand the rate of combustion of methanol was found to be very low in this case. Regarding figure 6.60, it will be recalled that the energy release model fails to take knock into account. The portion of the curve after the onset of knock should thus be disregarded.

As noted during the discussion of the combustion of diesel fuel, the strength of the temperature entropy diagram lies in the expansion of the region near TDC. In this regard, satisfactory burning of methanol is noted with low DME contribution, figures 6.57 and 6.59 and poor burning with high DME contribution, figures 6.58 and 6.60.

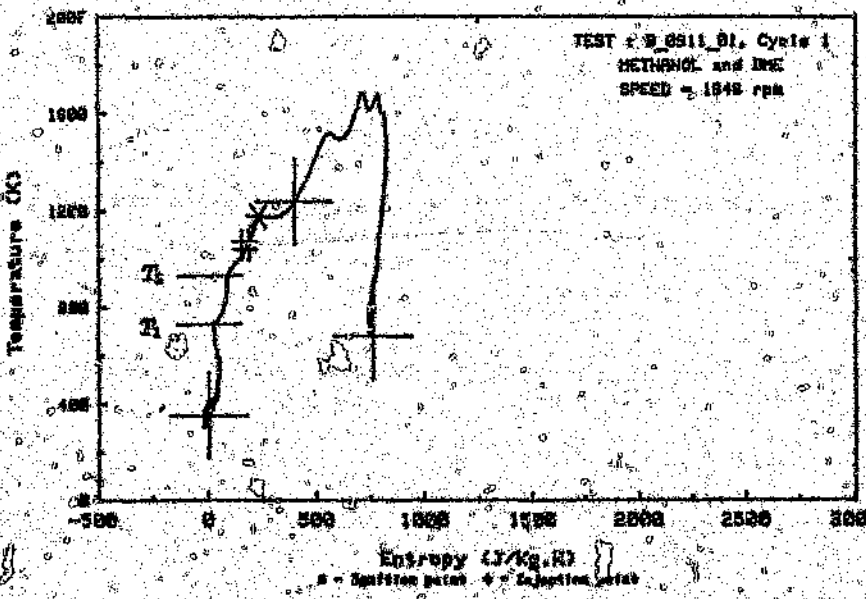

Figure 6.57: Temperature versus entropy for low load, low DME fuel contribution

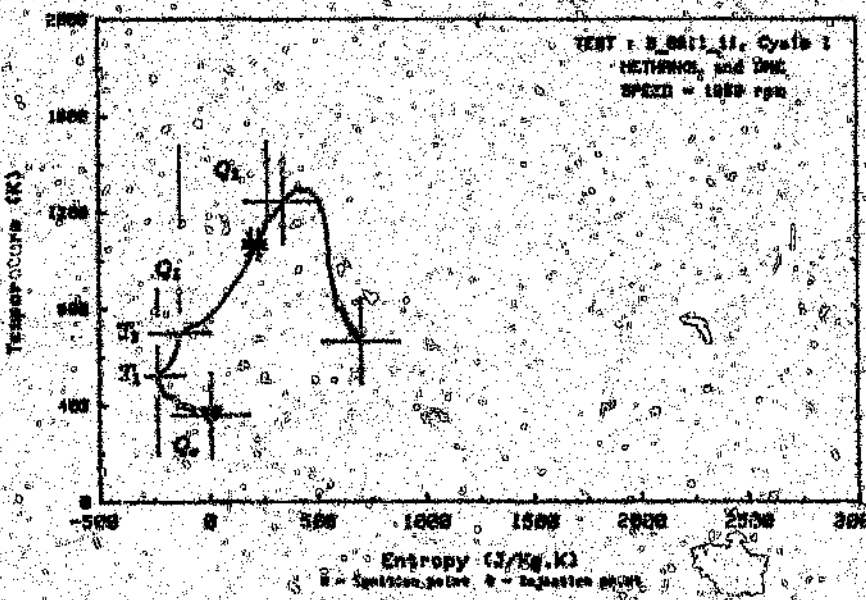

Figure 6.58: Temperature versus entropy for low load, high DME fuel contribution

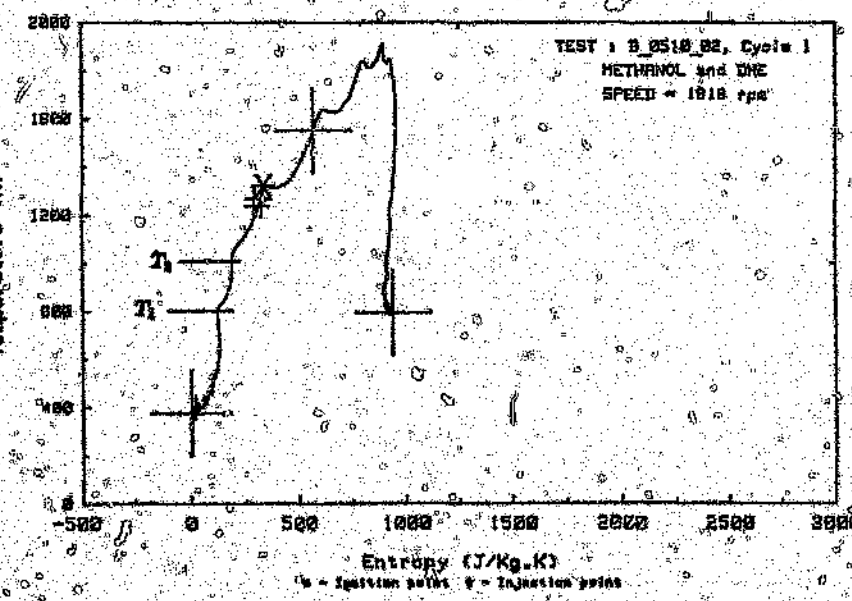

Figure 6.59: Temperature versus entropy for high load, low DME fuel contribution

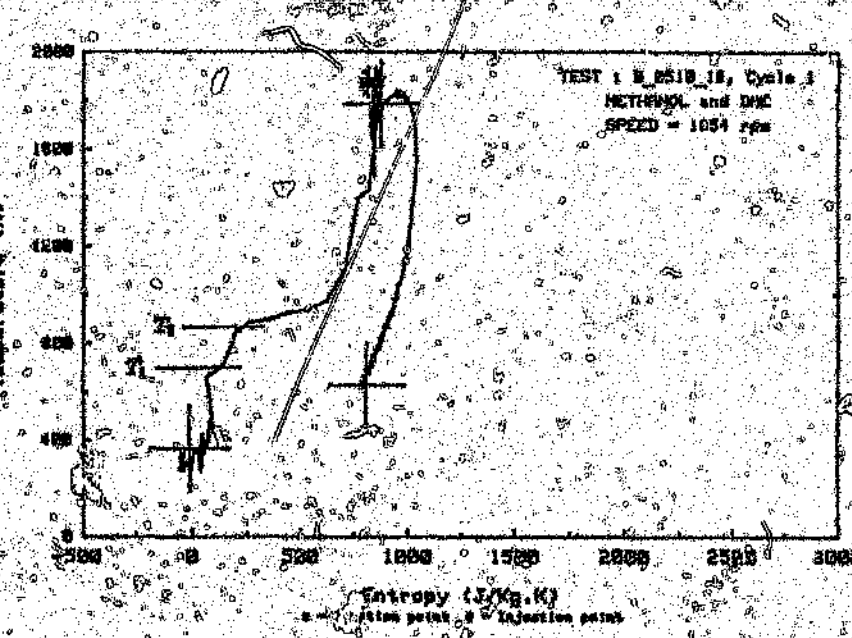

Figure 6.60: Temperature versus entropy for high load, high DME fuel contribution

Chapter 7

CLOSURE

Conclusions have already been stated or implied at various points, particularly in Chapter 6, of this thesis. The more important conclusions are summarised below, and an attempt is made to assess the novel contributions which this thesis makes. This is followed by suggestions for further work.

7.1 Summary, Conclusion and Comments

The main aim of this study was to develop and refine thermodynamic techniques for the study of combustion in compression ignition engines. These techniques were then applied to the incompletely understood case of methanol/DME fuelling. Prior to this application the techniques were to be 'calibrated' against test runs on diesel fuelling.

A general appraisal of methanol as a compression ignition engine fuel was given in order to place methanol/DME fuelling into perspective.

The only previously published work on this fuelling system (Brook, *et al* 1984) was preliminary in nature but revealed some unusual features of combustion. Exploratory tests were therefore conducted by the present author which indicated that the combustion was indeed complex in nature.

In order to unravel these complexities, attention was focused on energy release modelling and the relevant literature was reviewed. It was concluded that none of the available models was entirely suited for the methanol/DME system.

A number of thermodynamic techniques, both experimental and analytical, including a refinement of existing energy release models, was therefore developed and consolidated.

The first group of these techniques was the determination of data on: combustion chamber pressure (p) versus crank angle (θ), p versus combustion chamber volume (V), dimensionless $\ell n\ p$ versus $\ell n\ V$ and injector line pressure versus θ. This necessitated the presence of a combustion chamber pressure transducer and a shaft encoder. These techniques are well established. They were, however, executed in such a manner that the recording of a normal single firing cycle with methanol/DME fuelling (cycle 1) was followed immediately by a cycle on DME fuelling alone (cycle 2) at otherwise identical engine conditions. Further, in a similar manner a pure motoring cycle (no fuel at all) could be recorded, at engine speed and temperatures essentially identical to those of cycle 1, or of a diesel combustion cycle. Thereafter, the engine could immediately be restored to normal fuelling. Such special cycles were thus 'embedded' in normal firing cycles.

The recording of single non-firing cycles is well known in spark ignition engine work, but has not, to the author's knowledge, previously been achieved in compression ignition engine work. The recording of 'cycle 2' type data is also believed to be novel.

The recording of cycles 1 and 2 and their superimposition proved valuable in unraveling the interaction of the two fuels. The value of the motoring cycle lay mainly in the 'calibration' of the heat transfer model. (With heat transfer correctly accounted for, a motoring cycle is adiabatic).

These special cycles could be achieved very conveniently on the particular test rig that was used. The test rig of this study consisted of a two cylinder engine each with its own fuel pump. When desired, the fuel supply to the instrumented cylinder could be rapidly interrupted by decoupling the cam and plunger, while the other cylinder continued in normal operation. Similarly, the DME was supplied separately to each cylinder so that the flow to the instrumented cylinder could be interrupted and re-established

as desired. The technique could however, with slightly reduced convenience be adapted to an in-line fuel pump system.

The second group of techniques was analytical in nature and resulted from numerical modelling. The techniques involve the study of the interrelationship of the following: polytropic index n and the ratio of the principal thermal capacities γ versus θ, combustion chamber temperature T versus θ, cumulative energy release Q versus θ, and T versus entropy s. The data of γ, T and s are all obtained from the energy release model Q versus θ.

The model is a variant of that of Krieger and Borman (1966) featuring the following refinements: during compression DME is accounted for and assumed to go to its equilibrium products of combustion at each increment of θ. During the incremental combustion of methanol the equilibrium products of reaction (14 species) of both fuels determine the specific gas constant and the specific thermal capacities. Heat transfer to and from the trapped mass is evaluated by using a model specifically developed for this engine which takes into account convection resulting from longitudinal, radial and swirl flows in the combustion chamber, as well as radiation. In the case of the Krieger and Borman model, heat transfer was estimated according to the less comprehensive equations of Annand and Ma (1970).

A large number of tests were conducted on diesel fuelling for purposes of optimising the injection timing and for checking the correct functioning of the instrumentation and data gathering software. The techniques discussed above were then applied to a few of these tests. The information thus obtained showed the techniques to be free from major error and to be mutually corroborative and complementary. The modelling of the combustion chamber heat transfer was found to be imperfect but sufficiently effective so as not to mask the various features of combustion.

Having established confidence in these techniques, they were then applied to the little understood case of methanol/DME fuelling. Tests were performed at the same injection timing as that for diesel fuelling. Two loading conditions were chosen (termed 'high' and 'low'). At each condition the initial mass flowrate of DME was the lowest possible corresponding to the onset of misfire; the flowrate of DME was increased gradually and that of methanol decreased such that the load and speed were maintained essen-

tially constant. The procedure was continued until the onset of knock or until the selected speed could no longer be maintained. Thus for each load setting a number of tests at constant power were conducted with varying ratios of methanol to DME fuel.

The equivalence ratio ϕ_{TOTAL} (referred to both fuels) was less than unity throughout, that is, the mixtures were lean. The equivalence ratio ϕ_{DME} (referred to the DME component only) varied from 0,155 to 0,395.

Brake thermal efficiency (BTE) and indicated thermal efficiency (ITE) were defined on the basis that methanol and DME were separate fuels. Since the net energy gain or regeneration on catalytic conversion of methanol to DME is negligible, this definition holds also for the practical situation in which the engine/catalytic converter system is supplied with a single fuel, namely methanol.

Both BTE and ITE fell with increasing ϕ_{DME} but the drop was more gradual with the former. Correspondingly the mechanical efficiency increased with increasing ϕ_{DME}, that is, decreasing methanol fuel contribution. This increase in mechanical efficiency is largely due to a decrease in the methanol pumping work.

The thermodynamic techniques discussed above were now applied to individual combustion cycles, both on dual fuelling (cycle 1) and on DME fuelling alone (cycle 2). While each technique proved valuable, the simultaneous application of all of them, augmented the overall understanding of the combustion phenomena. Nevertheless, certain techniques were particularly informative. These are: the superposition of cycle 1, cycle 2, and in certain cases motoring cycle, data; the experimental methods that permit the recording of cycles 1 and 2; and energy release modelling as described above.

The DME was found to combust in a complex manner, which also affected the subsequent combustion of methanol. The DME releases energy in two stages, of magnitude termed Q_1 and Q_2, occurring at crank angles θ_1 and θ_2. The energy release Q_1 is preceded by what appears to be an endothermic pre-reaction, of magnitude Q_0. This pre-reaction is masked in some energy release diagrams, owing probably to inadequacies in the heat transfer model. Evidence for its presence is, however, inherent in the raw p versus θ data. The magnitude of the energy absorption Q_0 increases with ϕ_{DME},

and decreases with load. Exhaust temperatures and thus presumably also combustion chamber temperatures increased with load and ϕ_{DME}, the latter owing to slow burning of subsequently injected methanol. Since the heat transfer model assumes a constant combustion chamber wall temperature distribution, there is some doubt about the absolute magnitude of Q_o. The endothermic pre-reaction is equivalent to cooling during compression, thus leading to a reduction in negative work.

The first energy release Q_1 occurs at nearly constant crank angle, $\theta_1 \approx 330°$. The magnitude of Q_1 at high and low load is essentially independent of ϕ_{DME} and is of the order of 44 and 36 J respectively. The calculated gas temperature at the start of Q_1, that is, T_1, varies from approximately 800 to 700 K from minimum to maximum ϕ_{DME} at high load, and from approximately 750 to 500 K at low load. (These variations in temperature are the result of the preceding energy absorption Q_o). The magnitude of the energy release Q_1 thus appears to be independent of gas temperature. These effects suggest the following: Q_1 is associated with the preparation reaction for the second energy release Q_2. The latter starts when a fixed concentration of products of the reaction Q_1 has been attained in the mixture. (Additionally there is a time lag between the end of Q_1 and the start of Q_2). The above suggests that Q_1 might be constant overall and that the difference between high and low loads is due to error in the heat transfer modelling. Thus Q_1 might be constant at 40 J overall. This figure is equivalent to $2{,}19 \times 10^6$ $J/kmol$ of air/DME mixture. By way of comparison it should be noted that the largest value of Q_o is -75 J.

It is stated above that the onset of Q_1 occurs at 'nearly constant' crank angle. In fact θ_1 advances very slightly with load and ϕ_{DME}. Exhaust gas temperature and thus presumably combustion chamber wall temperature similarly increases with ϕ_{DME} and load. The gas temperature at θ_1, however, that is, T_1, falls with ϕ_{DME}, but less so at high load than at low load. Since additionally the combustion chamber wall temperature is not known with any certainty, no speculative explanations regarding the observed trend in θ_1 are offered here.

The second stage of energy release Q_2 occurs at crank angles θ_2 varying from 347° to 343° with increasing ϕ_{DME} for low load, and from 345° to 339° for high load. These trends are an accentuated version of those observed with θ_1. The magnitude of Q_2 increases with ϕ_{DME} and accounts (though not

in all cases perfectly) for the remaining DME fuel energy. The rate of pressure rise during energy release Q_2 increases with ϕ_{DME} and ultimately leads to knock. While the end of energy release Q_2 is difficult to detect (and particularly so in the presence of knock) it is reasonable to state that DME burns essentially to completion before TDC.

The three stages of reaction of DME/air mixtures have not to the author's knowledge been previously identified in CI engine fuelling studies. Although no suggestion regarding the mechanisms of these reactions are offered in this study, engine performance may be explained in terms of them.

Consideration is first given to fuelling on DME alone. A progressive increase in ϕ_{DME} leads to the following: the endothermic pre-reaction Q_0 increases in magnitude thus causing a progressive reduction in negative work; the energy release Q_1 is of approximately constant magnitude but occurs at increasingly earlier crank angles; the energy release Q_2 increases in magnitude, occurs at progressively earlier crank angles and is essentially completed before TDC; the latter two effects cause an increase in negative work. The ITE for cycle 2 (DME alone) initially increases up to $\phi_{DME} = 0{,}25$ and then decreases. Thus the cooling effect of Q_0 initially predominates and is then swamped by the unfavourable effects of Q_1 and Q_2.

DME, however, is intended to be used in conjunction with injected methanol fuel. At low levels of DME, a lag occurs between injection and ignition of methanol. Below $\phi_{DME} \approx 0{,}155$, methanol does not ignite at all. At high levels of DME however, methanol ignites immediately at injection and burns at the nozzle. The rate of burning of methanol is strongly dependent on the concentration of DME, the initial rate of pressure rise falling sharply with ϕ_{DME}. Since the DME is combusted essentially to completion before the ignition of methanol, the latter burns in an atmosphere containing increasing pre-existing concentrations of CO_2 and H_2O. This causes the progressively lower rate of burning of methanol. This decrease in the rate of burning is particularly sharp in the region $\phi_{DME} < 0{,}25$, that is, the range in which the ITE of DME by itself increases with ϕ_{DME}. The overall effect of these phenomena is a reduction in ITE with methanol/DME fuelling throughout the range of DME concentrations. The most favourable concentration of DME is thus the lowest above the misfire limit.

7.1.1 Suggestions for Further Work

A number of improvements could be made in the experimental techniques and software.

A dynamometer with constant speed and torque facility would ensure more consistent results. Furthermore this could be coupled to a computer able to capture many consecutive cycles, and average them, while retaining the cycle 1 and cycle 2 facility. (The present system accepts at most three cycles).

Tests should be conducted at varying speed and torque at a number of fixed low DME/methanol ratios. The effects of methanol injection timing on methanol ignition and on engine performance should be investigated.

On the software side the energy release/heat transfer model could profitably be refined. In particular the combustion chamber wall temperature distribution and the associated heat transfer should be automatically adjusted as a function of engine running conditions. Exhaust temperature could possibly serve as an indicator of wall temperature. The energy release model itself should be modified so as to cope with negative mass addition (from pressure fluctuations) in the determination of the atomic ratios of the combustion chamber constituents.

The physical chemistry of oxidation of DME appears to require a study, which is fundamental on the one hand, but is directed ultimately towards application in CI engines.

Appendix A

DERIVATION OF THE HEAT TRANSFER EQUATION

The heat transfer to and from the surface of the cylinder walls of a compression ignition engine is, in general, expressed in terms of a surface heat transfer coefficient, that is,

$$q = hA(T_g - T_w) \tag{A.1}$$

where

q = heat flux (W)
h = convective heat transfer coefficient (W/m^2K)
A = area of cylinder walls (m^2)
T_g = mean gas temperature (K)
T_w = mean wall surface temperature (K)

However, as is well recognized, heat transfer in a compression ignition engine occurs under turbulent conditions. The intensity and scale of turbulence during compression in the cylinder varies approximately linearly with engine speed (Sitkei and Ramanaiah, 1972). Thus, the above equation must be modified to evaluate the instantaneous heat transfer.

Heat transfer in a compression ignition engine generally takes the form of convection and radiation. These are discussed below.

A.1 Convective Heat Transfer

Equation A1 above may be expressed in a form to evaluate the instantaneous heat transfer at each crank angle increment, as follows:

$$Q(I) = h(I)A(I) \quad (T_g(I) - T_w(I)) \tag{A.2}$$

with the symbols having the same meaning as in equation A1.

The main problem in the determination of convective heat transfer lies in the estimation of the convective heat transfer coefficient h, in equation A2. However, consideration is now given to the determination of each variable in equation A2.

A.1.1 Convective Heat Transfer Coefficient

The convective heat transfer coefficient in engine work is based on the generally accepted correlation:

$$Nu = C_1\, Re^n\, Pr^m \tag{A.3}$$

where Nu, Re and Pr are the Nusselt, Reynolds and Prandtl numbers respectively, and C_1, m and n are constants. Thus from the definition of the above dimensionless groups, equation A3 is written as;

$$\frac{hD}{k} = C_1\left(\frac{\rho V D}{\mu}\right)^n \left(\frac{c_p \mu}{k}\right)^m \tag{A.4}$$

where

h = convective heat transfer coefficient (W/m^2K)
D = cylinder bore (m)
k = conductivity of cylinder gases (W/mK)
ρ = density of cylinder gases (kg/m^3)
V = piston velocity (m/s)
μ = dynamic viscosity of cylinder gases (Ns/m^2)
c_p = specific thermal capacity at constant pressure (J/kgK)

The initial values of the constants C_1, m and n are determined from the literature, and then adjusted for the particular engine. This is achieved from data recorded from a motoring cycle, where ideally the compression/expansion process is adiabatic.

Each of the above variables is calculated at each crank angle increment, from which the instantaneous value of h in equation A4 is determined. However, since h is a function of velocity, attention will now be focussed on the latter.

When air is drawn into the cylinder during the induction stroke and subsequently compressed, its motion can essentially be resolved into three components. These are

(i) swirl

(ii) radial

(iii) longitudinal

Swirl is the motion acquired by the air during the induction stroke resulting from the inlet valve geometry.

Radial motion is produced during the compression stroke as the air moves into the bowl in the centre of the piston crown.

The swirl and radial components of velocity were evaluated with equations developed by Dent and Derham (1974). These authors carried out a detailed investigation of the air motion in a four-stroke direct injection compression ignition engine.

The swirl component during compression was calculated using the equation:

$$\dot{W}_c = \left(\frac{D}{2}\right)^n \dot{W}_o \left[\frac{\pi(D/2)^2 S(I)/v + 1}{\pi(D/4)^4 S(I)/v + (d'/2)^2}\right] \qquad (A.5)$$

where:

$\dot{W}_c$	=	air swirl velocity in cylinder during compression (rad/s)
$\dot{W}_o$	=	air swirl velocity at beginning of compression (rad/s)
D	=	cylinder bore (m)
$S(I)$	=	distance of piston crown from cylinder head at any crank angle position (m)
v	=	combustion chamber volume (m^3)
d'	=	diameter of combustion bowl (m)

The radial velocity component was calculated from

$$V_r = \frac{d^2[(D/d')^2 - 1]}{4S(I)} \left[\frac{v}{A_c S(I) + v}\right] \frac{dS(I)}{dt} \qquad (A.6)$$

where

I	=	crank angle position
V_r	=	radial air flow velocity (m/s)
A_c	=	cross sectional area of cylinder (m^2)
$dS(I)$	=	derivative of distance of piston crown from cylinder head at any crank angle position with respect to time (m/s)

The longitudinal motion of the air is the result of the linear displacement of the centre of mass of the air as the piston moves towards and away from TDC. This velocity component was calculated from the derivative of the piston displacement equation for a crank slider mechanism:

$$V_L = wr\left[\sin I + c(2a_1 \sin 2I - 4a_2 \sin 4I + 6a_3 \sin 6I \ldots)\right] \qquad (A.7)$$

where:

V_t = longitudinal air flow velocity (m/s)
c = crank to connecting rod ratio
r = connecting rod length (m)
w = angular speed (rad/s)
$a_1 = \frac{1}{4c^2} + \frac{2}{15c^4} + \frac{15}{512c^6} + \ldots$
$a_2 = \frac{1}{64c^4} + \frac{3}{256c^6} + \frac{35}{4096c^8} + \ldots$
$a_3 = \frac{1}{256c^6} + \frac{5}{2048c^8} + \ldots$

The longitudinal and swirl velocity components were combined into a resultant velocity. However, the longitudinal velocity was assumed to be half that of the piston, as calculated from equation A7. The reason for this is that the centre of mass of the air was assumed to move half the distance of the piston.

Convective heat transfer coefficients were thus calculated with the resultant velocity and with radial velocity, using equation A4.

However, before calculating the heat transfer, the appropriate areas and temperatures, as required in equation A2, must be considered.

A.1.2 Exposed Combustion Chamber Area

The exposed area of the combustion chamber consists of the piston crown, the cylinder head and the cylinder walls. Of these, the area of the cylinder walls varies with each crank angle increment.

The exposed area for the convective heat transfer coefficient based on the resultant velocity, was considered as being that of the combustion chamber walls only. The corresponding area for the coefficient based on the radial velocity was simply that of the piston crown and cylinder head, and was thus constant in value.

A.1.3 Mean Combustion Chamber Wall Surface Temperature

The surface wall temperature distribution in the combustion chamber of an internal combustion engine is particularly complex. However, since such a study was not within the scope of this research, a simplified approach was used.

A linear distribution between BDC and TDC was assumed. The temperature of the walls at BDC was taken as that of the engine cooling water temperature, (350 K) as suggested by Obert (1973). The temperature at TDC was an average value as suggested in the literature, (540 K), Whitehouse (1970).

The mean cylinder wall temperature, was evaluated for each position of the crank angle marker.

A.1.4 Mean Gas Temperature

The mean gas temperature was calculated, at each degree crank angle increment, from the full energy release model. The details are given in section 4.2.3.

A.1.5 Total Convective Heat Transfer

The total convective heat transfer was thus the sum of two components, termed longitudinal and radial. These were calculated as follows:

$$Q_l = h_{instantaneous} A_{wall} \ (T_g - T_w) \qquad \text{(A.8)}$$

and

$$Q_r = h_{radial} A_{cr} + h_{cyl} \ (T_g - T_w) \qquad \text{(A.9)}$$

from which the total convective heat transfer was given by

$$Q_{CONV} = Q_l + Q_r \qquad (A.10)$$

where each component, and thus the total convective heat transfer, was calculated at each degree crank angle increment.

The symbols in equations A8 to A10 have the following meanings:

Q_l	=	longitudinal component of convective heat transfer (W)
$h_{resultant}$	=	convective heat transfer coefficient based on resultant velocity (W/m^2K)
A_{wall}	=	exposed area of combustion chamber walls (m^2)
T_g	=	mean gas temperature (K)
T_w	=	combustion chamber wall surface temperature (K)
Q_r	=	radial component of convective heat transfer (W)
$A_{crown+head}$	=	area of piston crown and cylinder head (m^2)
Q_{CONV}	=	total convective heat transfer (W)

A.2.6 Radiation Heat Transfer

The heat transfer resulting from radiation was calculated from:

$$Q_{RAD} = \varepsilon \sigma A (T_g^4 - T_w^4) \qquad (A.11)$$

where

Q_{RAD}	=	heat transfer resulting from radiation (W)
ε	=	emissivity of the gases
σ	=	Stefan-Boltzman constant
A	=	exposed area of combustion chamber walls, piston crown and cylinder head (m^2)
T_g	=	mean gas temperature (K)
T_w	=	combustion chamber wall surface temperature (K)

The radiation heat transfer was also calculated at each degree crank angle increment.

A.2 Total Heat Transfer

The total heat transfer to and from the trapped mass was thus the sum of the convective and radiation components as follows:

$$Q_{TOTAL} = Q_{CONV} + Q_{RAD} \tag{A.12}$$

As clearly indicated above, each component was evaluated at each degree crank angle increment.

Appendix B

SPECIFICATIONS

B.1 Petter Compression Ignition Engine

Bore	87,74 *mm*
Stroke	110 *mm*
Continuous power rating at 2000 *rev/min*	12,2 *kW* (BS 5514)
Displacement	1330 cm^3
Compression Ratio	16,5:1
Fuel injection release pressure:	
900 to 1099 *rev/min*	137/152 *bar*
1100 to 2000 *rev/min*	197/217 *bar*
Fuel injection timing:	
Up to 1650 *rev/min*	34 ° BTDC
1651 to 2000 *rev/min*	28 ° BTDC
Valve timing:	
Inlet valve opens	13,5 ° BTDC
Inlet valve closes	38,5 ° ABDC
Exhaust valve opens	38,5 ° BBDC
Exhaust valve closes	13,5° ATDC

B.1.1 Instrumentation

Data logger:
HP model 3497A with compensation for ambient temperature.

Air flow:
The air inlet system consisted of a two hundred litre drum with a 30 *mm* orifice plate bolted at the one end of the drum. The air was drawn through the orifice into the drum, and then through a fibre glass cone facing away from the orifice. This ensured a uniform flow into the engine's air intake manifold. A rubber diaphragm was placed across the other end of the drum so as to reduce pulsations in the flow. The drum was mounted on a frame above the engine in a vertical position with the orifice at the top end. The pressure drop across the orifice plate was measured with a micromanometer.

Strain gauges:
Kyowa KFC-2-C1-11, with a 6V DC input.

Micromanometer:
Air Instruments Resources Ltd model MP6KMD.

Fuel flow rate:
Pierburg flowmeter type PLU 116.

Transient Recorder:
Datalab model 2800, 6 channels with Master Time base.

Cylinder Pressure:
Kistler type 6121 A1 piezo-electric transducer with Kistler 5007 charge amplifier.

Injector lift:
RDP Electronics D7M linear variable differential transformer with model D7M amplifier.

Optical Crank Angle marker:
AVL List Type 360C/600 - 0,1 ° Resolution.

DME flow rate:
Fischer Porter rotameter calibrated for dimethyl ether, with a flow rate

range of 0,37 to 42,74 *g/min.*

Appendix C

CALIBRATION OF INSTRUMENTATION

The instrumentation was calibrated before testing so as to obtain the relevant calibration equations. This was repeated on several occasions for each instrument to ensure continued accuracy.

The results given here relate to a set of calibrations so as to outline the procedure followed. However, whenever a calibration was performed, the appropriate equation was used in the relevant computer program.

C.1 Load Cell

The load cell was calibrated by loading the dynamometer arm with known masses. The output voltages from the Wheatstone bridge were recorded using a Fluke 2240A data logger. The procedure was repeated for loading and unloading, and the average millivolt output was calculated. Knowing the dynamometer arm radius, the torque exerted on the load cell was calculated. The results are given in table C.1.

A calibration curve of torque versus load cell output is shown in figure C1.

Reading	Mass	Torque	Load cell output		
			Up	Down	Average
	kg	*Nm*	*mV*		*mV*
1	0,616	2,413	5,012	5,016	5,014
2	2,882	11,290	5,701	5,935	5,818
3	5,155	20,191	6,598	6,827	6,713
4	7,420	29,065	7,513	7,718	7,616
5	9,691	37,962	8,415	8,605	8,510
6	11,962	46,856	9,304	9,493	9,399
7	14,232	55,749	10,210	10,371	10,291
8	14,734	57,716	10,423	10,572	10,498
9	15,238	59,688	10,628	10,760	10,694
10	15,736	61,639	10,829	10,950	10,890
11	19,055	74,642	12,141	12,229	12,185
12	19,559	76,613	12,345	12,413	12,379
13	20,061	78,581	12,544	12,594	12,569
14	23,007	90,121	13,697	13,704	13,701

Table C.1: Calibration of load cell

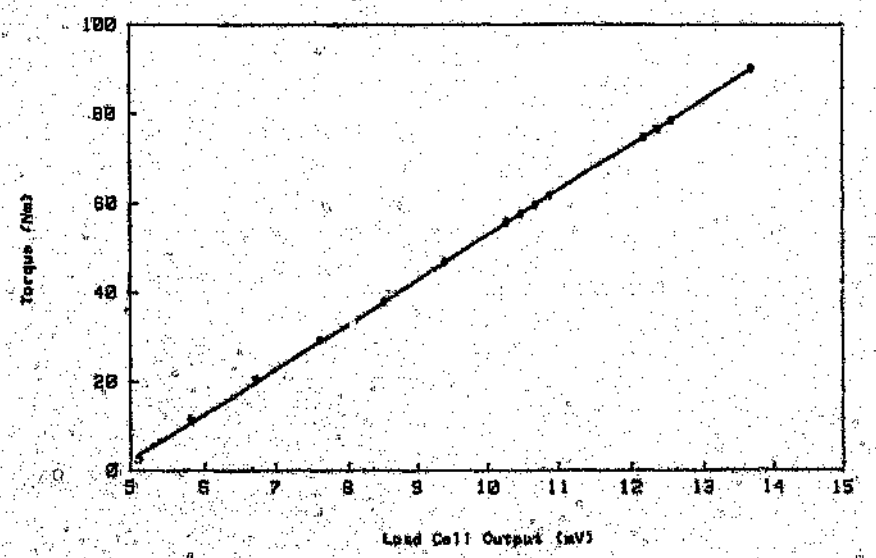

Figure C.1: Torque versus load cell output

Torque arm radius	0,4003 m
Wheatstone bridge supply voltage	6 V
Gravitational constant in Laboratory	9,78549 m/s^2

The relevant data for the above calibration was:

Slope of straight line	10.06 (Nm/V)
Y intercept	-47.82 (Nm)

Therefore torque in terms of load cell output was given by:

$$\text{Torque } (Nm) = \text{load cell output } (mV) \times 10.06 - 47.82$$

C.2 Tachometer

The tachogenerator was calibrated against a stroboscope. The stroboscope, a General Radio Model 1531-AB Strobotac, was calibrated as required by

the manufacturers. The engine was then started up and allowed to stabilize at a particular speed. Readings from the stroboscope and the engine tachogenerator were recorded as given in Table C.2. The tachogenerator output was displayed as a voltage on a Fluke 75 hand held digital voltmeter.

Reading	Stroboscope	Tachogenerator output
	rev/min	*V*
1	1169	1,791
2	1197	1,860
3	1217	1,896
4	1260	2,001
5	1327	2,077
6	1491	2,336
7	1526	2,486
8	1541	2,518
9	1678	2,655
10	1634	2,680
11	1664	2,745
12	1771	2,928
13	1866	3,072
14	1918	3,190
15	1961	3,270
16	1980	3,310

Table C.2: Calibration of tachogenerator

Figure C.2 shows the calibration curve of engine speed versus tachogenerator output.

Slope	539.87 (*rev/min*/V)
Y intercept	197.82 (*rev/min*)

The resulting calibration equation was:

$$\text{Speed } (rev/min) = \text{Tachogenerator output } (V) \times 539.87 + 197.82$$

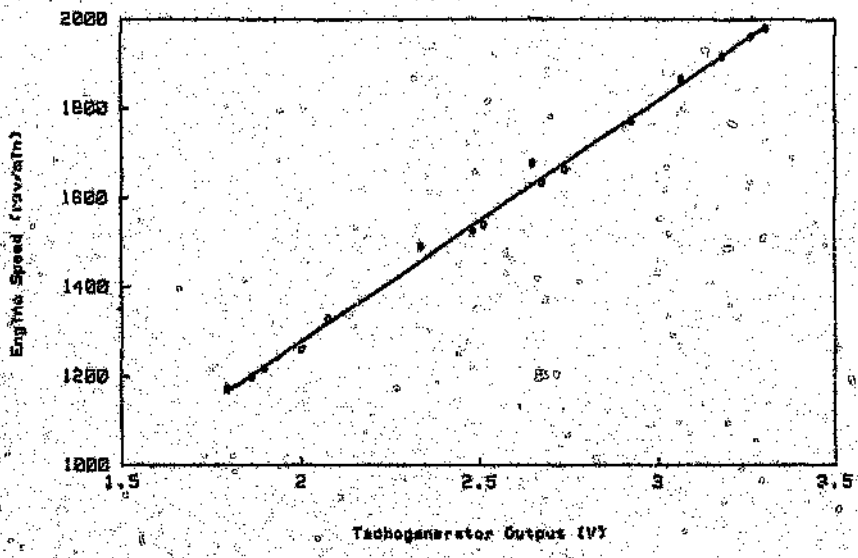

Figure C.2: Engine speed versus tachogenerator output

C.3 Fuel Flowmeter

The Pierburg fuel flowmeter was calibrated by measuring the mass of a quantity of fuel flowing through the flowmeter over a known period of time. The resulting mass flowrate was then plotted against the voltage output of the flowmeter display unit. This output was monitored using a Fluke 75 hand-held digital voltmeter. Table C.3 shows the calibration results and figure C.3 the corresponding calibration curve.

Slope	50.11	$((g/s)/V)$
Y Intercept	0.017	(g/s)

The fuel flowrate in g/s in terms of flowmeter output was given by:

$$\text{Fuel flowrate } (g/s) = \text{Flowmeter output } (V) \times 50.11 + 0.017$$

Reading	Fuel flowrate g/s	Flowmeter output V
1	0,1571	0,0030
2	0,2963	0,0057
3	0,5263	0,0103
4	0,7203	0,0140
5	1,000	0,0194
6	1,1712	0,0228
7	1,3889	0,0272
8	1,6239	0,0321
9	1,8349	0,0360
10	2,0354	0,0400
11	2,2321	0,0439
12	2,3333	0,0475
13	2,6549	0,0523

Table C.3: Calibration of fuel flowmeter

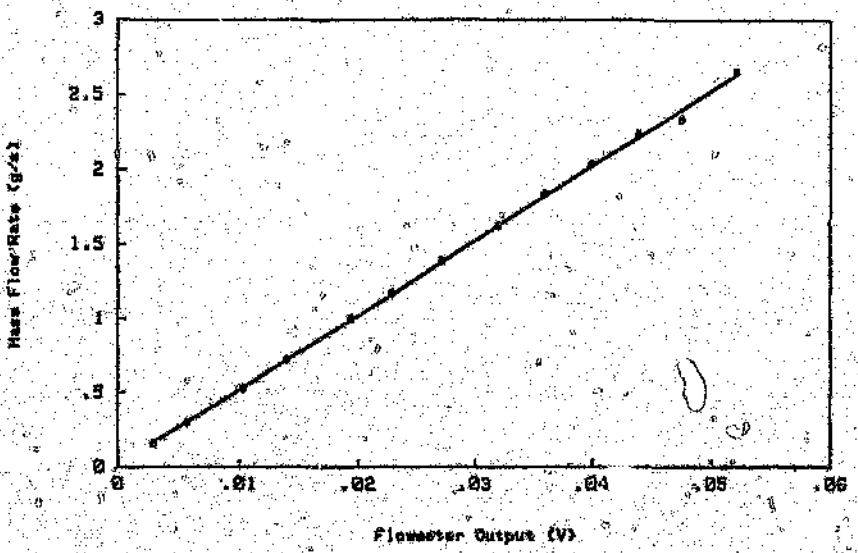

Figure C.3: Fuel flowrate versus flowmeter output

C.4 Airflow

The pressure difference across the orifice plate used to calculate the airflow rate to the engine was measured by an Air Instrument Resources Ltd micromanometer. The orifice plate was designed in accordance with British Standards BS1042: 1984. The engine speed was allowed to stabilize, and the readings in millimeters of water on the micromanometer and the corresponding voltage output were recorded. This procedure was repeated so as to cover the speed range of the engine.

The results are given in table C.4 and the calibration curve is shown in figure C.4.

Slope	200.82	(mm/V)
Y Intercept	0.24	(mm)

The resulting calibration equation is:

$$\text{Pressure drop } (mmH_2O) = \text{micromanometer output } (V) \times 200.82 + 0.24$$

Reading	Micromanometer Output V	Pressure Drop mmH_20
1	0,023	4,8
2	0,053	11,0
3	0,103	20,8
4	0,123	24,9
5	0,151	30,6
6	0,189	38,2
7	0,226	45,6
8	0,267	53,9
9	0,331	66,9
10	0,360	72,6
11	0,405	81,0
12	0,435	87,9

Table C.4: Calibration of micromanometer

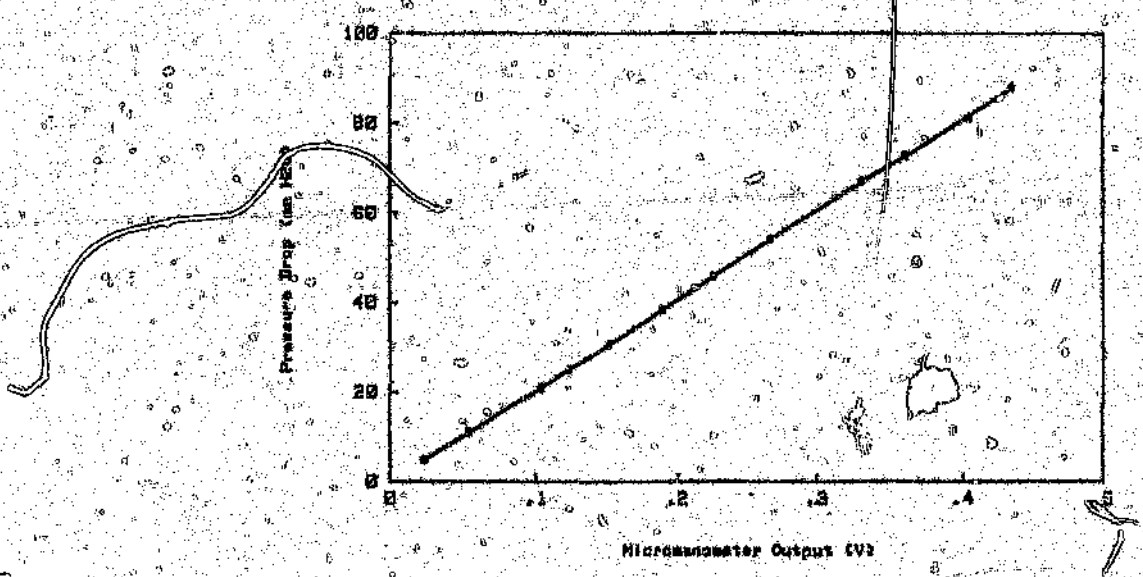

Figure C.4: Pressure drop across orifice versus micromanometer output

C.5 Combustion Chamber Pressure

Cylinder pressure was measured by means of a Kistler 6121A1 piezo electric transducer, coupled to a type 5007 charge amplifier.

Although the transducer's operating temperature ranged from -80 to 350°C, and could withstand intermittent flash temperatures of up to 2500°C, it was decided to cool the transducer during operation.

Therefore the transducer was mounted in a water jacket which was in turn fitted to the cylinder block. The transducer, water jacket, connecting cable and charge amplifier were calibrated as a system. Pressure was applied to the transducer by means of a Budenburg dead weight tester.

The calibration procedure adopted was as follows:

- The water jacket with the transducer inserted in it was connected to the Budenburg tester
- The charge amplifier was switched on and allowed to warm up for about one hour
- A Fluke 75 hand-held digital voltmeter was connected to the output of the charge amplifier to measure the output voltage
- The zero on the charge amplifier was checked and adjusted if necessary
- Weights were added successively to the Budenburg so that the pressure increased from 0 to 1000 *psi* in steps of 100 *psi*
- For each increment, the output voltage of the charge amplifier was recorded
- The procedure was repeated for loading and unloading and the average voltage was used in the plot.

It should be noted, however, that the sensitivity of the charge amplifier was adjusted to ensure that a linear relationship between applied pressure and output voltage was achieved. This was done prior to the calibration itself using random weights covering the required range.

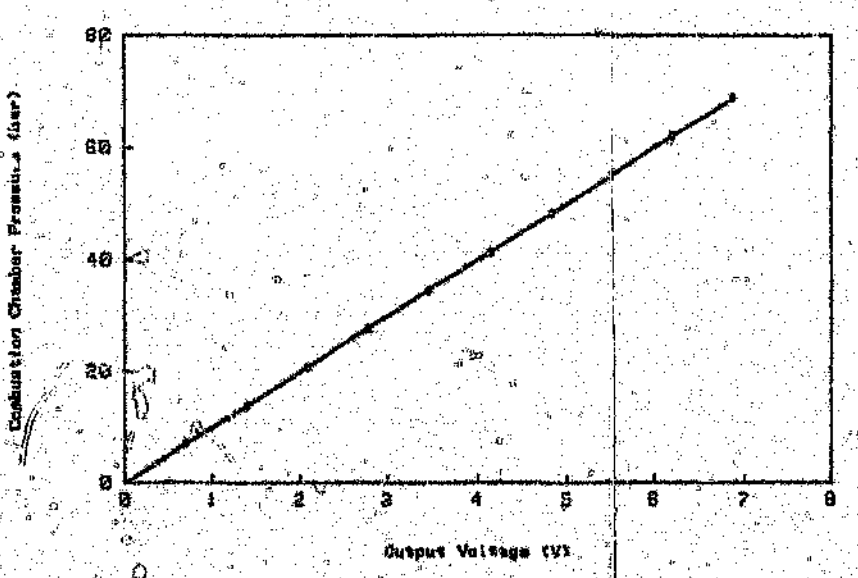

Figure C.5: Transducer pressure versus output voltage

The results obtained are shown in table C.5, and the corresponding calibration curve in figure C.5.

Slope	10.03 (bar/V)
Y Intercept	-0.21 (bar)

The charge amplifier was set on 10 mechanical units per volt. The resulting relationship was:

Pressure $(bar) = 10.03\ (V) - 0.21$

C.6 Injector Needle Lift

The displacement of the injector needle was measured using an RDP Electronics LVDT with a type D7M amplifier.

The LVDT slug was mounted in an adjustable housing fitted onto the injector body and cap. A dial gauge was set up so that the needle was resting on the housing. The amplifier output was recorded using a Fluke 75 voltmeter.

Reading	Applied Pressure		Output voltage
	psi	*Bar*	*V*
1	0	0	0,002
2	100	6,895	0,701
3	200	13,790	1,399
4	300	20,684	2,091
5	400	27,574	2,784
6	500	34,477	3,47
7	600	41,369	4,15
8	700	48,263	4,83
9	800	55,158	5,51
10	900	62,053	6,21
11	1000	68,948	6,88

Table C.5: Calibration of cylinder pressure transducer

The housing was slowly unscrewed until the output voltage showed no further change. This point was taken as zero displacement. The housing was screwed in slowly in steps of 0,1 *mm* as indicated on the dial gauge, and the corresponding LVDT output was recorded. The procedure was repeated until the housing was completely screwed in.

The calibration curve was then plotted and the calibration equation was established. The curve showed a linear portion in the middle range of the LVDT. The housing was therefore positioned so as to operate in this linear region.

The calibration data is given in table C.6. Figure C.6 shows the calibration curve for the injector needle lift.

Slope -0.16 (*mm/V*)
Y Intercept 1.51 (*mm*)

Therefore,
Injector lift (*mm*) = LVDT output (V) × (-0.16) + 1.51

Reading	Injector lift *mm*	LVDT output *V*
1	0	9,86
2	0,1	9,10
3	0,2	8,41
4	0,3	7,72
5	0,4	6,99
6	0,5	6,30
7	0,6	5,62
8	0,7	4,95
9	0,8	4,25
10	0,9	3,55
11	1,0	2,89
12	1,1	2,159
13	1,2	1,486
14	1,3	0,923
15	1,4	0,310
16	1,5	-0,301
17	1,6	-0,894
18	1,7	-1,445
19	1,8	-2,023
20	1,9	-2,596
21	2,0	-3,134
22	2,1	-3,68
23	2,2	-4,20
24	2,3	-4,76
25	2,4	-5,31
26	2,5	-5,84
27	2,6	-6,38
28	2,7	-6,92
29	2,8	-7,47
30	2,9	-8,07

Table C.6: Calibration of injector needle lift

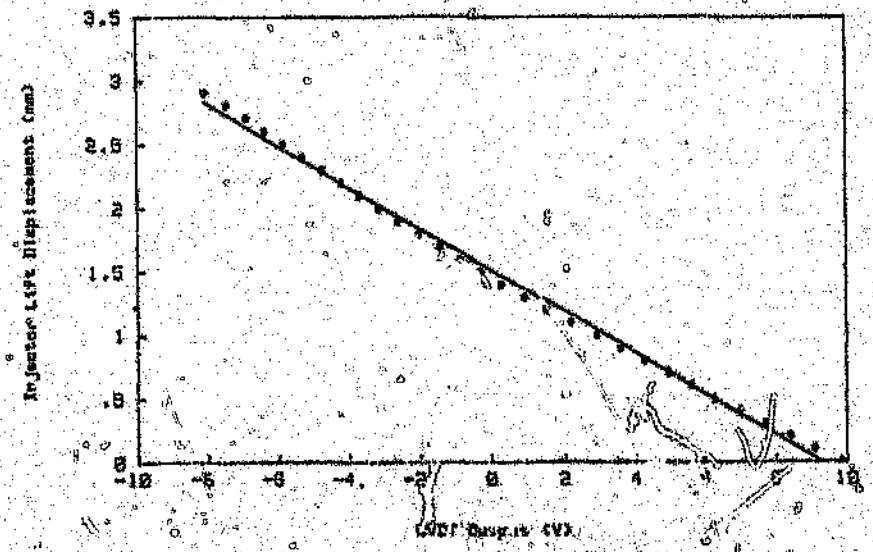

Figure C.6: Injector lift versus LVDT output

C.7 Fuel Line Pressure

Fuel line pressure was measured by means of an AVL 5QP2002 piezo-electric transducer, coupled to a Kistler type 5007 charge amplifier.

The transducer was mounted in a brass block made to AVL specification. The block and transducer were placed in the fuel line between the pump and the injector of cylinder number 1.

Before fitting the transducer, it was calibrated with its cable and charge amplifier with the aid of a Budenburg dead weight tester.

The procedure adopted for the calibration was as in C.5.

Table C.7 shows the observations recorded during a typical calibration, and figure C.7 the resulting calibration curve.

Slope 30.03 (bar/V)
Y Intercept -0.007 (bar)

The charge amplifier was set on 50 mechanical units per volt. The resulting

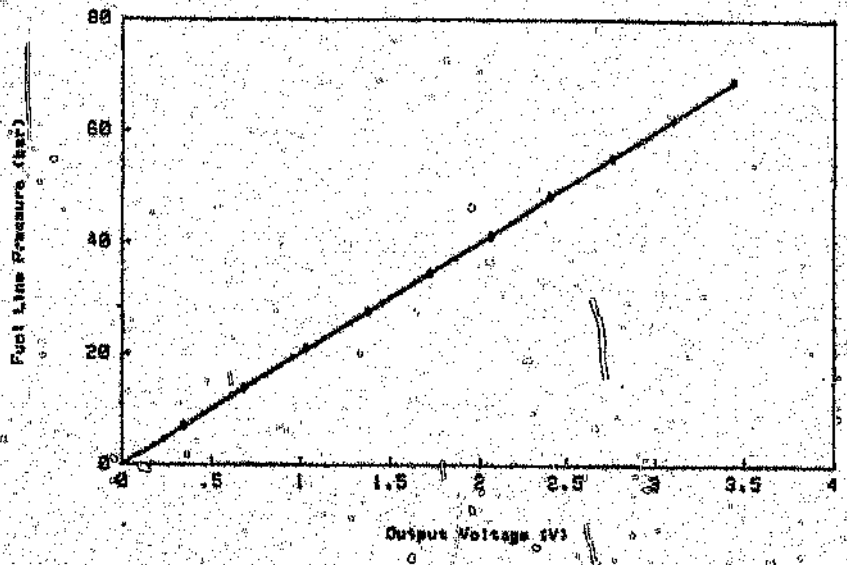

Figure C.7: Transducer pressure versus output voltage

relationship was:

$$\text{Pressure } (bar) = 20.03\ (V) - 0.007.$$

C.8 Rotameter

The mass flowrate of DME was measured with a Fischer and Porter Tri-Flat Variable-Area flowmeter. This device could not be calibrated by measuring the mass of a quantity of DME flowing through over a known period of time. The reason being that DME would change to a vapour phase on leaving the rotameter.

The mass flowrate of a liquid flowing through the rotameter can be calculated using the following equation provided by the manufacturers:

$$q_m = \alpha C' \sqrt{(\rho_s - \rho_1)\rho_1} \quad (g/min)$$

where

Reading No.	Applied Pressure		Output Voltage
	Psi	*Bar*	*V*
1	0	0	0,002
2	100	6,895	0,344
3	200	13,790	0,688
4	300	20,684	1,032
5	400	27,574	1,376
6	500	34,477	1,722
7	600	41,369	2,066
8	700	48,263	2,412
9	800	55,158	2,757
10	900	62,053	3,10
11	1000	68,948	3,44

Table C.7: Calibration of fuel line pressure transducer

q_m = mass flowrate of liquid (g/min)
α = flow coefficient
C' = size factor on the tube size or float diameter
ρ_f = float density (g/cm^3)
ρ_l = fluid density at operating conditions (g/cm^3)

Using the procedure and calibration charts supplied with the rotameter, an equation using water as a liquid was derived. Since certain factors required in the above equation are read off charts, the accuracy of the equation was tested. This was achieved by measuring the mass of a quantity of water flowing through the rotameter over a set time interval.

The calculated and experimental mass flowrate for the various rotameter readings are given in table C.8.

The calculated and experimental curves of mass flowrate versus rotameter readings are shown in figure C.8.

Calibration		Derivation	
Rotameter reading	Mass flowrate *g/min*	Rotameter reading	Mass flowrate *g/min*
1,6	0,31	2,0	0,467
2,4	0,63	3,0	1,070
3,0	1,05	4,0	2,220
3,9	2,12	5,0	4,000
5,0	3,94	6,0	5,999
6,0	6,10	8,0	10,866
7,0	8,35	10,0	16,665
7,7	10,00	12,0	22,398
8,8	13,10	14,0	28,664
9,7	15,58	16,0	35,196
10,9	18,72		
11,8	21,59		
12,9	24,35		
14,0	28,27		
14,9	31,14		
16,0	34,31		

Table C.8: Calibration of rotameter using water

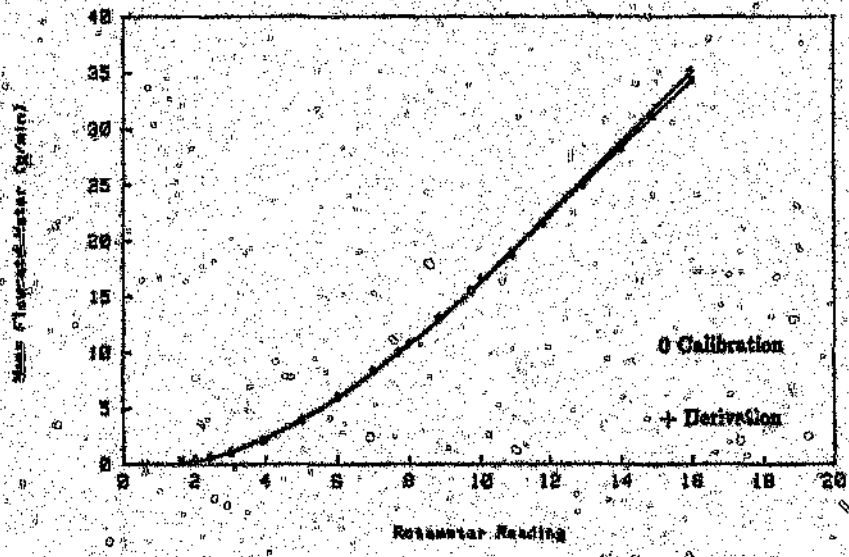

Figure C.8: Calculated and experimental mass flowrate versus rotameter reading using water

Using the same procedure as above, a calibration equation was derived for DME with the appropriate properties.

The resulting DME calibration equation was:

q_m = Rotameter scale reading × 2,807 - 2,437

Appendix D

EFFECT OF RESIDUALS ON INITIAL MIXTURE TEMPERATURE

The enthalpy of the mixture in the cylinder is the sum of the enthalpies of the residuals and of the fresh charge as follows:

$$H_M = H_R + H_{FC}$$

where

M = mixture
R = residuals
FC = fresh charge

therefore:

$$c_M(m_R + m_{FC})T_M = c_R m_R T_R + c_{FC} m_{FC} T_{FC}$$

where

m = mass (kg)
c = specific thermal capacity (J/kgK)
T = temperature (K)

Assuming specific thermal capacities to be essentially constant and the same, the above equation reduces to:

$$m_M T_M = m_R T_R + m_{FC} T_{FC}$$

where

m_M = mass of mixture
= $m_R + m_{FC}$

but

$$m_R T_R = \frac{p_{ex} V_{ex}}{R_{ex}}$$

where

p_{ex} = pressure (Pa)
V_{ex} = volume (m^3)
R_{ex} = specific gas constant (J/kgK)

all at TDC during the exhaust process.

These values are essentially constant, therefore the product $m_R T_R$ is also constant.

Therefore the temperature of the mixture is indenpendent of the load.

Appendix E

PHYSICAL PROPERTIES OF DME

Formula		$CH_3 - O - CH_3$	
Molecular mass		$g\ mole^{-1}$	46,069
Melting point (101,325 *kPa*):			
	Temperature	$°C$	-141
	Latent heat	$kcal\ kg^{-1}$	26,61
Boiling point (101,325 *kPa*):			
	Temperature	$°C$	-24,82
	Latent heat	$kcal\ kg^{-1}$	111,59
	Liquid density	$kg\ m^{-3}$	734,7
	Gas density	$kg\ m^{-3}$	2,34
Critical point			
	Temperature	$°C$	126,95
	Pressure	kPa	5269,0
	Density	$kg\ m^{-3}$	271,4
Heat capacity for the perfect gas at 25°C		$cal\ kg^{-1}K^{-1}$	0,341
Surface tension (liquid-gas interface) at -10°C		$dynes\ cm^{-1}$	16,4

Flammability in air (101,325 *kPa*, 20°*C*):

Lower	%	3,4
Upper	%	27
Minimum auto-ignition temperature (101,325 *kPa*)	°*C*	750

One litre of liquid liberates 374 litres of gas (expanded to 15°*C*, 101,325 *kPa*)

Density	Temperature	Pressure	Liquid	Gas
	°*C*	*kPa*	kgm^{-3}	kgm^{-3}
	0	256	698	5,75
	15	424	674	9,18
	50	1130	612	24,95

Viscosity (101,325 *kPa*)	Temperature	Viscosity
	°*C*	$\times 10^{-5}$ poises
		8,70
		9,06
		10,20
		11,68

Thermal conductivity (101,325 *kPa*)	Temperature	Conductivity
	°*C*	$\times 10^{-5}$
		$cal\ cm^{-1}s^{-1}K^{-1}$
	0	3,35
	15	3,68
	50	4,49
	100	5,75

Compressibility factor

Pressure	Temperature	
kPa	15°*C*	50°*C*
100	0,9777	0,9847
200	0,9544	0,9690
400	0,9037	0,9357
600		0,8997
800		0,8601
1000		0,8156
1100		0,7908

REFERENCES

1. Alkidas, A.C. (1987) Combustion characteristics of a single-cylinder open-chamber diesel engine. *Journal of Engineering for Gas Turbines and Power*, vol. 109, pp 419-425.

2. Alkidas, A.C. (1987a) Heat release studies in a divided-chamber diesel engine. *Journal of Engineering for Gas Turbines and Power*, vol. 109, pp 193-199.

3. Alkidas, A.C. (1987b) On the premixed combustion in a direct-injection diesel engine. *Journal of Engineering for Gas Turbines and Power*, vol. 109, pp 187-192.

4. Alternative Fuels Committee of the Engine Manufacturers Association. (1982) *A Technical Assessment of Alcohol Fuels*, SAE, no 820261, pp 1-37.

5. Annand, W.J.D. (1963) Heat transfer in the cylinders of reciprocating internal combustion engines. *Proceedings of the Institution of Mechanical Engineers*, vol 177, No 36, pp 973-990.

6. Annand, W.J.D. and Ma, T.H. (1970-71) Instantaneous heat transfer rates to the cylinder head surface of a small compression-ignition engine. *Proceedings of the Institution of Mechanical Engineers*, vol 185, No 72/71, pp 976-987.

7. Austen, A.E.W. and Lyn, W.T. (1960-61) Relation between fuel injection and heat release in a direct-injection engine and the nature of the combustion process. *Proceedings of the Institution of Mechanical Engineers (Automobile Division)*, no 1, pp 47-62.

8. Baker, Q.A. (1981) Use of alcohol-in-diesel fuel emulsions and solutions in a medium-speed diesel engine. *Alternative Fuels SP480*, SAE, no 810254, pp 71-82.

9. Berg, P.S., Holmer, E. and Bertilsson, B.I. (1979) The utilization of different fuels in a diesel engine with two separate systems. *Third International Symposium on Alcohol Fuels Technology*, California, USA, pp 1-8.

10. Bowden, C.M., Samaga, B.S. and Lyn, W.T. (1969-70) Rate of heat release in high-speed indirect injection diesel engines, *Proceedings of the Institution of Mechanical Engineers*, vol. 189, part 33, pp 122-129.

11. Borman, G. and Nishiwaki, K. (1987) Internal-combustion engine heat transfer. *Progress in Energy Combustion Science*, vol 13, pp 1-46.

12. Boyce, T.R., Karim, G.A. and Moore, N.P.W. (1969-70) The effects of some chemical factors on combustion processes in diesel engines, *Proceedings of the Institution of Mechanical Engineers*, vol. 184, part 33, pp 137-146.

13. Brook, D.L., Rallis, C.J., Lane, N.W. and Cipolat, D. (1984) Methanol with dimethylether ignition promoter as fuel for compression ignition engines. *Proceeding of the 19th IECEC*, San Francisco, California, pp 654-658.

14. Burnett, T.C., Vergeer, F.C. and Lawson, A. (1984) Utilization of methanol as a fuel for diesel powered mining operations. *Proceeding of the Sixth International Symposium on Alcohol Fuels Technology*, Ottowa, Canada, pp 78-86.

15. Campbell, A.S. (1979). *Thermodynamic Analysis of Combustion Engines*, John Wiley and Sons.

16. Chiu, C.P., Liang, Y.W. and Wu, H.W. (1984) Cyclic combustion variation and vibration characters in an indirect injection diesel engine with alcohol/diesel fuel blends. *Seventh International Symposium on Alcohol Fuels Technology*, Ottowa, Canada, pp 87-96.

17. Cipolat, D., Lane N.W., Jawurek, H.H. and Rallis, C.J. (1986) Performance comparisons of alcohol-based fuel systems in a dual-injection compression-ignition engine. *Proceeding of the Seventh International Symposium on Alcohol Fuels Technology*, Paris, France, pp 348-353.

18. Cruz, J.M., Chancellor, W.T. and Goss, J.R. (1979) Dual-fuelling a diesel engine with carburetted alcohol. *Third International Symposium on Alcohol Fuels Technology*, California, USA, pp 1-12.

19. Dent, J.C., and Derham, J.A. (1974) Air motion in a four-stroke direct injection diesel engine. *Proceedings of the Institution of Mechanical Engineers*, vol 188, no 21/74, pp 269- 280.

20. Dent, J.C. and Suliaman, S.J., (1977) Convective and radiative heat transfer in a high swirl direct injection diesel engine, *SAE no 770407*, pp 1-15.

21. Ecklund, E.E., Bechtold, R.L., Timbario, T.J. and McCallum, P.W. (1984) State-of-the-art report on the use of alcohols in diesel engines, *SAE no. 840118*, pp 1-19.

22. Edo, T. and Foster, D. (1984) A computer simulation of a dissociated methanol engine. *Proceeding of the Sixth International Symposium on Alcohol Fuels Technology*, Ottowa, Canada, pp 139-147.

23. Eichelberg, G. (1939) Some new investigations on old combustion engine problems. *Engineering*, vol 148, pp 463-466.

24. Faletti, J.J., Sorenson, S.C. and Goering, C.E. (1982) Energy release rates from hybrid fuels. *American Society of Agricultural Engineers*, no. 82-1548, pp 1-16.

25. Garcia, P. (1986) Static and field experience with the use of neat methanol in a transport fleet. *Seventh International Symposium on Alcohol Fuels Technology*, Paris, France, pp 311-316.

26. Ghojel, J.I. (1982) A study of combustion chamber arrangements and heat release in DI diesel engines. *SAE no 821034*, pp 1-13.

27. Grigg, H.C. and Syed, M.H. (1969-70) The problem of predicting rate of heat release in diesel engines. *Proceedings of the Institution of Mechanical Engineers*, vol 184, part 33, pp 192-202.

28. Gulder, O.L. (1988) Combustion gas properties: Part III - prediction of the thermodynamic properties of combustion gases of aviation and diesel fuels. *Transactions of the ASME*, vol 110, pp 94-99.

29. Hagen, D.L. (1977). Methanol as a fuel: a review with bibliography, *SAE no 770792*, pp 1-33.

30. Hayes, T.K., Savage, L.D. and Sorenson, S.C. (1986) Cylinder pressure data acquisition and heat release analysis on a personal computer. *SAE no. 860029*, pp 1-9.

31. Henein, N.A. (1965) Instantaneous heat transfer rates and coefficients between the gas and combustion chamber of a diesel engine. *SAE, no 969B*, pp 1-11.

32. Heywood, J.B. (1981) Automotive engines and fuels: A review of future options. *Progress in Energy Combustion Science*, vol. 7, pp 155-184.

33. Hohenberg, G.F. (1979) Advanced approaches for heat transfer calculations, *SAE no 790825*, pp 61-79.

34. Hsu, B.D. (1984) Heat release, cycle efficiency and maximum cylinder pressure in diesel engine - the use of an extended air cycle analysis. *SAE, no. 841054*, pp 13-25.

35. Jackson, M.D., Renner, R.A. and Smith, K.D. (1984) California's experience with methanol-fuelled transit buses. *Proceeding of the Sixth International Symposium on Alcohol Fuels Technology*, Ottowa, Canada, pp 291-300.

36. Jawurek, H.H., Lane, N.W. and Rallis, C.J. (1987) Biogas/petrol dual fuelling of SI engine for rural third world use. *Biomass, No 13*, pp 87-103.

37. Knight, B.E. (1964-65) The problem of predicting heat transfer in diesel engines. *Proceedings of the Institution of Mechanical Engineers*, vol 179, Part 3J, pp 99-112.

38. Krieger, R.B. and Borman, G. (1966) The computation of apparent heat release for internal combustion engines. *Transactions ASME*, no 66-WA/DGP- 4, pp 2-16.

39. Lawson, A., Last, A.J., Deaphande, A.S. and Simmonds, E.W. (1981) Heavy-duty truck diesel engine operation on unstabilised methanol/diesel fuel emulsions. *Alternative Fuels SP-480, SAE, no. 810846*, pp 99-108.

40. Lawson, A. and Last, A.J. (1979) Development of an on-board mechanical fuel emulsifier for utilization of diesel/methanol and methanol/ gasoline fuel emulsions in transportation. *Proceeding of the Third (International) Symposium on Alcohol Fuels Technology*, California, USA, pp 1-13.

41. Lawton, B. (1987) Effect of compression and expansion on instantaneous heat transfer in reciprocating internal combustion engines. *Proceedings of the Institution of Mechanical Engineers*, vol 201, no A32, pp 175-186.

42. Le Feuvre, T., Myers, P.S. and Uyehara, O.A. (1969) Experimental instantaneous heat fluxes in a diesel engine and their correction. *SAE, no 690464*, pp 1717-1733.

43. Lewis, B. and Von Elbe, G. (1951) Combustion, flames and explosion of gases. *Academic Press Inc*, New York, pp 461-466.

44. Lyn, W.T. (1960-61) Calculations of the effect of rate of heat release on the shape of cylinder-pressure diagram and cycle efficiency. *Proceedings of the Institution of Mechanical Engineers (Automobile Division)*, no 1, pp 34-46.

45. Lyn, W.T. (1962) Study of burning rate and nature of combustion in diesel engines. *Proceeding of the Ninth International Symposium on Combustion*, New York, pp 1069-1082.

46. Martin, J.K. and Ahmad, T. (1986) Heat-release characteristics of an open- chamber diesel engine employing a wall-wetting combustion system. *SAE no. 860120*, pp 1-10.

47. Myburgh, J.S. and Weiss, E.K.J. (1986) Evaluation of ignition-improved methanol as an alternative fuel for heavy-duty diesel engines. *Seventh International Symposium on Alcohol Fuels Technology*, Paris, France, pp 278- 283.

48. Obert, E.F. (1973) *Internal combustion engines and air pollution*. Harper and Row, New York.

49. Oguri, T. (1960) On the coefficient of heat transfer between gases and cylinder walls of the spark ignition engine. *Bulletin of JSME*, vol 3, No 11, pp 363-369.

50. Oguri, T. (1960) Theory of heat transfer in the working gases of internal combustion engines. *Bulletin of JSME*, vol 3, No 11, pp 370-377.

51. Overbye, V.D., Bennethum, J.E., Wyehara, O.A. and M[illegible], P.S. (1961) Unsteady Heat Transfer in Engines. *SAE, no 201[illegible]*, pp 461-494.

52. Picken, D.J., Soliman, H.A. and Fox, M.F. (1979) Heat release analysis of internal combustion engine indicator diagrams, *Institution of Mechanical Engineers and Umist, International Journal of Mechanical Engineering Educatio[illegible]*, vol 7, no 4, pp 165-170.

53. Pischinger, F.F. and [illegible]urghardt, P. (1984) Use of alcohol fuel in passenger car diesel en[illegible]. *Proceeding of the Sixth International Symposium on Alcohol Fuels Technology*, Ottowa, Canada, pp 310-318.

54. Pischinger, F.F. and Havenith, C. (1979) A new way of direct injection of methanol in a diesel engine. *Third International Symposium on Alcohol Fuels Technology*, California, USA, pp 1-11.

55. Prothero, A. (1969) Computing with thermochemical data. *Combustion and Flame*, vol [illegible] p 399-408.

56. Seko, T., Hori, M., F[illegible]il and Kobayashi, S. (1984) Methanol diesel engine and its application to a vehicle. *SAE, no. 840116*, pp 1-8.

57. Shimotsu, M. and Erdo, Y. (1982) An analysis of diesel combustion focusing on the combustion rate of the diesel spray. *Bulletin of JSME*, vol 25, no 200, pp 241-248.

58. Shipinsky, J. (1967) Relationships between rates-of-injection and rate-of-heat release in diesel engines. *PhD dissertation*, University of Wisconsin.

59. Sitkei, G. and Ramanaiah, G.V., (1972) A rational approach for calculation of heat transfer in diesel engines. *SAE, no 720087*, pp 165-174.

60. Sorenson, S.C. (1981) Simple computer simulations for internal combustion engine instruction. *International Journal of Mechanical Engineering Education*, vol 9, no 3, pp 237-249.

61. Storment, J.O. and Baker, Q.A. (1981) Dual fuelling of a two-stroke locomotive engine with alternate fuels. *Alternative Fuels SP-480, SAE, no. 810252*, pp 47-57.

62. Strehlow, R.A., (1984) *Combustion Fundamentals.* McGraw-Hill, New York.

63. Stull, D.R. and Prophet, M. (1971) *2nd Ed., Journal of Thermochemical Tables*, US Government Printing Office.

64. Swain, M.R. and Swain, M.N. (1984) A computer model for waste heat recovery in methanol fuelled engines. *Proceeding of the Sixth International Symposium on Alcohol Fuels Technology*, Ottowa, Canada, pp 365-370.

65. Tanasawa, Y. and Tesima, T. (1958) On the theory of combustion rate of liquid fuel spray. *Bulletin of JSME*, vol. 1, no. 1, pp 36-41.

66. Taylor, C.F. (1960) *The internal combustion engine in theory and practice, vol 1, Second Edition, MIT Press*, Chapter 8.

67. Toepel, R.R., Bennethum, M.J.E. and Heruth, R.E. (1983) Development of Detroit diesel Allison 6V-92TA methanol fuelled coach engine. *SAE, no. 831744*, pp 1 - 77.

68. Weidmann, K. and Menrad, H. (1984) Fleet test, performance and emissions of diesel engines using different alcohol-diesel fuel blends. *Alternative Fuels for Compression and SI Engines SP-587, SAE, no. 841331*, pp 1-14.

69. Weinberg, F.J. (1957) Explicit equations for the calculation, by successive approximation, of equilibrium gas compositions at high temperature: the hydrogen + carbon + oxygen and the hydrogen + carbon + oxygen + nitrogen systems without solid carbon formation. *Proceedings of the Royal Society London, Proceedings A241*, pp 132-140.

70. Whitehouse, N.D. (1970-71) Heat transfer in compression - ignition engines. *Proceeding of the Institution of Mechanical Engineers*, vol 185, no 72/71, pp 963-975.

71. Whitehouse, N.D. and Abughres, S.M. (1975) Calculation of fuel-air mixing in a diesel engine with swirl for the purpose of heat release prediction. *Combustion in engines sponsored by the Automobile Division of the Institution of Mechanical Engineers, Cranfield Institute of Technology*, C97/75, pp 147-154.

72. Whitehouse, N.D., Stotter, A., Goudie, G.O. and Prentice, B.W. (1962) Method of predicting some aspects of performance of a diesel engine using a digital computer. *Proceedings of the Institution of Mechanical Engineers*, vol. 176, no. 9, pp 195-217.

73. Whitehouse, N.D. and Way, R. (1969-70) Rate of heat release in diesel engines and its correlation with fuel injection data, *Proceedings of the Institution of Mechanical Engineers*, vol. 184, part 3J, pp 17-27.

74. Whitehouse, N.D. and Way, R.J.B. (1971) A simple method for the calculation of heat release rates in diesel engines based on the fuel injection rate. *SAE, no. 710134*, pp 1-10.

75. Woschni, G.A. (1967) A universally applicable equation for the instantaneous heat transfer coefficient in the internal combustion engine. *SAE, no 670931*, pp 3065-3083.

76. Woschni, G.A. and Anisits, F. (1974) Experimental investigation and mathematical presentation of rate of heat release in diesel engines dependent upon engine operating conditions. *SAE, no. 740086*, pp 1-14.

77. Yoshida, K., Yamaguchi, I., Seko, T., Suzuki, T., Hori, M. and Kim, Y.K. (1986) Use of dissociated methanol in heavy-duty DI engine with spark plug. *Seventh International Symposium on Alcohol Fuels Technology*, Paris, France, pp 285-290.

78. Zucrow, M.J. and Hoffman, J.D. (1976) *Gas Dynamics*, vol 1, John Wiley and Sons, NY.

The references listed below are those quoted in the historical back-ground based on the paper by D L Hagen (1977), whose format of referencing is retained.

1. Anderson, C.J. Berger, B. Carlson, J. Crothers, W. Gregg, D. Grens, J. and Pasternack, A. (1974) (Lawrence Livermore Labs) *LLL Contribution to the AEC Methanol Report: Fuel Utilization and Environmental Impact.* University of California, Livermore, California, UCID-16442, prepared for US AEC, Contract W-7405-Eng-48.

2. Baratz, B. Ouellette, W. and Stokes, B. (1975) (Mitre Corp.) *Survey of Alcohol Fuel Technology, vol. I.* M74-61-vol. I, 143 pp. NTIS no PB-256007/6WE.

3. Cassady, P.E. (1974) *The Use of Methanol as a Motor Vehicle Fuel.* Mathematical Sciences Northwest Inc. Seattle, Wash., MSNW Report 174-243-2 Prepared for the City of Seattle, Dept. of Lighting, Seattle, Washington, pp 111.

4. Cassady, P.E. (1975) (Mathematical Sciences North West Inc. Bellevue) *The Use of Methanol as a Motor Fuel.* 169th ASCE Meeting, Philadelphia.

5. Crothers, W.T. and Anderson, C.J. (1975) *A Practical Approach to the Introduction of Alternate Automotive Fuels,* University of California, Lawrence Livermore Labs. UCRL-51779, pp 23.

6. Crothers, W.T. (1974)(1975) (Lawrence Livermore Labs) *The Use of Methanol in Transportation.* UCID-16528 Rev. 1, USAEC Contract W-7405-Eng- 48, pp 35.

7. Energy Research and Development Administration, (1977) *Alternative Fuels Utilisation Report.* no 1, Published by Div. Trans. Energy Conserv., Alternative Fuels Utilization Branch, Washington, D.C., Edited and Distributed by Hueller Associated, Inc., 1900 Sulfur Spring Rd., Baltimore, Md. 21227.

8. Federal Ministry for Research and Technology, Bonn. *On the Trail of New Fuels–Alternative Fuels for Motor Vehicles.* 578 pp. Translated (may- June 1975) from the German *Neuen Kraftstoffen auf der*

Spur-Alternative Kraftstoffe fur Kraftfahrzeuge. Bundesministerium fur Forschung und Technologie Bonn, 1974, pp. 1-282, Gersbach & Sohn Verlag, Munchen, UCRL- Trans-10879; 2974, 395 pp., 155 ref. ERDA Res. Abs. 1 (1), 0417, 1976.

9. Gonnermann, C.H. Moore, J.S. and McCallum, P.W. (1975) (Mueller Assoc., Inc., Baltimore, Md.) *Fuelling Automotive Internal Combustion Engines with Methanol–Historical Development and Current State of the Art.* 10th IECEC, Newark, Paper no. 759127, pp.849-855, Contract E.P.A. no. 68-03-0388.

10. Johnson, R.T. (1975) (University of Missouri, Rolla) *Evaluation of Methyl Alcohol as a Vehicle Fuel Extender.* Dept. Transportation Contract DOT-05- 40104, pp 166., NTIS no. PU-251108.

11. Kant, F.H. Cahn, R.P. Cunningham, A.R. Farmer, M.H. and Herbst, W. (1974) *Feasibility Study of Alternative Fuels for Automotive Transportation. vol I, Executive Summary; vol. II, Technical Section; vol. III, Appendices,* by Exxon Research and Engineering Co., Linden, N.J., EPA 460/3-74-009-A, Band C., Contract no 68-01-21◯,NTIS no PB- 235582.

12. Lapedes, D.E. Hinton, M.G. and Meltzer, J. (1974) (Aerospace Corp. El Segundo, Calif.) *Current Status of Alternative Automotive Power Systems and Fuels. vol. I. Executive Summary; vol. II, Alt. Auto Engines; vol. III. Alternative Nonpetroleum-based Fuels; vol. IV. Electric and Hybrid Power Systems,* prepared by the Aerospace Corporation for the EPA. Alternative Automotive Power Systems Divs., Aerospace Report no.ATR-74 (7325)-1, vol. I-IV EPA no EPA-460/3-74-013-a (V.1), pp [illegible] -b (V.2), pp 463.; -c (V/3), pp 380., Contract no 68-01-0417.

13. Mathematical Sciences Northwest, Inc., Seattle, Wa., (1974) *Feasibility Study: Conversion of Solid Waste to Methanol or Ammonia.* MSNW 74-243-1, Sect. IV *Technical Assessment of Conversion Product Uses,* pp 109., 51 ref., prepared for the City of Seattle, Dept. of Lighting, Seattle, Washington.

14. Most, W.J. and Longwell, J.P. (1975) (Exxon Res. & Eng. Co.) *Single- Cylinder Engine Evaluation of Methanol–Improved Energy Economy and Reduced NO_x.* SAE, no. 750119.

15. Nash, A.W. and Howes, D.A. (1938) *Principles of Motor Fuel Preparation and Applications.* vol. I, 2nd Ed., John W. Wiley and Sons, N.Y., pp 461- 561.

16. Pangorn, J. and Gillis, J. (1974) (Institute of Gas Technology, Chicago, IL) *Alternative Fuels for Automotive Transportation–A Feasibility Study, vol. I - Executive Summary; vol. II - Technical Section; vol. III - Appendices*, EPA-460/3-74-012-a, b, and c, pp 26., pp 265., and pp 105.

17. Reed, T.B. and Lerner, R.M. (1973) (Lincoln Laboratory, MIT, Lexington, Mass.) *Methanol: Versatile Fuel for Immediate Use.* Science, vol. 182, pp. 1299-1304.

18. Reed, T.B. (M.I.T., Cambridge) (1975) *Use of Alcohols and Other Synthetic Fuels in Europe from 1930-1950.*

19. Stokes, B. and Park, W. (1975) (Mitre Corp.) *Survey of Alcohol Fuel Technology* vol. II. M74-61-vol. II, pp 68 PB-256908/4WE.

The four references listed below have not been read but have been quoted in the review of the literature on heat transfer in internal combustion engines.

1. Chirkov, A.A. and Stefanovski, B.S. (1958) Odom iruyushchem sposobye pyer edachi tepla v tsilindrach dvigatyelyei vnu tryennyevo sgoraniya, *Trudy rostov. Inst. Inzh. Fyelyeznodorpvnov. Transp.* 21.

2. Nusselt, W. (1923) Der Warmeubergang in der Verbrennungskraftmaschene, Z. *Verdt. Ing.* 67, 692, 708.

3. Pflaum, W. (1951) Warmeubergang bei dieselmaschienen mit und ohne aufladung MTZ, 22, 3.

4. Van Tyen, H.W. (1962) Methode zur berechung der Zylinderbuchsentemperaturen in dieselmotoren, *Dissertation Thesis*, U. Delft, Netherlands.

Author: Cipolat, Daniele.
Name of thesis: Thermodynamic analysis techniques for the study of combustion in compression ignition engines with application to methanol-dimethyl ether fuelling.

PUBLISHER:
University of the Witwatersrand, Johannesburg
©2015

LEGALNOTICES:

Copyright Notice: All materials on the University of the Witwatersrand, Johannesburg Library website are protected by South African copyright law and may not be distributed, transmitted, displayed or otherwise published in any format, without the prior written permission of the copyright owner.

Disclaimer and Terms of Use: Provided that you maintain all copyright and other notices contained therein, you may download material (one machine readable copy and one print copy per page)for your personal and/or educational non-commercial use only.

The University of the Witwatersrand, Johannesburg, is not responsible for any errors or omissions and excludes any and all liability for any errors in or omissions from the information on the Library website.